

# Impact of aromatic on emissions and seal compatibility of gas turbine engine

By Chenxing Ling

**Supervisors** 

Prof. W. Nimmo

Dr B. Khandelwal

A thesis submitted in partial fulfilment of the requirements for the degree of Doctor of Philosophy

The University of Sheffield

Faculty of Engineering

Department of Mechanical Engineering

December 18, 2024

## **Abstract**

This thesis investigates the impact of different aromatic species on emissions using a Tay engine combustor. Intermediate species were identified for soot prediction using Chemkin models. A new experimental configuration was also established to investigate seal compatibility in alternative jet fuels.

Since alternative jet fuels usually contain very little aromatics in their formulation, which significantly reducing PM production but also causing fuel leakage. Therefore, it is necessary to investigate the appropriate aromatic species to add into current alternative jet fuels to solve the leakage problem without compromising the reduction of PM emissions. A wide range of aromatics (15 species) were blended with normal paraffin at two different aromatic concentrations (8% vol. and 18% vol.) to provide a complete investigation of aromatics regarding PM emissions. Gaseous emissions were also considered for better understanding of aromatics. Results indicate that the different aromatics will affect PM production differently at both concentrations. It was found that additional ring structure in aromatic will significantly promote PM production, density was also found to be an indicator of PM production potential. Further investigation is required since the fuel blends used in this experiment were relatively simpler than actual commercial jet fuel, and density should be coupled with other fuel properties for accurate PM prediction.

Chemkin models were established to investigate the production pathway of soot from selected aromatics and identify intermediate species as potential soot tracer in a costeffective way. Both 0-D and 1-D models were created based on a model Tay combustor for the first time. The experimental results guided the analysis of simulation results. Simulation results suggest that compare with small molecules such as acetylene, larger molecules containing benzene structure show better agreement with the experimental findings and have potential as soot tracer. Due to the limitation of Chemkin models, more complex 3-D simulations are recommended for further investigating.

Since the O-ring seal compatibility in alternative jet fuels is currently a hot topic, a new configuration was established to provide a more realistic test environment for seal ageing experiments. Alternative jet fuels are used as drop-in fuels in current aviation combustors, and leakage problems usually occur after fuel changing. Therefore, a complex fuel change strategy was designed to examine sealing performance which is rarely investigated previously. O-ring samples were tested under various temperatures and fuel environments while maintaining high compression. High-temperature ageing processes within the fuel are achieve using newly designed pressured vessels. The results show the replicability of this new test configuration and also present that FKM maintains superior seal compatibility across various temperatures and fuels under realistic conditions. This new test setup will benefit the future investigations of seals in innovative alternative jet fuels.

# **Acknowledgements**

I wish to express my sincere appreciation to my supervisors, Dr. Bhupendra Khandelwal and Prof. Bill Nimmo, for their patience, guidance, and support. Moreover, I would like to acknowledge the technical and research team at the LCCC: Mr I. Ahmed, Mr. D. Dunstan and Mr. T. Haycock for their help with the rig setup. Without them, the completion of this study would not be possible.

# **Content**

| Ab:  | stract                                     | i     |
|------|--|-------|
| Acł  | knowledgements                             | iii   |
| Соі  | ntent                                      | iv    |
| List | t of figures                               | xi    |
| List | t of tables                                | xvii  |
| No   | menclature                                 | xviii |
| List | t of publications                          | XX    |
| 1.   | Introduction                               | 1     |
|      | 1.1 Development of air transport           | 2     |
|      | 1.2 Development of gas turbine engine      | 4     |
|      | 1.3 Overview of aviation emissions         | 6     |
|      | 1.3.1 PM / Soot                            | 8     |
|      | 1.3.2 Nitrogen Oxides (NO <sub>x</sub> )   | 11    |
|      | 1.3.3 Carbon Monoxide and Carbon Dioxide   | 12    |
|      | 1.3.4 Unburned hydrocarbon (UHC)           | 13    |
|      | 1.4 Alternative Jet Fuel                   | 13    |
|      | 1.4.1 Composition of Conventional Jet Fuel | 17    |
|      | 1.4.2 Composition of alternative jet fuels | 19    |
|      | 1.5 Emissions reduction methods            | 19    |
|      | 1.6 Research question                      | 22    |

| 1.7 Thesis Structure                                     | 23 |
|--|----|
| 2. Literature review                                     | 25 |
| 2.1 Previous research on emissions                       | 25 |
| 2.2 Previous research on combustor modelling             | 32 |
| 2.2.1 Stirred reactor model/0-D model                    | 33 |
| 2.2.2 Chemical reactor network/1-D model                 | 34 |
| 2.2.3 Turbulent combustion simulation                    | 37 |
| 2.3 Seal compatibility of alternative jet fuel           | 39 |
| 2.3.1 Fuel leaking                                       | 40 |
| 2.3.2 Past research on elastomer compatibility           | 41 |
| 2.4 Overall summary                                      | 44 |
| 3. Methodology   | 46 |
| 3.1 Experimental configuration of emissions test         | 46 |
| 3.1.1 Fuel blends  | 47 |
| 3.1.2 Tay rig  | 50 |
| 3.1.3 Tay Combustor                                      | 52 |
| 3.1.4 Laser-induced incandescence (LII)/ Artium LII 300  | 55 |
| 3.1.5 Mobile emissions laboratory                        | 56 |
| 3.1.6 3000HM THC analyser                                | 58 |
| 3.1.7 4000VM heated vacuum chemiluminescent NOx analyser | 59 |
| 3.1.8 9000MGA multi gas analyser                         | 60 |
| 3.2 Kinetic modelling                                    | 61 |

| 3.2.1 Zero-D model  | 63 |
|---|----|
| 3.2.1.1 Chemistry mechanism   | 64 |
| 3.2.1.2 Reactant selection  | 64 |
| 3.2.1.3 Reaction temperature  | 65 |
| 3.2.1.4 Residence time, flow rate and volume                                  | 65 |
| 3.2.1.5 Air-fuel ratio (AFR) / $^{\lambda}$                                   | 66 |
| 3.2.1.6 Tracer selection  | 67 |
| 3.2.2 CRN (Chemical reactor network)  | 67 |
| 3.2.1.1 Simple 1D model   | 70 |
| 3.2.2.1 1-D recirculation model   | 71 |
| 3.2.2.3 Detailed 1-D model  | 73 |
| 3.3 Fuel, O-ring, and experiment apparatus                                    | 75 |
| 3.3.1 Candidate fuels   | 75 |
| 3.3.2 O-ring selection  | 77 |
| 3.3.3 C11 jig   | 77 |
| 3.3.4 Elastocon kits  | 79 |
| 3.3.5 Heating vessel and oven   | 83 |
| 3.3.6 Compression strategy  | 84 |
| 3.3.7 Heating treatment and the ageing process                                | 87 |
| 3.3.8 Low-temperature treatment   | 88 |
| 3.4 Unforeseen obstacles and real force majeure                               | 88 |
| 4. Emissions characteristics of a gas turbine combustor and alternative fuels | 90 |

| 4.1 Introduction  | 90              |
|---|-----------------|
| 4.3 Result and Discussion   |                 |
|   |                 |
| 4.3.2 PM emissions  | 93              |
| 4.3.2.1 Molecular weight  | 96              |
| 4.3.2.2 H/C ratio / H%  | 97              |
| 4.3.2.3 Density   | 99              |
| 4.3.2.4 Molecular structure   | 102             |
| 4.3.1 Comparison of gas turbine combustor and IC engine                       | 102             |
| 4.3.3 Gaseous emission  | 104             |
| 4.3.3.1 Unburned hydrocarbon (UHC)  | 104             |
| 4.3.3.2 CO  | 108             |
| 4.3.3.3 NOx   | 112             |
| 4.4 Conclusion  | 116             |
| 5. Investigation of potential intermediate tracers for soot production from c | hemical kinetic |
| modelling   | 118             |
| 5.1 Introduction  | 118             |
| 5.2 Results and Discussion  | 120             |
| 5.2.1 Stoichiometric combustion ( $\lambda$ =1)                               | 121             |
| 5.2.1.1 C <sub>2</sub> H <sub>2</sub> (acetylene)                             | 121             |
| 5.2.1.2 C <sub>2</sub> H₃ (ethenyl)   | 123             |
| 5.2.1.3 C <sub>6</sub> H <sub>6</sub> (benzene)                               | 125             |
| 5.2.1.4 C <sub>14</sub> H <sub>10</sub> (phenanthrene + anthracene)           | 126             |

|           | 5.2.2 Lean combustion (AFR=65)                                | 127 |
|-----------|---|-----|
|           | 5.2.3 Fuel-rich combustion ( $\lambda$ =0.5)                  | 129 |
|           | 5.2.4 Temperature impact                                      | 130 |
|           | 5.2.4.1 1700 K  | 130 |
|           | 5.2.4.2 1300 K  | 131 |
|           | 5.3 1-D model   | 132 |
| 5.4 (     | Conclusion  | 140 |
| 6. Impact | of alternative fuels on seal compatibility                    | 143 |
| 6.1 l     | ntroduction   | 143 |
| 6.2 F     | Result and Discussion   | 145 |
|           | 6.2.1 Jet A-1   | 147 |
|           | 6.2.2 Jet A-1 to Alternative Jet Fuel (#13)                   | 150 |
|           | 6.2.3 Alternative Jet Fuel (#13) to Alternative Jet Fuel (#4) | 151 |
|           | 6.2.4 Alternative Jet Fuel (#4) to Jet A-1                    | 153 |
|           | 6.2.5 High-temperature treatment                              | 155 |
|           | 6.2.6 Low-temperature impact                                  | 160 |
|           | 6.2.7 Experiment replicability                                | 162 |
|           | 6.2.7.1 Fuel impacts and heat ageing treatment                | 163 |
|           | 6.2.7.2 Low-temperature impact                                | 164 |
|           | 6.2.8 Physical appearance of O-rings after the experiment     | 165 |
| 6.3 (     | Conclusion  | 167 |
|           |   |     |

|   | 169 |
|---|-----|
| 7.1 Overall conclusions                                   | 169 |
| 7.2 Suggestions on future work                            | 172 |
| Bibliography  | 174 |
| APPENDIX A - Feedstock of alternative jet fuels           | 199 |
| A.1 Feedstock of alternative jet fuels                    | 199 |
| A.2 Bio-based feedstock                                   | 200 |
| A.2.1 Starch and sugar                                    | 201 |
| A.2.2 Palm oil  | 202 |
| A.2.3 Lignocellulose resources                            | 203 |
| A.2.4 Energy crops  | 204 |
| A.2.5 Waste oil   | 205 |
| A.2.6 Algae   | 205 |
| A.3 Fossil feedstock                                      | 206 |
| A.3.1 Natural gas   | 206 |
| A.3.2 Coal  | 207 |
| APPENDIX B - Production pathways of alternative jet fuels | 209 |
| B.1 Fischer-Tropsch (FT)                                  | 210 |
| B.2 Hydrotreatment Esters and fatty acids (HEFA)          | 211 |
| B.3 Alcohol-to-Jet (ATJ)                                  | 213 |
| B.4 Direct sugars to hydrocarbons (DSHC)                  | 214 |
| B.5 Catalytic hydrothermolysis (CH)                       | 215 |

| B.b Lite cycle analysis21 |
|---------------------------|
|---------------------------|

# **List of figures**

## Chapter 1

| Figure 1. 1: World aviation traffic evolution 1945-2022. Reproduced from [3]3       |
|---|
| Figure 1. 2: Gas turbine engine structure. Reproduced from [8]5                     |
| Figure 1. 3: Gas turbine engine emissions and corresponding effects. Reproduced     |
| from [11]7  |
| Figure 1. 4: Sequence of soot formation. Reproduced from [14]8                      |
| Figure 1. 5: Structure of a conventional combustor. Reproduced from [16]9           |
| Figure 1. 6: Flight tests using alternative jet fuels. Reproduced from [36]16       |
| Figure 1. 7: Gas chromatograph of the composition of jet fuel (Jet-A/JP-5/JP-8).    |
| Reproduced from [16]  |
| Figure 1. 8: Emissions Production due to temperature and AFR. Reproduced from [16], |
| [51]21  |

#### Chapter 2

|    | Figure 2. 3: PM results for IC engine. Adapt from [75]                      | 31    |
|----|---|-------|
|    | Figure 2.4: Perfectly stirred reactor. Reproduced from [77]                 | 33    |
|    | Figure 2.5 Recirculation model. Reproduced from[78]                         | 34    |
|    | Figure 2.6 Schematic of a plug-flow reactor. Reproduced from[77]            | 35    |
|    | Figure 2.7: Recirculation reactor model. Reproduced from [79]               | 36    |
|    | Figure 2.8: Diagram of emission model. Reproduced from[81]                  | 37    |
|    | Figure 2.9: Seal Swelling Phenomenon  | 40    |
|    | Figure 2.10: Fuel leaking due to the sealing problem. Reproduced from [73]  | 41    |
|    | Figure 2.11: Schematic of an optical dilatometer. Reproduced from [90]      | 42    |
| Ch | apter 3   |       |
|    | Figure 3.1: Tay rig setup   | 50    |
|    | Figure 3. 2 The Tay combustion and turbine system (04 module). Reproduced f | rom   |
|    | [94]  | 52    |
|    | Figure 3. 3 Single combustor can from Tay engine. Reproduced from [95]      | 53    |
|    | Figure 3. 4 Airflow inside Transply material. Reproduced from[96]           | 54    |
|    | Figure 3.5: Typical laser-induced incandescence. Reproduced from [97]       | 56    |
|    | Figure 3.6: Mobile Emissions Laboratory. Reproduced from [98]               | 57    |
|    | Figure 3.7: THC system. Reproduced from [100]                               | 59    |
|    | Figure 3.8: Working principles of heated vacuum chemiluminescent NOx analy  | /ser. |
|    | Reproduced from [99]  | 60    |
|    | Figure 3.9: Infrared Photometer working principle. Reproduced from [101]    | 61    |
|    | Figure 3. 10: 0-D model   | 63    |

|    | Figure 3. 11 (a) Sketch of Tay Combustor Model. Reproduced from [112]; (b) 3- | ·D  |
|----|---|-----|
|    | geometry of Tay combustor model   | 38  |
|    | Figure 3. 12 Flow field in model Tay combustor. Reproduced from [83] (a) Mid  | - k |
|    | horizontal plan plane; (b) Mid-vertical plan                                  | 39  |
|    | Figure 3. 13: Simplest CRN  | 70  |
|    | Figure 3. 14: CRN model layout 1  | 71  |
|    | Figure 3. 15: CRN model layout 2  | 71  |
|    | Figure 3. 16: CRN model Layout 3  | 74  |
|    | Figure 3. 17: Section view of C11 jig under pressure. Reproduced from [119]   | 78  |
|    | Figure 3. 18: Critical parts of C11 jig                                       | 79  |
|    | Figure 3. 19: Overview of the Elastocon kits                                  | 30  |
|    | Figure 3. 20: Stress relaxation unit. Reproduced from [117]                   | 31  |
|    | Figure 3. 21: Elastocon unit with environment control hood                    | 32  |
|    | Figure 3. 22: Structure of heating vessel                                     | 33  |
|    | Figure 3. 23: Compression strategy in one jig. Reproduced from [119]          | 35  |
| Ch | apter 4   |     |
|    | Figure 4. 1: Effect of aromatic species on PM mass concentration              | )4  |
|    | Figure 4. 2: Molecular weight impact on PM                                    | 96  |
|    | Figure 4. 3: H/C ratio impact on PM   | 98  |
|    | Figure 4. 4: Blend density impact on PM production10                          | )() |
|    | Figure 4. 5: Correlation between H/C ratio and density                        | )1  |
|    | Figure 4. 6: Aromatics impact on UHC1   | )5  |

|    | Figure 4. 7: Correlation between PM and UHC105   |
|----|--|
|    | Figure 4. 8: Corrlation between molecular weight and UHC, (b) Corrlation between                               |
|    | Density UHC, (c) Corrlation between H/C ratio UHC108   |
|    | Figure 4. 9: Aromatics impact on CO  |
|    | Figure 4. 10: Correlation between PM and CO110   |
|    | Figure 4. 11: (a) Correlation between molecular weight and CO, (b) Correlation                                 |
|    | between Density CO, (c) Correlation between H/C ratio CO112  |
|    | Figure 4. 12: Aromatics impact on NOx,   |
|    | Figure 4. 13: Correlation between PM and NOx114  |
|    | Figure 4. 14: (a)Correlation between molecular weight and NOx, (b) Corrlation                                  |
|    | between Density NOx, (c) Corrlation between H/C ratio NOx116   |
| Ch | apter 5  |
|    | Figure 5. 1: Mole Fraction of C <sub>2</sub> H <sub>2</sub> as a function of residence time122                 |
|    | Figure 5. 2: Mole Fraction $C_2H_3$ as a function of residence time  |
|    | Figure 5. 3: Mole Fraction $C_6H_6$ as a function of residence time  |
|    | Figure 5. 4: Mole Fraction $C_{14}H_{10}$ (phenanthrene + anthracene) as a function of                         |
|    | residence time126  |
|    | Figure 5. 5: Mole Fraction $C_{14}H_{10}$ (phenanthrene + anthracene) as a function of                         |
|    | residence time128  |
|    | Figure 5. 6: Mole Fraction $C_{14}H_{10}$ (phenanthrene + anthracene) as a function of                         |
|    | residence time129  |
|    | Figure 5. 7: Mole Fraction C <sub>14</sub> H <sub>10</sub> (phenanthrene + anthracene) at 1700 K as a function |

| of residence time  |
|--|
| Figure 5. 8: Mole Fraction C14H10 (phenanthrene + anthracene) in 1300k13:              |
| Figure 5. 9: Mole fraction of C2H2 of fuel blends in PFR                               |
| Figure 5. 10: Mole fraction of C2H3 of fuel blends in PFR13!                           |
| Figure 5. 11: Mole fraction (C6H6) in PFR130   |
| Figure 5. 12: Mole fraction of BIN groups for Methylnaphthalene fuel blends13          |
| Figure 5. 13 (a)Production pathways to BIN1A, (b) Production pathways to BIN1B, (c     |
| Production pathways to BIN1C139  |
| Figure 5. 14: Possible reaction net between methylnaphthalene, indenyl, and C6H0       |
| 140  |
| Chapter 6  |
| Figure 6. 1: Initial stress relaxation curve for 5 hours                               |
| Figure 6. 2: The stress relaxation behaviour in Jet A-1 for 80 hours149                |
| Figure 6. 3: The stress relaxation behaviour from Jet A-1 to Alternative Jet Fuel (#13 |
| 150  |
| Figure 6. 4: The stress relaxation behaviour from Alternative Jet Fuel (#13) to        |
| Alternative Jet Fuel (#4)152   |
| Figure 6. 5: The stress relaxation behaviour from Alternative Jet Fuel (#13) to Jet A- |
| 15-  |
| Figure 6. 6: Stress relaxation curve after the first heating process150                |
| Figure 6. 7: Fuels impact on heat-treated sample after the first heating process15     |
| Figure 6. 8: All high-temperature ageing processes and fuel exchanges of Set 615       |

| Figure 6. 9: Low-temperature impacts on Set 6 (a) stress relaxation curve for different  |
|--|
| materials (b) temperature curve161   |
| Figure 6. 10: Stress relaxation curve for Set 7  |
| Figure 6. 11: Low-temperature impacts on Set 7 (a) stress relaxation curve for different |
| materials (b) temperature curve  |
| Figure 6. 12: O-ring physical appearance   |

# **List of tables**

| Chapter ' |
|-----------|
|-----------|

| Table 1. 1: Emissions control based on the engine operation condition [8], [16], [26] | 26]. |  |
|---|------|--|
|   | 20   |  |
|   |      |  |
|   |      |  |
| Chapter 3   |      |  |
| Table 3.1: List of candidate aromatics  | 47   |  |
| Table 3.2: Properties of Banner NP1014  | 49   |  |
| Table 3.3: Test conditions  | 51   |  |
| Table 3.4: Gaseous emissions measurement equipment                                    | 58   |  |
| Table 3. 5: Fuel Selection  | 76   |  |
| Table 3. 6: O-rings   | 77   |  |
| Table 3. 7: Pre-compression of Set 6  | 86   |  |
| Table 3. 8: Pre-compression of Set 7  | 87   |  |

# Nomenclature

| AFR  | Air fuel ratio   |
|------|--|
| ATJ  | Alcohol-to-jet   |
| BC   | Black carbon   |
| CBTL | Coal-biomass to liquids                                |
| CO   | Carbon monoxide  |
| CO2  | Carbon dioxide   |
| CRN  | chemical reactor network                               |
| CSD  | cross-section diameter                                 |
| CTL  | coal to liquids  |
| EI   | Emission index   |
| FAO  | Food and Agriculture Organization of the United Nation |
| FAR  | Fuel air ratio   |
| FKM  | Fluorocarbon   |
| FS   | Fluorosilicone   |
| FT   | Fischer-Tropsch  |
| GTL  | Gas to liquids   |
| HEFA | Hydrotreatment Esters and fatty acids                  |
| HRJ  | Hydrotreated Renewable Jet                             |
| LES  | large eddy simulation                                  |
| NVP  | non-volatile PM  |
| PFR  | plug flow reactor                                      |
| PM   | Particulate matter                                     |
| PSR  | perfect stirred reactor                                |
| RQL  | Rich-burn Quick-quench Lean-burn<br>Combustor          |
| SAF  | Sustainable aviation fuel                              |

| UHC | Unburn hydrocarbons   |
|-----|-----------------------|
| VP  | volatile particulates |
| WSR | well-stirred reactor  |

# **List of publications**

Authored during the course of this PhD programme.

- 1. Zheng, Lukai; Ling, Chenxing; Ubogu, Emamode A; Cronly, James; Ahmed, Ihab; Zhang, Yang; Khandelwal, Bhupendra. Effects of Alternative Fuel Properties on Particulate Matter Produced in a Gas Turbine CombustorEnergy & fuels, 32(9), pp. 9883–9897. doi: 10.1021/acs.energyfuels.8b01442.
- 2. Zheng, Lukai; Singh, Paramvir; Cronly, James; Ubogu, Emamode A; Ahmed, Ihab; Ling, Chenxing; Zhang, Yang; Khandelwal, Bhupendra. Impact of Aromatic Structures and Content in Formulated Fuel for Jet Engine Applications on Particulate Matter Emissions. Journal of energy resources technology, 143(12). doi: 10.1115/1.4049905.

## 1. Introduction

The consumption of conventional aviation fuel has continued to increase for decades. This demand for aviation transportation dropped significantly due to the COVID-19 pandemic. However, the market appears to be recovering, suggesting that the need for jet fuel will continue to increase.

Particulate matter (PM) or soot ranks among the most significant pollutants emitted by gas turbine engines. Other emissions, such as CO<sub>2</sub> and NOx, substantially affect the environment. The quantity of jet fuel used represents a smaller fraction than other sectors such as internal combustion engines. Only 10.5% of each 44-gallon crude oil in the US [1]. However, given projected aviation growth, environmental pollution is anticipated to intensify due to large-scale jet fuel combustion. Therefore, introducing low-emission alternative jet fuels is one of the most logical solutions to replace conventional fossil fuels environmentally.

The ideal scenario would be direct usage of alternative jet fuels without modifying existing gas turbine engines, though this presents significant challenges. Therefore, additional experimentation and testing are required to investigate potential interactions between alternative jet fuels and gas turbine engines, particularly regarding the emissions characteristics and seal compatibility.

Research confirms that burning alternative jet fuels reduces PM and gaseous emissions relative to conventional jet fuels. However, most researchers focus solely on the fuel as a single entity, analysing results by the type of alternative jet fuels. Particularly for full-scale engines, the prohibitive cost of customized fuel blends has limited most studies from examining individual fuel components.

Almost all alternative jet fuels test results demonstrate a significant reduction in PM emissions, and most researchers correlate this phenomenon with the absence of aromatic content in alternative jet fuels. However, aromatics are the general name for a large group of chemical substances, including various species, which could result in different PM emissions. Few studies examine a wide range of aromatic species and their impact on PM emissions. Moreover, whether aromatic species affect gaseous emissions remains unclear. This study will aim to address this knowledge gap through a well-developed test rig.

In addition, there is a significant problem when using alternative jet fuels in gas turbine engines since their low aromatic content stems from production methods and feedstocks. The sealing performance of elastomer seals will decline without aromatic content, potentially causing leaks. Some literature has examined how different aromatic species will affect seal compatibility. However, these tests often neglect the actual operation environment in gas turbine engines, such as high pressure and extreme temperature. Current methodologies require updating to better assess alternative fuel-seal interactions. This study will develop an improved experimental approach to evaluate alternative fuel effects on multiple elastomer types.

## 1.1 Development of air transport

The world's first commercial airline service began in St. Petersburg, Florida, in 1914 [2]. Since then, the demand for the aviation market has continued to increase. Figure 1. 1 provided by the international civil aviation organization (ICAO), shows the history of aviation market development. This figure shows that despite events like terrorist attacks and financial crisis temporarily slowing growth the market consistently recovers and expands within years.

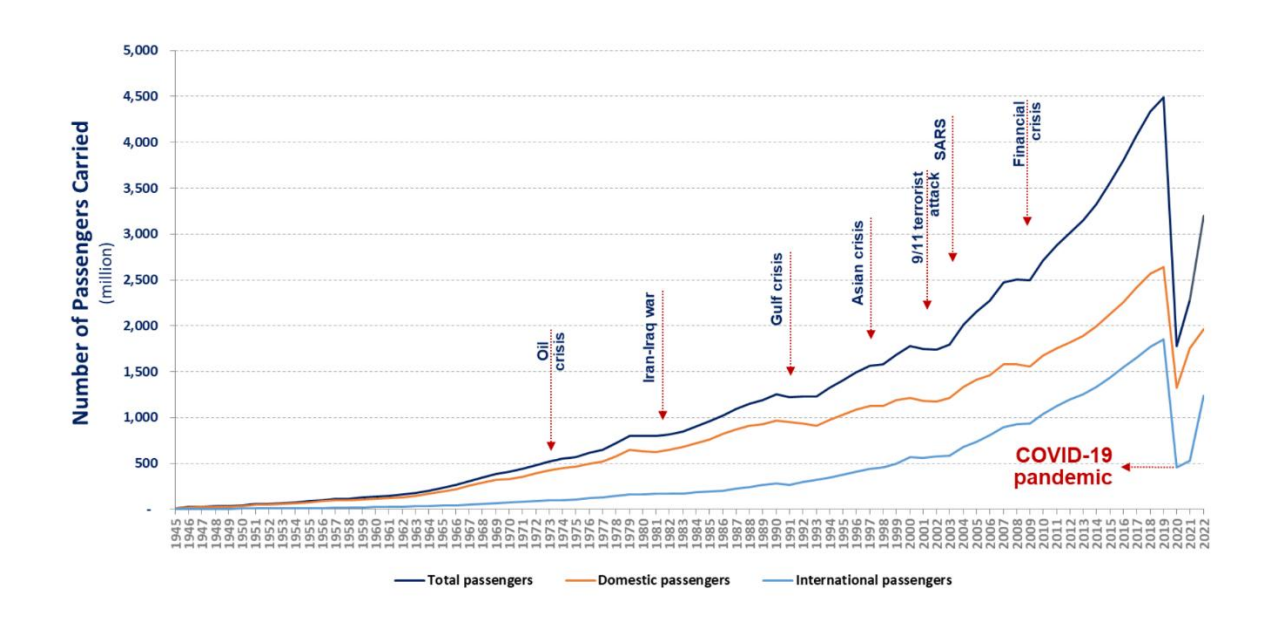


Figure 1. 1: World aviation traffic evolution 1945-2022. Reproduced from [3]

Air transportation capacity reached its historical peak between 2018 and 2019 before declining dramatically due to COVID-19. ICAO data comparing 2020 and 2019 world-scheduled passenger traffic shows, a 60% passenger reduction and nearly \$372 billion in losses [3]. The pandemic's impact was unprecedented, raising concerns about air transportation's future. However, Figure 1. 1 within a few years after the end of the pandemic shows a steep recovery trend post-pandemic. While capacity hasn't fully recovered to pre-pandemic levels, industry and society remain optimistic about its recovery.

In the "Commercial Market Outlook 2022-2041 [4]", Boeing states that over the next two decades, the industry will experience an annual 4.8% growth in global fleets and 5.3% passenger traffic growth. An annual 4.1% air cargo growth is projected through 2024. Meanwhile, Airbus forecasts an annual 3.6% growth in passenger traffic and 3.2% growth in freight traffic in its "Global Market Forecast 2022-2024 [5]". Although their growth estimates vary slightly, both aviation leaders share the same opinion: the market will continue to grow for the foreseeable future.

In general, the development of air transport continued by COVID-19, and the market will continues expanding rapidly. However, this situation implies the corresponding emissions problem from aviation growth will intensify. Therefore, the public and industry must stay vigilant, and emission-reduction technologies require advancement.

## 1.2 Development of gas turbine engine

Many incarnations of gas turbines have appeared in the history of humankind, but these prototypes were never mass-produced. The first operational modern gas turbine engine, the Jumo 004B, was developed in 1942 during World War II [6]. It was designed by Anselm Franz and powered the Messerschmitt Me 262, the world's first operational jet fighter [6]. Meanwhile, the first commercial airline equipped with a gas turbine engine was the DH.106 Comet, introduced by de Havilland in 1949 [7]. The superior performance of gas turbine engines led to their rapid replacement of piston engines in both military and civilian applications. The dramatic development of gas turbine engines resulted in numerous specialized designs and manufacturing branches. Although many gas turbine engine variants exist worldwide, the core mechanism remains consistent.

A typical operating principle of a modern gas turbine engine is shown in Figure 1. 2. Generally, all gas turbine engines operate on a Brayton cycle and include three main parts: compressor, combustor, and turbine. Atmospheric air is first compressed by the compressor to the designed pressure before entering the combustor. Jet fuel is sprayed and vaporised inside the combustor into tiny droplets. Air and fuel are then mixed and ignited within the combustor to generate high-temperature gas flow. Finally, these high-temperature pressurized gases enter the turbine and rotate the turbine connected to the compressor.

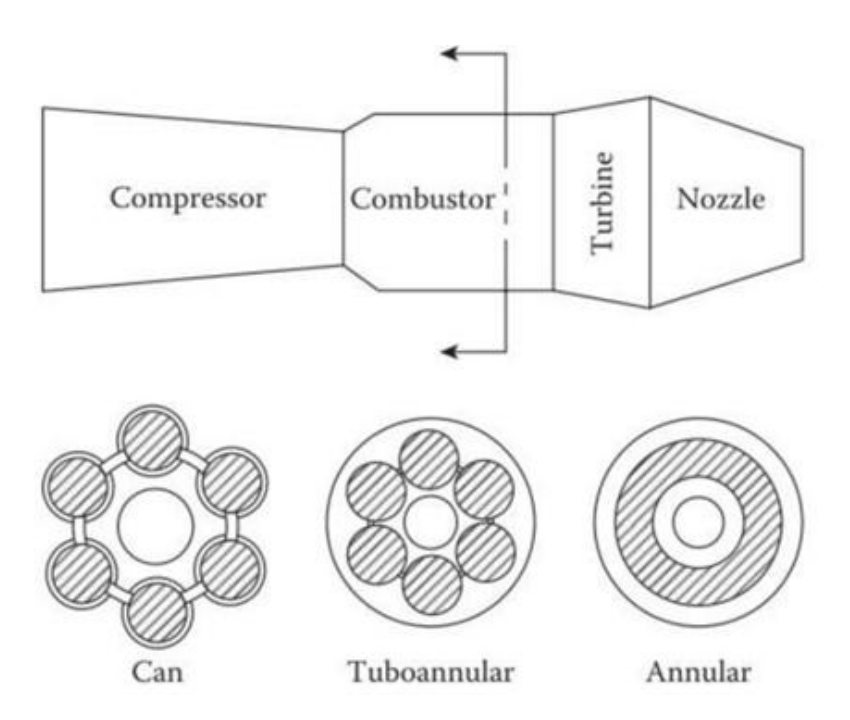


Figure 1. 2: Gas turbine engine structure. Reproduced from [8]

Although most aircraft in service today use gas turbine engines, given concerns about the emissions problem from aviation transport, some voices have urged abandoning the current propulsion method and replacing it with a more environmentally friendly system like hydrogen [9], [10]. However, replacing gas turbine engines remains challenging.

Decades and countless investments have been spent on developing gas turbine engines, securing their technological advantage over other potential aviation propulsion methods. Therefore, the complete switch from gas turbine systems in aircraft will first require consist global policy support. Second, a breakthrough propulsion technology capable of matching gas turbine performance is needed. However, either requirement has been met to date.

Therefore, the attempt to replace the current aviation propulsion system in a short time is unrealistic. Considering the difficulty of changing the current propulsion system, gas turbine engines will remain operational for the foreseeable future. However, following the natural law, there will eventually emerge an advanced propulsion system to replace

the gas turbine engine, and considering the current development rate of alternative propulsion systems, a relatively long transition phase will be required between the iteration of propulsion technology.

Certainly, the emissions problem caused by gas turbine engines has become a significant issue. Until the transition to a new propulsion method, improving the existing gas turbine system to achieve the emission reduction goal becomes extremely necessary.

### 1.3 Overview of aviation emissions

A detailed characterization of analysis of aviation emissions should be prioritised before developing mitigation strategies for a modern gas turbine engine. Generally, aviation emissions can be divided into gaseous emissions and soot. For gaseous emissions, the industry primarily focuses on four types: carbon monoxide, carbon dioxide, unburned hydrocarbon (gaseous form) and nitrogen oxides. Soot is another significant emission, consisting of particulate matter of varying sizes. These emissions are proven to harm the environment and human health in multiple ways. For example, CO<sub>2</sub> is one of the primary greenhouse gases that contributes to global warming. Meanwhile, inhaled soot can cause permanent lung damage. A detailed discussion of these aviation emissions will be presented later in this chapter.

The cause of jet fuel emissions varies, but in general, two factors significantly affect emissions production: combustion conditions and fuel content. Figure 1. 3 provides an overview of the emissions production pathway and its relative impact on the environment or human health. According to the jet fuel combustion formula in Figure 1. 3, there is a difference in emissions species for ideal combustion and actual combustion. It should be pointed out that ideal combustion usually refers to complete combustion,

and actual combustion stands for incomplete combustion. Moreover, different air-fuel ratios significantly the combustion conditions. Higher AFRs promote complete combustion, while lower AFRs increase incomplete combustion risk.

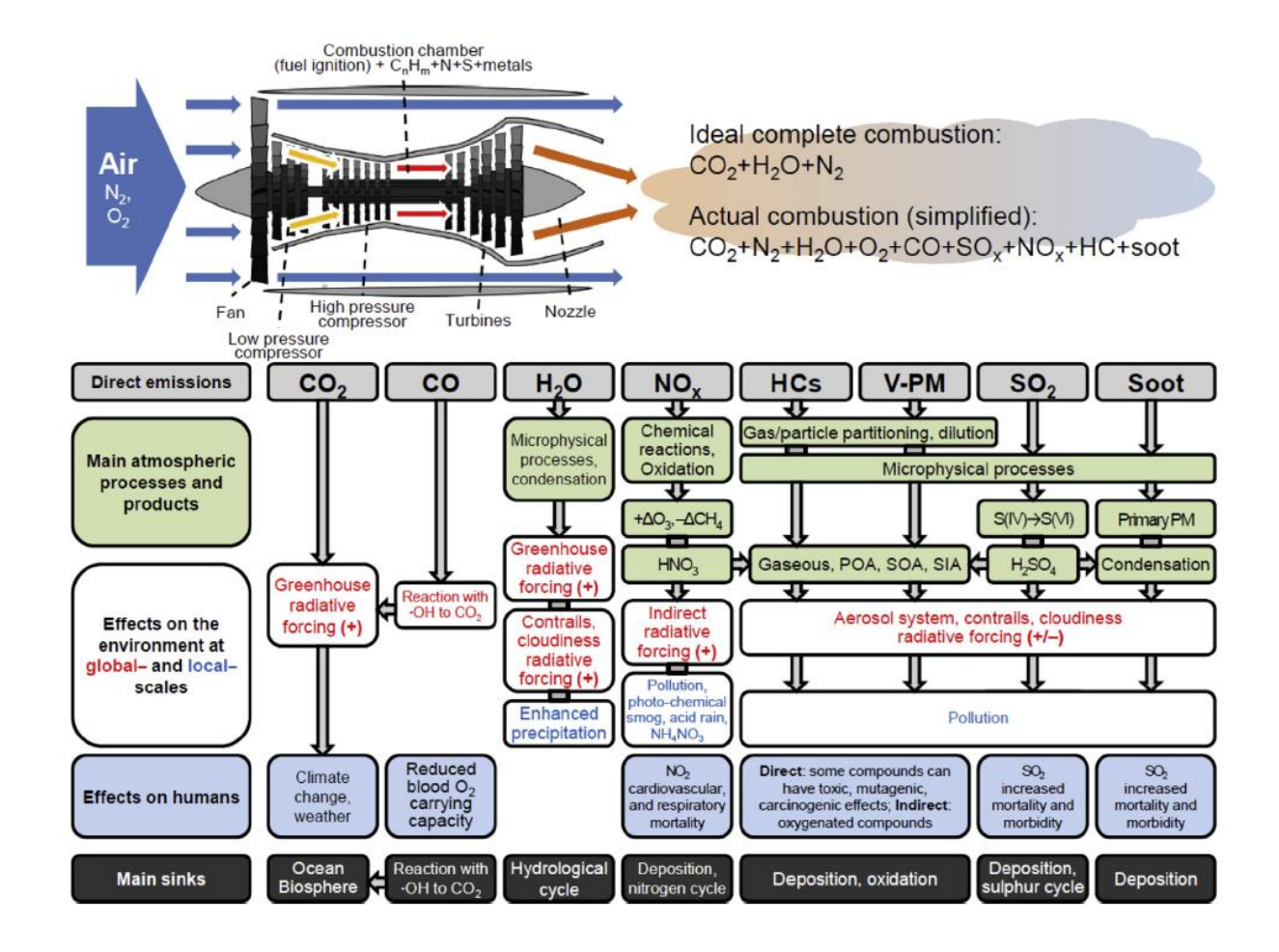


Figure 1. 3: Gas turbine engine emissions and corresponding effects. Reproduced from [11]

Under ideal jet fuel combustion produces only emit  $CO_2$ ,  $H_2O$  and  $N_2$ . Only  $CO_2$  will significantly impact the environment through this combustion pathway since  $CO_2$  is one of the major greenhouse gases. However, the actual situation is worse. Due to the nature of the combustor design and fuel formula, emissions such as  $SO_2$ , CO, and soot are also emitted, causing environmental harm. Moreover, although nitrogen content is nearly negligible in jet fuel, abundant  $N_2$  remains in the air. High combustion temperatures facilitate N and O combination, generating  $NO_x$  - a known air pollutant. This section will provide more details about jet fuel emissions.

#### 1.3.1 PM / Soot

Soot or PM, collectively termed particulate pollution, consisting of different sizes of solid particles and liquid droplets. According to their formation principle, they are categorized as primary and secondary emissions. Primary emissions are the particles generated directly from the combustion process, and secondary particle form subsequently in the atmosphere from combustor-emitted gaseous precursors. The black coloration of high soot concentrations results from carbon content. Since soot is visibly polluting, its environmental and health impact have been extensively studied [12], and fundamental formation theories exist [13]. A general soot formation pathway is shown in Figure 1. 4.

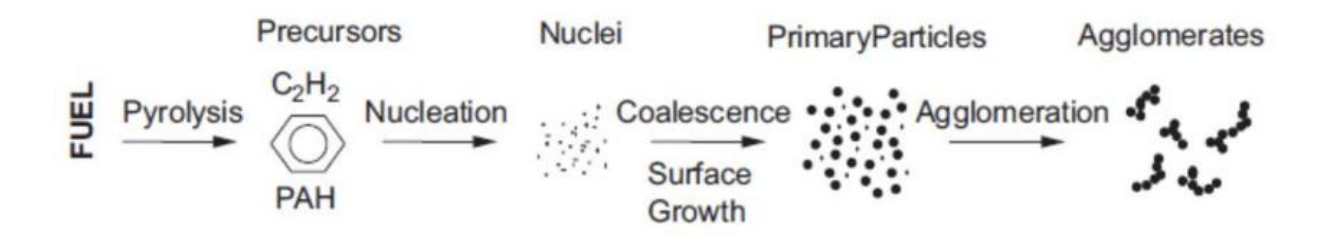


Figure 1. 4: Sequence of soot formation. Reproduced from [14]

Although the exact soot formation pathway remains under study, especially regarding nucleation [15], combustion theory (Figure 1. 3) suggests the majority of PM or soot results from incomplete combustion with hydrocarbons being the primary carbon source. Furthermore, two key factors affecting combustion conditions in gas turbines are fuel formula and combustor design.

Figure 1. 5 illustrates the general structure of a gas turbine combustor. The combustion process can be divided into three zones: primary, secondary, and dilution. To establish a necessary high-temperature region, 15- 20 percent air is introduced with fuel in the primary zone to trigger the rapid combustion. About 30 percent of air passes through

the holes in the secondary zone completing combustion. The remaining air cools the mixed combustion products to achieve the required inlet temperature of the turbine.

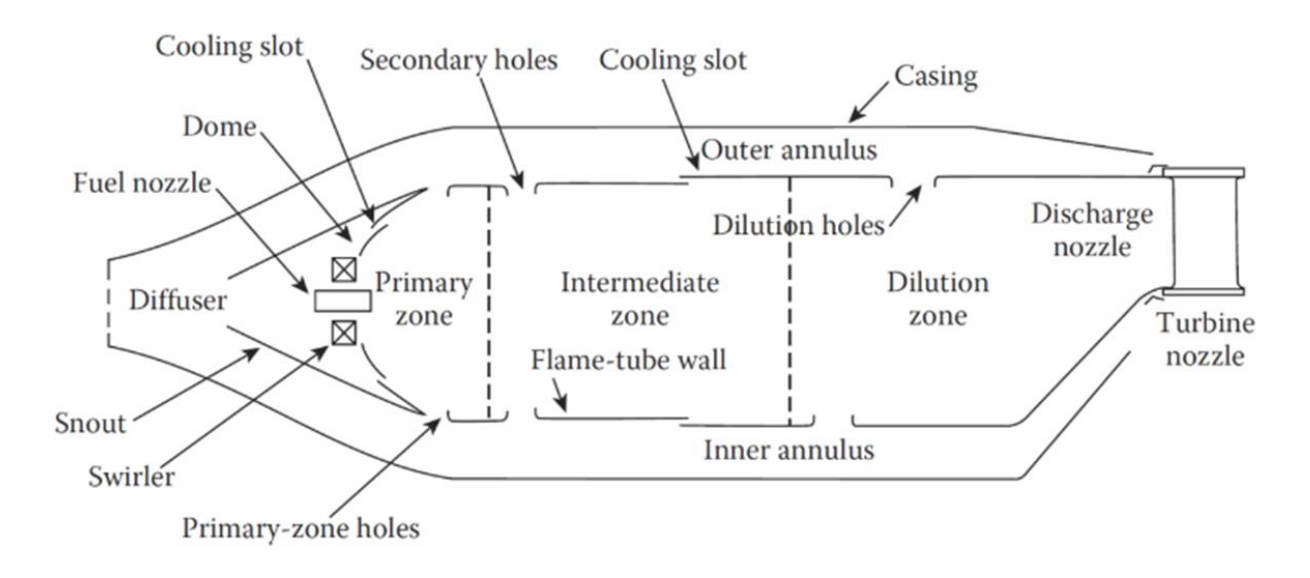


Figure 1. 5: Structure of a conventional combustor. Reproduced from [16]

In the combustor geometry aspect, soot is produced in the fuel-rich regions of the flames, where burned gases move toward the fuel injector. Deficient oxygen gases envelop local rich fuel pockets at high temperatures. Also, it can be produced anywhere in the combustor where fuel-air mixing is insufficient. Generally, most soot is formed in the primary zone and consumed downstream at high temperatures. In gereral, The primary zone determines the soot production rate, while the dilution zone governs the consumption rate.

Modern engines have put a lot of effort on combustor modification to achieve soot reduction. As mentioned, insufficient air in the primary zone prevents complete hydrocarbon combustion, creating small intermediate species that grow into PAHs. Therefore, there are several methods that could solve the soot problem through combustor design.

First of all, upgrading the fuel injector creates a finer fuel-air mix, Modern aviation-grade fuel injectors are typically air-blasted and feature complex internal geometries that guide air and fuel to produce extremely fine fuel droplets. Second, introducing more oxygen after the primary zone promotes the consumption of the unburned hydrocarbons. For example, the Rich-burn Quick-quench Lean-burn Combustor (RQL) concept introduces a high amount of quenching air after the primary zone. Although the primary purpose of this quenching air is NOx reduction, it also effectively reduces soot. In fact, studies show that RQL-like air injection methods can eliminate up to 99.6% of initial soot volume fraction from jet fuels [17]. It should be noted that the timing of quench air injection should be carefully controlled; early injection could actually increase PM production.

The specific content in the fuel composition could also cause incomplete combustion. Hydrocarbon is the primary component in jet fuel, and paraffin, aromatic, and naphthene are hydrocarbon classes, which will be discussed further in this chapter. Many previous studies have proved that alternative fuels can reduce soot emissions due to their low aromatic content. In addition, in theory, all hydrocarbons could cause soot generation if the combustion is incomplete. Therefore, some research [18], [19], [20] comparing soot production tendencies of jet fuel hydrocarbons shows the following order: "naphthalenes > alkylbenzenes > alkynes > alkenes > cycloparaffins  $\approx$  iso-paraffins > n-paraffins, which is independent of carbon number. This sequence provides a clear framework of how different fuel components influence PM production. It indicates that although other major fuel content, such as cycloparaffin, could promote PM production, the effectiveness cannot compare with aromatic.

Since different fuel components could affect PM production differently, and aromatics comprise numerous chemical species, and it is easy to speculate that different aromatic species will exhibit distinct soot formation behaviours. Therefore, further study on soot

formation focusing on different aromatic species forms a key objective of this investigation.

## 1.3.2 Nitrogen Oxides (NO<sub>x</sub>)

It used to be believed that aviation activity was not the major source for NOx emissions since it was not the primary transportation method [21]. However, with the increasing demand for aircraft travel in recent decades, a significant increase in NOx emissions has been observed. NOx, including NO and NO<sub>2</sub>, contributes to the formation of smog and acid rain [22]. Moreover, the most significant impact of NOx is altering the O<sub>3</sub> concentration in both the troposphere and stratospheric ozone layer [23], [24]. In detail, most gas turbine engines operating in the troposphere produce O<sub>3</sub>, while subsonic aircraft reduce the ozone layer in the stratosphere. Both situations impact the ozone concentration, climate and human health.

The sources of nitrogen oxides are nitrogen present in the air and jet fuel. Due to the extremely high temperature during the combustion, this nitrogen will be oxidized into NOx through oxidation. However, it is believed that the primary source is the nitrogen in the air, since jet fuel contains only trace nitrogen [25]. The nitrogen content in jet fuel is typically unregulated industrially, and the possible range is between 0 ppm and 20 ppm [26]. Therefore, fuel-bound nitrogen minimally affects NOx emissions under ideal and full-power engine operation conditions.

Compared to fuel formula, the most effective approach focuses on combustion conditions to achieve significant NOx reduction goal. The previous studies demonstrate a strong correlation between NOx production and high flame temperature in gas turbine combustors [27], [28]. Many combustor design innovations have been implemented. For example, modifying the combustor geometry design [29] achieves a more rapid and

uniform flame temperature reducing the duration and magnitude of peak temperature while lowering NOx emissions. Excess air dilution in a combustor further decreases NOx emissions by lowering the overall flow temperature [30].

#### 1.3.3 Carbon Monoxide and Carbon Dioxide

Both carbon monoxide and carbon dioxide are emissions directly resulting from the fuel composition. The amount of CO<sub>2</sub> and CO in gas turbine exhaust is complementary. These emissions are highly tied to the combustion conditions. In general, complete combustion produces predominantly CO<sub>2</sub> and incomplete combustion favours CO production.

CO<sub>2</sub> is one of the final products of combustion according to the jet fuel combustion principle. It is not toxic but serves as a key indicator for monitoring the engine combustion conditions. Moreover, CO<sub>2</sub> is considered the primary contributor to global warming. In the atmosphere, CO<sub>2</sub> can absorb longwave radiation from the Earth's surface and prevent this radiation from escaping to space. This phenomenon is commonly known as the greenhouse effect [31].

Unlike CO<sub>2</sub>, CO is a toxic chemical that impairs red blood cells' oxygen capacity [32]. Since the combustion process is not always ideal, incomplete combustion converts some fuel carbon to CO. The causes of incomplete combustion are various: Inappropriate air-fuel ratio, combustor design, and fuel injector performance all influence the combustion condition. Elevated flame temperatures increase CO output through significant CO<sub>2</sub> dissociation.

Approximately 2.1% of total global human carbon emissions come from aviation transportation [33], [34]. Moreover, as demand grows, annual CO<sub>2</sub> emissions are projected to rise from 705 Mt in 2013 to 1000-3100 Mt by 2050 [35]. Significant efforts

have focused on reducing CO<sub>2</sub> emissions from gas turbine engines. However, as mentioned, reducing CO<sub>2</sub> emissions often increases CO production. Therefore, rather than modifying combustion conditions, alternative jet fuel is considered an effective approach to reduce carbon emissions overall [36].

#### 1.3.4 Unburned hydrocarbon (UHC)

Unburned hydrocarbon (UHC) primarily results from the incomplete decomposition of jet fuel during the combustion process, and they serve as combustion condition indicators. Elevated UHC levels often correlate with increased CO production. Exposure to unburned hydrocarbons can lead to significant health risks, even in the gaseous form. Different hydrocarbons vary in health impact severity due to their distinct toxicological properties [37]. Therefore, monitoring and reducing UHC remains essential for gas turbine combustion.

## 1.4 Alternative Jet Fuel

According to data provide by IEA [38], in the United States, conventional jet fuel accounts for a significant portion of petroleum products, and approximately 65 million gallons of jet fuel were consumed in 2002. The shortage of fossil-based fuels is worsened due to the increasing demand for global aviation transportation. Moreover, as aviation transportation expands worldwide, the consequence of environmental damage due to conventional jet fuel usage becomes much more serious. Hence, urgent adoption of alternative jet fuels from novel feedstocks is critical.

Alternative aviation propulsion systems are not a new concept. Aircraft powered by hydrogen or nuclear were extensively studied throughout human history [39], [40]. Unlike today, which also focuses on environmental protection, these projects mainly focused on energy security, and through these investigations, the feasibility of using

alternative power sources has been examined. However, as discussed, gas turbine engines using hydrocarbon jet fuel will continue to dominate the market until a huge breakthrough appears in other power systems. Therefore, introducing low-emission alternative jet fuels with various feedstocks that are directly compatible with the current gas turbine engine system is essential. This type of alternative jet fuels is also called a drop-in fuel. The drop-in alternative jet fuels refer to fuels that can replace conventional fuel without compromising engine performance and maintenance [41], and are the focus of this thesis. More information on feedstock and production pathways of alternative jet fuels are available in Appendix A and Appendix B.

Generally, there are two primary advantages of using alternative jet fuels: environmental security and supply security. While environmental security fuels reduce the emissions problem, supply security types offer a continuous supply in the future. The industry and the public more frequently hear the broad concept of alternative jet fuel. However, the name alternative jet fuel is not always used. Different organizations and entities have bestowed it with different names for various purposes. Sustainable aviation fuel (SAF), bio-jet fuel, FT fuel, and synthetic jet fuel all belong to the category of alternative jet fuels. The difference between them includes feedstock, production process, and manufacturer, which will be discussed in detail later in this section. Governments sometimes prefer sustainable aviation fuel (SAF) to emphasis the benefits of its fuel security and feedstock sustainability. A drop-in fuel is commonly of interest in the industry since it can be used directly in existing gas turbine engines. Other names, such as environmentally friendly jet fuel or renewable jet fuel, have also been used. Again, the general term alternative jet fuels will refer to all drop-in alternative jet fuels in this thesis.

As discussed in the previous section, it is imperative to develop alternative aviation fuels since they will produce less particulate matter (PM) and gaseous emissions due to their

cleaner fuel formula. In general, the large proportion of aromatics content in conventional jet fuel results in high PM emissions, and most alternative jet fuels have extremely low aromatic or are even aromatic-free due to their feedstock and production pathway. However, aromatics in jet fuel also enhance the sealing performance of an aircraft's fuel system. Therefore, removing all aromatic content from the fuel formula is impractical for actual usage in a gas turbine engine.

The solution to the current sealing problem in the industry is to blend alternative jet fuels with conventional jet fuel. New feedstocks and production pathways have proved the possibility of mass production for aromatic-free alternative fuels. By blending alternative fuels with conventional fuels, enough aromatics remain to provide the required sealing capability, and the emissions could also be reduced. Jet fuel blends produced through the alternative jet fuels pathway, or alternative jet fuels-SPK, must be approved by ASTM D7566 as part of Annex A5 [42]. The exact blend formula varies depending on the alternative jet fuel types, but it is generally a 50/50 ratio.

The feasibility of using these fuel blends has been tested in some actual flights. Figure 1. 6 shows some important practical flight tests using alternative jet fuels since 2006.

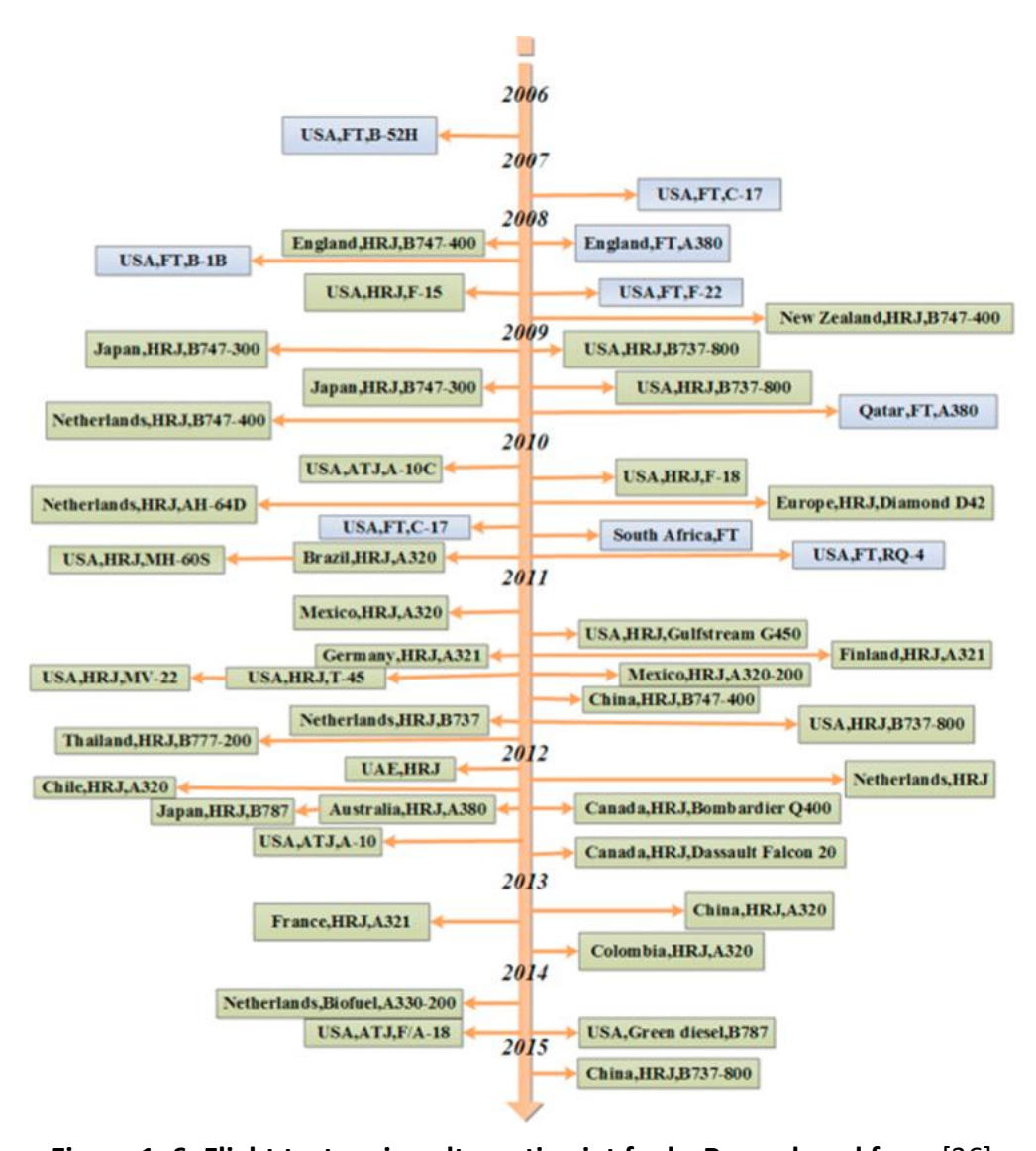


Figure 1. 6: Flight tests using alternative jet fuels. Reproduced from [36]

These flight tests include various alternative jet fuels product types, aircraft types and organizations. All these airline tests have been successfully finished which confirmed some feasibility of using alternative jet fuels in actual flight and proved the ability to promote the usage of alternative jet fuels in the commercial market further. While many studies report the benefits on PM reduction using alternative jet fuels [43], it is still important to further understand of emissions caused by these alternative jet fuels blends.

### 1.4.1 Composition of Conventional Jet Fuel

Conventional jet fuel is designed for modern aviation gas turbine engines. It differs from piston-powered engine fuel (avgas) as it has higher flash points, resulting in a safer operation and transportation environment. Up to now, the major types of jet fuel used in the world are Jet A and Jet A-1. The United States uses Jet A and Jet A-1 is used worldwide. Most components in conventional jet fuel are paraffin; other trace components and additives exist in conventional jet fuel to meet usage requirement. In general, conventional jet fuel usually has an extremely complex fuel formula. A gas chromatograph of jet fuel composition is presented in Figure 1. 7, which shows the complexity of fuel components in typical conventional jet fuel.

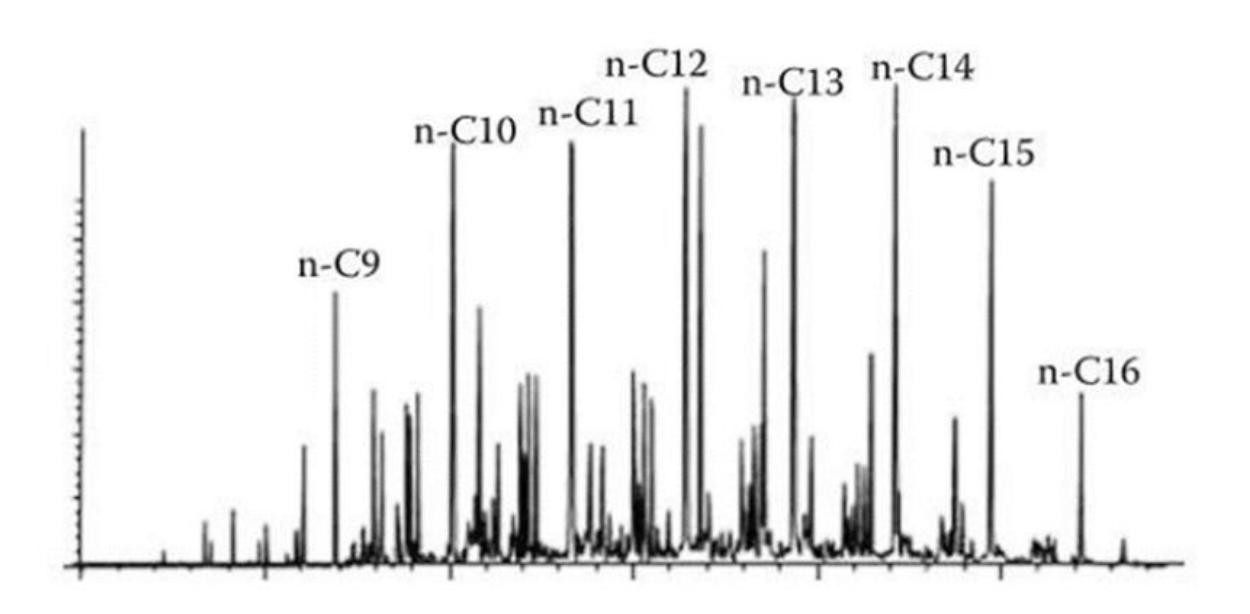


Figure 1. 7: Gas chromatograph of the composition of jet fuel (Jet-A/JP-5/JP-8). Reproduced from [16]

Long-chain hydrocarbons are not the only components comprising current in-service aviation jet fuels, but rather hundreds of different species that collectively meet aviation fuel requirements. Typically, three main key components exist in conventional aviation jet fuels: paraffin, naphthene, and aromatics.

The general formula of paraffin is  $C_nH_{2n+2}$ . According to the molecular structure, paraffin can be divided into three types: normal paraffin, isoparaffins, and cycloparaffins. The simplest form of paraffin is methane, and approximately 60% of the total content in jet fuel is paraffin.

Naphthene, or cycloparaffins, differs from normal paraffin in molecular structure, where carbon atoms in naphthene form a ring structure rather than a long chain structure. For naphthene, the general formula is written as C<sub>n</sub>H<sub>2n</sub>. Compared with normal paraffin, the concentration of naphthene typically 25-35%, in conventional jet fuel but is still considered one of the major components of jet fuel [26].

The chemical formula of olefin is  $C_nH_{2n}$ . Similar to other hydrocarbon compounds, olefins are constituted by only hydrogen and carbon, while at least one pair of carbon atoms are connected in the form of a double bond. Olefins are a unsaturated compound with high chemical activity and react readily with other fuel components [16]. The product of these reactions is a gum-like substance. As olefin is an undesirable compound in fuel, the total amount is small.

The formula for aromatic compounds could be written as C<sub>n</sub>H<sub>2n-6</sub>, and the simplest aromatic is benzene. Aromatics generally contain at least one six-carbon benzene ring with three double carbon bonds". However, the double bond in aromatics is different from the traditional concept. A double bond in aromatics is usually shorter than a single bond due to the extra overlap of Pi orbitals, which shortens the distance between two atoms. The bond length of a typical carbon-carbon double bond and single bond is 0.134nm and 0.154nm, respectively. However, in the case of aromatics, all bonds have the same bond length, which is 0.142nm, because these bonds are neither a signal nor a double bond but delocalized electrons over the ring. As mentioned, aromatics are considered the primary cause of PM production [44], [45], [46], [47], [48], [49], [50].

Since various types of aromatic compounds exist in jet fuel, and due to their different structures, functional groups and physical properties, the PM production behaviour will show significant differences. In addition, having aromatics in the fuel formula still has some advantages in the aircraft fuel system. The most significant advantage of fuel aromatics compounds is that they cause swelling behaviour on engine seals, improving the sealing capability in the fuel system.

## 1.4.2 Composition of alternative jet fuels

Compared with conventional jet fuel, alternative jet fuels usually have a shorter list of fuel composition species. Especially for the aromatic group, most alternative jet fuels contain only extremely low aromatic species or even free of aromatic. It should be noted that due to the production pathway, different alternative jet fuels or manufacturers will have various fuel formulas. Some alternative jet fuels have been post-processed to meet jet fuel requirement by altering their composition. However, in general, the majority of alternative jet fuels are composed of paraffin. The relatively clean structure of the fuel formula gives alternative jet fuels advantage of low emissions output, especially for soot.

## 1.5 Emissions reduction methods

Achieving the purpose of emission reduction within the current aviation propulsion framework is relatively straightforward. In theory, the modification will occur either in the gas turbine engine or jet fuel aspect, representing two primary approaches to improve incomplete combustion and combustion temperature. General emissions control techniques in engine thrust conditions are shown in Table 1. 1.

Table 1. 1: Emissions control based on the engine operation condition [8], [16], [26].

|                | Causes                     | Effects                         | Pollution                | Solution                                    |
|----------------|----------------------------|---------------------------------|--------------------------|---|
| Low<br>Thrust  | Low<br>temperature,<br>FAR | Poor combustion<br>Stability    | Carbon<br>Monoxide       | Increase residence time.                    |
|                |                            | Poor fuel atomization and       | Unburned<br>Hydrocarbons | Reduce flow velocity.                       |
|                |                            | distribution                    |                          | Improve fuel mixing.                        |
|                |                            |                                 |                          | Increase fuel atomization and distribution. |
| High<br>Thrust | High<br>temperature,       | Excess residence time           | Oxides of<br>Nitrogen    | Reduce residence time.                      |
|                | FAR                        | High flame<br>temperature       | Smoke                    | Introduce dilution flow.                    |
|                |                            | poor local fuel<br>distribution |                          | Reduce equivalent ratio to 0.5-0.7          |
|                |                            |                                 |                          | Improve local fuel distribution.            |

According to Table 1. 1, it is clear that although the emission problem varies in different conditions for of a gas turbine engine, by changing some combustor parameters, it is possible to reduce the emissions as desired. In addition, injector configurations could also significantly affect emissions. The modern injector commonly used airblast injector to provide much better fuel atomisation which promote the complete combustion and hence reduce soot.

Figure 1. 8 also presents the correlation between combustion temperature and AFR. It indicates that manipulating the primary zone temperature and AFR in the combustor could achieve the goal of gaseous emission reduction. This manipulation of combustion conditions requires redesigning the combustor components, such as the geometry and fuel spray pattern.

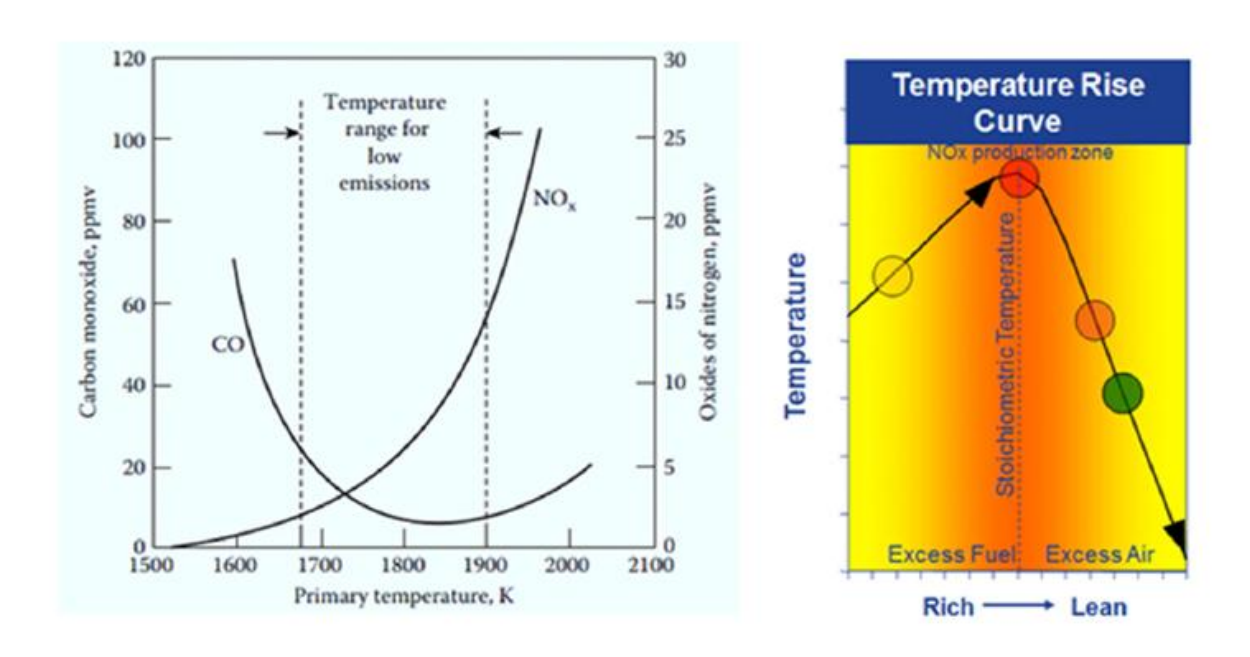


Figure 1. 8: Emissions Production due to temperature and AFR. Reproduced from [16], [51]

In terms of combustor modification, several novel combustor designs have been developed in the last few decades, such as Rich-burn Quick-quench Lean-burn Combustor (RQL) [29], [51], [52], [53], Double Annular Combustor (DAC) [54], [55], [56], and Variable Geometry Combustor (VGC) [57], [58], [59]. Among these relativity innovative combustor designs, the RQL technique is worth mentioning in this section since it is already in service in commercial aircraft, and many fuel tests were initially based on it.

The concept of RQL was first introduced to reduce Nox emissions by Mosier et al. [60] in 1980. Early development of RQL was based on the conventional combustor by adjusting stoichiometry distribution [61]. However, without modification to the physical geometry of the combustor, it is extremely difficult to constrain flow behaviour. This leads to some aggressive change in combustor appearance in the later design such as the RQL designed by GE [62] in 1998. Experimental-scale RQL systems have also been developed for research purposes, such as the one developed by Makida et al. [63], which is also used as a fundamental model for some more recent RQL design [64]. The

design of Makida et al. [63] is based on a conventional can-type combustor with modified air distribution to achieve RQL concept, which is challenging. It also reported that some initial design arrangements failed to show RQL feature, which might be due to unexpected flow changes.

In general, these novel combustor design technologies mainly focus on rearranging the air-fuel ratio and maximum flame temperature during combustion to avoid high emissions, as shown in Figure 1. 8. The attempt to implement emissions reduction measures through engine design modification has been successful. Compared with the original gas turbine engine, modern models have significantly reduced emissions without affecting engine performance.

As mentioned, two factors affect emissions production: combustion conditions and fuel formula. Therefore, changing the fuel formula could also reduce emissions, in addition to redesigning the combustor. Using alternative jet fuels could achieve the goal of low emissions since the composition of alternative jet fuels is relatively simple compared to conventional jet fuel. Recently, alternative jet fuels have been widely developed, and unlike conventional kerosene fuel, alternative jet fuels have various feedstocks ranging from waste oil to energy crops [65]. Alternative jet fuels are mainly introduced due to emission reduction and fuel security concerns in conventional jet fuel markets. Due to the nature of alternative jet fuel compositions (lack of aromatic compounds and sulphur), soot, PM and polycyclic aromatic hydrocarbon (PAH), could be diminished significantly [66].

# 1.6 Research question

The main objective of the thesis is to advance understanding in the design of future fuel formulations and fuel system for a gas turbine engine for emission reduction purposes.

To meet this aim, the following objectives need to be achieved:

- An understanding of fuel composition and corresponding impact on emissions. A
  wide range of aromatic species and their respective impacts on PM and gaseous
  emissions were tested using a realistic aviation combustor (a Rolls-Royce Tay
  combustor in LCCC, Sheffield).
- A comparison and discussion of PM and gaseous emissions from different aromatic species was performed. Important properties of aromatic species, such as molecular structure and density, were also be included in the discussion.
- Kinetic models that can represent the Tay combustor were constructed for further investigation of both soot formation and tracer selection. A further understanding of soot formation pathways and suitable tracers were informed by experimental results.
- An experimental platform to test various O-ring materials and jet fuels was
  established. More practical testing conditions were adopted for this new test rig. A
  fuel-switching test was conducted using this rig. A comparison of different O-ring
  materials and their sealing performance under various operating conditions were
  discussed to select suitable materials in the fuel system.

## 1.7 Thesis Structure

The thesis structure consists of seven chapters: an introduction, a literature review, a methodology chapter, three results chapters and a conclusion chapter. The results chapters contain two experimental studies and one simulation studies. The main topic of each chapter is presented below.

Chapter 1 is an introduction which provides a brief background of the thesis.

Chapter 2 is the literature review chapter, which provides an overview of previous research on emissions and seal compatibility. Corresponding methodology, contributions and drawbacks will also be discussed.

Chapter 3 is the methodology chapter. It discusses the experimental method, instructions, and procedure. Strategies for constructing a 1-D kinetic model are also discussed here.

Chapter 4 is the result chapter of the emissions champaign for various aromatic species. The impact of different aromatic species on emissions, especially PM is examined. The key properties such as molecular structure and density were analysed for their emission impacts.

Chapter 5 is the modelling chapter using CHEMKIN-Pro. Both 0-D and 1-D models were created based on a model Tay combustor. The Performance of each model is discussed, and potential soot tracers are identified with the guidance from experimental results

Chapter 6 is the result chapter of sealing campaign where different types of O-rings were evaluated at various temperatures with constant compression under a new experimental configuration. Complex fuel switching process was also performed. The performance of each O-ring was evaluated and discussed at the end.

Chapter 7 is the conclusion. It summarises all the works in this thesis. Achievements and drawbacks will be briefly discussed with some recommendation of future work.

# 2. Literature review

This chapter will present an overview background on the thesis topic. It will also highlight previous theories, research and investigations. In general, the chapter will focus on the following topics:

- Jet fuel emissions. With an examination of some essential previous studies regarding emissions.
- Past investigations on combustor modelling
- The compatibility between alternative jet fuels and elastomers, including relevant studies.

## 2.1 Previous research on emissions.

With the awareness of potential environmental damage caused by burning jet fuels, several experiments have been conducted in the past decades. Significant effort has been spent identifying the key factors affecting emissions, such as aromatics. Many of these emission studies have been done on laboratory test rigs or gas turbine engines. Moreover, due to the concern about the shortage of feedstock of gasoline-based jet fuel and its environmental impact, alternative jet fuels must be tested for their emissions production before they can replace conventional jet fuel in the near future. Briefly, emissions and engine capability tests of alternative jet fuels have been conducted by various organisations, including a wide range of engine types [67].

PM emissions for conventional fuel have been widely investigated on a lab scale and in actual in-service engines [68]. Compared to lab-scale testing, the actual engine seems more practical. In 2005, a Rolls-Royce Allison T56-A-15 turboprop engine in a C-130H aircraft was used to investigate the impact of engine power on emissions [69]. This experiment uses the emission index (EI) to represent pollutant intensity, which is typically expressed as the mass of pollutant generated per kilogram of fuel consumed.

The results show that EI of soot is 40%-50% higher in idle conditions, which suggests that soot production is inversely related to the engine power, and increased engine power could burn fuel more effectively and reduce soot emissions. FT fuel also showed a noticeable soot reduction in all engine conditions. For gaseous emissions, NOx increases with increasing FAR, while CO decreases with higher FAR. Notably, CO emissions decrease dramatically from low-speed idle to high-speed idle conditions. For CO<sub>2</sub> emissions, the trend is not linear with increasing engine power.

This work established an excellent framework for emission measurement. It also provided a preliminary indication that, in addition to engine operation conditions, fuel composition significantly affects emissions production. However, this experiment was limited in scope. Only FT fuel was tested, and the impact of fuel composition on emissions was not thoroughly investigated.

NASA performed a more complex study of emissions, including one of the most noticeable tests in California in 2004 [70]. The test platform was a DC-8 aircraft with CFM-56-2C1 engines. The CFM-56-2 is a high-bypass turbine engine with an overall compression ratio of 23.5. The primary objective of this test is to examine the impact of aromatic and sulphur content on PM emissions.

According to test results, there is a significant difference in EI measured at 1m and 30m away from the exhaust. The EI at in 30m is 5 to 30 times greater than at 1m. Additionally, particle size distribution showed a peak at <12nm, indicating freshly nucleated aerosols. Therefore, the project suggests that particles collected at 1m distance are non-volatile PM (NVP).

It should be point out that fuel composition was also taken into consideration in this test. Three jet fuel blends were selected: JP8, high sulphur fuel and high aromatic fuel. Interestingly, results showed similar NVP production across all engine power settings for all test fuels, implying that NVP might not be affected by fuel formula, which is different to other research showing that fuel composition, especially aromatic content, have a significant impact on NVP formation [16], [41], [71], [72], [73].

In 2009 [72], NASA conducted an experiment project named Alternative Aviation Fuel Experiment (AAFEX). The experimental setup was similar to the previous APEX study [70], using an in-service CFM-56 engine. Two alternative jet fuels (Fischer-Tropsch products from natural gas and coal) were tested alongside JP-8. Exhaust sampling occurred at 1 m and 30 m from the engine, with thrust varied from 4% to 100%. One engine used JP-8 as baseline, while the other tested five fuel blends: 100% JP-8, 100% FT-1 (GTL), 100% FT-2(CTL), 50/50 FT-1 with JP8 and 50/50 FT-2 with JP-8. Selected AAFEX emission results are shown in Figure 2. 1 and Figure 2.2.

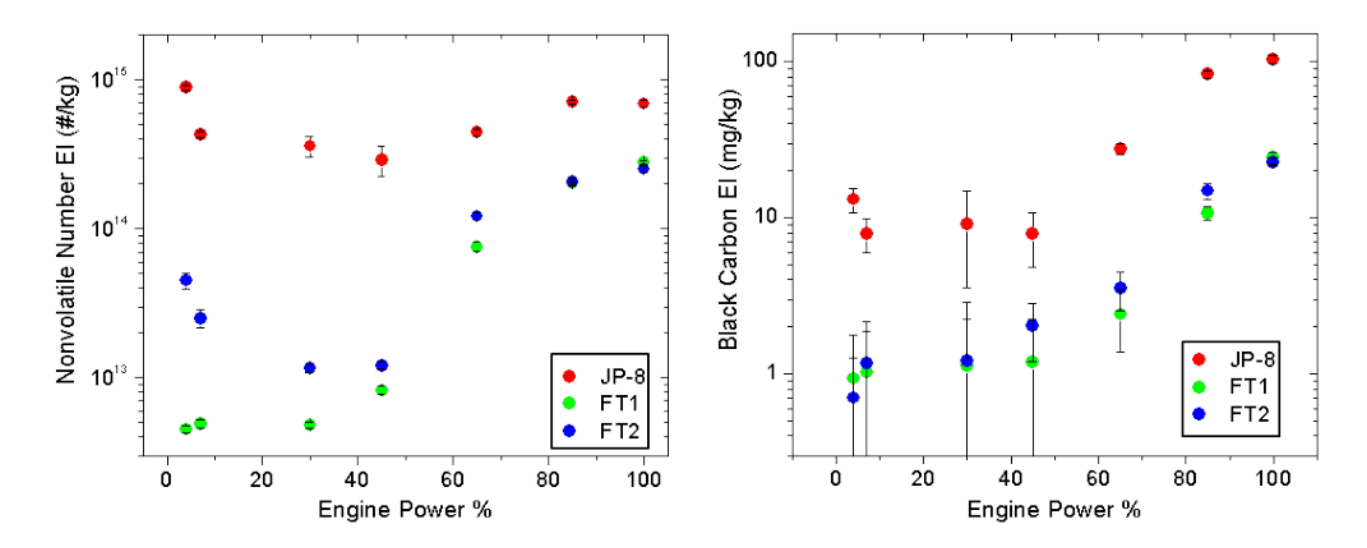


Figure 2. 1: Nonvolatile particle number (left) and black carbon mass (right) emission indices as functions of per cent maximum thrust for the starboard engine as it burned each of the indicated fuels. Reproduced from [72].

Figure 2. 1 indicates that burning alternative jet fuels have significantly reduced NVP emissions, especially for El<sub>n</sub> and El<sub>BC</sub> of FT-1, which are lower than the baseline JP-8 by factors of 200 and 20, respectively, at low power conditions. In the case of FT-2, El<sub>n</sub> and El<sub>BC</sub> show reduce factor of 35 and 20 compared with JP8.

Chemically, these results demonstrate that NVP emissions (both number and mass) are proportional to aromatic content and vary inversely with hydrogen content. Additionally, FT fuel produces smaller diameter PM emissions than conventional fuels.

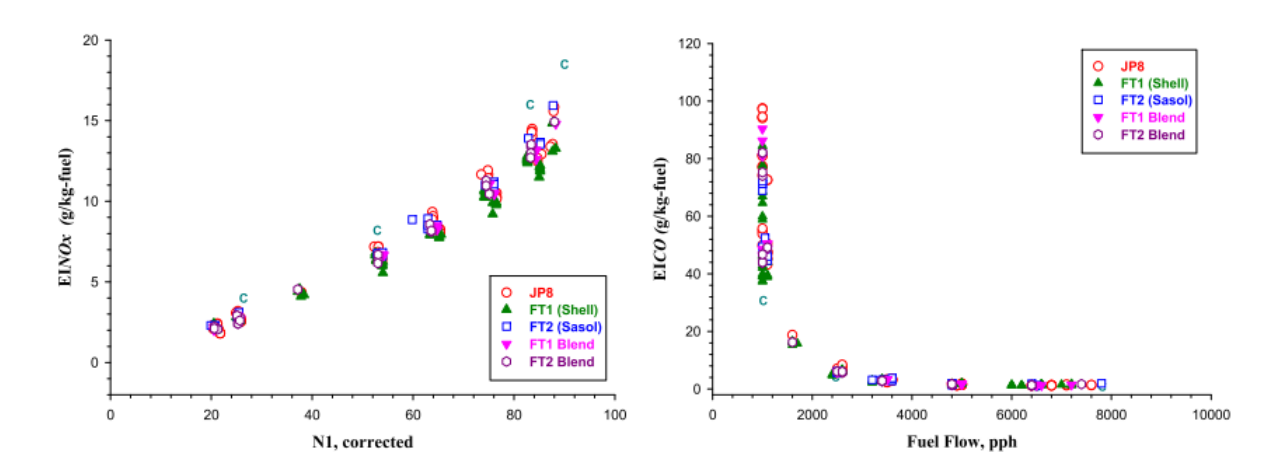


Figure 2.2: NOx emission index plotted versus corrected N1(right) and CO emission index plotted versus corrected fuel flow rate (left). The "C" points correspond to ICAO certification values for the CFM56-2C engine. Reproduced from[72].

This project specifically reported an approximately 10% reduction in NOx and CO at full power and idle engine conditions, respectively, when using FT fuel [72].

Compared to the experiment discussed previously, this research tested more alternative jet fuels with different feedstocks. Both PM and gaseous emissions were significantly reduced when using alternative jet fuels. The result also indicated that blending alternative jet fuels with conventional jet fuel can dramatically reduce PM emissions without compromising engine performance. Moreover, emission of NOx, CO and CO<sub>2</sub> show little dependence on fuels type. Furthermore, UHC and CO strongly correlate with engine combustion conditions, especially the ambition temperature, resulting in different inlet temperatures.

The main drawback of this study is that only FT-based fuels were tested, excluding other alternative fuel types. Since different alternative jet fuels have varying fuel compositions due to different production pathways, the emission results could vary significantly. Additionally, the study treated fuels as homogeneous mixtures without analysing individual components' effects on PM emissions.

Soot production from FT fuel was also reported by Timko et al. [74]. The study examined the emissions performance of FT fuel (GTL) using a PW308 aircraft engine at power settings from 7% to 85%. Comparing JP-8 and FT fuel (which was nearly aromatic and sulphur-free). Samples taken at 1m and 50m downstream showed significantly lower soot production from pure FT fuel versus the 50/50 blend. Additionally, FT fuel produced smaller, more spherical particles than JP-8.

The drawback of this test was similar to other projects presented above. First, only FT fuels were tested. Second, detailed fuel composition (including aromatic species) was not considered for soot emission analysis.

Using alternative jet fuels could significantly reduce PM emissions including non-volatile (NVP) and volatile particulates (VP), as demonstrated in NASA's Alternative Aviation Fuels Experiment Project (AAFEX II) [73]. Beyond FT fuels, Hydrotreated Renewable Jet (HRJ) showed significant PM reduction versus JP-8 baseline. In addition, the project found that fuel with less sulphur could reduce aerosol formation in the exhaust plume. AAFEX II results also indicated a slight reduction in NOx emissions when using FT fuel compared with JP8 [73]. Moreover, this project suggested that in ideal conditions, HC and CO emissions are more sensitive to temperature rather than fuel type.

In the AAFEX II study, more types of alternative jet fuels were investigated, and aromatics were identified as the primary cause of soot emissions. However, aromatics are a group of compounds with many different species, and different aromatic species affect soot emissions differently. While the impact of different aromatic species on gaseous emissions remains understudied, different fuel formulations affect combustion conditions such as temperature and residence time, and these variations may influence gaseous emissions differently. For example, NOx formation depends on combustion temperature, which varies with fuel composition.

Harper [64] conducted a series of emission tests on two RQL type combustor. The first RQL design based on the RQL proposed by Makida et al. [63] discussed earlier, while the second is a modified version with enhanced primary zone cooling. Several alternative jet fuels were examined, showing that NVP correlates with fuel composition and properties, ranked: Hydrogen content > Total aromatics content > Total Paraffins > Cycloparaffin + Monoaromatics. While this experiment providing insights into of other fuel components like cycloparaffin, individual species effects weren't analysed.

Another experiment worth mentioning in this section was conducted by Almohammadi et al [75]. which included a series of emission tests in LCCC, Sheffield. Unlike the experiments presented above, this study used a single-cylinder direct-injection IC engine operating at a constant speed of 1500 rpm and under 5kW load. A wide range of aromatics was selected to assess their impact of emissions, especially soot. Results are shown in Figure 2. 3.

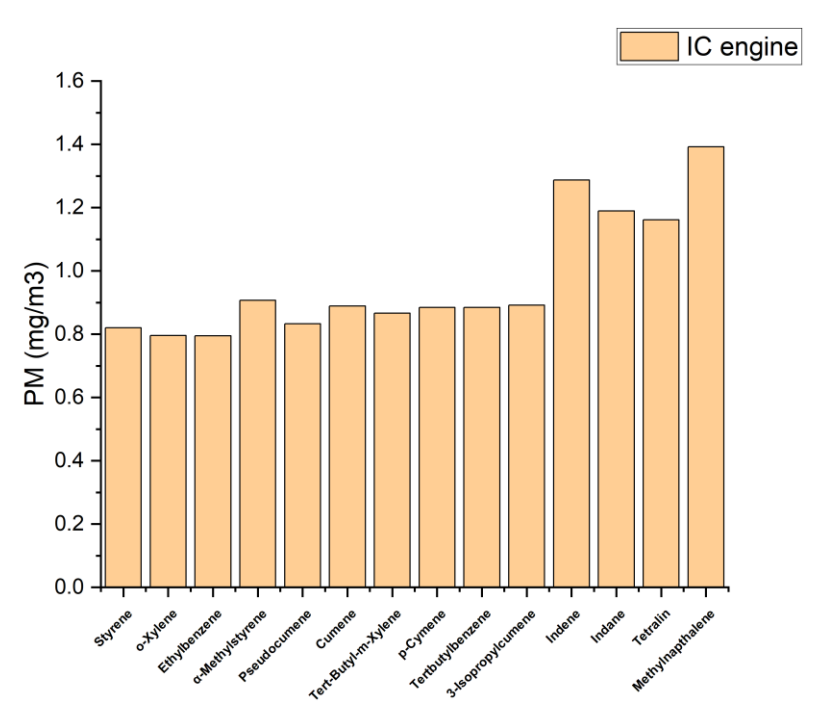


Figure 2. 3: PM results for IC engine. Adapt from [75].

According to Figure 2. 3, diaromatic compounds produces significantly higher PM than monoaromatic, matching founding from gas turbine engines.

This work is relevant because the selected aromatics match those used in this thesis. Moreover, identical sampling and measurement systems were employed. The main difference between Bander's work and the experiment in this thesis lies in the combustor design. This study uses a real gas turbine combustor (Rolls-Royce Tay combustor). Therefore, it is interesting to investigate whether these aromatics affect PM formation differently in gas turbine engines.

# 2.2 Previous research on combustor modelling

Since increasingly stringent emission regulations for gas turbine engines, modification of combustor design and formulation of alternative jet fuels are necessary. Meanwhile, extensive tests must validate the requirements of engine performance, emission reduction and operational safety.

There is no doubt that employing a more realistic experiment setup, such as full-scale combustor testing will reduce the discrepancy between lab data and real-world operation. However, such testing volume may be impractical due to prohibitive time and resources costs. Therefore, developing analytical models to predict combustor performance and emissions, combined with experimental validation, would improve efficiency.

Significant challenges remain in modelling an entire combustor. The major problem is capturing three-dimensional flows with recirculation, which is extremely difficult to simulate in analytical model. One solution involves assuming extremely high turbulence and negligible mixing times relative to chemical kinetics. Based on this hypothesis, kinetic models employ idealized reactors to represent the combustion process. The

complexity of these types of kinetic models ranges from simple 0-D model with only one rector to complex connected reactor groups (CRN). Each model balances accuracy and computational cost differently.

### 2.2.1 Stirred reactor model/0-D model

In general, stirred reactor can be divided into two types, perfect stirred reactor (PSR) and well-stirred reactor (WSR). In 1953, the concept of applying stirred reactors to combustor modelling was first introduced by Longwell et al. [76]. As shown in Figure 2.4, PSR refer to an arbitrary region with unform combustion condition including temperature, mixing and pressure within a fixed volume. Different from PSR, inside a well-stirred reactor, recants are mixed fast but not instantaneously, which involves a mixing delay time.

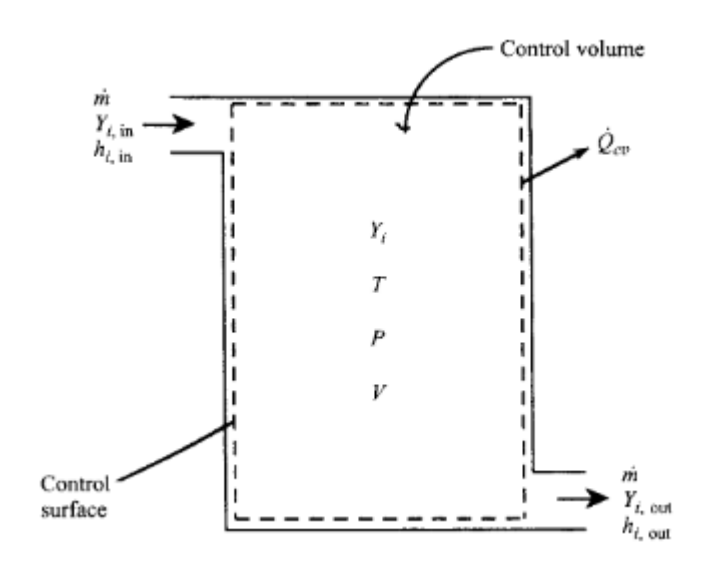


Figure 2.4: Perfectly stirred reactor. Reproduced from [77]

The PSR approach presumes sufficiently high turbulence for negligible mixing times relative to chemical kinetics. Summarizing the entire combustor as a single reactor eliminates flow simulation complexities while focusing more on chemical mechanisms. This constitutes the 0-D model. While computationally efficient, it neglects key aspects

like incomplete mixing and residue flame. The reactor volume and residence time parameter significantly influence simulation accuracy.

### 2.2.2 Chemical reactor network/1-D model

The 0-D model has advantages in combustion simulation, like low computational cost, which is particularly valuable for chemical mechanism development. However, to model a combustor more accurately, especially a secondary zone multiple reactors are needed, leading to a chemical reactor network (CRN). In CRNs, reactors are interconnected, passing flow parameters like velocity and composition between stages.

The recirculation model shown in Figure 2.5 represents an early CRN concept first proposed by Hottel et al. [78].

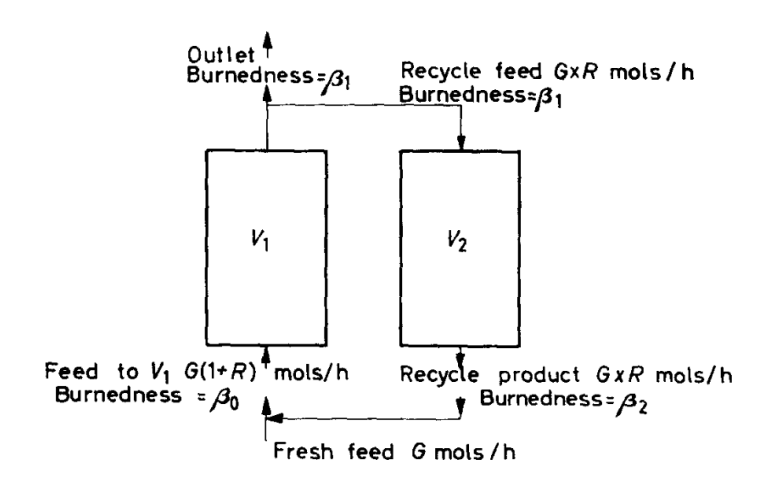


Figure 2.5 Recirculation model. Reproduced from [78]

This model simulates the recirculation behaviour in the combustor, providing a more detailed combustion environment than a single stirred reactor. However, post-flame zones (secondary and dilution) are excluded, potentially omitting critical soot nucleation processes. For complete post-flame modelling, a plug-flow reactor must be incorporated, as shown in Figure 2.6.

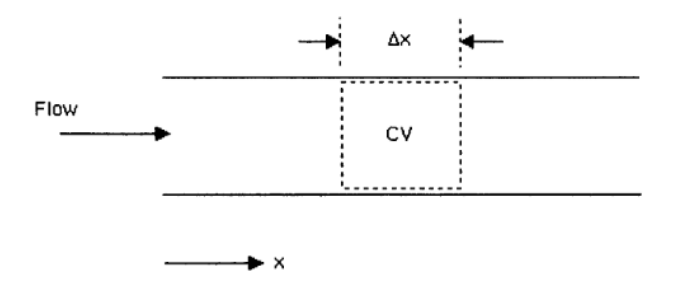


Figure 2.6 Schematic of a plug-flow reactor. Reproduced from[77]

In combustor modelling, plug flow reactors (PFRs) are typically used to simulate secondary and dilution zones when coupled with stirred reactors. Mellor et al. [79] introduced a more complex model for combustor simulation which is an update version on model by Hottel et al. This model considers both recirculation behaviour in the primary zone and post-flame conditions. In this model, the primary zone uses two parallel PSR while a series of PFRs represent the secondary zone and dilution zone. The configuration of model by Mellor et al. is present in Figure 2.7. This layout of model is widely used in other CRN models [80], [81] and it is also one of the reference models in this thesis.

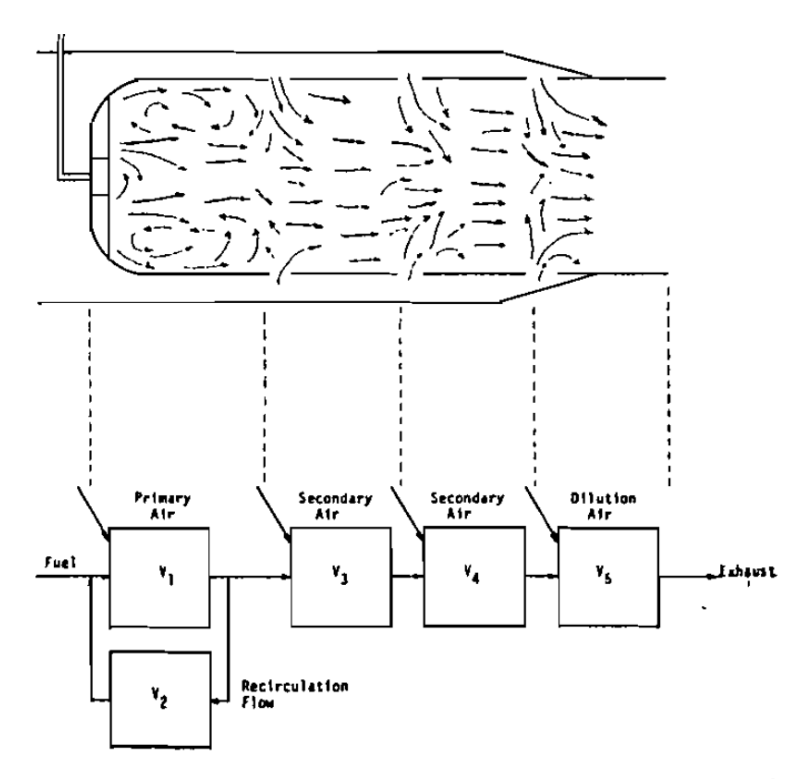


Figure 2.7: Recirculation reactor model. Reproduced from [79]

Besides recirculation models, a notable primary zone modelling approach involves fuel vaporization distribution [82]. In this solution, fuel vaporization distribution in the primary zone assumes a normal distribution function. This assumption has remained a common solution for modelling fuel distribution for quite a long time, and some recent combustor modelling still employ this hypothesis. The drawback is its limitation to initial conditions, ignoring injector-specific droplet patterns.

Allaire [81] proposed a physics-based emissions model using CRN principles. This model incorporates the fuel vaporization distribution hypothesis. It divides the combustor into three parts: primary zone, intermediate zone and dilution zone. The primary zone used 16 parallel PSRs. The intermediate zone employs a PFR, while the dilution zone uses two PFRs. Intermediate zone is model by a PFR, and dilution zone is modelled by two PFRs. See Figure 2.8 for the layout.

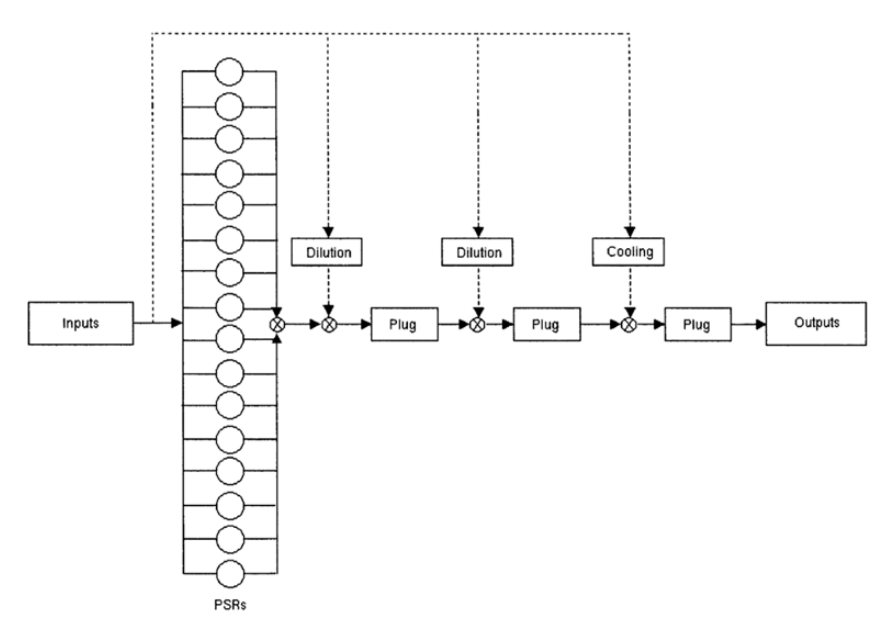


Figure 2.8: Diagram of emission model. Reproduced from[81]

One of the problems in previous studies is the arbitrary selection of reactor residence time. Although this work argues residence time should be determined using 3-D modelling, some CRN models still use abstract values or adopt times from dissimilar combustors[80]. This likely reflects the difficulty to performing full 3-D simulations or the need for CRN flexibility. Still, to build a persuasive CRN model, suitable residence time is necessary. Moreover, most CRN applications focus only on temperature or gaseous emissions, and the investigation did not take further into soot production due to the challenges in soot formation mechanisms and high computational requirements.

#### 2.2.3 Turbulent combustion simulation

With advances in turbulent combustion, whole-combustor simulations have become feasible. These typically 3-D model that provide more detailed information than 1-D or 0-D models. Although 3-D combustion modelling benefits from improved computing power, significant computational costs remain a key drawback versus simpler 1-D approaches.

Two 3-D simulation studies are presented in this section using a model Tay combustor. The same model Tay combustor was select for the CRN model proposed in this thesis; more detail will be provided in Chapter 3. The understanding of these 3-D models will help the construction of 1-D model including resident time and reactor selection. More information about how to use these 3-D simulation results will also be covered in Chapter 3.

Mare et al. [83] applied large eddy simulation (LES) to simulate the combustion process in a model Tay combustor. The heat losses through walls were negligible due to constant pressure and low Mach number. The dimensions selected matched the model Tay combustor. This was the first simulation of the entire combustion process in a model Tay combustor, and the time required to finish the simulation was extremely high and unacceptable for further emission investigation using different fuels. The most valuable information obtained from this study was the detailed flow field simulation, proving crucial for CRN model development. They also observed a small recirculation zone where the flow encountered the dilution air, which might significantly affect soot production.

Zhang[84] took the 3-D combustion simulation of this model Tay combustor further. The primary achievement was significantly reducing computation time by combining stress transport K-omega model (SSTKW) turbulence and the Zimont turbulent flame speed closure (ZTFSC) combustion model. This approach required only 1/164 of the computing time of conventional LES.

One limitation of Zhang's model is that the combustor dimensions were modified to better agree with experimental data. For example, the diameter of the air inlet hole was reduced by 14%. Moreover, like other models, it struggles with cooling air simulation. Since the Tay combustor uses porous Transply walls (with no existing physical flow

model), fixed mass flow rates were assumed at chamber walls, this could affect combustion temperature and emission formation, especially in the primary zone. More details about Transply will be discussed later in the thesis. This work also focused only on temperature/gaseous emissions (using reduced chemistry), omitting PM prediction. In addition, it used only propane rather than realistic aviation fuels

# 2.3 Seal compatibility of alternative jet fuel

With the development of alternative jet fuels, their use offers potential for soot reduction through lower aromatic content. However, significant challenges remain, preventing full replacement with conventional jet fuels. As mentioned, pure alternative jet fuels typically contain low aromatic content, reducing elastomer sealing performance in fuel system and potentially causing leaks. This has led to an 8% minimum aromatic requirement to prevent operational leaks, and most commercialized alternative fuels require blending with conventional fuel before use.

The sealing performance of an elastomer is determined by two factors: elasticity and swelling ability. Swelling ability is primarily affected by the fuel composition. When exposed to fuel, the elastomer's volume expands through swelling, enhancing sealing. Swelling behaviour occurs in both natural and synthetic elastomers. When the elastomer is immersed into the fuel, some fuel content will be absorbed into the elastomer, increasing the elastomer volume. Simultaneously, fuel will extract content from the elastomer and cause the elastomer to shrink. A general swelling phenomenon is shown in Figure 2.9.

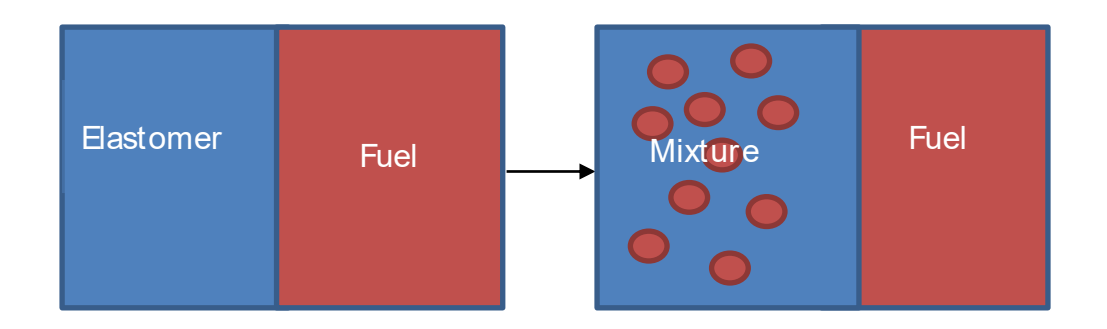


Figure 2.9: Seal Swelling Phenomenon

All fuel components could participate in the swelling process of elastomers, but aromatics are believed to have the major impact on promoting swelling [85]. Other factors affecting fuel and elastomer properties could also affect swelling, which include the strength of interaction, molar volume, structure of fuel component, polarity, and the ability to serve as a hydrogen bond donor. Usually, a large molar volume will inhibit the swelling behaviour. Polarity and the ability to serve as hydrogen bond donors also participate. Due to the lack of ability to form hydrogen bonds, the swelling problem for alternative jet fuels is mainly molar volume and structure dependent.

## 2.3.1 Fuel leaking

As mentioned, aromatic content contributes to PM emissions and seal performance simultaneously. In theory, lack of aromatic content in fuels means reduced emission but declining sealing performance in fuel systems. The potential seal problem caused by using pure alternative jet fuels was not widely recognized until recent years [86]. With more extensive studies on alternative jet fuels tested in actual gas turbine engines, some research has begun to report leakage problem when alternative jet fuels are used. Figure 2.10 shows the fuel leakage problem reported when using neat Hydroprocessed Renewable Jet (HRJ) and Fischer-Tropsch (FT) fuels in AAFEX II project [73].



Figure 2.10: Fuel leaking due to the sealing problem. Reproduced from [73]

The frequency of these fuel leakage problems is expected to become more often since more and more similar alternative fuels test will be conducted in the future. Thus, the key question is whether the leakage problem can be stopped by changing seal materials or introducing additional fuel components, which are a focus of this thesis investigation.

# 2.3.2 Past research on elastomer compatibility

Most research has investigated the impact of fuel content on elastomer swelling behaviour [87], [88], [89]. Among these experiments, Graham et al. [90] conducted the most complex experiment on seal swelling behaviour with a wide range of fuel contents. An optical method was used to detect the volume change of samples during contact with selected fuel blends and fuel contents. The standard experimental setup is shown in Figure 2.11.

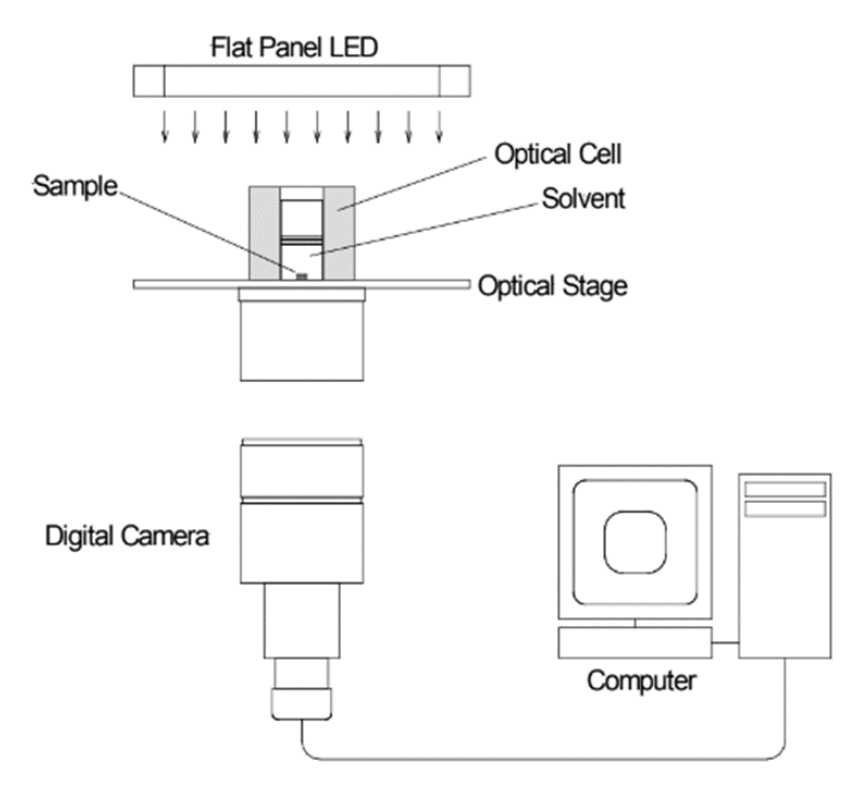


Figure 2.11: Schematic of an optical dilatometer. Reproduced from [90].

This experiment provides a detailed understanding of the impact of swelling behaviour caused by different fuel contents. It indicates that aromatics are indeed the primary cause of swelling in elastomers. Moreover, different aromatics affect the swelling differently. In addition, the impact of cycloparaffins on sealing performance was also investigated; the results indicated that similar to aromatics, cycloparaffins also promote sweal behaviour, which suggests that for future formulations of alternative jet fuels, increasing cycloparaffins content might be an option to solve the leakage problem. This study also shows that after switching fuels from JP-8 to FT, nitrile starts to show a strong reaction, and the volume swelling decreased dramatically, which indicates poor sealing performance.

One of the major drawbacks of this experiment is that O-ring samples are placed on the optical stage freely, but in actual applications significant pressure will be applied to samples. This could significantly affect the O-ring swelling behaviours. Moreover, the entire experiment was conducted under constant temperature conditions, which did not

reflect the actual environment in gas turbine fuel systems. In addition, the impact of switching fuels from conventional jet fuel to alternative jet fuel was not investigated, which is one of the major reasons for fuel leakage while using alternative jet fuel.

Liu [91] presents another experiment called stress-relaxation texting to investigate the seal behaviour of different materials in various fuels. During the experiment, an O-ring sample was placed on a platform that contained a groove. A piston connected by a load cell and data acquisition unit was pressed to just contact the O-ring sample. Then, the O-ring sample was immersed in selected fuels. Any change in O-ring volume was directly measured and recorded by the load cell unit. Different environmental temperatures were also investigated.

Results indicated that using alternative jet fuels such as SPK and HVOs did not significantly affect seal performance for fluorosilicone and fluorocarbon O-rings. However, nitrile is extremely sensitive to alternative jet fuels due to the lack of aromatic content in the fuel. Moreover, different types of alternative jet fuels affect O-rings differently, and fully synthetic jet fuel (FSJF) shows extraordinary capability for maintaining seal performance for O-rings. Furthermore, it also states that temperature significantly influences O-rings' sealing performance, especially for fluorocarbon-type O-rings, which are relatively sensitive to low temperatures due to their high glass transition temperature.

The advantage of Liu's work is that it provides a more practical and direct view of swelling behaviour compared to Graham's work, since force is recorded instead of volume change. Moreover, temperature impact was also considered in this experiment. However, this experiment also did not consider the actual service environment such as high pressure. In addition, Liu further suggested that a fuel-switching experiment

between conventional fuel and alternative jet fuels could be conducted in the future to investigate the interaction between fuels and O-rings in more detail.

# 2.4 Overall summary

An overall review of past research related to the topic of this thesis is presented in this chapter. In this section, a summary and corresponding unanswered question will be presented below:

- A lot of work has been done on emissions from conventional fuels and alternative jet fuels. The results indicate that alternative jet fuels are valuable in emissions reduction, especially for PM. However, very few alternative jet fuels were tested, which resulted in a lack of understanding of the relationship between fuel content and emissions. Especially for aromatics, some investigations indicated that certain aromatic groups would produce noticeably more soot compared to others. Still, a wide range of aromatics should be tested regarding their emission impacts, which will certainly benefit the design of future fuel formulations.
- Kinetic models have been used to simulate a combustor for decades. A general review of these models was discussed, from simple 0-D models to more complex 1-D models. However, most models are only used to predict gaseous emissions, and soot prediction seems rarely incorporated in these models. Moreover, the model Tay combustor used to represent an actual one has not yet had a corresponding CRN model in emission prediction. Some 3-D simulation studies on this model Tay combustor have been discussed in this chapter, and the knowledge gained through these complex and time-intensive models will be used to construct a simple, cost-effective CRN model in this thesis.

• Works on the compatibility of O-ring seals with different materials in various fuels were also comprehensively presented and discussed in this chapter. Although these investigations indicate that different fuel contents could have significantly different impacts on different seal materials, the real seals' operation environment was not completely taken into consideration. A test platform using more practical test conditions seems necessary to be developed to fill these gaps.

# 3. Methodology

This chapter will discuss the detailed experimental configuration used in the emissions campaign. The experimental work presented in this thesis were carried out at the LCCC (Low Carbon Combustion Centre) at the University of Sheffield. In general, two experimental sections were included. The first section involved a series of emission tests for selected aromatic fuel blends. One actual Tay engine combustor can was used to perform this emissions campaign. The second experimental section was a stress relaxation test for different fuels and seal materials used in gas turbine fuel systems.

The methodology for numerical simulation using Ansys Chemkin-Pro will be presented. Key settings will also be discussed, including reactant selection, residence time, and reaction temperature used in the model. Since the actual Tay combustor used in the experiment was lost during the flood, the reference for the simulation work is a model Tay combustor built in 1988[92]. More details about this Tay model combustor will be described later in this section.

Finally, the consequences and remediation measures of the impact on both experimental and simulation work caused by the flood will be elaborated.

# 3.1 Experimental configuration of emissions test

In this section, the fuel blend strategy will be explained in detail. Fuel blends consist of base fuel and aromatic candidates. They will be divided into two groups according to the aromatic concentration. Candidate aromatics were selected carefully based on previous experiments and chemical composition in standard jet fuels. Moreover, details of the experimental setup will also be illustrated, including instrument selection and

operating principles. This section will also provide an overlook configuration of the entire experiment.

#### 3.1.1 Fuel blends

In total, 15 aromatic species shown in Table 3.1 are selected to investigate their impact on emissions, including PM/soot and gaseous emissions. These aromatics are chosen carefully according to their structure, cost, and presence in conventional jet fuel such as jet A-1. The detailed critical properties of the aromatics are also presented. Pure aromatics should be used in experiments to gain the best sensitivity results. However, considering the cost-efficiency, all aromatics are blended with a solvent (NP1014) to form two blend categories (8% vol. and 18% vol.).

Table 3.1: List of candidate aromatics

|               | Chemical Molecular              |        | н/с   | Density (kg/m³) |  |
|---------------|---------------------------------|--------|-------|-----------------|--|
| Aromatic Name | Structure                       | Weight |       |                 |  |
| Toluene       | CH₃                             | 92.14  | 1.143 | 865             |  |
| Styrene       |                                 | 104.15 | 1     | 906             |  |
| o-Xylene      | CH <sub>3</sub> CH <sub>3</sub> | 106.16 | 1.25  | 879             |  |
| Ethylbenzene  |                                 | 106.16 | 1.25  | 867             |  |

| Indene                |                                    | 116.16 | 0.889 | 996  |
|-----------------------|------------------------------------|--------|-------|------|
| Indane                |                                    | 118.18 | 1.111 | 965  |
| α-Methylstyrene       | CH <sub>3</sub>                    | 118.18 | 1.111 | 909  |
| Pseudocumene          | H <sub>3</sub> C CH <sub>3</sub>   | 120.19 | 1.333 | 876  |
| Cumene                | CH <sub>3</sub>                    | 120.19 | 1.333 | 864  |
| Tetralin              |                                    | 132.2  | 1.2   | 973  |
| p-cymene              | CH <sub>3</sub><br>CH <sub>3</sub> | 134.22 | 1.4   | 860  |
| Tertbutylbenzene      | CH <sub>3</sub><br>CH <sub>3</sub> | 134.22 | 1.4   | 867  |
| Methylnaphthale<br>ne | CH <sub>3</sub>                    | 142.2  | 0.909 | 1001 |

| Tert-Butyl-m-<br>Xylene | H <sub>3</sub> C CH <sub>3</sub> H <sub>3</sub> C CH <sub>3</sub> | 162.27 | 1.5 | 867 |
|-------------------------|---|--------|-----|-----|
| 3-<br>Isopropylcumene   | H <sub>3</sub> C CH <sub>3</sub> CH <sub>3</sub> CH <sub>3</sub>  | 162.27 | 1.5 | 856 |

Banner NP1014 is the base fuel used to blend with aromatic candidates to form test fuels in this testing campaign. It is a commercial solvent-type product manufactured by Banner Chemicals Group UK. The official applications listed by the company is lamp oil and fuel additives. According to the information provided by the manufacturer, NP1014 contains 99% straight long-chain hydrocarbon, including C9, C10, C11, C12 and C14 by volume, and the remaining 1% consists of hydrocarbons with molecule sizes larger than C14. The impurities in NP1014, also according to the statement by the manufacturer, are less than 1% by volume. This solvent is the ideal base fuel for this testing campaign since the fuel formulation is close to existing aromatic-free alternative jet fuels. Some basic properties of Banner NP1014 solvent are shown in Table 3.2.

**Table 3.2: Properties of Banner NP1014** 

| Density (15℃)    | 751 kg/m3 |
|------------------|-----------|
| Aromatic content | 0.15% wt. |

Fuel properties, such as density and aromatic content, are one of the easiest methods to judge jet fuel quality in combustion. Most existing commercial fuel standards, such as the UK DEF STAN 91 and the US ASTM D1655, require specific fuel properties for desired engine performance and emissions. The correlation between fuel properties and emissions has been widely investigated. For example, PM emissions are closely related to combustion performance and hydrogen content. NOx emissions are proportional to the combustion temperature in the engine. Hence, it is possible to predict the emissions roughly by examining key fuel properties. This testing campaign will examine critical fuel properties, including density, H/C ratio, and molecular weight, and their impact on emissions.

### **3.1.2** Tay rig

All emission tests in this thesis were conducted in the Tay rig located in LCCC at the University of Sheffield. This rig was upgraded and modified from an existing test platform, and the reliability has been proven by previous test campaigns [41], [93]. Figure 3.1 shows the overall rig setup.

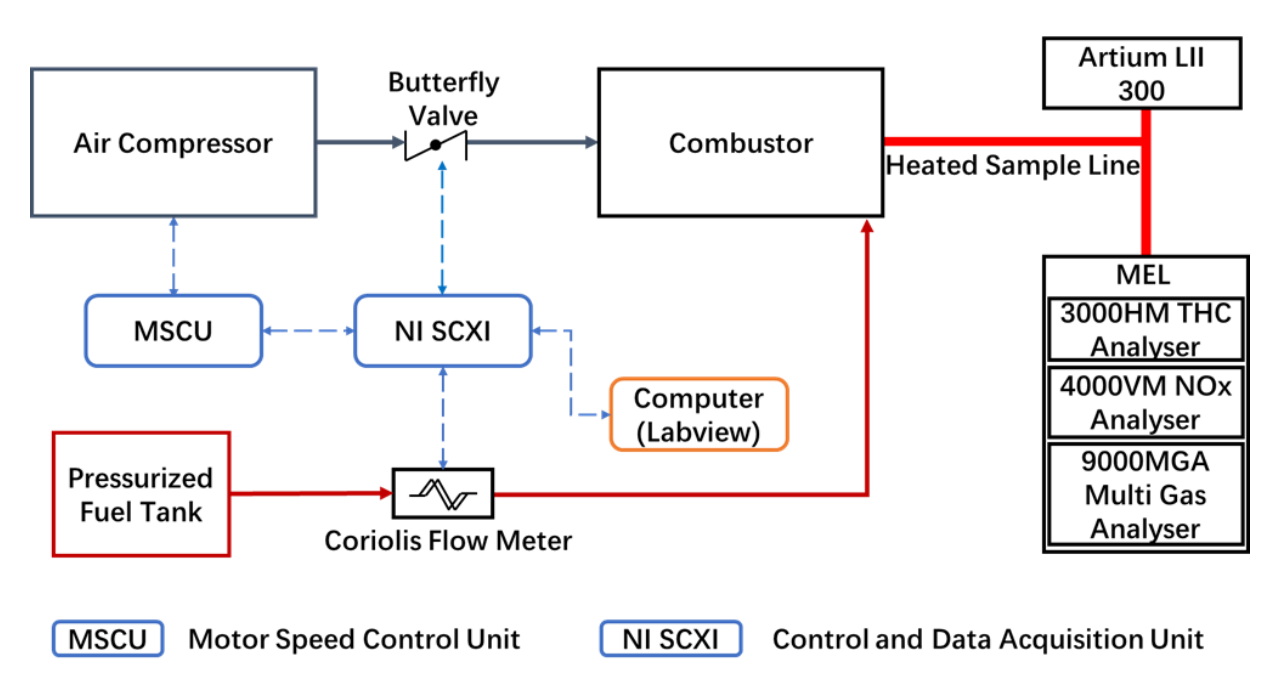


Figure 3.1: Tay rig setup

The main components of the Tay rig could be divided into three units: the combustion unit, the emission sampling unit and the control unit. Air was sent to the combustor by an atmosphere-pressure compressor and a computer controlled the speed of the compressor motor, maintaining the uncertainty of the measured air flow rate within ±2%. The fuel feed system includes a pressure vessel, flow control valves and an air-assisted fuel injector. The fuel vessel was pressurized by nitrogen to provide smooth fuel flow, and a series of computer-controlled air-actuated valves controlled the fuel flow rate. The exhaust was sampled by a non-reactive stainless-steel probe. The probe maintained the sample temperature at no less than 150 °C to avoid water vapour condensation. A 6-meter-long heated sample line was used to transport the exhaust sample to the Mobile Emissions Laboratory. Inside the MEL a group of external emission measurement instruments were deployed for emission analysis.

The operating parameters were fixed and presented in Table 3.3. Air-assistance pressure for fuel injection was set at 1 bar to produce poor atomization and enhance the PM emissions.

Table 3.3: Test conditions

| Condition | Fuel Pressure | Air-assistance<br>Pressure | Air-mass<br>flow g/s | Fuel flow<br>rate g/s | wCalculated<br>AFR |
|-----------|---------------|----------------------------|----------------------|-----------------------|--------------------|
| 1         | 300 kPa       | 1 bar                      | 130                  | 0.5                   | 260                |
| 2         | 300 kPa       | 1 bar                      | 200                  | 1.7                   | 117.64             |
| 3         | 300 kPa       | 1 bar                      | 60                   | 0.5                   | 120                |

It should be note that Condition 1 and Condition 3 were used for rig initiation and other purposes such as equipment diagnostics. Only Condition 2 was successful in getting sufficient PM readings and used in this thesis.

### 3.1.3 Tay Combustor

The Combustor in the Tay rig was a can combustor isolated from a full-scale Tay engine. The Tay engine was developed by Rolls-Royce, and the program was first launched in March 1983 by Gulfstream Aircraft (GIV), but early work on this engine could be traced to 1980. Modified engines from the Tay series were also equipped on Fokker 100 (Tay 620) and BAC 1-11 (Tay 650). In general, the Tay engine could be treated as the successor of the Rolls-Royce Spey family, and according to N. J. Wilson, chief engineer of Tay, the core of RB183 Mk 555 (Spey) was selected as the heart of the Tay engine [94].

The combustor equipped in the Tay engine is a tubo-annular combustion system also inherited from the Spey engine with some modifications, but many hardwire components were directly taken from the Spey engine. An overview of the Tay engine combustion system is presented in Figure 3. 2.

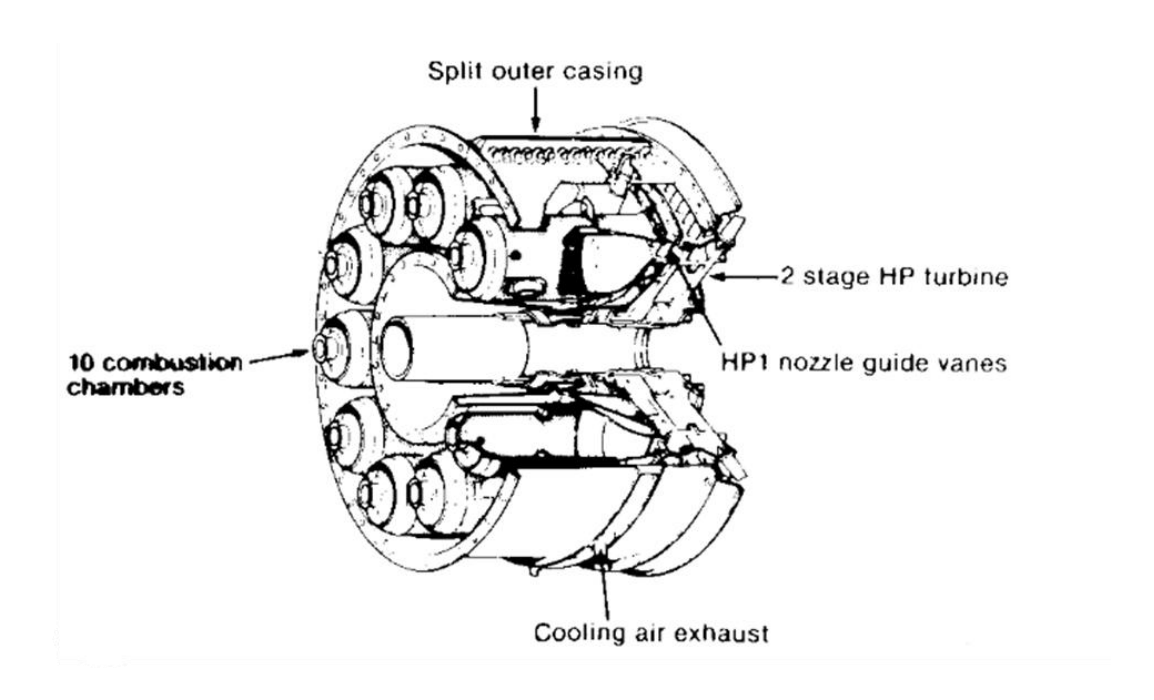


Figure 3. 2 The Tay combustion and turbine system (04 module). Reproduced from [94]

Ten combustion chambers surrounding a turbine shaft constitute the main body of the combustion system which is a typical arrangement of a tubo-annular combustor. One important advantage of using this system is that a single combustion chamber could be easily equipped on other ground-based test rigs, which benefits the engine modifications in faster and more cost-effective manner, and the Tay rig built in LCCC is based on this idea.

The general geometry of the combustion chamber is similar to other conventional cantype combustors. As presented in Figure 3. 3 the chamber mainly consists of three regions: the primary zone, the intermediate zone and the dilution zone. Fuel is injected by an air-assisted fuel injector for fine droplet atomization. Air is mainly supplied by air holes located at the body of the chamber. A swirler is also mounted at the head of the chamber to provide combustion air and stabilized the flame within the primary zone due to its aerodynamic curved vanes.

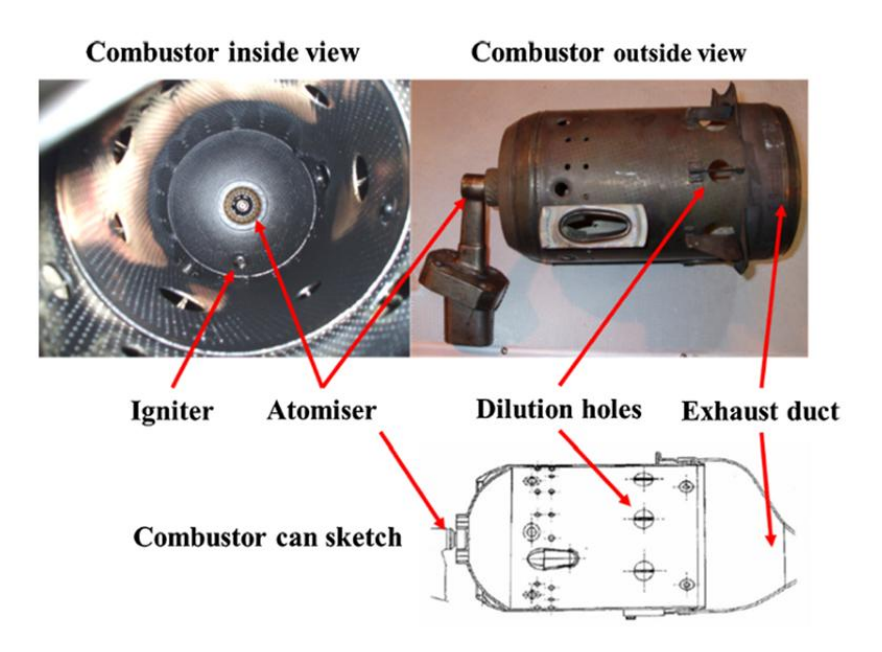


Figure 3. 3 Single combustor can from Tay engine. Reproduced from [95]

The major improvement of the Tay combustor, compared to other similar conventional can-type combustors, is the material. Tay used a specially designed material called

Transply, which is essentially made from two brazed metal sheets. Air passages were made on the inner face by chemical etching, and air moved freely through holes in the sheet and entered the combustor through air passages. Figure 3. 4 illustrates the structure of Transply material.

According to Wilson [94], the original intention of using Transply in the Tay combustor was the need for emission reduction. Since the Tay combustor uses turbo-annular configurations, the ratio of surface area to volume is higher than other combustors, which leads to a larger amount of cooling air. It is believed that more cooling air introduced means the quenching effect is more intense, which will partially burn hydrocarbons to form soot. Therefore, it is necessary to reduce the amount of cooling air below average to meet the emission requirements of that era.

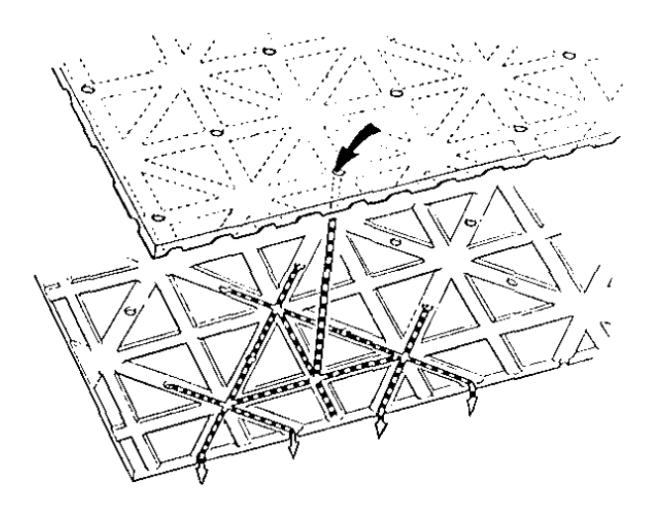


Figure 3. 4 Airflow inside Transply material. Reproduced from [96]

Transply is specifically highlighted in this section, because compared to other combustors existing in the same period, it alters the combustion environment and has the potential to affect emission results when using fuel blends with different aromatic species. Moreover, it modifies the overall air distribution, which is essential for developing the simulation model. More information about the simulation model will be described in the later subsequent sections.

Compared with some modern engines, such as Rolls-Royce Trent, the Tay engine does not have significant advantages in efficiency, bypass ratio, material, emissions or noise. The Trent uses a more advanced single annular combustor with 18 fuel spray nozzles, and RQL technology is also adopted. These technologies allow the Trent engine to have more uniform outlet temperatures and lower emissions. While The Tay engine uses tubo-annular arrangement.

However, compared to older combustor designs, they still share many similarities. They all use airblast fuel injectors and multi-stage combustion (primary zone and dilution zone) to provide more stable combustion, though modern engines enhance this with lean-burn and premixed combustion for lower emissions. They both provide cooling on the combustor liner: Transply in Tay and tiling in the Trent. In general, Trent and other modern engines can be treated as updated versions based on Tay, just as the Tay evolved from the Spey. Since the core technology of Tay and modern combustors is similar, aromatic emissions experiments on Tay could also be considered valid for other modern combustors, but in a more cost-effective and convenient way.

# 3.1.4 Laser-induced incandescence (LII)/ Artium LII 300

The smoke meter was commonly used in PM measurement, but LII was select in this thesis. Unlike the smoke meter, LII offers a more accurate, non-intrusive, and real-time measurements, including PM concentration and primary particle diameter. The LII system used in this testing champaign is an Artium LII-300 unite, and he standard configuration of this unit is present in Figure 3.5.

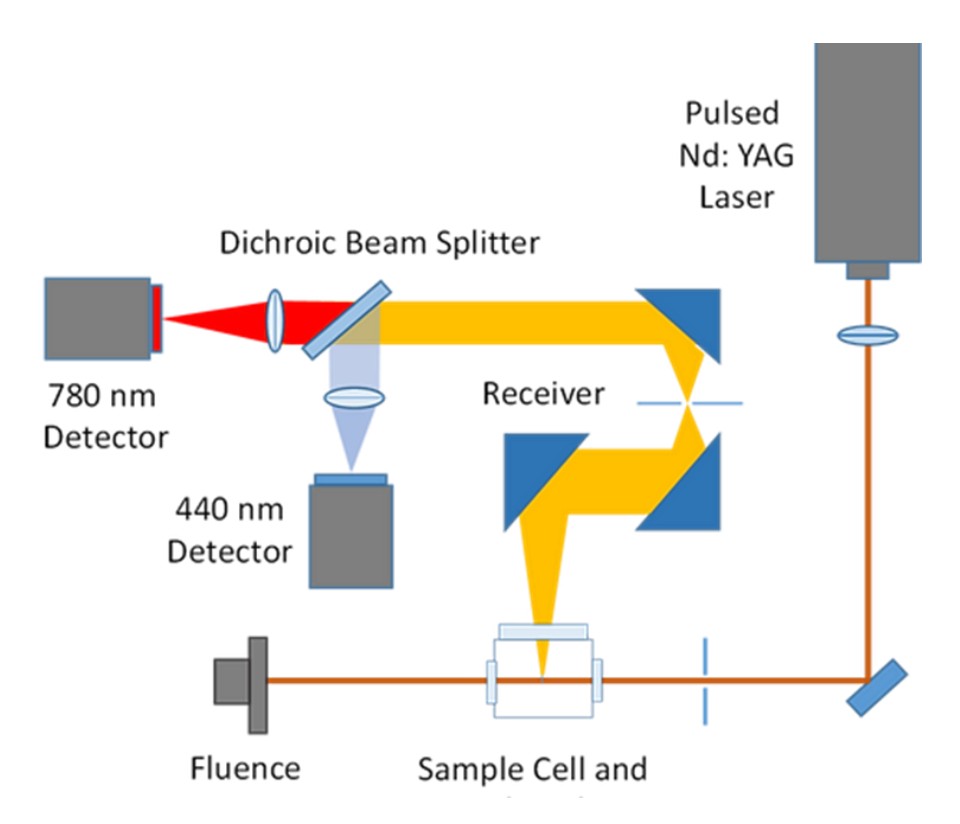


Figure 3.5: Typical laser-induced incandescence. Reproduced from [97]

It uses a pulsed Nd: YAG laser as the excitation source, emitting 1064-nm laser pulses to heat PM samples. Heated particles emit thermal radiation (incandescence) and are detected by two detectors via optical receivers.

# 3.1.5 Mobile Emissions Laboratory

A series of devices are involved in this investigation for gaseous measurements to provide reliable and continuous emission measurements. This suite of analytical instruments is called the MEL (Mobile Emissions Laboratory). The MEL is constructed on a trailer that can be easily connected to a car. This setting provides good mobility for the emissions laboratory, enabling emissions testing at virtually any location. An overview of the analytical hardware and the operational principles of each instrument are summarised in Figure 3.6 and Table 3.4. MEL shares the same sampling system with PM instruments, consisting primarily of heated sample lines and connection units.

A prefilter was installed at the input of MEL to prevent liquid jet fuel from entering the system, which could damage the instruments.

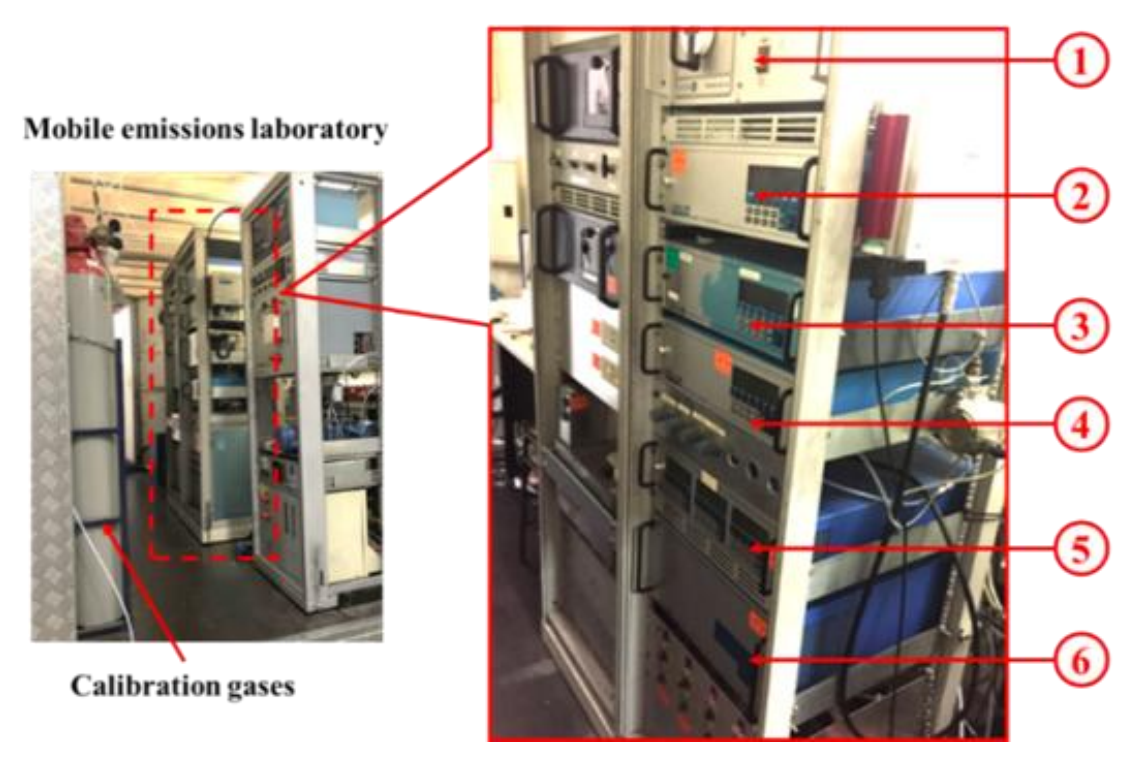


Figure 3.6: Mobile Emissions Laboratory. Reproduced from [98]

MEL contains equipment capable of characterising an exhaust plume regarding gaseous emissions concentrations (CO, CO<sub>2</sub>, NO<sub>x</sub>, Total Unburned Hydrocarbons, and O<sub>2</sub>). All instruments are calibrated by calibration gas cylinders located inside the trailer before running the Tay rig. Calibration gases are mainly divided into two categories: zero gas (nitrogen) and corresponding span gas, and the calibration procedure is convenient. Before testing, all instruments in MEL are activated for routine diagnostic and preheating. If all instruments are ready, the zero-gas valve will be opened, and nitrogen will pass through the piping to all instruments. If all instruments successful display a zero reading, the zero calibration is complete. Otherwise, manual calibration is required. Subsequently, the zero-gas supply will be shut off and each device will be calibrated using the corresponding span gas. Similar to zero calibration, if all

instruments display readings matching those recorded on the span gas cylinders, the calibration is successful. Otherwise, manual calibration would be necessary.

Readings from MEL are recorded by computer using LabVIEW, which is adequate to accurately capture reading fluctuations within the measurement period. The testing instrument's uncertainty was investigated and discussed in previous experiments that us the MEL [99].

Table 3.4: Gaseous emissions measurement equipment

| Number in Figure 3.6 | instrument   | Method   | Uncertainty |
|----------------------|--|--|-------------|
| 1                    | Signal Prefilter Unit 333                                  | -  | -           |
| 2                    | 3000HM THC<br>Analyser                                     | Flame Ionisation<br>Detector (FID)   | ± 8 ppm     |
| 3/4                  | 4000vm NOx<br>Analyser                                     | Heated, vacuum<br>Chemiluminescence  | ± 15 ppm    |
| 5                    | Multi Gas Analyser<br>CO, CO <sub>2</sub> , O <sub>2</sub> | Duel GFC Non-<br>Dispersive Infrared<br>Analyser (NDIR) plus<br>paramagnetic | ± 6 ppm     |
| 6                    | Signal 200sm<br>Series Cooler                              | -  | -           |

# 3.1.6 3000HM THC analyser

3000HM THC Analyser is selected to detect total unburned hydrocarbon (THC) in the exhaust. It uses a flame ionization detection (FID) in which a hydrogen flame ionizes any hydrocarbon passing through the flame inside the device. This technique allows THC detection at a ppm levels. A heated sample system is necessary to maintain

sample exhaust in gaseous form since combustion exhaust usually contains unburned liquid fuel. A typical THC working principle is shown in Figure 3.7.

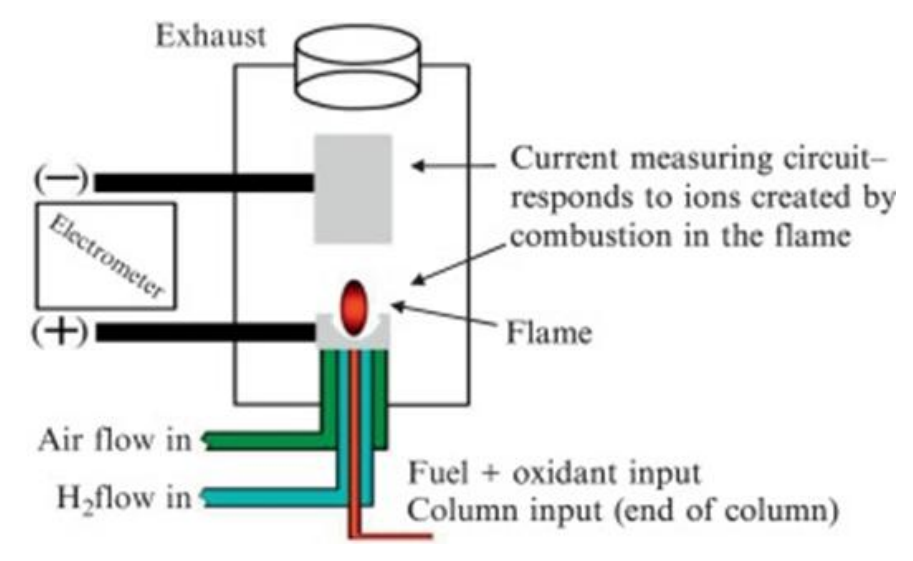


Figure 3.7: THC system. Reproduced from [100]

## 3.1.7 4000VM heated vacuum chemiluminescent NOx analyser

The operating principle of the 4000VM NOx analyser is based on the chemiluminescent reaction between nitric oxide and ozone which are shown in Equation 3. 1 and Equation 3. 2.

$$NO + O_3 \Rightarrow NO_2 + O_2$$
 Equation 3. 1

$$NO + O_3 \Rightarrow NO_2 + O_2 + photon$$
 Equation 3. 2

Figure 3.8 shows a typical analyser using the heated vacuum chemiluminescent method. The majority of the output through this reaction is nitrogen monoxide and oxygen, and only 10% of NO<sub>2</sub> is electrically excited. Excited NO<sub>2</sub> will return to ground state and emit a photon (wavelength between 0.6µm and 0.3µm) due to the loss of molecular energy. A photomultiplier and associated electronics then detect photons. The production of

photons is directly proportional to the mass flow rate of NO. The primary pathway for NO<sub>2</sub>\* to lose energy is molecular collision. Only a tiny fraction of NO<sub>2</sub>\* will emit a photon. Since the probability for this molecule collision is proportional to the pressure, it is essential to maintain low pressure inside the analyser.

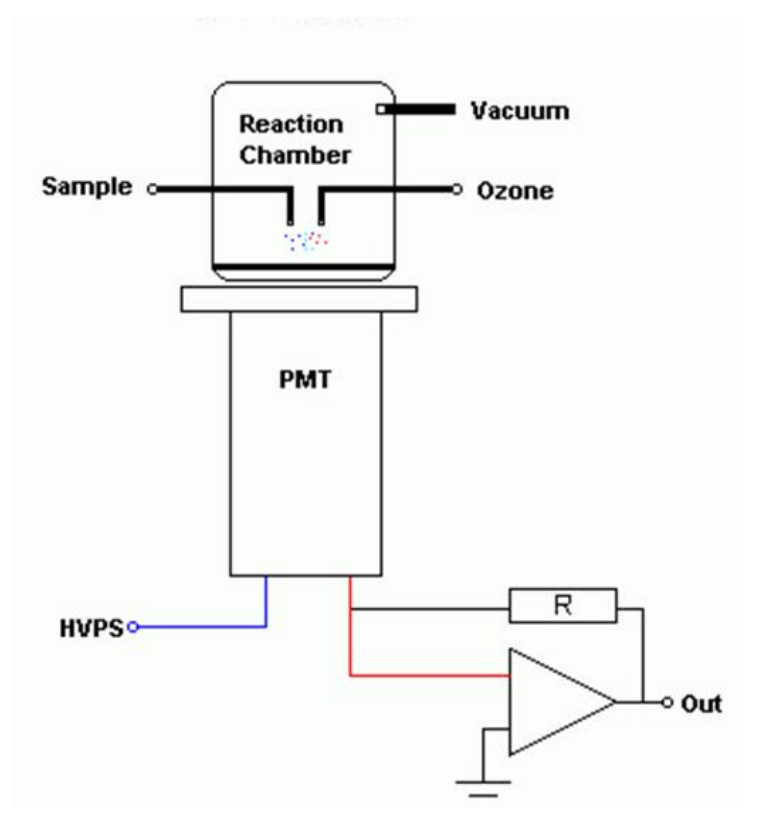


Figure 3.8: Working principles of heated vacuum chemiluminescent NOx analyser.

Reproduced from [99]

The 4000VM operates at low pressure to maximize photon output and minimize interference from other gases, such as CO<sub>2</sub>, which can deactivate NO<sub>2</sub>\*.

# 3.1.8 9000MGA multi gas analyser

The Signal 9000MGA Multi Gas Analyser detects the exhaust's O<sub>2</sub>, CO, and CO<sub>2</sub> concentration. The basic operating principle is that most gases absorb infrared energy at wavelengths specific to each gas species. Each gas species has a preference to absorb a particular wavelength. Therefore, measuring the absorbed energy could

represent the amount of the specific gas species. A typical infrared photometer is shown in Figure 3.9.

# **Typical Infrared Photometer**

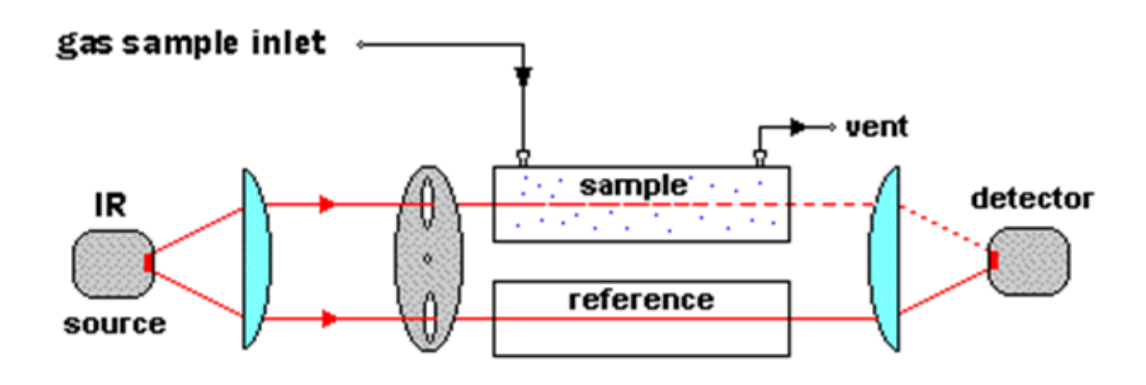


Figure 3.9: Infrared Photometer working principle. Reproduced from [101]

In this analyser, CO and CO<sub>2</sub> have their dedicated infrared detection modules. Each module contains two sealed cells: one filled with a non-absorbing reference gas and the other with the target analyte gas. Radiation passes through each cell sequentially, and absorption ratio is measured. This ratio changes when the sample gas enters the optical path due to radiation absorption. By comparing the differential absorption between the reference and sample cells, the gas concentration is determined.

# 3.2 Kinetic modelling

To understand the chemical reactions behind the experimental results, a simulation model with a group of detailed chemical mechanism was built. This simulation work has two primary objectives. First, the simulation results should match the experiment results regarding how different aromatic species affect soot production. Second, to identify an appropriate intermediate tracer for soot prediction.

As a reminder, the common recognition of soot or black carbon is the aggregation of numerous small carbon particles across a wide sizes distribution, typically referred to as polycyclic aromatic hydrocarbons (PAHs). The exact formation mechanism of PAHs has various theories, but it is generally accepted that the nucleation centre originates from small molecules such as acetylene [102]. The following reaction pathway represents one proposed mechanism for the initial stage of PAH formation.

$$C_2H_3 + C_3H_3 \leftrightarrow C_6H_5 + H$$

$$C_3H_3 + C_3H_3 \leftrightarrow C_6H_6$$

$$n - C_4H_5 + C_2H_2 \leftrightarrow C_6H_6 + H$$

$$n - C_4H_3 + C_2H_2 \leftrightarrow C_6H_5$$

Therefore, one method of soot prediction involves identifying intermediate tracers that correlate with final soot production, which is one of the primary purposes of this research.

CHEMKIN-Pro 2019 R3 was used for all simulations. This software specializes in solving complex chemical kinetics problems, supporting multiple chemical species, reaction equations, concentration ranges, and temperatures. By solving reaction equations, researchers can establish comprehensive understanding of chemical processes. Its reliability and efficiency for combustion and emissions analysis have been widely demonstrated [103].

Two major challenges were encountered during model development. First, simulating full-scale combustor combustion processes remains extremely challenging due to environmental complexity and computational demands. Detailed combustor characterization would require prohibitive computational resources, necessitating trade-offs between simulation complexity, accuracy, and computational costs. To address this, both a simplified 0-D model and a detailed chemical reactor network (CRN) 1-D model

were developed to balance accuracy and computational feasibility. These simulations aim to study aromatic impacts on emissions rather than precise prediction.

The second challenge resulted from the Tay combustor's destruction during a flood. With limited publicly available information, the detailed combustor can geometry became irretrievable, making identification of an accurate representative model critically important.

#### 3.2.1 Zero-D model

The primary objective of this simulation work is to identify intermediate tracers that could represent final soot production. By cross-referencing with experimental results from Chapter 3, this approach will evaluate how aromatic species influence PM formation.

To start the investigation, a 0-D model was used to investigate chemistry mechanism performance varied residence times, air-fuel ratios, and temperatures. The model in CHEMKIN-Pro consists of a stirred reactor with reactant inflow and product outflow, shown in Figure 3. 10.

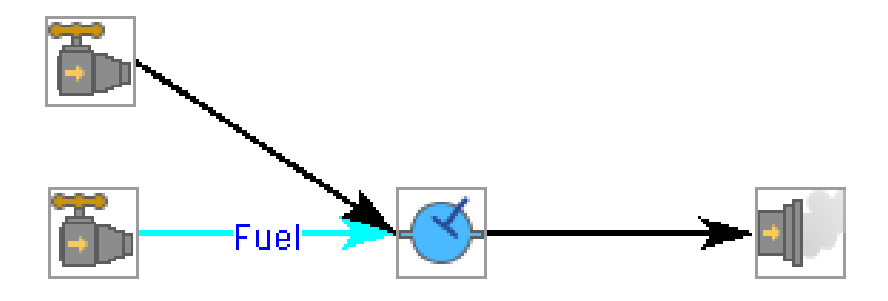


Figure 3. 10: 0-D model

A perfect stirred reactor is selected assuming perfect mixing and operating at a steady state condition within a fixed control volume. Although 0-D models cannot fully replicate detailed combustion environments, their simplicity and computational efficiency make them ideal for investigating parameter sensitivity. This approach also informs the development of more complex models.

### 3.2.1.1 Chemistry mechanism

To investigate soot production using kinetic model, using a complex kinetic mechanism will not significantly affect simulation time. Moreover, keeping the mechanism component as complex as possible will benefit the accuracy of the simulation results in theory. The kinetic mechanism used in this research is a detailed mechanism provided by CRECK Modelling Group [104], which includes 621 species and 27369 reactions from C1 to C16.

Unlike simple or sim-detailed mechanism used in other Chemkin studies [80], [81], this mechanism was chosen because it is one of the most detailed kinetic mechanisms available. It incorporates the chemistry of relevant intermediates and aromatic components that need to be investigated. Multiple studies have verified this chemistry mechanism and proven its reliability [105], [106], [107]. Same mechanism is also used in 1-D models in later section,

#### 3.2.1.2 Reactant selection

Reactants used in this research are carefully selected. The main criterion of reactant selection is accurately representing fuel properties while simplifying the calculation process. Instead of reducing the chemistry mechanism, the number of reactants is simplified as much as possible. Since available species in the mechanism were also

considered, not all fuel blend compositions will be involved in the simulation. NC<sub>16</sub>H<sub>34</sub> (n-hexadecane) was selected to represent the base fuel, with aromatic additives comprising the remaining components. Four aromatics (methylnaphthalene, indene, styrene, and ethylbenzene) were selected in the simulation as they represent three different types of aromatic classes investigated previously.

### 3.2.1.3 Reaction temperature

The maximum reaction temperature inside a typical gas turbine combustor could reach 2500°F (2071°C) [108], making it nearly impossible to measure during experiments. It is also difficult to predict the combustion temperature since the temperature inside the combustor chamber is not uniform due to the complex flow pattern. Detailed combustor chamber geometry is needed to simulate the entire combustor temperature profile. Moreover, many factors affect the actual combustion temperature in a real experiment, such as fuel spray and degree of mixing. In conclusion, not only is detecting actual combustion temperature challenging, but simulating the accurate temperature profile is also extremely difficult. In this thesis, a wide range of reaction temperature was selected for simply 0-D model. For complex CRN model, reaction temperature was consult from other experiment and simulation work in a model Tay combustor [84], [92].

### 3.2.1.4 Residence time, flow rate and volume

Residence time refers to the time that reactants spend in the reactor and it is related to volume and mass flow rate. When constructing a CRN model with fixed mass flow, either the residence time or volume must be defined initially. For a 0-D model, due to their relative low simulation time cost, multiple residence time could be used to investigate their impact on emissions. However, more complex models such as CRN require more precise definition of residence time. The residence time of CRN models

presented in this thesis are calculated by Chemkin according to the geometry information (volume) and flow characteristics (mass flow rate) presented in literatures [83], [84], [92]. For example, in a simple 1-D model, 10.091ms, 2.19ms and 0.957ms may represent the residence times for the total primary zone, the secondary zone and the nozzle respectively.

### 3.2.1.5 Air-fuel ratio (AFR) $/ \lambda$

Air-fuel ratio is a fundamental parameter in combustion science, representing the mass ratio of air to fuel. AFR directly a direct characterizes mixture stoichiometry. The air-fuel equivalence ratio ( $\lambda$ ) represents AFR relative to the stoichiometric AFR for a specific fuel blend. AFR and  $\lambda$  could be easily transferred to each other using the following Equation 3. 3.

$$\lambda = \frac{AFR}{AFR_{stoich}}$$

Equation 3.3

Where AFR<sub>stoich</sub> is the stoichiometric air-fuel ratio for a particular fuel.

Three mixture ratios were selected in this simulation investigation, including lean combustion (AFR=65), stoichiometric combustion ( $\lambda$ =1), and fuel-rich combustion ( $\lambda$ =0.5). These fuel mixture ratios were determined based on actual combustor operating conditions. For an actual combustor used in an aviation gas turbine engine, the fuel-air mixture is non-uniform. Rather, due to the combustor geometry and fuel injection method, different regions inside the combustor will have significant mixture ratio variations. For instance, the region near the fuel injector will have an extremely fuel-rich mixture condition. Moreover, different types of combustors will have different characteristics, making it reasonable to investigate various AFR conditions.

#### 3.2.1.6 Tracer selection

As mentioned, one of the objectives of this research is to identify appropriate soot tracers. The election of optimal soot tracers remains debated in the field [109], [110]. Species selection varies depending on the selected combustion model and chemical mechanism. The prevailing view suggests small molecules such as acetylene (C<sub>2</sub>H<sub>2</sub>) are the most suitable intermediate tracers for PM production across chemical mechanisms. This statement, based on established PAH formation pathways, is supported by research since theoretically they initiate aromatic molecule formation. Accordingly, small molecules such as acetylene, ethylene and ethane were monitored during the reaction process. Larger molecules and early-stage PAHs were also monitored as they directly represent PAH production.

## 3.2.2 CRN (Chemical reactor network)

Due to the concern that 0-D models might insufficiently represent combustion environment in actual combustors, a 1-D chemical reactor network (CRN) was developed for PM prediction purpose. The chemistry mechanism matches that used in the 0-D model.

The CRN configuration is empirically determined minor structural modifications may affect simulation results. Therefore, experimental or simulation references aid model construction. The CRN model proposed in this thesis incorporates data from both 3-D simulations and experiments using a model combustor burns propane. This model combustor is developed by Bicen et al. [92] in a Rolls-Royce-founded project at the Imperial College, which was used to represent an actual Tay combustor chamber at that time. The geometry information of this model Tay combustor is shown in Figure 3. 11, same geometry was also used in other works [83], [84], [111].

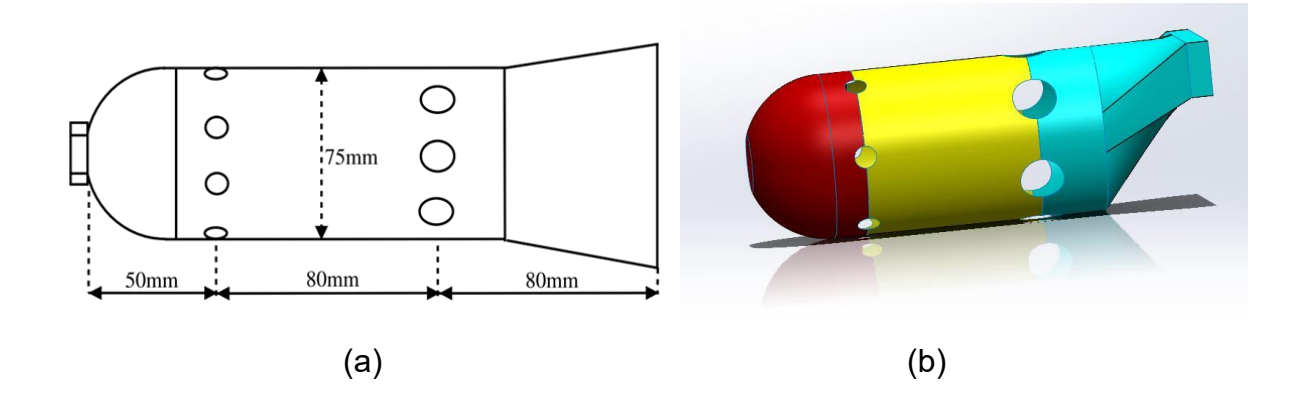


Figure 3. 11 (a) Sketch of Tay Combustor Model. Reproduced from [112]; (b) 3-D geometry of Tay combustor model

In general, this model Tay combustor preserves most features in an actual Tay combustor, and some research states that it is a three-fourth-scales model of an actual one [83]. It was built with a 75mm circular barrel that included six primary air holes and six dilution holes. The diameter of the primary holes and dilution holes is 10mm and 80mm, respectively. A hemispherical head is attached at the start point of the barrel in front of the primary holes, and a circular to rectangular nozzle was also assembled at the end. A swirler is equipped at the beginning of the hemispherical for flow stabilization. The swirler delivers 6.9% airflow, and the swirler number and discharge coefficient are 0.56 and 0.74, respectively; more detail on this swirler can be found at [113].

The material of the model combustor is Transply which is identical material used in an actual Tay combustor. Transply delivers 26.2% total airflow into combustor (6.6% at hemispherical head, 13.8% at barrel and 5.8% at nozzle). Other than that, primary holes introduce 13.6% airflow, dilution holes 53.5%. The mass flow rate was also scaled down based on the actual Tay engine using the parameter of mT<sub>inlet</sub><sup>0.5</sup>/(AP). The operation parameter of this model combustor is set as 57 for total AFR, 1.76 g/s for fuel mas flow rate and air inlet temperature is set as 315°C. All these air distribution and operation parameters were used in the CRN model.

Works of 3-D simulation on this model Tay combustor was also used in this thesis to help the decision on the selection of reactor types, numbers and corresponding volume (residence time) [83], [84]. Flow field of this model combustor was presented in Figure 3. 12.

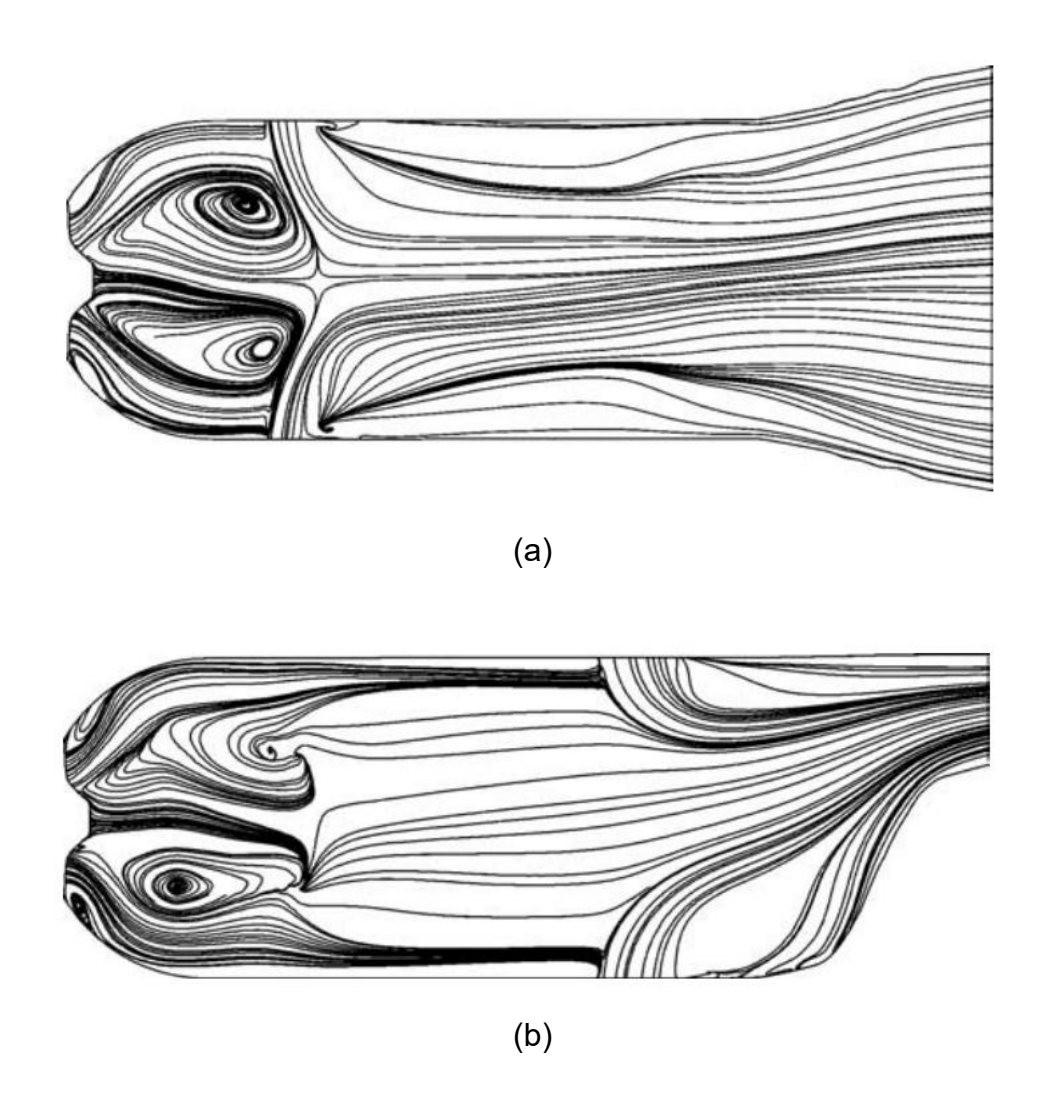


Figure 3. 12 Flow field in model Tay combustor. Reproduced from [83] (a) Mid-horizontal plan plane; (b) Mid-vertical plan

The flow field created by LES and other combustion models closely matches experimental results. Figure 3. 12 shows significant recirculation occurs in the primary zone, and the majority of combustion flow is restrict whining the zone by air flow from primary air holes. For this type of flow, a prefect stirred reactor (PSR) is the best option

since large eddies enhance the mixing process. Both the intermediate and dilution zones can be modelled as plug flow reactors (PFRs) due to minimal vertical mixing, and no large eddy is observed. Therefore, the simplest CRN structure to represent this model Tay combustor is a PSR connected to two PFRs in series, as shown in Figure 3. 13.

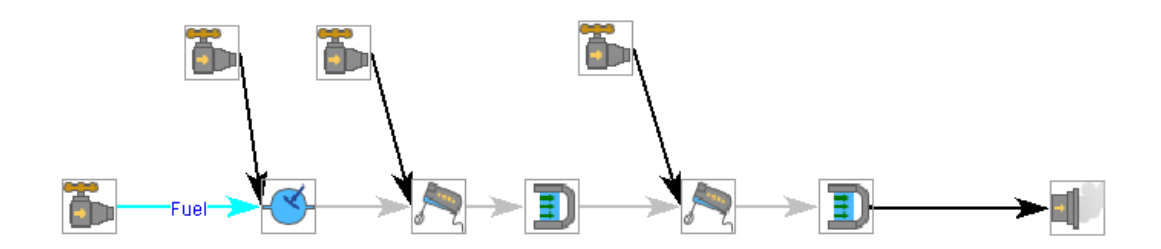


Figure 3. 13: Simplest CRN

In this model, each reactor represents different combustion zones, and the residence time is determined by the volume of each zone. To calculate reactor volumes, zone boundaries must be defined. Osgerby[82] suggested that the midpoint between two set of air holes could be treated as the boundary such as midpoint between primary and secondary jet holes. Swithenbank et al. [114], [115] proposed an experimental method using a salt-tipped probe to identify primary zone since the combustion flow in this region will be easily sodium coloured. However, the experiment method is impractical, and Osgerby's method is too generalized different combustor designs. Therefore, reactor volumes in this thesis were calculated by consult geometry information present in Figure 3. 11 and simulated results present in Figure 3. 12.

### 3.2.1.1 Simple 1-D model

The first 1-D model proposed in this thesis is shown in Figure 3. 14. It is a modified version of the simplest CRN structure mentioned above. An extra PSR is deployed at

the beginning to simulate mixing processes. The two rows of sources inlets at the top of the model are air inlet for the swirler, air holes and Transply.

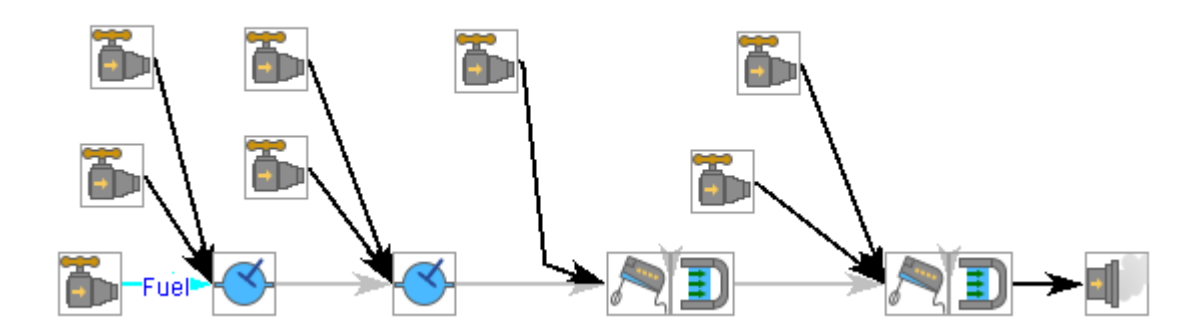


Figure 3. 14: CRN model layout 1

This model layout balance both computational efficiency and fidelity to the model Tay combustor.

### 3.2.2.1 1-D recirculation model

A more complex 1-D model is also created in tend to replicate the recirculation behaviour in primary zone. The structure of this model is present in Figure 3. 15.

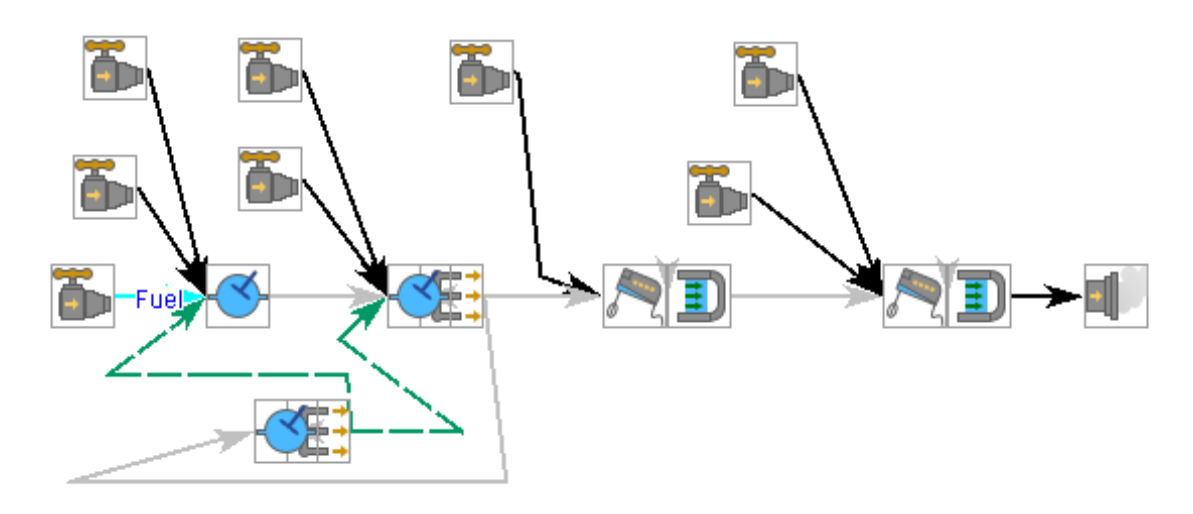


Figure 3. 15: CRN model layout 2

One of the challenges to build a recirculation model is determining the percentage of recirculation flow back to the primary zone. Since experimental measurement is challenging, several methods for estimation will be discussed.

First, in a conventional can-type combustor, most fuel burns in the primary zone. Osgerby [82] suggest that around 90% of the fuel combustion occurs in the primary zone. This assumption enables rough calculation of recirculated air requirements and its percentage.

A second method to calculate recirculation flow uses a simply jet entrainment model introduced by Swithenbank et al. [114] given by:

$$\frac{\dot{m}}{\dot{m}_j} = 0.32 \frac{x}{d_j} \left(\frac{\rho}{\rho_j}\right)^{\frac{1}{2}}$$

#### Equation 3.4

Where  $\dot{m}_j$  refer to mass flow rate of air into the combustor chamber through air holes, x is the distance penetrated by air into the combustor chamber,  $\rho/\rho_j$  is the ratio of air density which is assume equal to 4 by Swithenbank.  $d_j$  could be calculated by the diameter of air hole  $d_0$  and correspond discharge coefficient  $\mathcal{C}_D$  by

$$d_j = d_0(C_D)^{0.5}$$

#### Equation 3.5

Bicen et al. [92] proposed a solution to calculate the percentage of recirculation jet by using flow temperature by

$$\frac{m_{pr}}{m_{ni}} = 0.5 \sin \theta T_r^{-0.5}$$

#### Equation 3.6

The value of  $\theta$  is suggested as 15°, and  $T_r$  is the temperature measure as 1850K/1500K. According to this method, 45% of primary jet participates in the primary zone to create recirculation behaviour.

Among these three methods to estimate the amount of recirculation flow, Osgerby provides a simple and quick solution, but the solution is based more on the design principle of the combustor; the practical combustion situation in a combustor might be different. Method from Swithenbank et al. requires more detailed information, such as the discharge coefficient of the air hole, which is not available for the model Tay combustor. Method by Bicen et al. is the most appropriate to use in this thesis since the temperature required to calculate the mass flow was taken directly from the experiment in the Tay model combustor. This means that the calculated result might be more accurate and closer to the actual condition. This estimation method was also used in other works [116]. Therefore, a 45% primary jet recirculation rate was used in this thesis to build the recirculation model. The volume of each reactor in the primary zone is equal to the ratio of corresponding mass flow suggested by Osgerby [82].

#### 3.2.2.3 Detailed 1-D model

Based on the flow field shown in Figure 3. 12, it is noticed that some combustion flow in primary zone escaped to the secondary zone between the gap of primary air holes and eventually stopped by the dilution air. This hot primary flow created a local high-temperature area that may affect emission production. The same behaviour was observed in other studies of this combustor [84]. This flow pattern represents a signature feature of the Tay model combustor in this thesis, and it is worth to bring it into the CRN model which is present in Figure 3. 16.

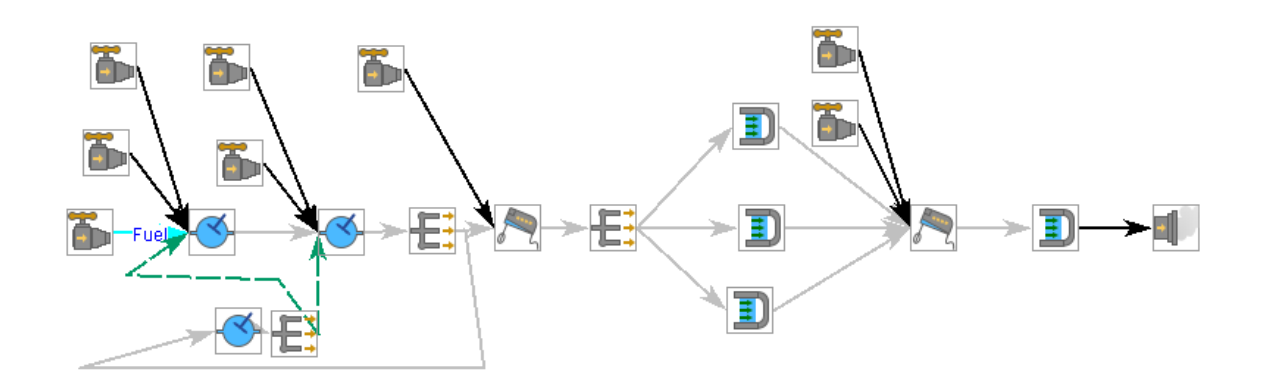


Figure 3. 16: CRN model Layout 3

Model Layout 3 added two extra PFRs parallel to the main PFR representing the secondary zone. A relatively high reaction temperature is selected for these two PFRs, with the initial temperature for the middle PFR is assumed as 1200K and the two extra PFRs as 1400K. The residence times of PFRs are calculated by Chemkin according to the volume and inlet mass flow rate. The corresponding volume of the three PFRs is assumed based on the distance of the gap between two air holes and the number of gaps. The middle main PFR is assumed as 59.29270967 mm³, while the upper and bottom PFRs are 29.04737667 mm³ and 35.5756256 mm³ respectively. The reason for using two PFRs (rather than one) is to replicate the asymmetry of the combustor due to the nozzle, and a slightly larger volume was selected for the bottom PFR. The ratio of mass flow rate between the three PFRs is assumed same as the ratio of their volumes suggested by Osgerby[82].

# 3.3 Fuel, O-ring, and experiment apparatus

This section describes experimental apparatus and specimens. The operating principles of each instrument are explained in detail. Fuels were selected mainly based on commercial jet fuel formulations and laboratory availability. Due to cost considerations and a flood during testing, the fuels selection was less comprehensive than initially planned.

However, the final selection of fuels remains representative, covering two commercial jet fuel types (LanzaTech alternative jet fuels and Jet A-1). O-ring samples included nearly all popular material options in the aviation industry. Note that O-rings from different manufacturers exhibit different physical characteristics even though the material is identical due to the different manufacturing pathways. Thus, the experiment included identical material O-rings with different standards. The test rig's framework was adapted from prior O-ring elastomer research [117], with many modifications for the new test objectives.

#### 3.3.1 Candidate fuels

One objective of this test is to develop testing technologies suitable for all existing jet fuels. Jet fuels are divided into two categories: conventional and alternative jet fuels. Some past research identified that lack of aromatics is the main course of fuel leakage in alternative jet fuels [87]. However, aromatics are also the primary soot source, which is the advantage of using alternative jet fuels since it has little aromatic content. Therefore, precise aromatic concentration in alternative fuels is essential to balance sealing and soot production, which is still in limbo. Thus, the strategy of fuel selection in this experiment should meet two requirements. First, selections should cover both

two categories, conventional and alternative jet fuels. Second, the impact of aromatic concentration should also be represented in the fuel selections.

Three fuel types were selected in this investigation, and details are shown in Table 3. 5.

Table 3. 5: Fuel Selection

|                      | Jet A-1                                  | Alternative Jet Fuel<br>#13    | Alternative Jet Fuel<br>#4                              |
|----------------------|--|--------------------------------|---|
| Source               | LCCC                                     | LanzaTech                      | LanzaTech   |
| Description          | Neat Jet A-1,<br>Hydrotreated<br>product | -                              | >60% Paraffin, isoparaffins and cycloparaffins (C8-C16) |
| Aromatic content (%) | 16.8                                     | 10-20 (1,3,5-trimethy benzene) | 1-10 (1,3,5-trimethy benzene)                           |

Jet A-1 was selected since it is a standard commercial jet fuels, representing conventional fossil-based jet fuels. Two other types of drop-in alternative jet fuels produced by LanzaTech use industrial waste CO<sub>2</sub> as the raw feedstock. According to the information provided by the manufacturer, which is also shown in Table 3. 5, their composition is primarily long-chain paraffin and cycloparaffins (C8-C16). The key difference between these two fuels is the percentage of aromatic content. Alternative Jet Fuel #13 contains 10-20% aromatic, and Alternative Jet Fuel #4 contains 1-10% aromatic. It should be mentioned that the aromatic that exists in both alternative jet fuels is 1,3,5-trimethyl benzene only. These two alternative jet fuels provide an ideal opportunity to study the impact of aromatic concentration on sealing.

### 3.3.2 O-ring selection

Three O-ring types were involved in the test: fluorocarbon (FKM, also called Viton), nitrile and fluorosilicone (FVMQ). Specifications of O-rings is shown in Table 3. 6. These elastomers were selected as the most widely used aviation-grade materials.

Table 3. 6: O-rings

|              | Material       | Source       | Colour Appearance |
|--------------|----------------|--------------|-------------------|
| FKM 607C     | Fluorocarbon   | Escudier SAS | Black             |
| FKM AMS7287  | Fluorocarbon   | Sheffield    | Black             |
| FKM AMS7276  | Fluorocarbon   | Sheffield    | Black             |
| NITRILE 2186 | Nitrile        | Escudier SAS | Black             |
| FVMQ 61D6    | Fluorosilicone | Escudier SAS | Blue              |

The O-rings were randomly selected from the same batch for each type to ensure consistent physical properties and manufacturing conditions. Note that, even within the same batch, O-ring dimensions vary slightly due to manufacturing processes and elastomer characteristics. However, these minor dimensional variations significantly influence results under high pressure. Therefore, each O-ring was measured individually to calculate the precompression, which will be presented later.

# 3.3.3 C11 jig

A set of custom jigs applies and maintain most compressions on O-ring samples. These jigs were previously used in the Wallace Compression Stress Relax Meter (WAC11), a testing rig to measure cross-section diameter (CSD) via electrical contact method, also known as the Shawbury-Wallace method [118]. Their proven stability and reliability justified their use in this research. A section view of the C11 jig is shown in Figure 3. 17.

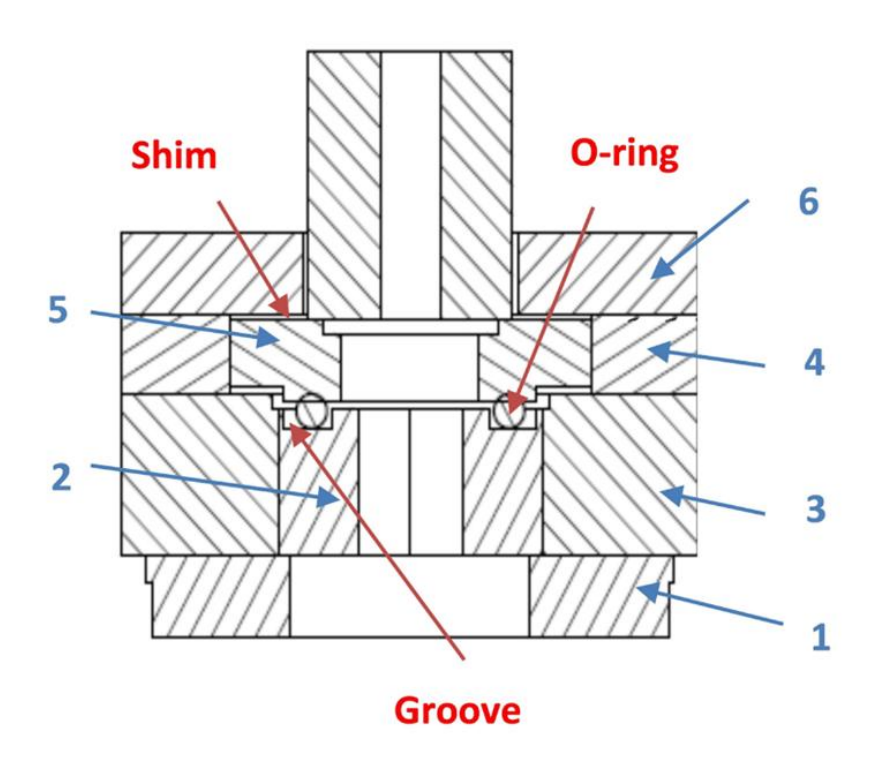


Figure 3. 17: Section view of C11 jig under pressure. Reproduced from [119]

In this test campaign, these jigs maintain 20% CSD compression for O-rings samples through testing, including temperature treatment. Figure 3. 17 shows the jig body comprises six stainless steel annular plates with a groove in Part 2 for O-ring placement. Three screws secure all plates together.

Figure 3. 18 shows the actual C11 jig components used, which were measured for precompression calculations. The number of each part in Figure 3. 18 matches the number present in Figure 3. 17 for better understanding.

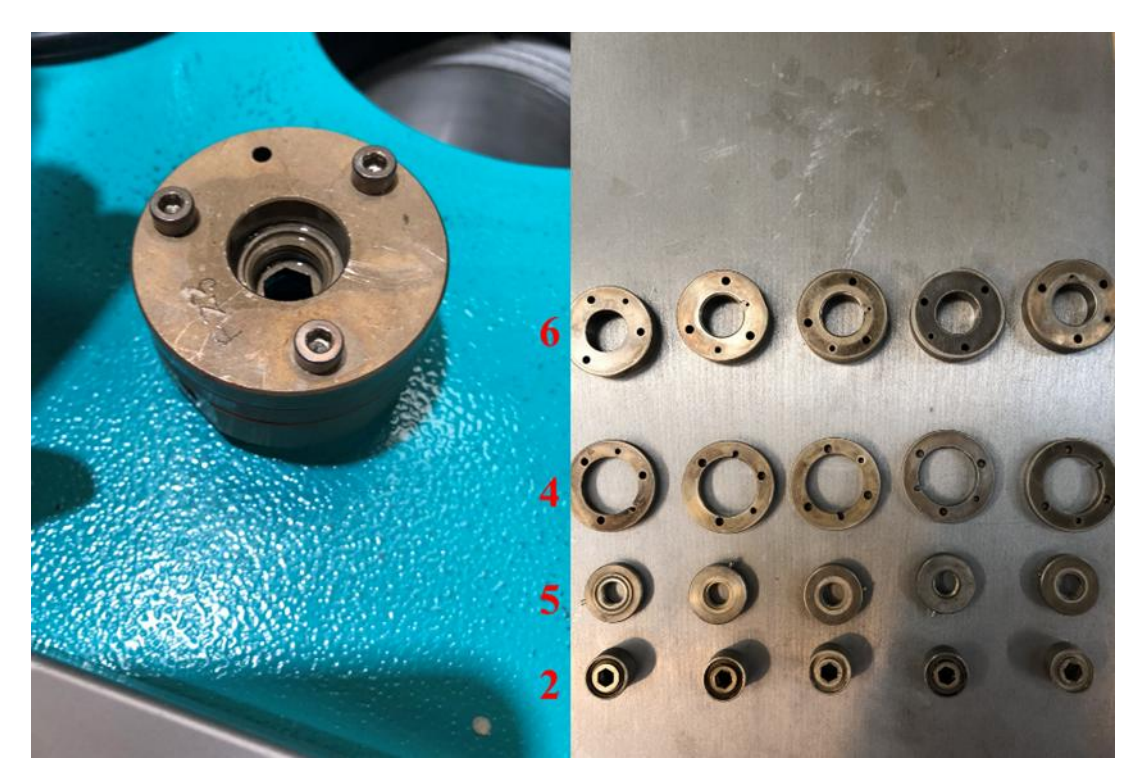


Figure 3. 18: Critical parts of C11 jig

### 3.3.4 Elastocon kits

Elastocon systems serve as the primary test rigs used in this experiment. they contain several instruments: stress relaxation units, an Elastocon environment control unit, a chiller, a signal amplifier and a state monitoring computer.

Figure 3. 19 shows the Elastocon system configuration. Jigs containing O-ring samples are placed in stress relaxation units inside the temperature-controlled Elastocon unit. An environmental control hood atop the unit maintains uniform temperature across all units. The Elastocon unit connects to a chiller for fuel temperature regulation.

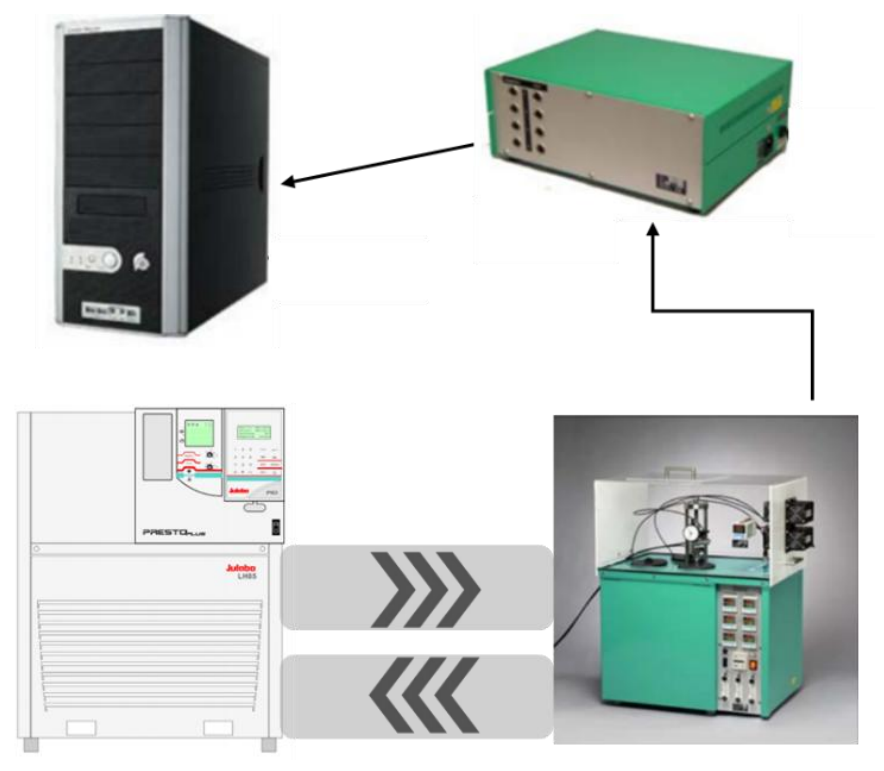


Figure 3. 19: Overview of the Elastocon kits

The counterforce signal from each load cell is amplified and received by the computer via a communication box. LabVIEW code in the computer process and record data.

The stress relaxation unit is a modified version (Figure 3. 20) consisting of four parts: a supporting frame, a force adjustment screw, a load cell with the force sensor, and a set of compression plates. Samples are placed between the compression plates, with force applied via the adjustment screw. Compression is controlled and monitored using a dial gauge. The load cell continuously records reaction force changes from O-ring compression set deflection.

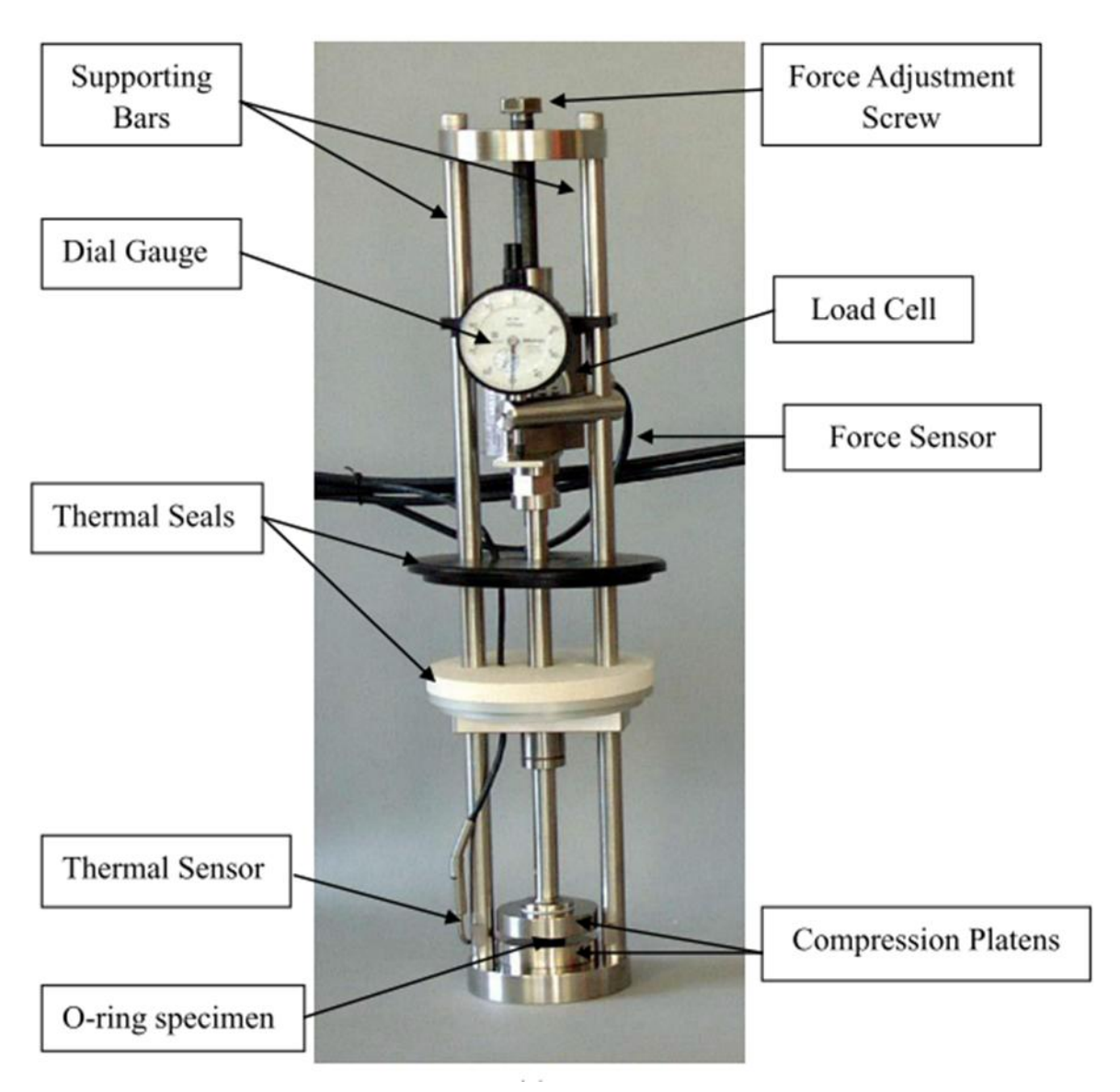


Figure 3. 20: Stress relaxation unit. Reproduced from [117]

In this experiment, the unit's bottom section was replaced with modified C11 jigs to maintain constant compression. The jig and shim provide 80% of the total compression, with the remaining 20% applied by the force adjustment screw.

A closed view of the Elastocon unit with an environmental control hood is shown in Figure 3. 21.



Figure 3. 21: Elastocon unit with environment control hood

A draft hood (environment control hood) is installed on the Elastocon unit. It is manufactured from polycarbonate, which prevents any temperature fluctuation caused by ambient temperature variations around the exposed upper section of the stress relaxation unit. The temperature control unit of this raft hood is a Peltier cooling system that can maintain the temperature within  $\pm 0.25$ °C.

The PRESTO A80 chiller provided high cooling capacity (theoretically to -80°C) with dynamic temperature control, making this unit a perfect choice for low-temperature treatment. It should be mentioned that, during the latter stages of the testing, the chiller unit failed and was removed from service by the suppliers. A significant delay was incurred in sourcing a replacement unit by the supplier as the unit was no longer in production. After replacing the chiller with the latest unit, a few attempts at low-

temperature treatment were performed, and the flood occurred, wiping the test plan once and for all.

## 3.3.5 Heating vessel and oven

The heating vessel is manufactured in the workshop and designed to contain multiple jigs during heating. An overview of the test vessel structure appears in Figure 3. 22. The vessel's main body is stainless steel preventing chemical reactions between fuel and vessel at high temperatures. The pressurized vessel prevents fuel vaporization during high-temperature heating.

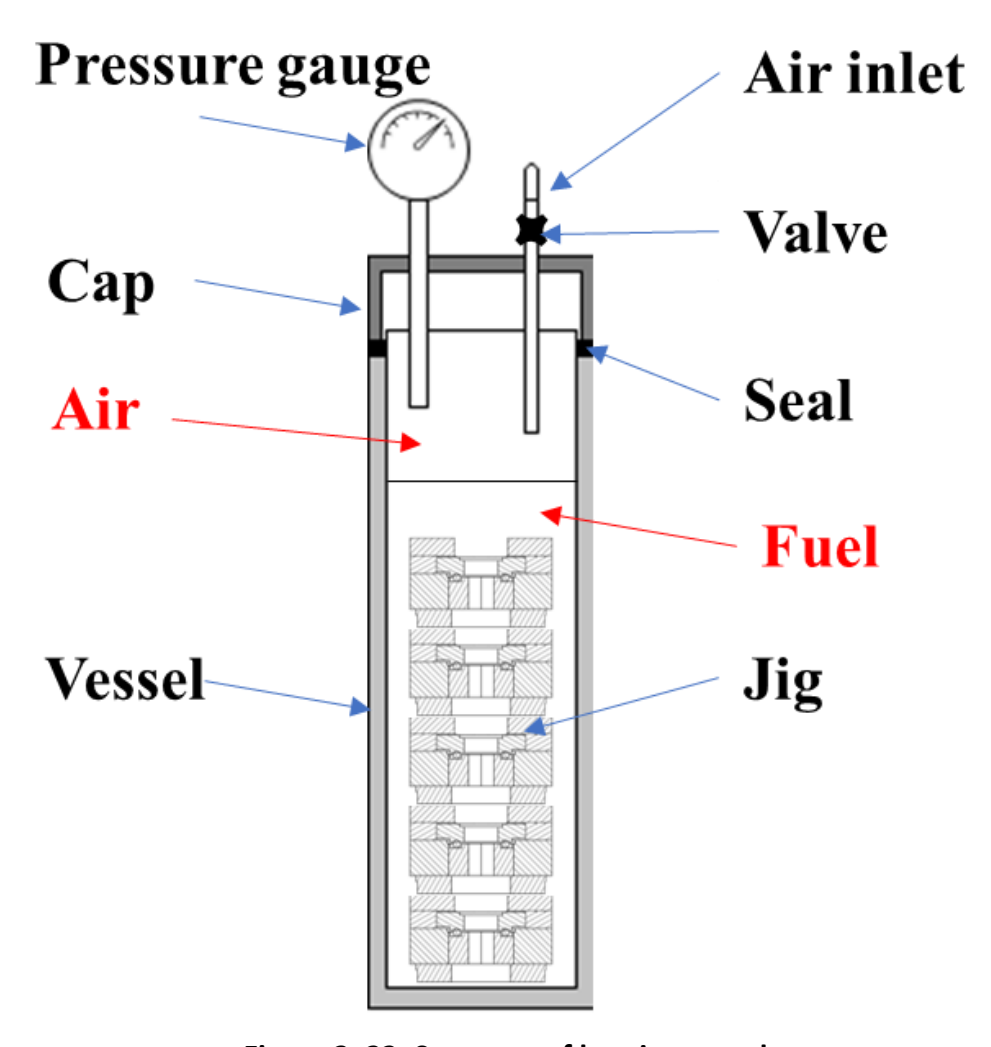


Figure 3. 22: Structure of heating vessel

An air inlet is mounted on the cap connects to the lab's compressed air system, delivering 10 bar compressed air. The 10-bar pressure used in this experiment is selected for convenience reasons, and this pressure is enough to prevent fuel vaporization at the selected temperature. Meanwhile, a pressure gauge is also equipped for pressure monitoring purposes.

In this experiment, a cell-ageing oven contains all heating vessels simultaneously and heats the fuel temperature as required. It is properly thermally insulated, with sufficient capacity for all vessels.

### 3.3.6 Compression strategy

A total of 25% compression in millimetres based on the CSD of test O-ring samples will be applied. Totally, three units are involved (C11 jigs, shims and Elastocon). The compression strategy shown in Figure 3. 23 has improved compared to past tests [117], [120]. C11 jigs with shims maintain consistent compression. Applying compression by using C11 jigs has many advantages. First, it substantially reduces the load of Elastocon and increases measurement accuracy since the sensor is extremely sensitive. Moreover, it provides mobility for the test sample across different facilities or test instruments, for example, between Elastocon and the oven.

In this set of experiments, 80% of total compression (20% of sample cross-section diameter) is provided by precompression. Generally, the precompression sources could be divided into two parts: C11 jig and Elastocon. Compression caused by C11 jigs is due to the groove carved on the jigs, the weight of the metal part and the shim applied inside the jigs. The groove on the jigs is designed to hold the O-ring samples during the test, and the depth of the groove will reduce the final compression after the jig is fully assembled. Therefore, a precise measurement of the thickness for each part, including

groove depth in the compression direction, is required to calculate the initial compression applied by the C11 jig. The overall compression strategy is shown in Figure 3. 23. Both C11 jig and internal shims proved constant compression (20% of CSD) even throughout the high temperature ageing process. A 5% compression was applied by Elastocon.

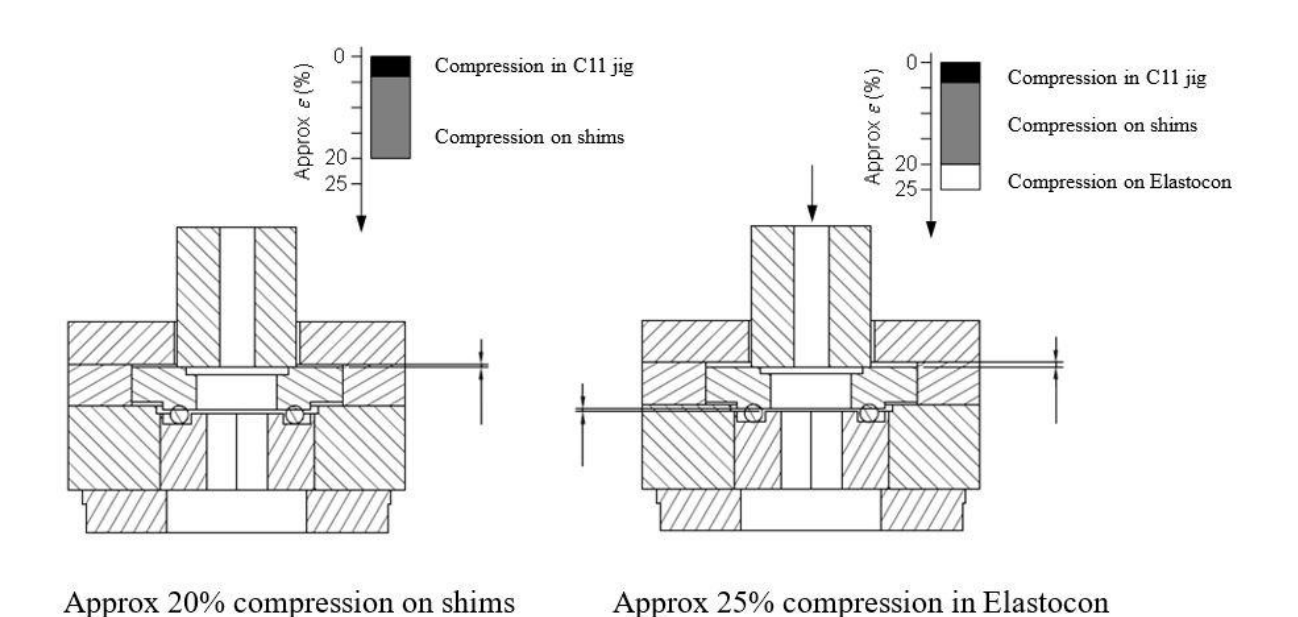


Figure 3. 23: Compression strategy in one jig. Reproduced from [119]

A dial gauge with ±0.01 mm accuracy measured the O-ring's cross-section diameter (CSD) before placing the seal in the test jig. All C11 parts were measured using a micrometre (±0.01 mm) and Vernier calliper. The formula to calculate the precompression due to C11 jigs is shown in Equation 3. 7.

**Precompression** 

= (Part 2 Thickness + CSD of Oring - Groove Thickness + Part 5 Thinckness) - (Part 3 Thickness + Part 4 Thickness)

Equation 3.7

After determining the value of the pre-compression due to the C11 jigs, a series of shims was added to achieve 20% of total compression. Once the jigs were placed into the stress relaxation unit, an additional 5% compression was added by this unit, providing a total compression of 25%. Thus, the O-ring seal is continuously cycled between 25% compression in the rig and 20% in the high-temperature ageing treatment. The jig will not be opened during the entire test campaign.

The detailed measurements and calculation of pre-compression are shown in Table 3. 7 and Table 3. 8 for the final test, Set 6 and Set 7, respectively.

Table 3. 7: Pre-compression of Set 6

| Jig Code  | A15(FS) | A27(FKM7282) | AA(NI)  | R(FKM7276) | P(FKM) |
|---|---------|--------------|---------|------------|--------|
| Average CSD (mm)                                | 2.375   | 2.45         | 2.413   | 2.487      | 2.472  |
| Pre-compression (mm)                            | 0.075   | 0.13         | 0.083   | 0.177      | 0.142  |
| 20%CSD (mm)                                     | 0.475   | 0.49         | 0.4826  | 0.4974     | 0.4944 |
| Compression<br>required to reach<br>25% CSD(mm) | 0.4     | 0.36         | 0.3996  | 0.3204     | 0.3524 |
| Shim (mm)                                       | 0.4     | 0.35         | 0.4     | 0.325      | 0.35   |
| 5% CSD (mm)                                     | 0.11875 | 0.1225       | 0.12065 | 0.12435    | 0.1236 |
| Compression from Elastocon (mm)                 | 0.12    | 0.1325       | 0.12    | 0.12       | 0.125  |

Table 3. 8: Pre-compression of Set 7

| Jig Code                                   | A25(FS) | G(FKM7287) | A23<br>(NI) | N(FKM7276) | M(FKM)  |
|--|---------|------------|-------------|------------|---------|
| Average CSD (mm)                           | 2.375   | 2.453      | 2.412       | 2.581      | 2.467   |
| Pre-compression (mm)                       | 0.055   | 0.133      | 0.092       | 0.198      | 0.147   |
| 20%CSD (mm)                                | 0.475   | 0.4906     | 0.4824      | 0.5036     | 0.4934  |
| Compression required to reach 25% CSD (mm) | 0.42    | 0.3576     | 0.3904      | 0.3056     | 0.3464  |
| Shim (mm)                                  | 0.425   | 0.35       | 0.4         | 0.3        | 0.35    |
| 5% CSD (mm)                                | 0.11875 | 0.12265    | 0.1206      | 0.1259     | 0.12335 |
| Compression from Elastocon (mm)            | 0.11375 | 0.11505    | 0.111       | 0.1315     | 0.11975 |

# 3.3.7 Heating treatment and the ageing process

As mentioned, establishing a test configuration with the ability to investigate seal performance across various fuels, O-ring types, and temperatures is the primary objective of this experiment. Therefore, studying the sealing behaviour of O-rings under high temperatures is essential. The heating treatment in this experiment is mainly performed as an ageing process to shorten the experimental time. However, it could still provide information on the high-temperature impact of different O-ring materials.

The temperature is set as close to the physical limit of each O-ring material to maximise the ageing performance. However, considering the difference in O-ring material, different temperatures are applied. For fluorocarbon (FKM) and fluorosilicate (FS), the ageing temperature is  $180\,^{\circ}\mathrm{C}$ ; for nitrile, the ageing temperature is  $110\,^{\circ}\mathrm{C}$ . These ageing temperatures are carefully selected based on material properties, following consultations and recommendations from researchers at Rolls-Royce who also

provided some test O-ring samples. These temperatures enable maximum accelerated ageing without damaging the samples themselves

# 3.3.8 Low-temperature treatment

The low-temperature treatment is performed to assess the O-ring material's physical limit and simulate the in-service condition as closely as possible. During the treatment, the minimum temperature in this experiment is set as -40°C. This temperature was selected based on the chiller's cooling capacity and potential real-world operating conditions. The general experimental setup for each sample is identical to that used in the high-temperature treatment.

# 3.4 Unforeseen obstacles and real force majeure

It should be stated that the research was heavily affected by the flood that occurred at Sheffield in 2019 and the following COVID-19 pandemic as well. Due to the flood, most of the test equipment in LCCC was either damaged or completely destroyed. The lockdown during the pandemic made recovery efforts more difficult and some testing rigs were deemed unrecoverable. Details of the impact on each part of this research will be presented below

First, the emission tests in the Tay rig were not fully completed according to the original plan. Instead of 15 aromatic species, 9 were tested for an 8% vol. fuel blend, and 14 were tested for high concertation (18% vol.). Fortunately, the high aromatic groups are the most important as they are close to the aromatic concentration in conventional jet fuels. Thus, since most 18% fuel blends (covering the majority of aromatic species) were tested, the flood's impact on the study's scientific value (investigating how different aromatic species and fuel properties affect emissions) was minimal.

Second, there are several methods to investigate the chemical reactions for soot generation. One of the most common ways is analysing the chemical composition of exhaust from different combusted fuel blends. The original plan was to collect soot from all candidate fuel blends and investigate the soot composition. However, the plan was changed due to the uncontrollable natural hazard - the flood mentioned previously. Instead of analysing actual soot formation, using software to simulate the chemistry was pursued. simulation model of the Tay combustor was developed using CHEMKIN-Pro. The scope of the model could represent Tay combustor used in the experiment and identify potential soot tracers for future emission predictions and enable soot production forecasting.

It should be noted that due to missing dimensional information for the original Tay combustor used in the experiment, a model Tay combustor is used instead for the simulation work. The exact flow behaviour might be different between the actual combustor and the model Tay combustor. The real Tay combustor has more dilution holes which should lead to a lower exit temperature. Moreover, a relatively large igniter is also required to be inserted into the combustor body, and the geometry of the igniter could have some influence on flow behaviour. In addition, a more refined fuel pattern is expected in the real Tay combustor as it uses an aviation-grade fuel injector. Despite all these differences between the two combustors, the downscaled model Tay combustor is still the most appropriate option available in the public domain to serve as the basis for the simulation model.

Finally, the flood disrupted the progress of O-ring tests in Elastocon rig. The entire rig was destroyed during this period, together with O-ring samples. This situation halted further investigation into different aromatics, fuels and O-ring materials. However, the general setup of the rig has been established before the flood, and enough data were preserved to present this new, more realistic experimental configuration.

# 4. Emissions characteristics of a gas turbine combustor and alternative fuels

# 4.1 Introduction

Choosing suitable jet fuel formulations is always the major topic for gas turbine engines to achieve better performance and lower emissions. As discussed in the literature review, due to the rapid growth of aviation transport demands, the environmental impact of jet emissions has increased substantially, promoting the trend of applying alternative jet fuel.

Alternative jet fuels used here are synthetic fuels that require appropriate chemical formulations to fit into the gas turbine combustion system without affecting its performance. Compared with the chemical complexity of fossil fuel, the composition of alternative jet fuels is simpler due to its unique manufacturing pathways. In the alternative jet fuels formulation, aromatic concentration is usually extremely low and even zero. It has been proven that the primary cause of emissions is the aromatic compounds in jet fuel [46]. However, aromatics are essential in fuel formulations since they promote the sealing performance of elastomers in fuel systems.

Therefore, to use alternative jet fuels in a gas turbine engine, aromatic species must be added to its fuel formula, either by blending with conventional fuel or adding aromatic compounds. However, many different aromatic species exist in jet fuel, and they have widely molecular structures and properties in both chemical and physical properties. Therefore, it is essential to investigate the combustion behaviour of different aromatics regarding emission production ability.

This investigation provides a good approach for evaluating a wide selection of aromatic species with different concentrations in an actual gas turbine combustor regarding emissions, which has never been done before. This test campaign blended selected aromatics with a base fuel in two categories (8% vol. and 18% vol.). A fully established and tested combustion rig was used to burn these blends. Emissions from the exhaust are delivered to emission instruments for further analysis.

# 4.3 Result and Discussion

The results of this experimental campaign are elaborated in this section. These results present a complete investigation of the impact on PM and gaseous emissions from introducing different aromatics. PM and gaseous emissions will be discussed separately for better clarity.

All results indicated that the different aromatics behave differently regarding PM production. Meanwhile, fuel properties might play a significant role in PM production, especially fuel blend density, which showed a relatively high correlation toward PM production. However, this observation should be treated with extra caution since it might be different in other combustion environments. In addition to PM emissions, the impact on gaseous emissions is also presented in this section. The common assumption is that aromatics will not affect gaseous emissions, especially NOx, which is theoretically determined to the combustion residence time, reaction rate and mixing rate [121]. However, adding different aromatics into the fuel blend should alter overall fuel properties, and NOx emission production could also be affected accordingly. Therefore, analysing gaseous emissions results still has its value in terms of aromatic species.

Several statistical methods were selected in this section to help understand emission results, including regression analysis, Pearson correlation coefficient (PCC), coefficient of determination (COD) and 95% confidence.

Linear regression analysis was employed, assuming a linear relationship between variables (best-fit line), calculated using the least squares method. Detailed calculations are presented in the following equations.

$$y = mx + b$$

Equation 4. 1

$$m = \frac{\sum (x - \bar{x})(y - \bar{y})}{\sum (x - \bar{x})^2}$$

Equation 4. 2

$$b = \bar{y} - m\bar{x}$$

Equation 4.3

Where x and y refer to the x-variable and y-variable respectively.  $\bar{x}$  and  $\bar{y}$  refer to sample means.

The Coefficient of Determination (R²) method is using in this thesis. Similar method also used in other literature [64]. It is statistical method typically associated with linear regression to determine the correlation level between a dataset and its corresponding best-fit line. Value of R² ranges from 0 to 1, and a higher value means best-fit line better represents the dataset statistically. The equation to calculate r² is presented below

$$R^2 = \frac{sstotal - ssresid}{sstotal}$$

Equation 4.4

Where ssresid refer to residual sum of squares, sstotal refer to the total sum of squares.

PCC is another static method that measured linear coefficient between two datasets. The value ranges from -1 to 1, and a higher value indicated a stronger correlation. It is used in this chapter to assist the understanding of two variables.

It should be emphasized that these methods are ultimately statistical methods. They might not accurately reflect the actual relationship between two variables. Since emissions are affected by a lot of factors, variables with good correlation don't necessarily represent emission production.

#### 4.3.2 PM emissions

With findings from two combustion rigs in the previous section, the overall results collected from the gas turbine combustor rig are presented individually with extra information for better understanding. Figure 4. 1 shows the general view of PM data collected from The Tay rig using LII. Both fuel blend groups (8% vol. and 18% vol. aromatic) are presented with their respective aromatic species.

The result in Figure 4. 1 was normalized to reference fuel (Jet A-1) using Equation 4. 5, in order to give a rough comparison in emissions. Similar method was also used in another emissions study[95].

$$\textit{Change\%} = \frac{\textit{Result}_{\textit{blend}} - \textit{Result}_{\textit{Jet A}-1}}{\textit{Result}_{\textit{Jet A}-1}} * 100\%$$

Equation 4.5

A positive value indicates the emission production is worse than Jet A-1, and a negative value represent the advantage in emission reduction compared to Jet A-1.

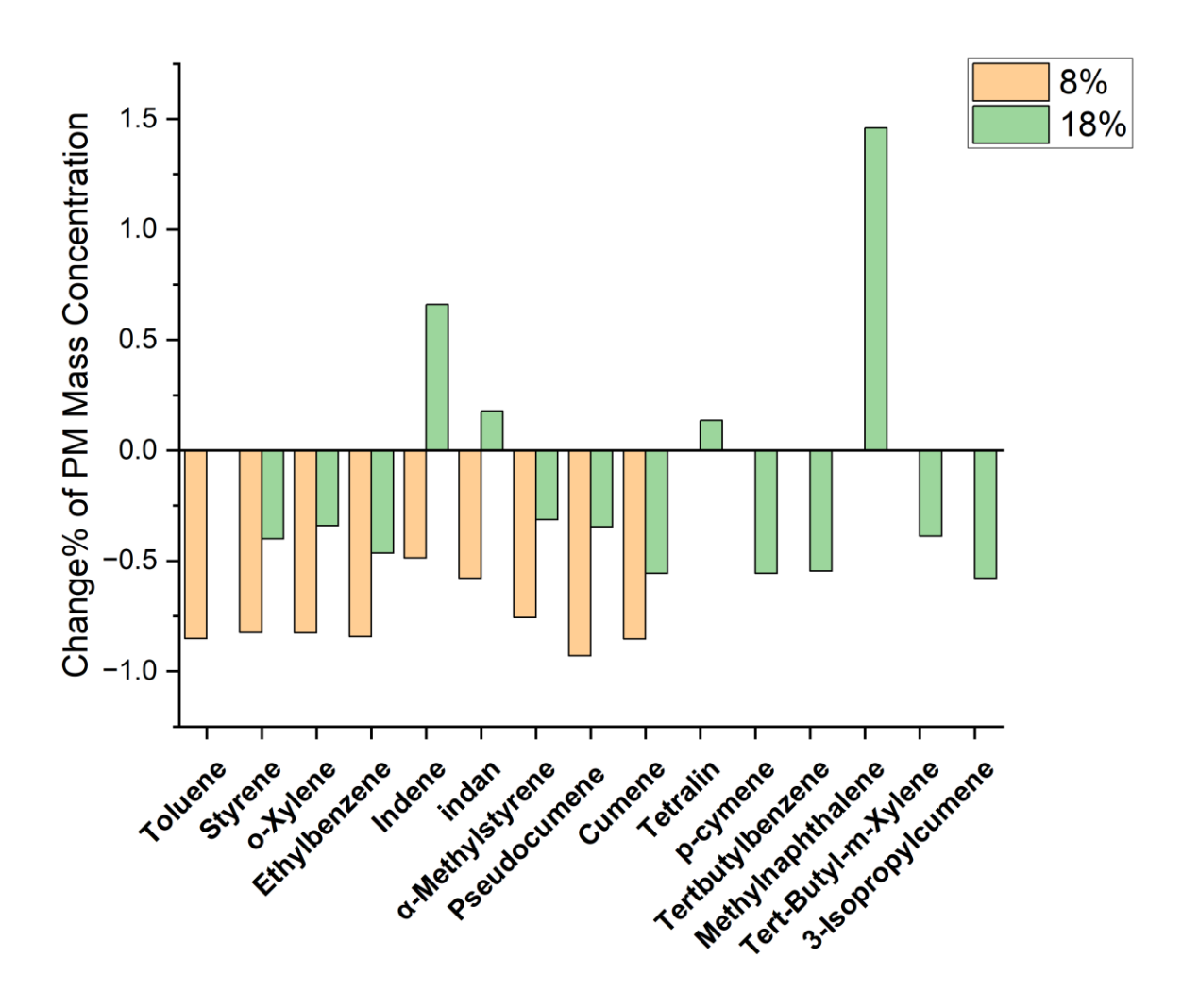


Figure 4. 1: Effect of aromatic species on PM mass concentration

Overall, 18% vol. aromatic blends produce more PM than 8% vol. aromatic blends, confirming previous findings that high aromatic concentration promotes PM production [122]. On average, by increasing 10% vol. aromatic concertation in blends formula, final PM production will rise approximately 3.22 times higher. One exception, Pseudocumene, is 9.31 times increase compared to low aromatic concentration blends. This phenomenon may occur because pseudocumene's molecular structure with more methyl branches increase decomposition difficulty during combustion, potentially promoting incomplete combustion and higher PM production.

Moreover, from these data, it could be concluded that the relationship between PM production and aromatic concentration is not a simple 1:1 linear relationship. The PM will increase dramatically for some species by slightly changing the fuel formulation's aromatic concentration. However, the accurate influence on PM production by simply increasing the concentration of individual aromatic species needs much further investigation.

In addition, the difference in PM intensity among aromatic species is shown in the 18% vol. aromatic fuel blends group: methylnaphthalene has the highest PM production (0.455 mg/m³), followed by indene and indane. In contrast, cumene and p-cumene have the lowest PM production (0.082 mg/m³). The results of 8% vol. aromatic fuel blends are not complete. However, it is still apparent that, even in this low aromatic concentration group, the PM production of indene and indane is noticeably higher than others. Meanwhile, pseudocumene produces the lowest PM intensity in 8% vol. aromatic fuel blends, and this phenomenon is not found in high aromatic concentration fuel blends.

Compared with emissions from Jet A-1(18.66% vol. aromatic), Most fuel blends (18% vol. aromatic) produce lower PM. However, indene, indane, tetralin, and methylnaphthalene show significantly higher PM than Jet A-1. This phenomenon indicates that at similar aromatic concentrations, some aromatics dramatically increase PM production (even exceeding conventional jet fuel levels) suggesting these species share some common properties. Previous research typically attributes these properties to molecular weight or hydrogen content percentage.

Therefore, this thesis will examine how aromatic properties (molecular weight, H/C ratio, and density) affect emissions.

# 4.3.2.1 Molecular weight

Logically, molecular weight should affect PM production significantly or at least have some connection because large molecules are usually difficult to decompose during combustion. Figure 4. 2 presents the relationship between molecular weight and PM production. The aromatic species with the highest molecular weight in this test campaign are tert-butyl-m-xylene and 3-isopropylcumene. However, according to Figure 4. 2, the highest PM production is methylnaphthalene, which has a molecular weight of 142.2. In addition, in Figure 4. 2, the PM intensity starts to diverge along with the molecular weight increase, indicating the correlation between molecular weight and PM production may be weak.

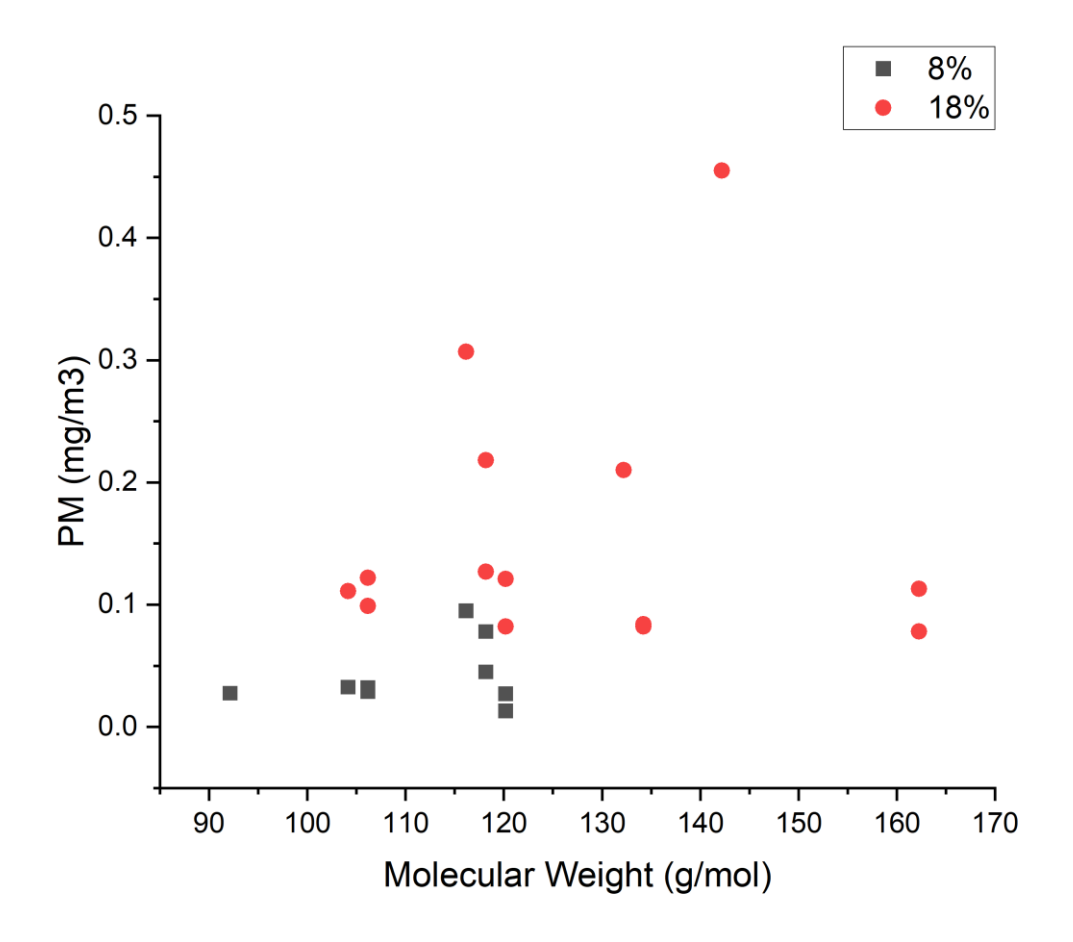


Figure 4. 2: Molecular weight impact on PM

This finding could be due to the low representativeness of molecular weight for molecular structure. As previously suggested, PM production is highly correlated with the aromatic structure. The more complex the molecular structure, the more difficult it is to burn completely, increasing PM production. Meanwhile, molecular weight does not entirely reflect structural differences among molecules. It simply represents the combination of the number of carbon and hydrogen atoms. The molecular structure, such as rings or branches is not captured by molecular weight yet significantly affects PM production. For example, high molecular weight may indicate a long-chain paraffin, which have negligible contributions on PM production.

# 4.3.2.2 H/C ratio / H%

The correlation between the H/C ratio and PM production is shown in Figure 4. 3. Trend lines are generated for both aromatic fuel blends. In some research, the H/C ratio is used to predict PM production. A high H/C ratio usually indicates low PM production. The effectiveness of using the H/C ratio on PM prediction is valid for comparing different conventional jet fuels. Due to the complex composition of the fuel blends, a high H/C ratio will mean fewer carbon atoms available for PM formation. However, when considering the impact of different aromatic blends with the same base fuel, the H/C ratio method becomes unreliable. Different aromatic species can have the same H/C ratio but produce different PM outputs.

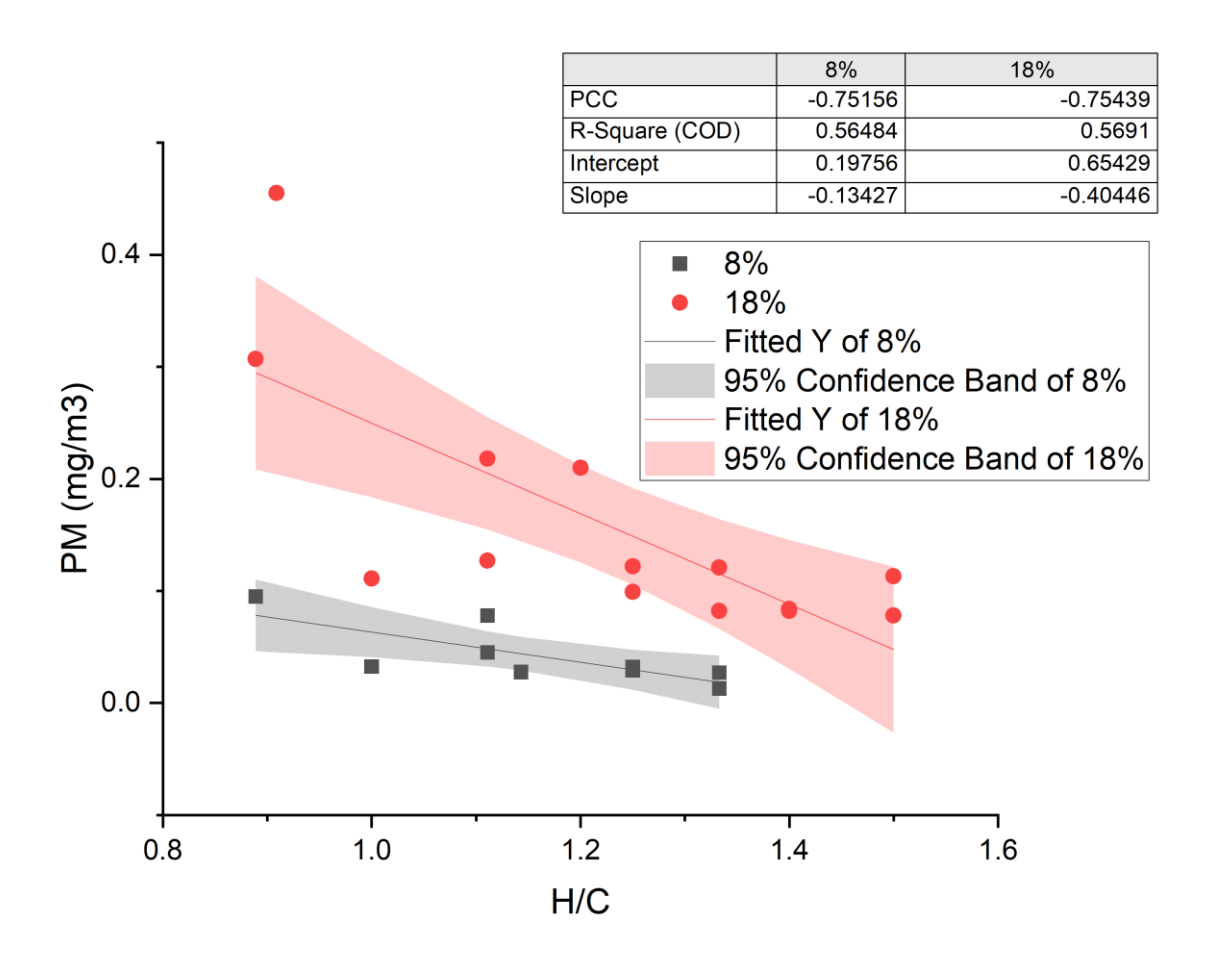


Figure 4. 3: H/C ratio impact on PM

The highest H/C ratio occurs in p-cymene and tert-butylbenzene fuel blends, and generally PM production decreases as H/C ratio increases, shown in Figure 4. 3. This occurs because aromatics with lower H/C ratios contain fewer carbon atoms (the primary sources of PM), resulting in lower PM production. Nevertheless, the relation between the H/C ratio and PM is not linear. A higher H/C ratio will have a minor effect on decreasing PM production. Interestingly, although methylnaphthalene has a recognizably higher H/C ratio than indene, its PM production is also higher, invalidating the H/C ratio as a PM prediction factor.

R<sup>2</sup> factors for two aromatic concentration fuel blends are also present in the figure to represent the correlation between the H/C ratio and PM sensitivity. In Figure 4. 3, R<sup>2</sup> values are 0.565 and 0.569 for the 8% vol. and 18% vol. aromatic fuel blend. The R<sup>2</sup>

value is low, which suggests a weak connection between the H/C ratio and PM production and the accuracy of predicting PM production using the H/C ratio is also low.

These findings indicate the drawbacks of using the H/C ratio as the reference for PM prediction. It could also be described from the perspective of molecular structure. Methylnaphthalene has two complete benzene rings, which are difficult to break during combustion, compared with indene, which only has one full benzene ring. Therefore, in theory, the methylnaphthalene fuel blend could cause incomplete combustion, and the partially decomposed molecule might contain more carbon ring structure, which are the preliminary forms of PM. However, the H/C ratio cannot represent the molecular structure completely. The ring structure difference between methylnaphthalene and indene could not be distinguished solely by their H/C ratio.

But in general, as mentioned, in conventional jet fuel, the H/C ratio has its value because conventional jet fuel contains many different components. Aromatics are only a tiny part. In this situation, the H/C ratio usually represents the energy efficiency of the fuel.

#### 4.3.2.3 Density

Fuel density is also an essential factor in terms of PM prediction. Figure 4. 4 compares the blend density with PM production. The x-axis represents the global density calculated from the concentration of aromatics and NP1014 used to form the fuel blend. The highest blend density is 18% vol. methylnaphthalene fuel blend, which also has the highest PM production.

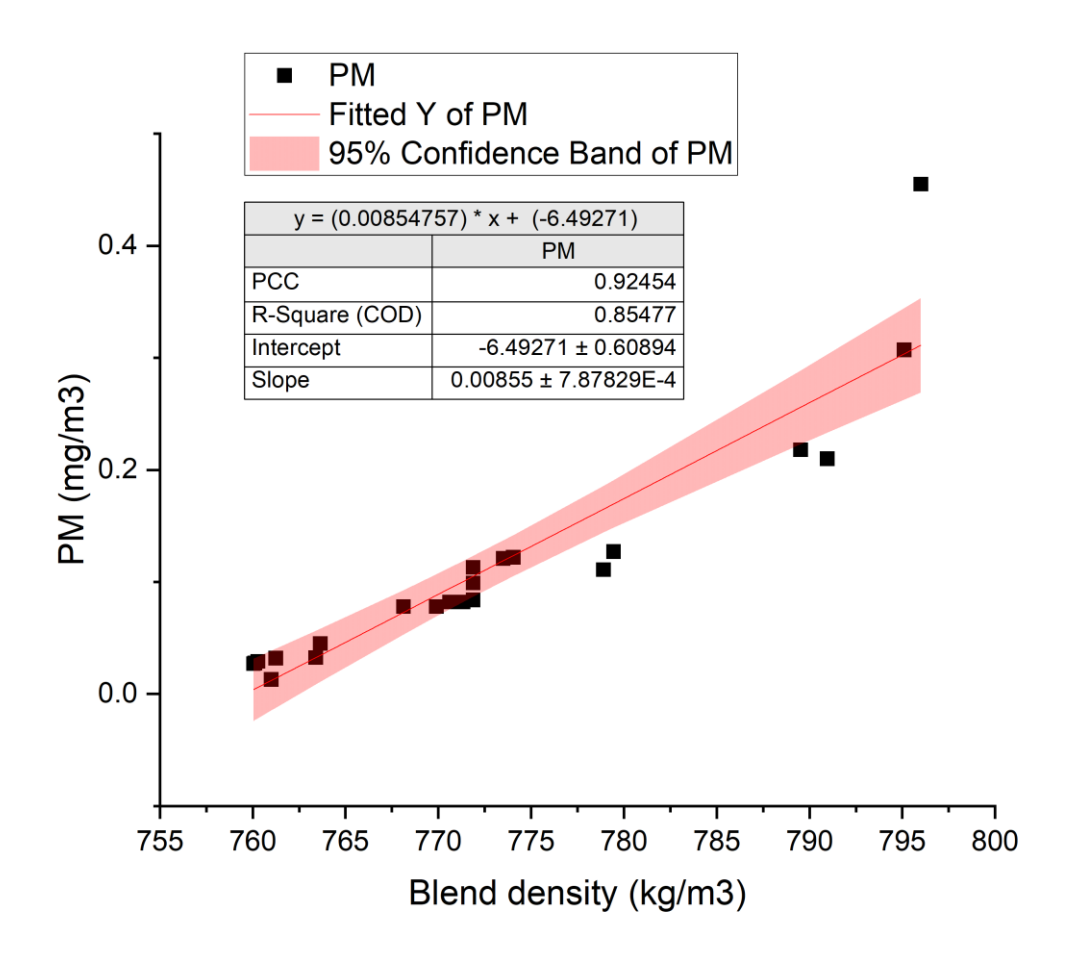


Figure 4. 4: Blend density impact on PM production

In general, according to Figure 4. 4, there is a relatively strong relation between density and PM production since data points are quite clustered around the best-fit line. The R<sup>2</sup> and PCC values for the trend line are 0.854 and 0.925 respectively, indicating a strong correlation from a statistical viewpoint. Unlike the H/C, the density has more connections to the aromatic structure. All aromatics containing two closed carbon rings show high PM production and blend density. In other words, fuel density might predict PM production more accurately. Moreover, longer residence times are required to completely combusted the fuel blends with high density, since they contain more fuel contents within the same volume. Therefore, high density fuel blends can promote incomplete combustion and increase PM production,

It should be pointed out that some fuel blends have the same density but produce different PM mass concentrations. This finding means density could not 100% represent the difference between aromatics but might be a good reference for PM prediction since the R<sup>2</sup> value is noticeably high. Moreover, different to the fuel blends used in this thesis, commercial fuels usually have more complex fuel formulations, and their properties cannot be described by density only. Multiple fuel properties are necessary to be considered together to predict the soot emissions.

The correlation between the H/C ratio and density is present in Figure 4. 5.

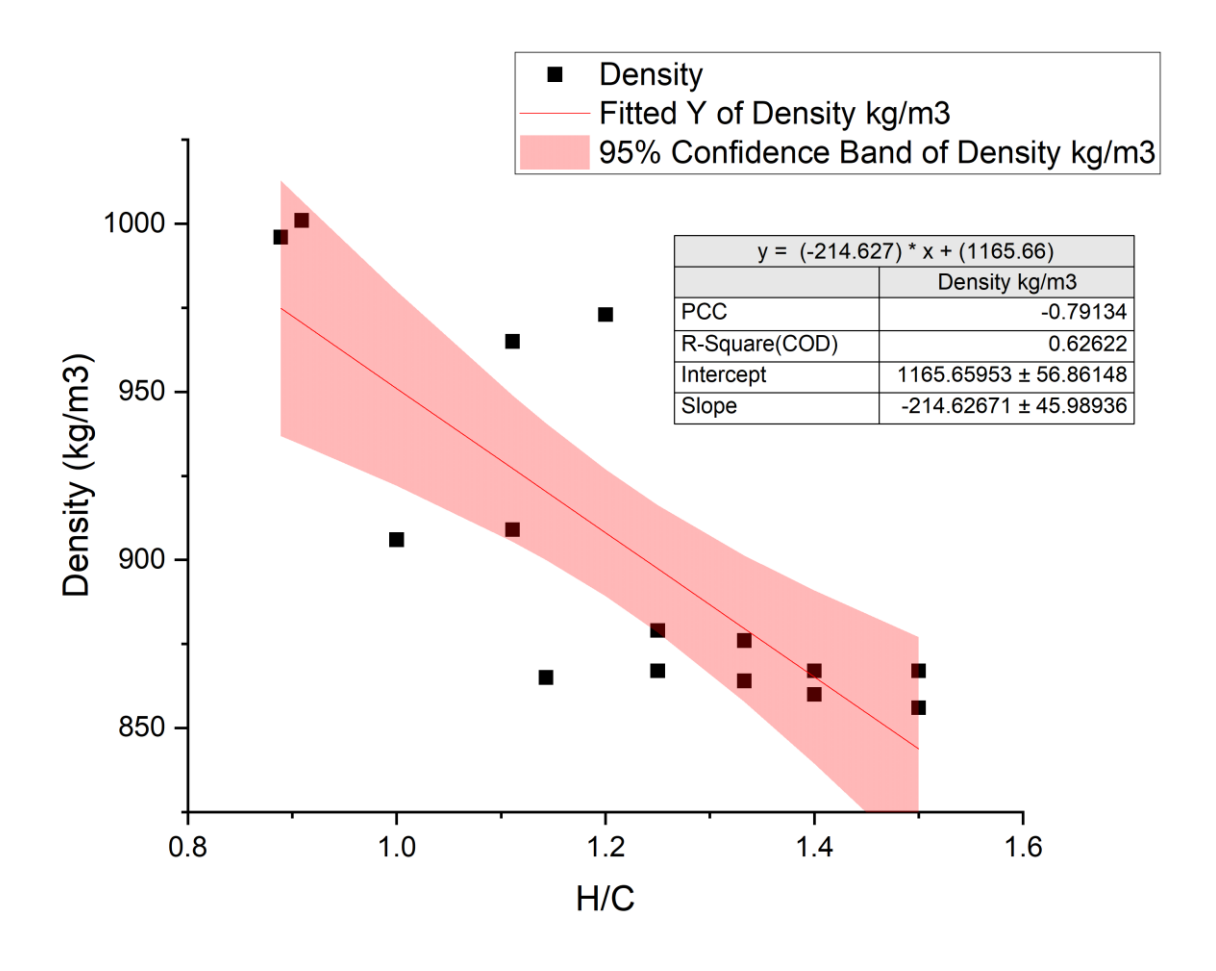


Figure 4. 5: Correlation between H/C ratio and density

Figure 4. 5 indicates the correlation between density and H/C ratio. In general, it shows that density decreases with increasing H/C ratio. The R<sup>2</sup> value is 0.626, which is quite weak, suggests the correlation might not be very strong.

#### 4.3.2.4 Molecular structure

It could be concluded that PM production is highly sensitive to diaromatic compounds with two complete closed carbon rings. These produce significantly higher PM than monoaromatic at equivalent concentrations. Therefore, depending on the PM production, candidate aromatics could be categorized based on their carbon ring structure. An alicyclic compound is a molecule that is either saturated or unsaturated but has no aromatic character. Typically, an alicyclic compound attached to an aromatic significantly promotes the formation of PM or soot. The PM production for indene is noticeably higher than for indane and tetralin because indene is a benzene ring fused with a cyclopentene ring. The presence of a double bond makes the cyclopentene ring more resistant to decomposition and potentially provides a shortcut in the nucleation process, significantly promoting soot production.

# 4.3.1 Comparison of gas turbine combustor and IC engine

Public awareness [44] of aromatics is that they significantly increase PM emissions. Still, some research indicates that particular aromatic species have a greater influence on PM production more than others [41]. Therefore, it is reasonable to predict that some aromatic species will always produce more PM than others.

It is interesting that the trend of different PM production measured in the Tay rig is similar to the trend measured in the IC rig as described in Chapter 2, Figure 2. 1. These two rigs used the same aromatic additive but different base fuel and aromatic concentrations. High aromatic concentration (18% vol.) fuel blends were used for the gas turbine

combustor rig to enhance PM production for better presentation. The fuel blends used in the Tay rig contain only aromatic and Banner NP1014, but the IC rig uses different blend formulas that contain 15% aromatic by mass and low aromatic diesel as base fuel.

Although different base fuel was used in these two rigs, the aromatic species added to the fuel blend are the same, meaning that the same aromatic species might have the same overall behaviour in different combustors. PM from IC engines was significantly higher than that from gas turbine combustors due to the nature of the combustion process.

It should be pointed out that the length of the sample line is different for these two experimental rigs, which will affect the final emissions intensity slightly in theory. However, according to the sample collection system's working principles and experience, this difference is tiny. Moreover, PM emissions from IC rigs will always be significantly higher than those from gas turbine combustor rigs. In conclusion, these slight differences could be ignored, and the results will not be affected.

According to results from both rigs, PM production is higher for IC engine rigs than for gas turbine combustor rigs, as predicted, due to the nature of IC engines. Moreover, the IC engine used diesel as base fuel, significantly boosting PM production compared with NP1014. However, it is noticeable that the overall PM trend of different aromatics for the two test rigs is similar. For example, both rigs show that methylnaphthalene produces the highest PM, followed by indene, indane and tetralin. Moreover, PM production for these four aromatic species blends is higher than the rest. These phenomena support the previous assumption that, besides the combustion environment, aromatic species will significantly affect PM production. Therefore, it is essential to distinguish the high PM production aromatic species for better alternative jet fuels formulations and emissions reduction purposes.

#### 4.3.3 Gaseous emission

This section will discuss the aromatic influence on gaseous emissions. Data for both PM and gaseous emissions were taken simultaneously during the test campaign to eliminate experimental errors. As mentioned, by adding different aromatics into the blend, fuel properties change, affecting gaseous emissions. This is particularly true for CO, which is highly tied to incomplete combustion. Moreover, PM intensity is also correlated with incomplete combustion. Therefore, it is predicted that there should be some correlations between gaseous emissions, PM and aromatic. These correlations are lack of description in the past.

# 4.3.3.1 Unburned hydrocarbon (UHC)

As mentioned, similar to PM emissions, it is suspected that different aromatic species could affect gaseous emissions differently. UHC refers to the hydrocarbons that are not fully consumed during the combustion process. Hence, it could potentially indicate the degree of incomplete combustion. Moreover, a correlation between PM and UHC is expected since both are heavily affected by combustion conditions. The results of UHC emissions and aromatic species are presented in Figure 4. 6. The x-axis represents different aromatics listed according to their molecular weight (low to high).

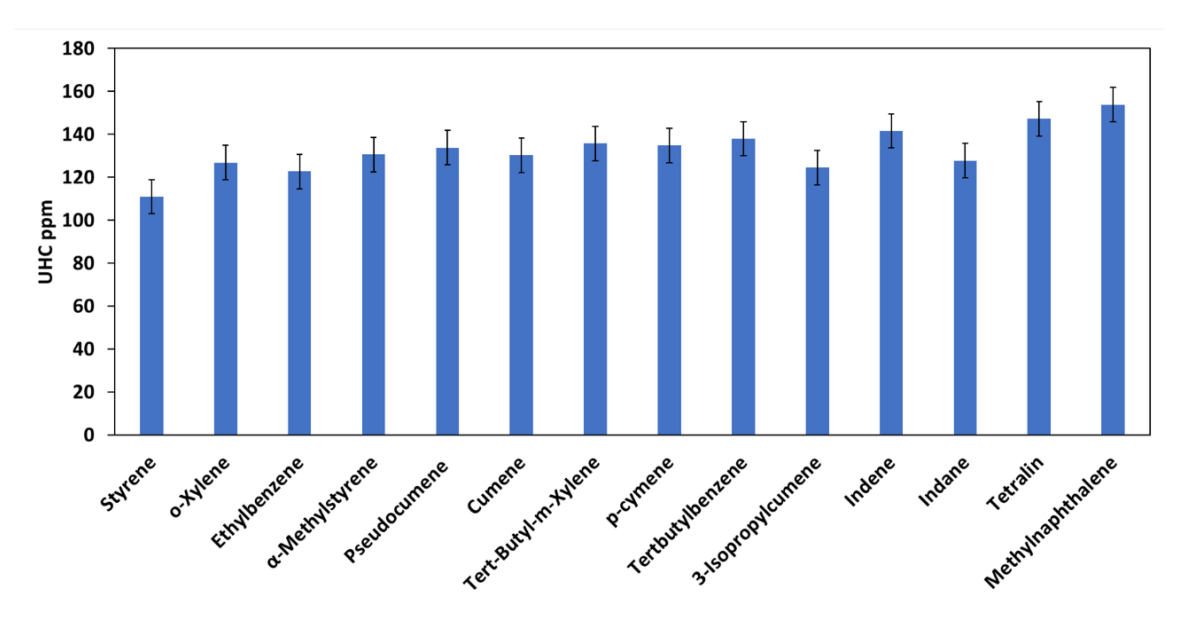


Figure 4. 6: Aromatics impact on UHC

Figure 4. 6 indicates that UHC production is affected by different aromatic species. Overall, it does not show a strong difference between aromatic species. In this figure, styrene produces less UHC, and methylnaphthalene produces the most UHC. Tetralin and indene also show relatively higher UHC intensities than other aromatics. Although the difference is not as significant as expected, this result still shows some interesting information.

Most polycyclic aromatics generally have higher UHC than alkylbenzene aromatics in UHC emission, meaning UHC is also tied to aromatic structure. Since polycyclic aromatics have more complex structures, which makes it difficult to decomposition, this phenomenon has also been found in PM production, as discussed previously. The only exception is indane, which appears to have relatively low UHC emissions compared to alkylbenzenes.

Moreover, since UHC and PM are both strongly correlated with incomplete combustion, it could be predicted that a correlation exists between them. Therefore, the relationship between PM and UHC is investigated and presented in Figure 4. 7.

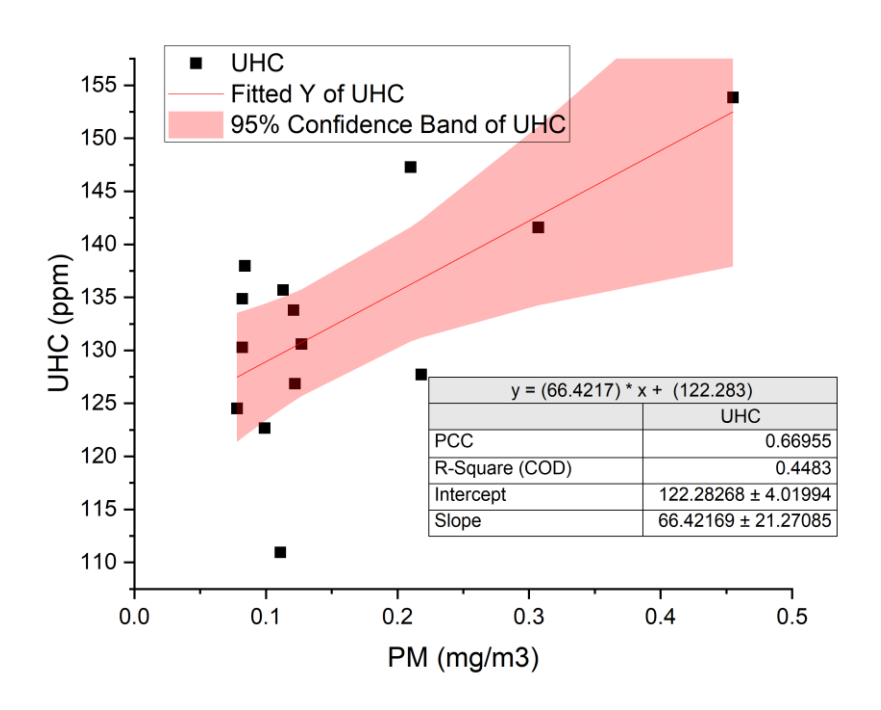
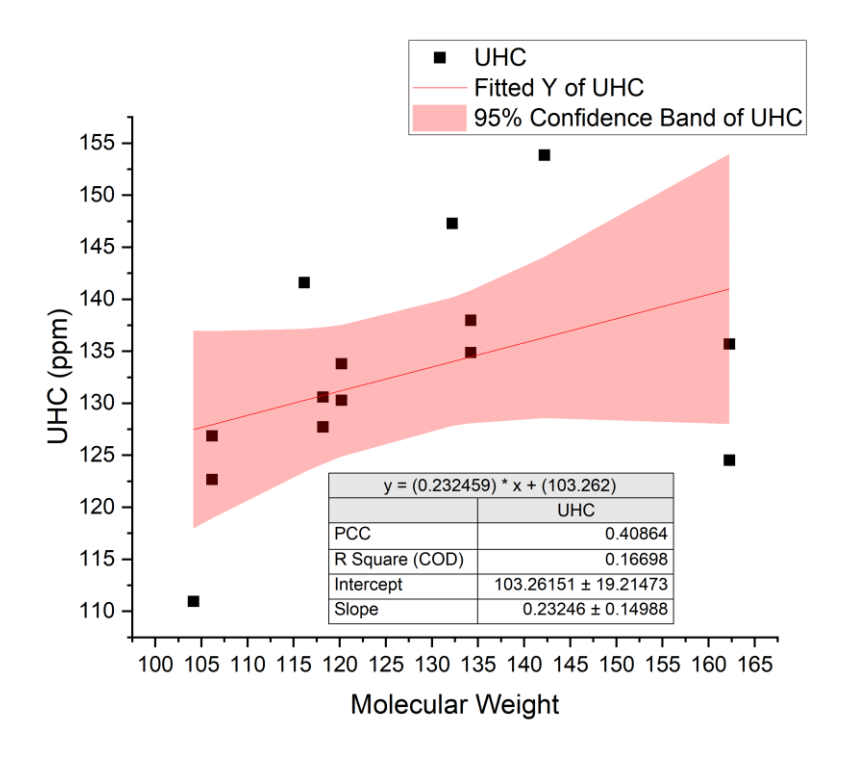


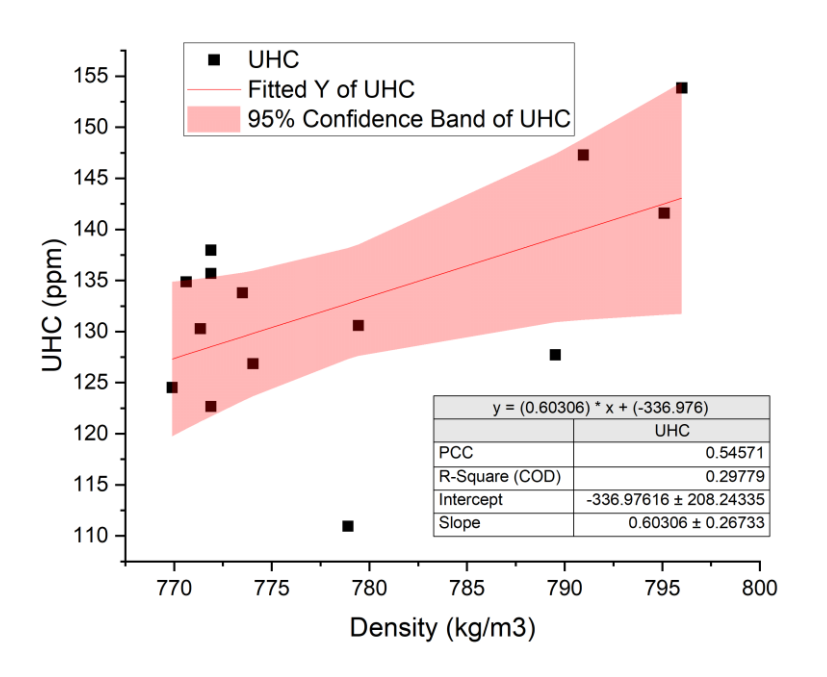
Figure 4. 7: Correlation between PM and UHC

According to Figure 4. 7, the overall correlation between PM and UHC is weak, with an R<sup>2</sup> value of 0.448. Although the influence is not as strong as predicted, it still demonstrates that aromatic species have some impact on UHC. Moreover, this finding could be explained through the combustion pathway. In general, large hydrocarbons will decompose into small molecules during combustion. The scale of these partially decomposed hydrocarbons might be too small to be classified and detected as UHC but still large enough to serve as effective nucleation sites for PM formation. Further investigation is necessary to verify this hypothesis.

In addition, incomplete combustion could also be due to the difference in overall fuel properties. Therefore, Figure 4. 8 illustrates the correlations between UHC and some essential fuel properties.



(a)



(b)

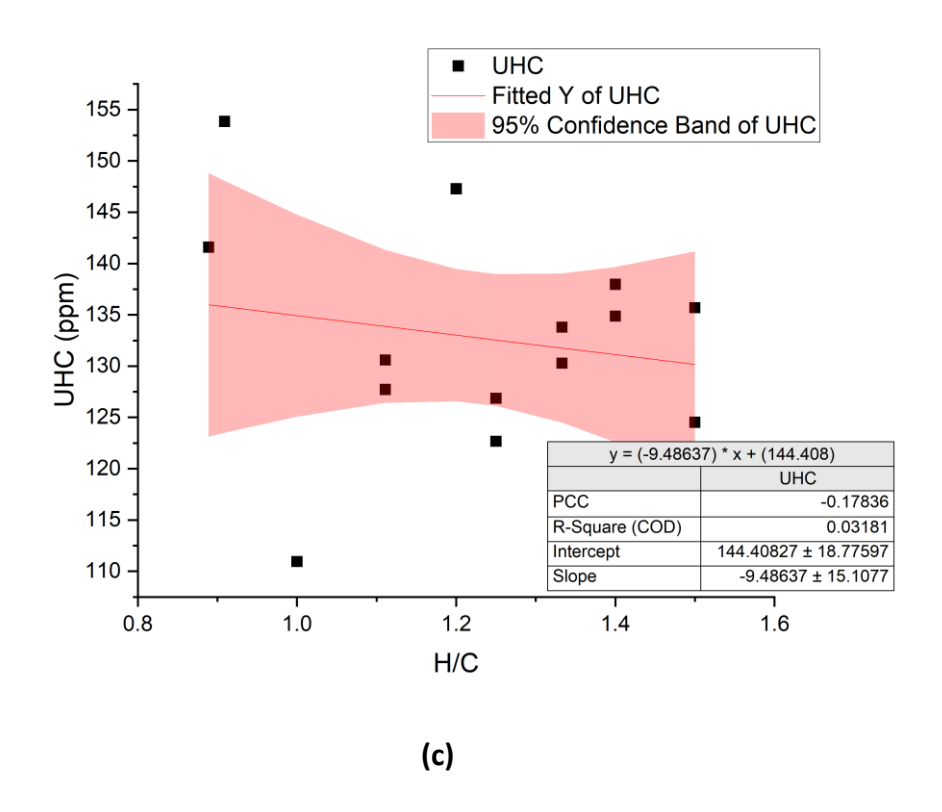


Figure 4. 8: Corrlation between molecular weight and UHC, (b) Corrlation between Density UHC, (c) Corrlation between H/C ratio UHC.

Generally speaking, according to Figure 4. 8, all three basic fuel properties have only minimal effects on UHC emissions, especially for the H/C ratio. It could be concluded that the influence on UHC is limited for these three fuel properties. However, further investigation is required since the range of fuel properties discussed here is limited. Other fuel properties, such as viscosity, have shown that they can significantly influence spray patterns and fuel mixture conditions, thereby impacting combustion and PM generation.

#### 4.3.3.2 CO

CO emissions result from incomplete combustion or poor fuel-air mixing. The correlation between CO emissions and aromatic species is presented in Figure 4. 9.

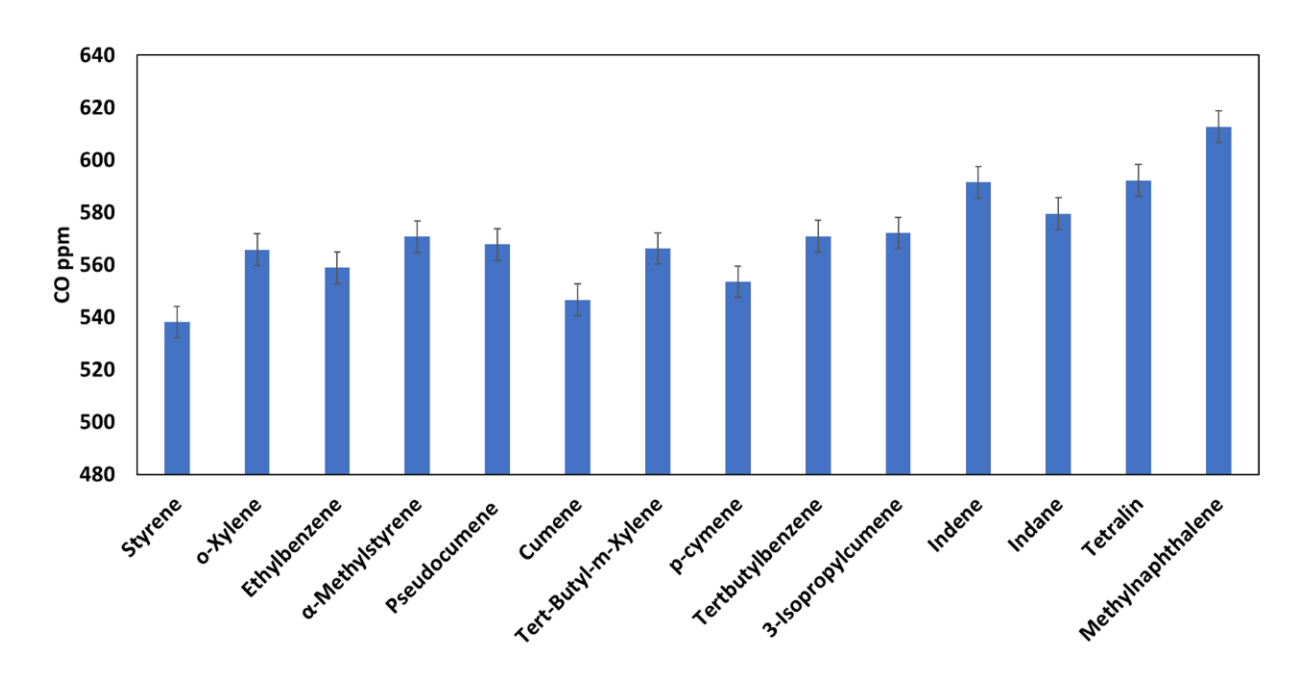


Figure 4. 9: Aromatics impact on CO

According to Figure 4. 9, different aromatics affect CO emissions. Moreover, polycyclic aromatics generally produce more CO emissions than alkylbenzenes. The same theory could explain this phenomenon for PM emissions. Polycyclic aromatics have more ring structures than alkylbenzenes, making them harder to combust and producing poor spray droplets.

PM, as mentioned, also has a strong connection with incomplete combustion. Therefore, a correlation might exist between PM and CO production. The correlation between CO and PM emissions is shown in Figure 4. 10.

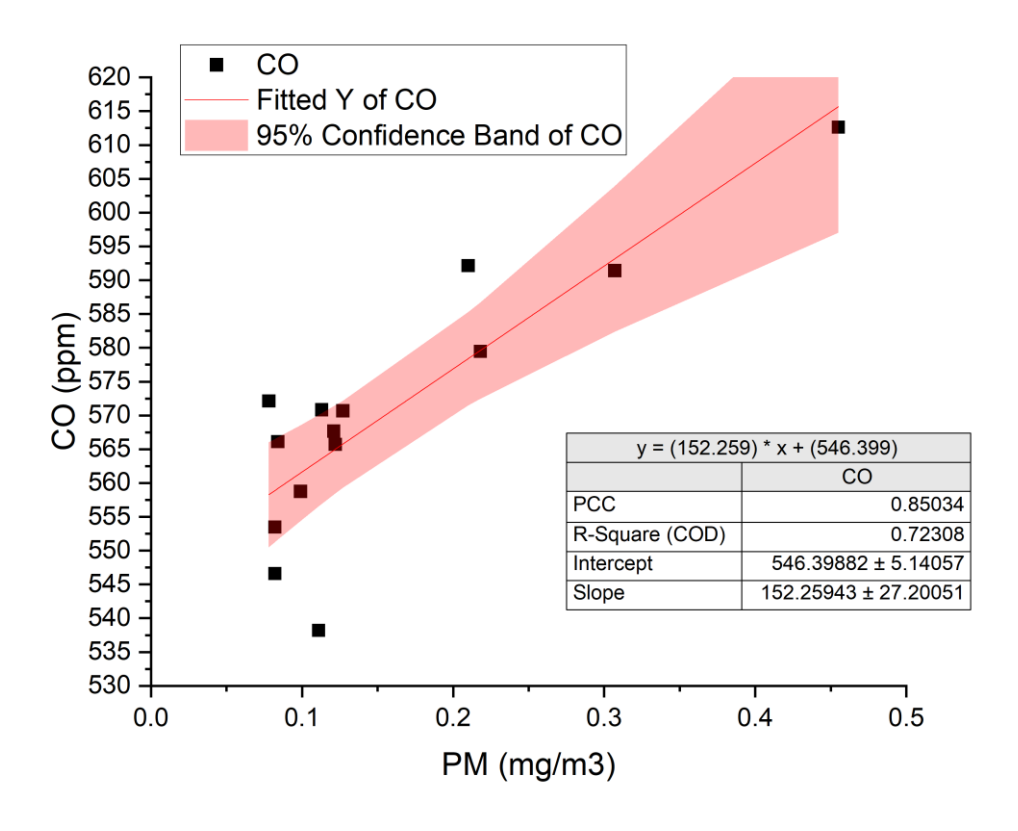
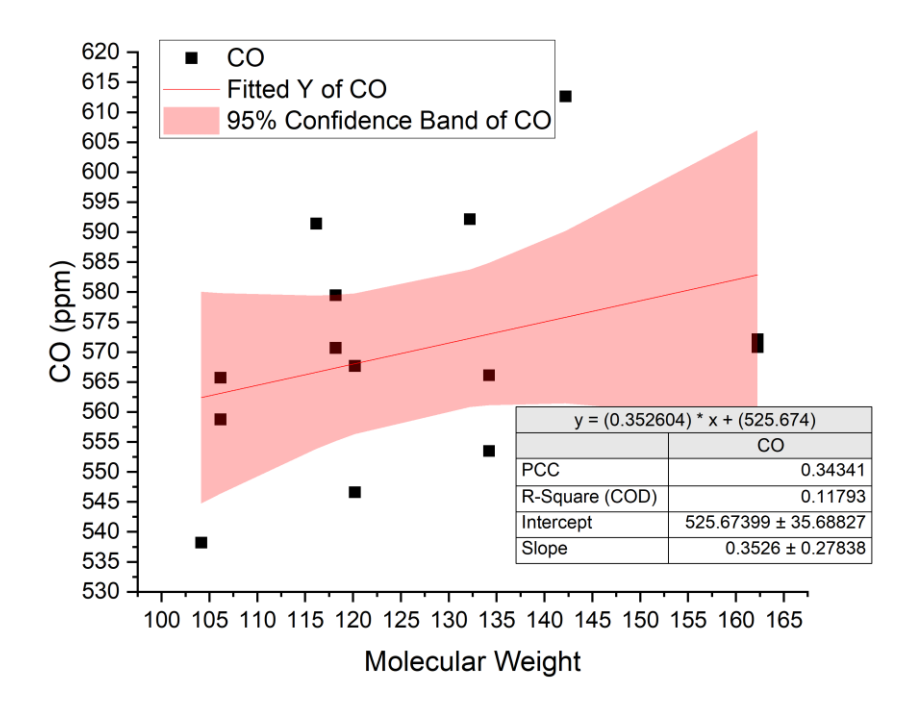


Figure 4. 10: Correlation between PM and CO

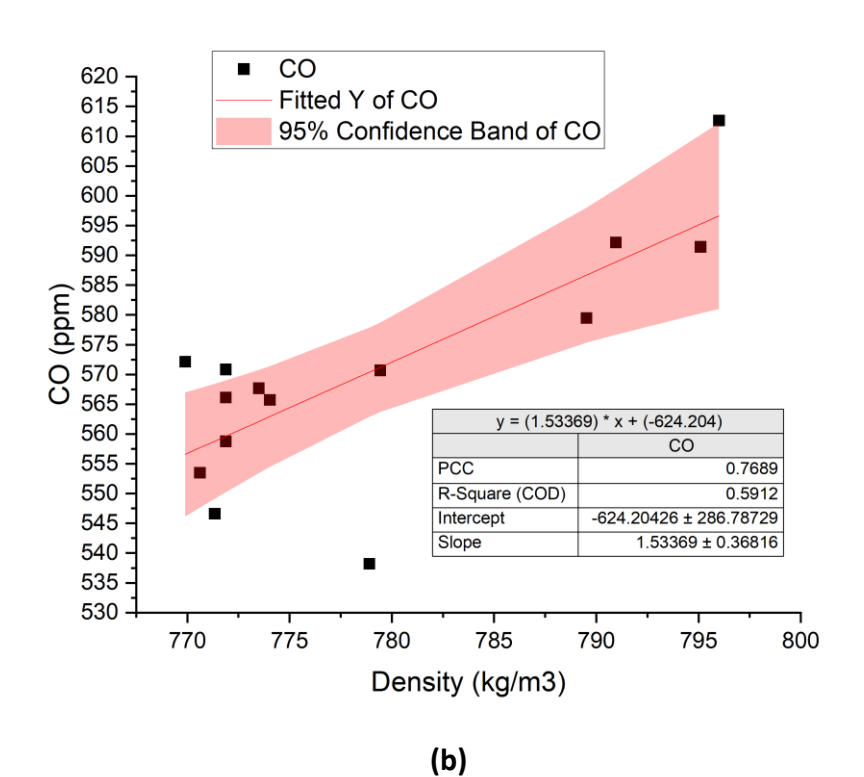
According to Figure 4. 10, the R<sup>2</sup> value is 0.723, indicating a strong correlation between CO and PM emissions. This finding proves that the previous statement is correct. Both PM and CO are primarily produced by incomplete combustion and partial decomposition on the molecular scale.

Moreover, it should be noticed that methylnaphthalene has the highest CO emissions, followed by tetralin, indene and indane, which follow the same sequence for PM production as shown in Figure 4. 1.

Besides aromatics themselves, fuel properties could also affect CO production through incomplete combustion. Figure 4. 11 shows CO emissions compared with fuel properties.



(a)



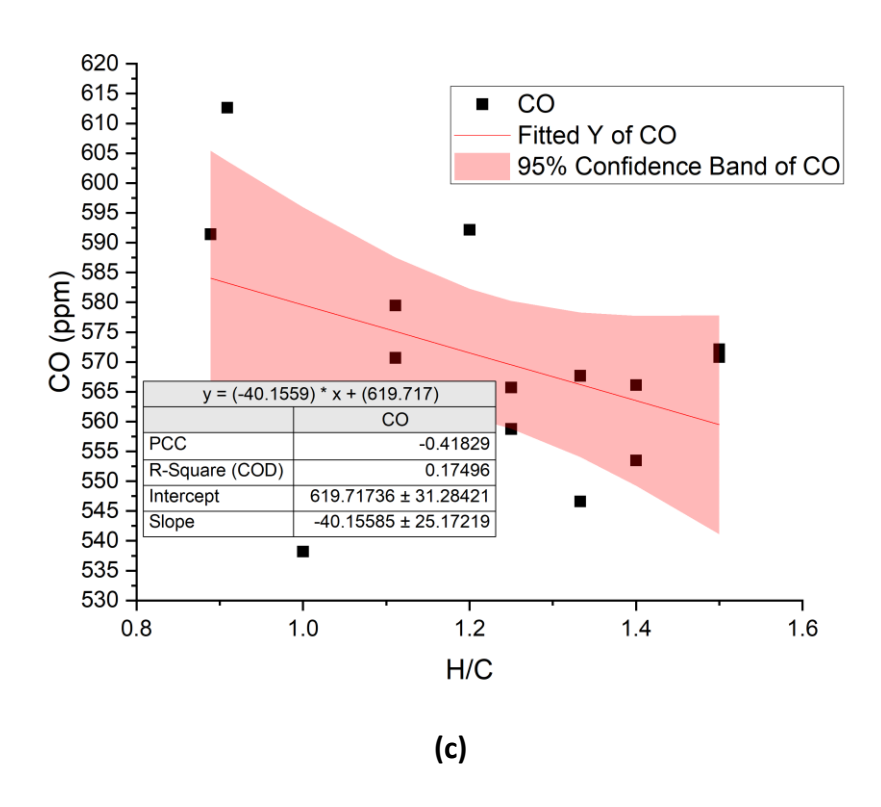


Figure 4. 11: (a) Correlation between molecular weight and CO, (b) Correlation between Density CO, (c) Correlation between H/C ratio CO.

Generally, CO emissions are not sensitive to molecular weight and H/C ratio. However, the relatively strong correlation between CO and density is shown in Figure 4. 11 (b) which has an R<sup>2</sup> value of 0.5912. Density also shows relatively high correlation with PM emissions discussed previously which suggest that the primary formation mechanism of CO and PM might be similar (incomplete combustion). Moreover, fuel density could be a good indicator for both PM and CO emissions. As discussed, higher density fuel might mean that more compositions requiring decomposition in the same volume or residence time which enhance the degree of incomplete combustion.

#### 4.3.3.3 NOx

In general, there are two pathways to form NOx in a combustor. First, NOx could be generated from nitrogen inside the fuel. However, standard jet fuel has negligible nitrogen. Second, NOx emission could be produced in a high-temperature zone in a

combustor, which is the primary pathway for aviation NOx production. According to the previous statements, different aromatics will affect incomplete combustion differently. Therefore, in theory, the combustion temperature for different fuels should also be different, and the trend should be similar. Figure 4. 12 shows the correlation between aromatic species and NOx production.

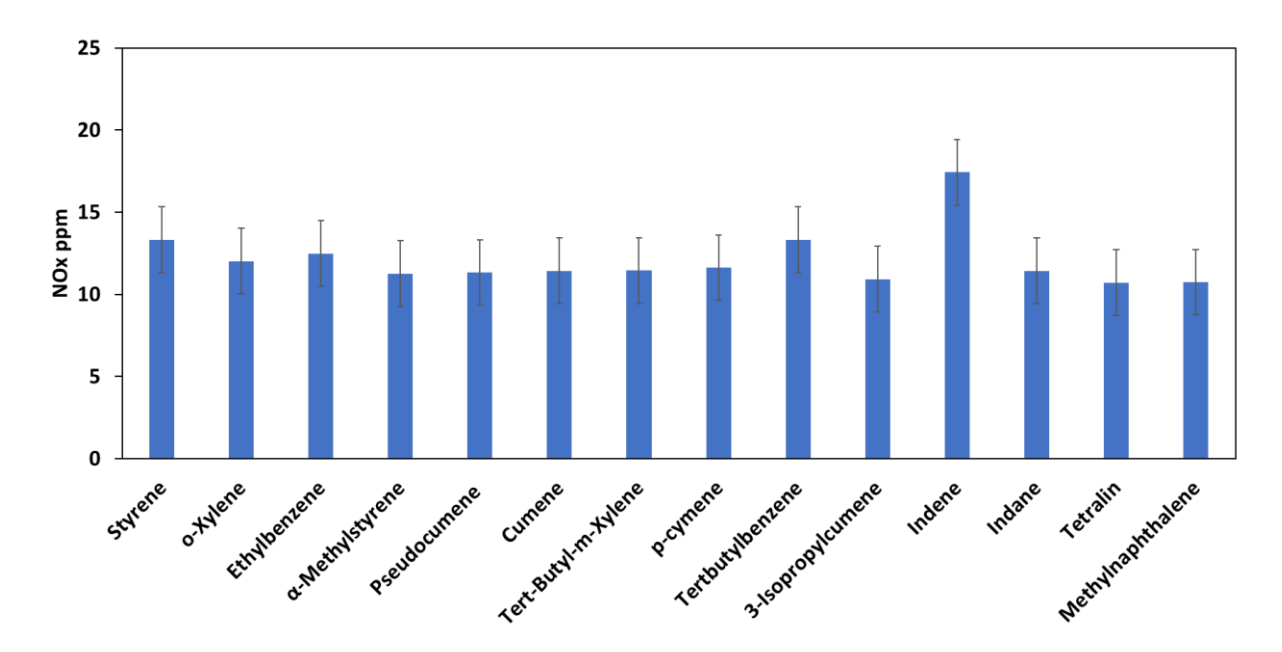


Figure 4. 12: Aromatics impact on NOx,

According to Figure 4. 12, aromatic species have similar NOx emissions, with only indene significantly higher. The reason could be multiple, either due to the test equipment's limited sensitivity or incomplete flame structure data. The exhaust temperature for all test fuel blends is very similar (between 435 and 452 °C). The influence of NOx emissions due to the temperature difference may be too minor for test equipment to detect. However, the value for indene is particularly higher than for other aromatics, which might be due to the unique ring structure, potentially creating localized high-temperature zones, or possible experimental errors affecting results.

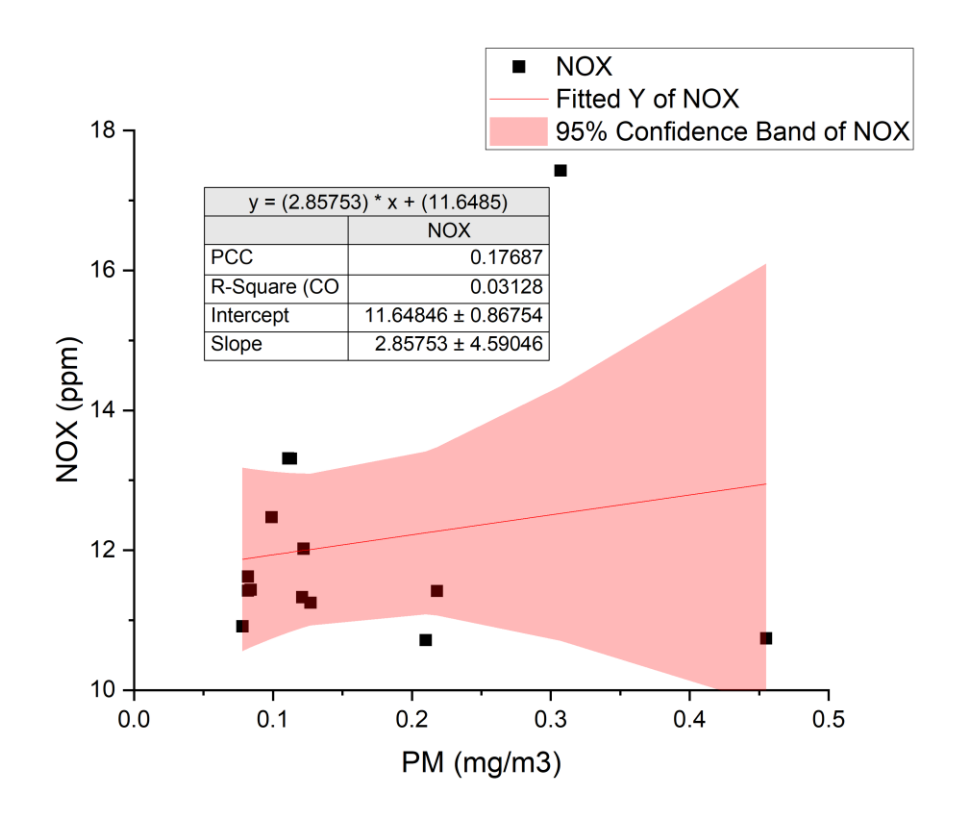
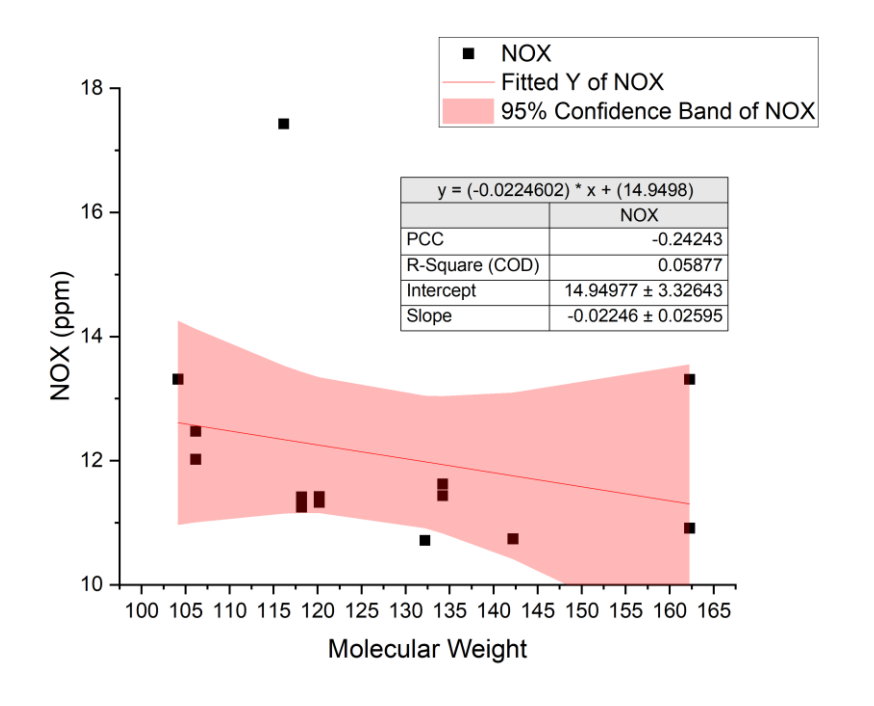


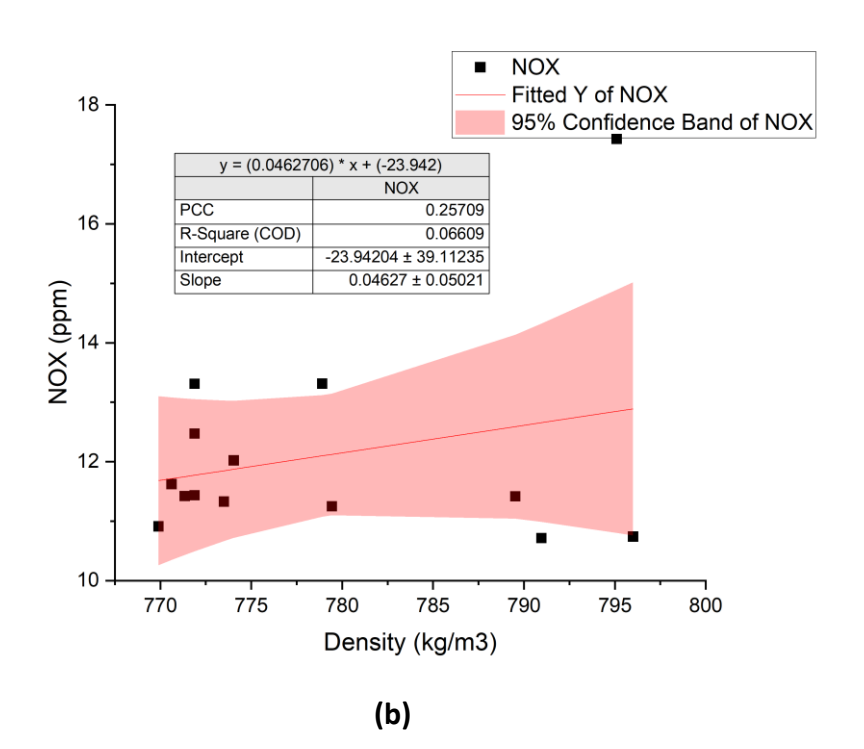
Figure 4. 13: Correlation between PM and NOx

According to Figure 4. 13, NOx emission has very little connection with PM production, which also shows that the fuel composition mainly affects PM emissions and has little impact on NOx emissions.

Figure 4. 14 shows the effects of key fuel properties (molecular weight, density, and H/C ratio) on NOx emissions.



(a)



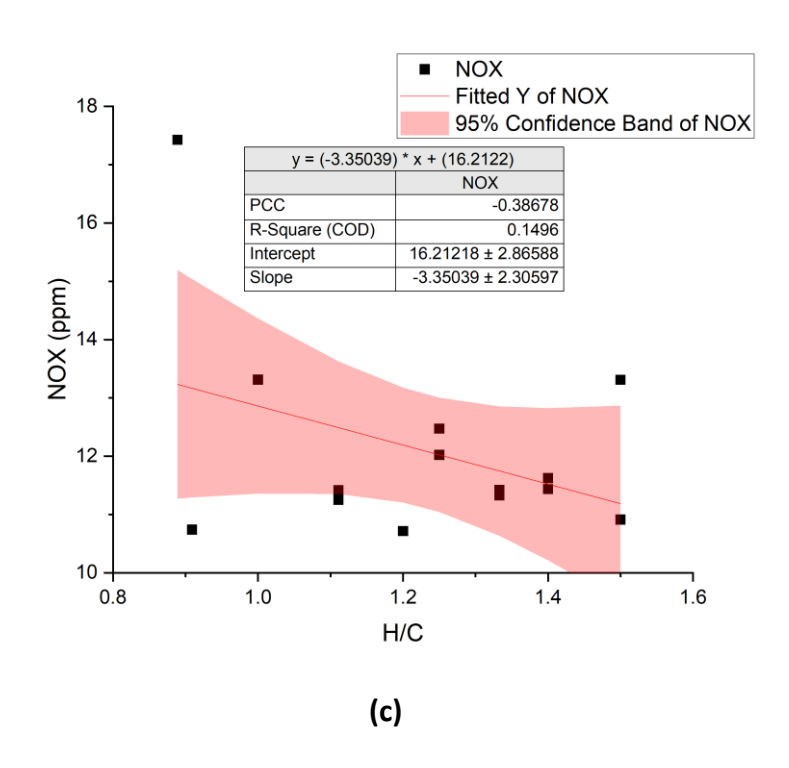


Figure 4. 14: (a)Correlation between molecular weight and NOx, (b) Corrlation between Density NOx, (c) Corrlation between H/C ratio NOx.

In general, none of them significantly affect NOx emissions, as supported by theory that only combustion temperature significantly affects NOx production.

# 4.4 Conclusion

The primary objective of this test campaign is to investigate the impact of various aromatics and some essential fuel properties on PM and gaseous emissions. Through the discussion, results obtained from this experimental campaign indicate that different aromatics have a noticeable impact on the production of both PM and gaseous emissions, which fulfils the primary objective.

Results of both 8% and 18% vol. aromatic blends were presented, and higher aromatic concentration blends significantly promote PM production. Moreover, results show that aromatic species noticeably impact emissions production in addition to aromatic concentration. It is found that in general, the ability to form PM for different aromatic

groups is followed by the trend: Diaromatic groups > Monoaromatic groups consistent with other works [75], [123]. Further observation indicated that even within the same aromatic groups, species with different structures could still behaviour differently in terms of PM production. Generally, cyclic aliphatic or benzene attached to a single aromatic compound will elevate PM production significantly. Moreover, the attached benzene ring structure produces significantly more PM than cyclic aliphatic.

Three basic fuel properties were discussed regarding PM production. Only the H/C ratio and density show a reasonable correlation with PM production, especially the density of the fuel blend, which shows strong correlation to PM values. However, this observation should be treated carefully since the high correlation is based on statistical analysis which might not reflect actual relationship between two variables. Different combustion environment might also affect results noticeably. Therefore, a further understanding of how overall fuel properties affect PM production needs further investigation. For example, in theory, changing the fuel formula could affect other fuel properties, such as viscosity, which could significantly impact fuel spray patterns and PM production from fuel mixtures.

In terms of gaseous emissions, results indicated that different aromatic species may have the ability to affect UHC and CO emissions. On the other hand, NOx shows weak correlation between emissions intensity and aromatic species since the formation of NOx is normally connected to the local combustion temperature.

# 5. Investigation of potential intermediate tracers for soot production from chemical kinetic modelling

# 5.1 Introduction

As presented in Chapter 4, results collected from a gas turbine combustor have potentially indicated that distinct aromatic species affect soot production differently. The general trend of how aromatic species affect soot production follows the order: (diaromatics > monoaromatics). Results obtained from other experiments also show this trend in soot production [124], [125], [126]. Therefore, the conclusion might be that the same aromatic behaves similarly in different combustion environments in terms of PM production.

In the past, combustion properties were believed to dominate soot production. However, this similar soot production trend observed in different combustion tests might suggest that fuel chemistry also plays an essential role in soot generation regardless of the combustion environment. Based on the fuel formulations used in these experiments, aromatic species could affect the trend of soot production. It is possible that changing fuel chemistry will also affect the combustion environment, such as the spray pattern, which will significantly influence the fuel-air mixture and hence affect soot production. Still, it is meaningful to investigate how aromatic species affect soot formation in terms of fuel chemistry.

Empirically, different fuel components will have different reaction pathways during the combustion process, affecting the final soot production. For example, in theory, large molecules require more steps to be fully consumed; in other words, fuel containing these large molecules trends to combust incompletely. Therefore, large molecules trends to combust incompletely and more likely to promote soot production. In addition, as described in Chapter 4, molecular size and species could affect soot production. More aromatic rings in the molecular structure are also difficult to break down because the aromatic structure requires more energy to break the bonds than a straight C-C bond.

Previous research suggests there is likely an intermediate species representing the final soot production [127]. Therefore, monitoring the generation of these intermediate species during the simulation makes it possible to predict the final soot concentration in reality. In the end, simulation results should correlate with the experimental results.

In conclusion, this simulation work has two main objectives. First, to develop a simple, cost-effective model to simulate soot production in a combustor. Second, to find an intermediate tracer that can predict soot. Both 0-D and 1-D models are considered in this thesis.

It should be noted that, the results calculated by Chemkin model should not be treated as accurate prediction for a real combustor, but indictors to analysing the potential impact of aromatics on emissions which will benefit the selection of soot tracers, future fuel formulations and combustor design. This is because, as mentioned in Chapter 2, the Chemkin model is typically 0-D or 1-D models, and fundamental assumption of these models assumes that the chemical reaction time is extreme fast to neglect the effects of turbulence flow. Moreover, reactors in Chemkin models are usually assumed to be steady-state conditions. Therefore, although Chemkin models could significantly reduce the simulation time, they also lack descriptions of complex 3-D flow

characteristics in realistic environments leading to the difference between simulation results and actual combustor behaviour. To improve the accuracy of Chemkin models for real applications, complex 3-D turbulence models are necessary to couple with Chemkin results.

# 5.2 Results and Discussion

Results obtained from CHEMKIN Pro simulations are plotted and presented in this section. As mentioned, the main objective is to determine any intermediate species that could predict an aviation fuel's final soot production. Conclusions drawn from experimental results presented in Chapter 4 were involved as a reference of simulation results. The fundamental methodology is to plot the mole fraction of selected intermediate species from different fuel blends against other variables such as residence time and position in a PFR. A sequence of candidate fuel blends will be obtained by checking the peak value of each fuel blend. If the sequence obtained from the simulation matches the sequence found in the experiment, this chemical species is considered to potentially have the capability to predict soot production.

For the 0-D model, two critical variables, air-fuel ratio and temperature, which theoretically significantly influence simulation results significantly, are also considered. The impact of different air-fuel ratio will be presented first with a reaction temperature of 1900K. This temperature selected first to ensure complete reaction within the given residence time. Moreover, the results of temperature effects will be discussed last.

Simulation results using CRN models will also be presented and discussed, since the variables in this model are set to the same value of the operation condition for the model Tay combustor described in [92] and Chapter 3, these 1-D models will mainly focus on investigating potential soot tracers and soot formation pathways.

# 5.2.1 Stoichiometric combustion ( $\lambda$ =1)

Stoichiometric combustion is one of the most critical fuel mixture ratios that must be investigated first. In theory, the stoichiometric condition means that fuel will be fully oxidized with precisely the required oxygen. In a real combustion environment, stoichiometric combustion is extremely difficult to achieve due to the complexity of the fuel injection method and combustor geometry. However, this condition could be easily simulated using a perfect stirred reactor in CHEMKIN, which is applied in this simulation model. The performance of four candidate intermediate tracers, C<sub>2</sub>H<sub>2</sub>, C<sub>2</sub>H<sub>3</sub>, C<sub>6</sub>H<sub>6</sub>, and C<sub>14</sub>H<sub>10</sub>, will be discussed first under stoichiometric combustion conditions.

# 5.2.1.1 C<sub>2</sub>H<sub>2</sub> (acetylene)

Figure 5. 1 shows the changing mole fraction of acetylene (C<sub>2</sub>H<sub>2</sub>) for different fuel blends with increasing residence time. According to this figure, the mole fraction curve of methylnaphthalene is significantly lower than the others, especially at its peak. Other curves of fuel blends have almost the same trend, while ethylbenzene has a slightly lower mole fraction value at its peak. Therefore, based on this finding, the four fuel blends could be categorized into two groups. Group 1 includes ethylbenzene, styrene and indene, while Group 2 consists solely of methylnaphthalene.

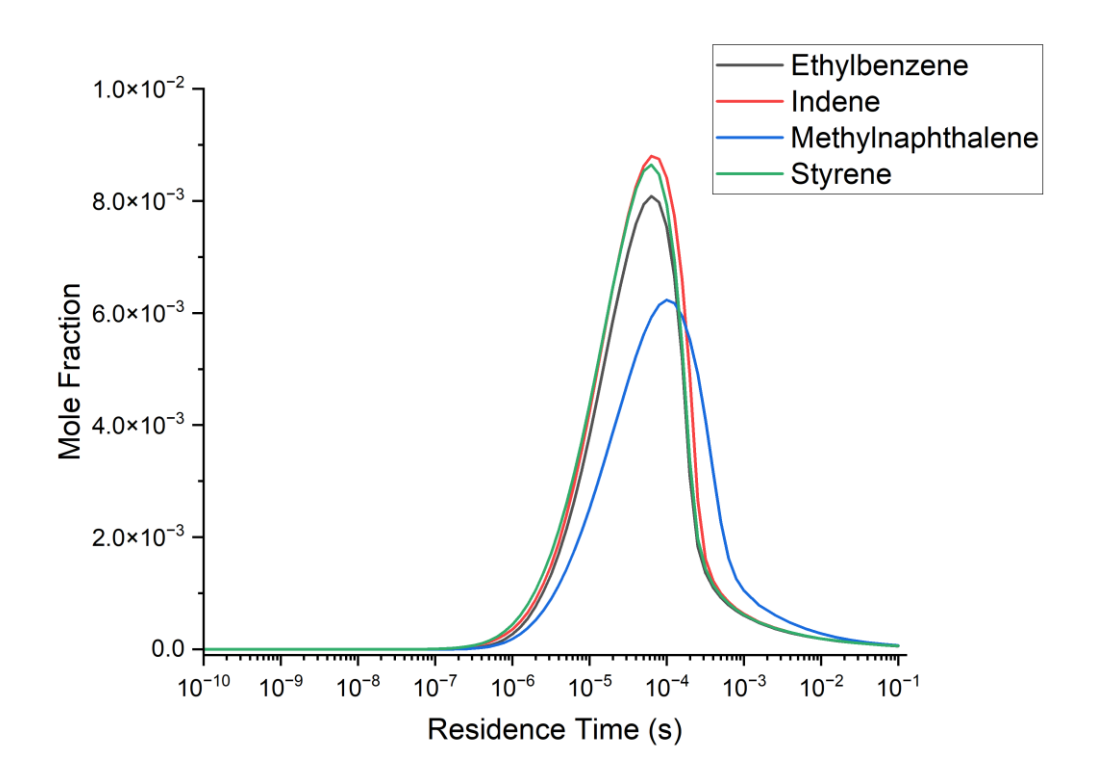


Figure 5. 1: Mole Fraction of C<sub>2</sub>H<sub>2</sub> as a function of residence time

This finding is roughly based on the diversity of aromatic structures. Members in Group 1 all belong to monoaromatics, which have only one complete benzene ring, while in Group 2, methylnaphthalene is a diaromatic with two benzene rings. In addition, the whole curve of the methylnaphthalene fuel blend shifts slightly to the right compared with other fuel blends. This phenomenon could be due to diaromatics having higher molecular weight and structural complexity, which requires more reaction steps to be fully broken into small molecules like acetylene. Therefore, methylnaphthalene requires more time to achieve a peak mole fraction of acetylene within a given reactor volume. In real combustion, this large molecule characteristic leads to difficult combustion, and incompletely combusted molecules tend to form PAH, significantly increasing soot production. A typical methylnaphthalene reaction pathway is shown below:

$$OH + C10H7CH3 => H2O + C10H6CH3$$

Moreover, all monoaromatic fuel blends have very close peak positions in residence time, even if the peak value is slightly different. It should be noted although ethylbenzene, styrene, and indene are categorized as monoaromatic, they have different molecular structures. One of the significant differences is indene, which has two complete ring structures, one benzene ring and one cyclopentene ring. While the other two monoaromatics only have one full benzene ring, this implies that more benzene ring structures in aromatics will significantly increase molecular decomposition difficulty, or in other words, the challenge of achieving complete combustion.

In general, combining results from both simulation and experimental data, using acetylene as a soot tracer can effectively differentiate soot production between diaromatic and monoaromatic compounds. However, it cannot readily distinguish among different monoaromatic species. Based on the experimental findings presented in Chapter 4, monoaromatics with only one complete ring structure should produce comparable quantities of soot. If acetylene were an ideal soot tracer, the simulation result should show identical peak value for ethylbenzene and styrene. However, Figure 5. 1 reveals that the peak value of styrene is noticeably lower than that of ethylbenzene and even lower than that of indene. Notably, indene generates significantly higher PM in experiments, a characteristic accurately reflected by acetylene concentrations in simulations.

# 5.2.1.2 C<sub>2</sub>H<sub>3</sub> (ethenyl)

C<sub>2</sub>H<sub>3</sub> is another intermediate that has the potential to predict soot production since it is one of the essential components in the pathway of PAH generation. The mole fraction of C<sub>2</sub>H<sub>3</sub> versus residence time is shown in Figure 5. 2. According to Figure 5. 2, the entire profile of methylnaphthalene and indene is significantly lower than those of ethylbenzene and styrene. Particularly at peak concentrations, methylnaphthalene and

indene show substantially lower values compared to ethylbenzene and styrene. Moreover, although ethylbenzene and styrene exhibit similar mole fraction trends, styrene achieves a slightly higher peak value than ethylbenzene.

Figure 5. 2 reveals an interesting pattern not observed with other intermediates: three fuel blends (ethylbenzene, styrene, and indene) show a secondary hump in their post-peak profiles. This feature is particularly pronounced in ethylbenzene and styrene, where their profiles and values are nearly identical. Additionally, the decay rate of the ethenyl mole fraction is lower for methylnaphthalene.

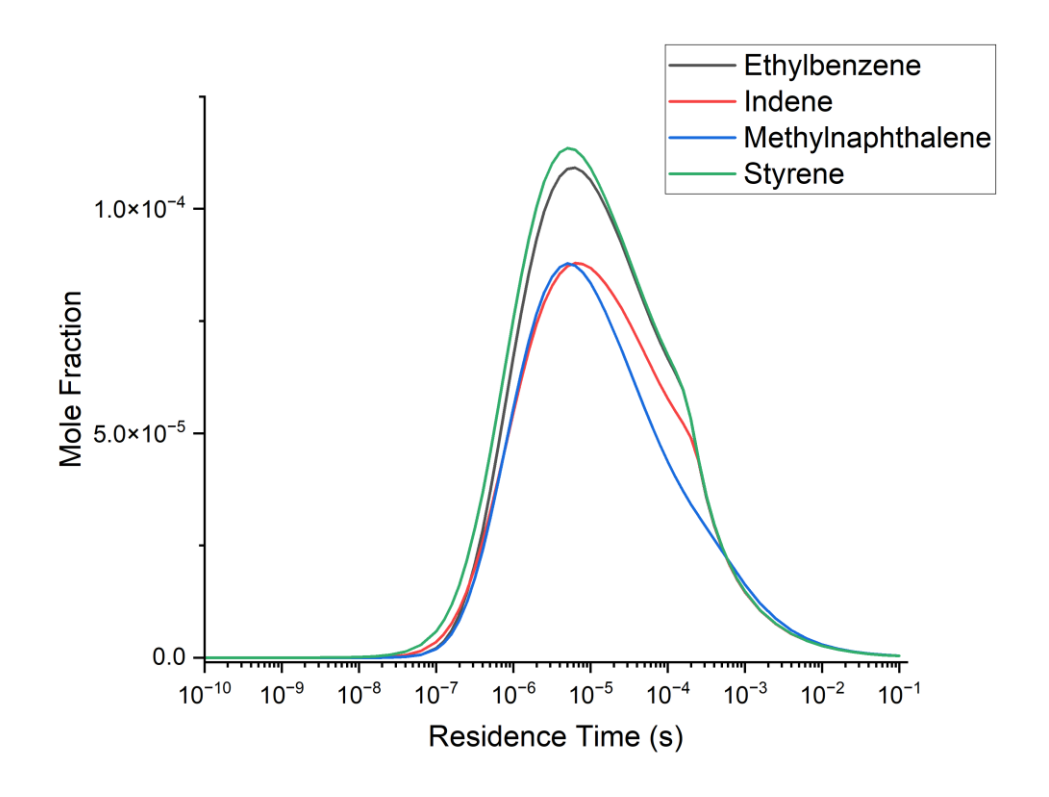


Figure 5. 2: Mole Fraction C<sub>2</sub>H<sub>3</sub> as a function of residence time

In conclusion, using C<sub>2</sub>H<sub>3</sub> as an intermediate tracer to predict final PM production effectively distinguishes compounds based on their ring structures. Species with two fused rings exhibit lower peak values in C<sub>2</sub>H<sub>3</sub> mole fraction. However, one limitation is its inability to differentiate between indene and methylnaphthalene. While methylnaphthalene contains two fused complete benzene rings, indene has only one

benzene ring. Experiment results show methylnaphthalene produces significantly higher PM than indene, a difference not captured by C<sub>2</sub>H<sub>3</sub> concentrations.

# 5.2.1.3 C<sub>6</sub>H<sub>6</sub> (benzene)

Figure 5. 3 presents the mole fraction of  $C_6H_6$  against residence time for four fuel blends. From this figure, the peak value of methylnaphthalene is noticeably lower than those of other three monoaromatic fuel blends, and the entire curve is shifted rightward, implying reduced fuel reactivity.

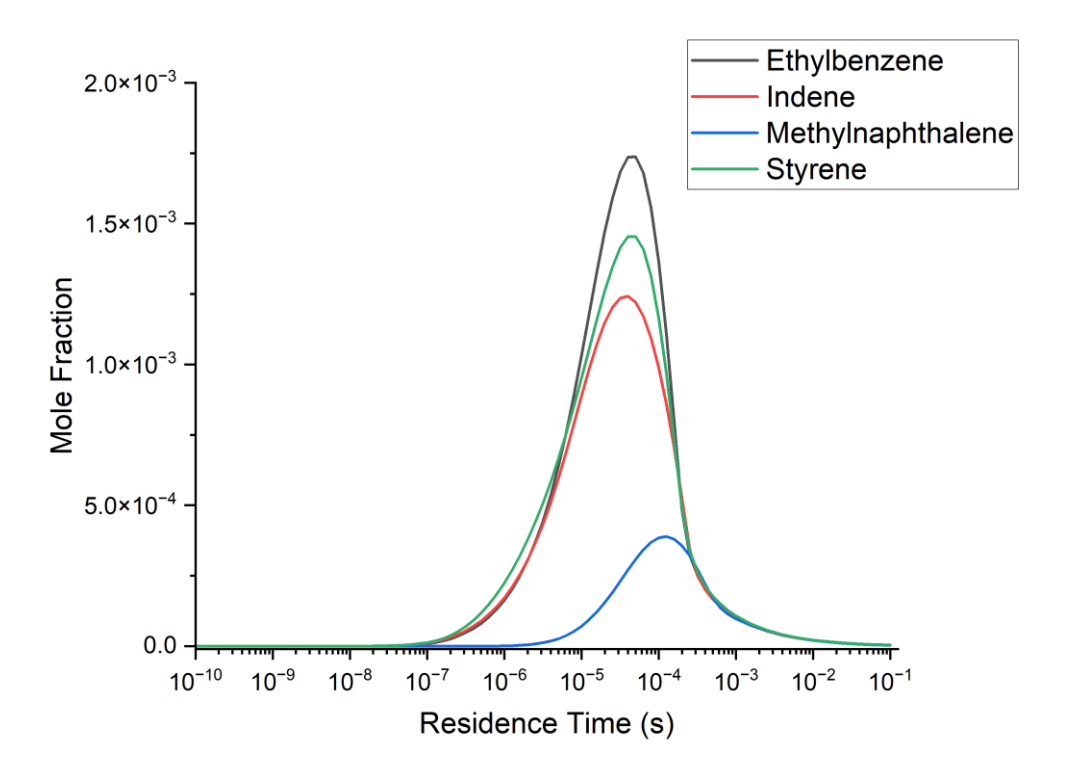


Figure 5. 3: Mole Fraction C<sub>6</sub>H<sub>6</sub> as a function of residence time

The ethylbenzene, indene, and styrene fuel blends exhibit similar peak values and curve trends, which contrast markedly with those of methylnaphthalene.

In conclusion, using benzene effectively differentiates diaromatics from monoaromatics.

The simulation results show an inverse trend compared to experimental findings.

However, the difference in peak value between indene and other monoaromatics is less pronounced than the dramatic PM intensity differences observed experimentally.

# 5.2.1.4 $C_{14}H_{10}$ (phenanthrene + anthracene)

Figure 5. 4 presents the mole fraction of C<sub>14</sub>H<sub>10</sub> against residence time for candidate fuel blends. Based on their aromatic structures, C14H10 combines phenanthrene and anthracene in the chemistry mechanism used in this research. The data reveal that methylnaphthalene has an extremely high peak value relative to other species. The mole fraction curve of indene is noticeably higher than those of ethylbenzene and styrene. Moreover, the curves of styrene and ethylbenzene are close, with styrene maintaining marginally higher concentrations of the residence time period. Consistent with Chapter 3 experimental results, the PM production ranking aligns with the C<sub>14</sub>H<sub>10</sub> mole fraction trends, particularly in peak value.

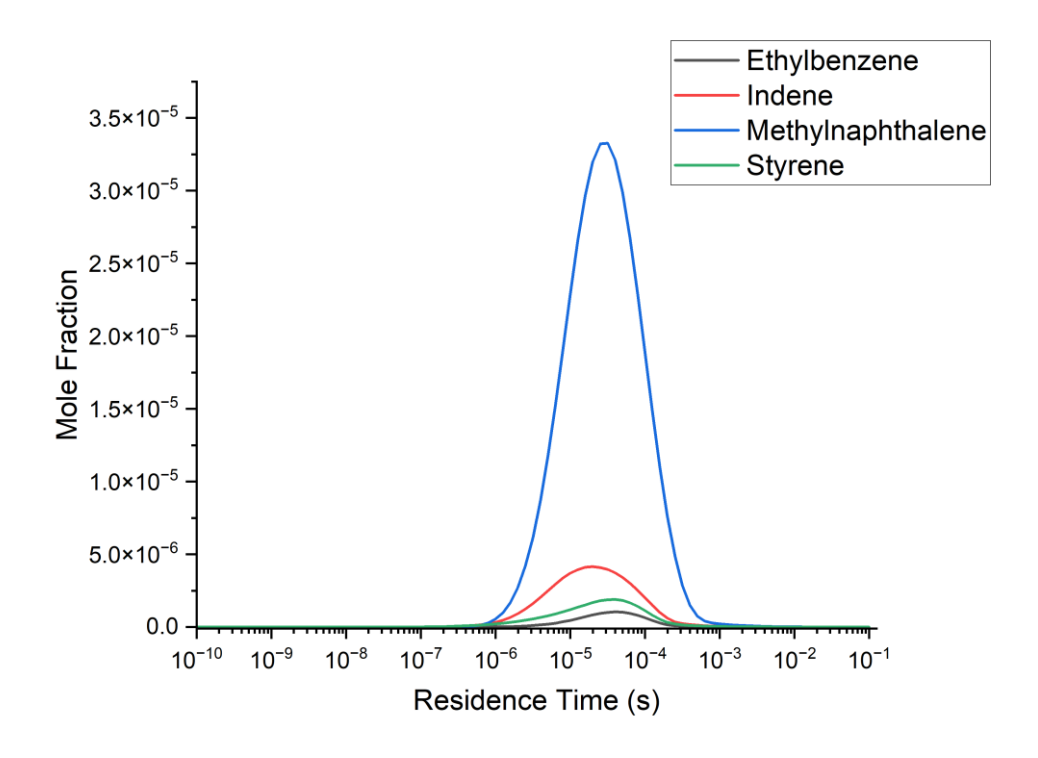


Figure 5. 4: Mole Fraction C<sub>14</sub>H<sub>10</sub> (phenanthrene + anthracene) as a function of residence time

Compared to other intermediate tracers,  $C_{14}H_{10}$ 's key distinction lies in being the smallest PAH species and the primary building block for larger PAH formation. This structural characteristic may enhance its predictive capability for PM emissions, as it represents a more direct precursor to final soot particles in the molecular evolution pathway.

In conclusion, while C<sub>14</sub>H<sub>10</sub> demonstrates promise as an intermediate tracer for soot production, its sensitivity to indene remains limited. Nevertheless, it effectively differentiates indene from other monoaromatic fuel blends.

# 5.2.2 Lean combustion (AFR=65)

Although stoichiometric conditions for different intermediates were analysed in the previous section, the high air-fuel ratio is still worth analysing since most commercial aviation combustors operate in lean combustion conditions. The reason for using lean combustion is well-founded. One of the main purposes is that it could significantly reduce fuel consumption while an aircraft is cruising. In addition, due to the complex geometry of a modern combustor, some high air-fuel ratio zones inevitably form in the combustor. Moreover, these high AFR zones depend on the combustor type and fuel injection method. Therefore, whether a high air-fuel ratio will affect the phenomena observed in previous sections and experimental results is worth investigating. In this section, a high AFR (65) is selected to simulate an extreme environment to cover the majority of lean combustion AFR ranges and to better present results. Only C<sub>14</sub>H<sub>10</sub> will be discussed in this section since it is the most eligible soot tracer in stoichiometric conditions.

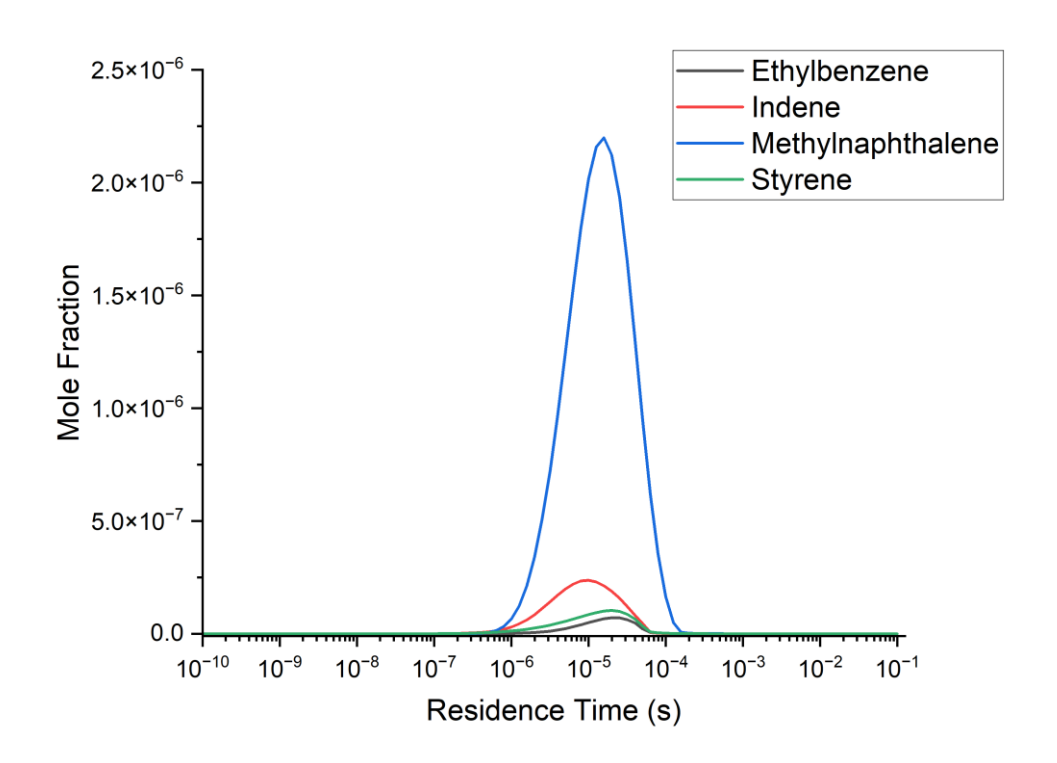


Figure 5. 5: Mole Fraction C<sub>14</sub>H<sub>10</sub> (phenanthrene + anthracene) as a function of residence time

Figure 5. 5 presents the mole fraction of  $C_{14}H_{10}$  against residence time under an air-fuel ratio of 65. In this figure, the curve of methylnaphthalene is noticeably higher than the other three aromatic blends, especially in the peak position.

The same phenomena were observed in the stoichiometric condition shown in Figure 5. 5. Moreover, the arrangement of all four aromatic blends is identical to the stoichiometric case, which indicates that excess air does not have a visible effect on soot generation from the fuel composition perspective. However, the peak value of C<sub>14</sub>H<sub>10</sub> is lower than under stoichiometric conditions, which will theoretically decrease final PM production. Consistent with experimental studies that lean combustion reduces PM production [128], [129]. In addition, the peak position of Figure 5. 5 was shifted left compared with Figure 5. 4, which may indicate that higher air-fuel ratios will shorten fuel consumption, promote combustion efficiency and reduce PM production ultimately.

# 5.2.3 Fuel-rich combustion ( $\lambda$ =0.5)

The investigation of the fuel-rich condition is equally important since commercial fuel injectors and combustor design will unavoidably provide a fuel-rich mixture zone. Therefore, this section examines an extreme air-fuel mixture condition with an equivalence ratio of 0.5.

Figure 5. 6 illustrates the intermediate ( $C_{14}H_{10}$ ) mole fraction curves for four candidate fuel blends. The methylnaphthalene curve is significantly higher than the others, a phenomenon consistent across all air-fuel ratio conditions. The relative ordering of the four fuel blends remains unchanged from other mixture conditions, confirming that  $C_{14}H_{10}$  remains a reliable tracer in fuel-rich environments.

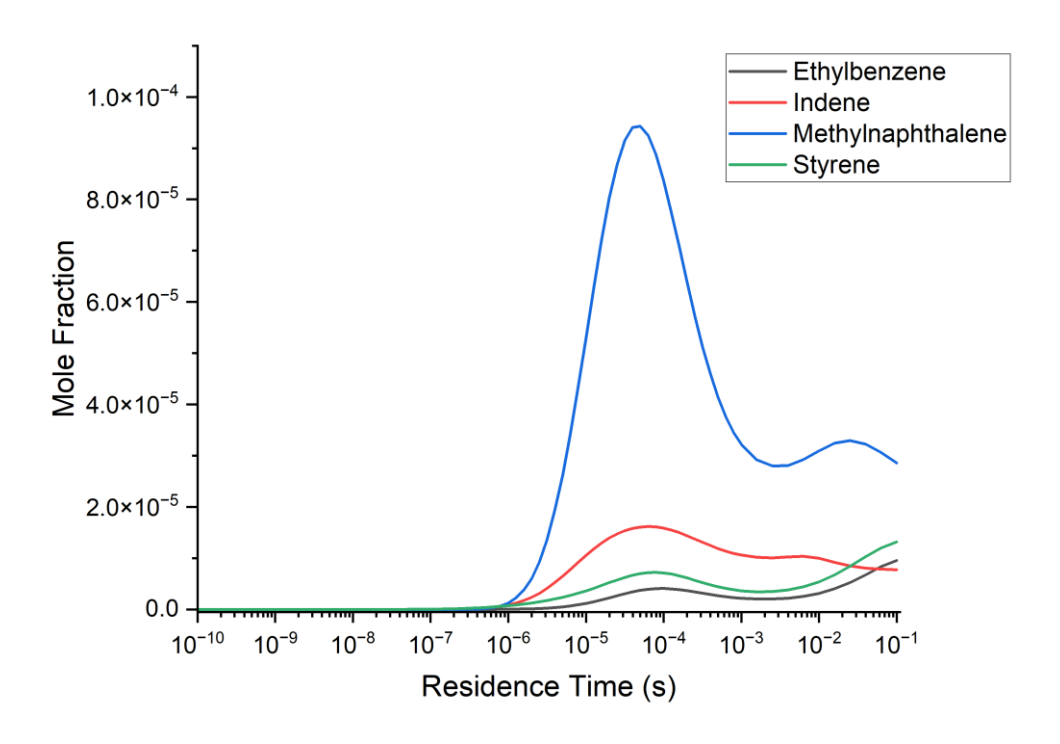


Figure 5. 6: Mole Fraction C<sub>14</sub>H<sub>10</sub> (phenanthrene + anthracene) as a function of residence time

A major difference in Figure 5. 6 compared with Figure 5. 4 and Figure 5. 5 is that all four curves have secondary C<sub>14</sub>H<sub>10</sub> peaks. This occurs due to incomplete reactions in

fuel-rich conditions. Large fuel molecules cannot fully decompose in the available residence time.

# 5.2.4 Temperature impact

The reaction temperature is a significant factor affecting simulation results. As mentioned, several fixed reaction temperatures were used instead of variable temperatures in the simulation setup. Therefore, any results affected by temperature change were easily identifiable.

### 5.2.4.1 1700 K

Figure 5. 7 presents the mole fraction curve of four aromatic fuel blends under a slightly higher temperature, 1700 K. The conclusions from the 1500 K condition remain valid.

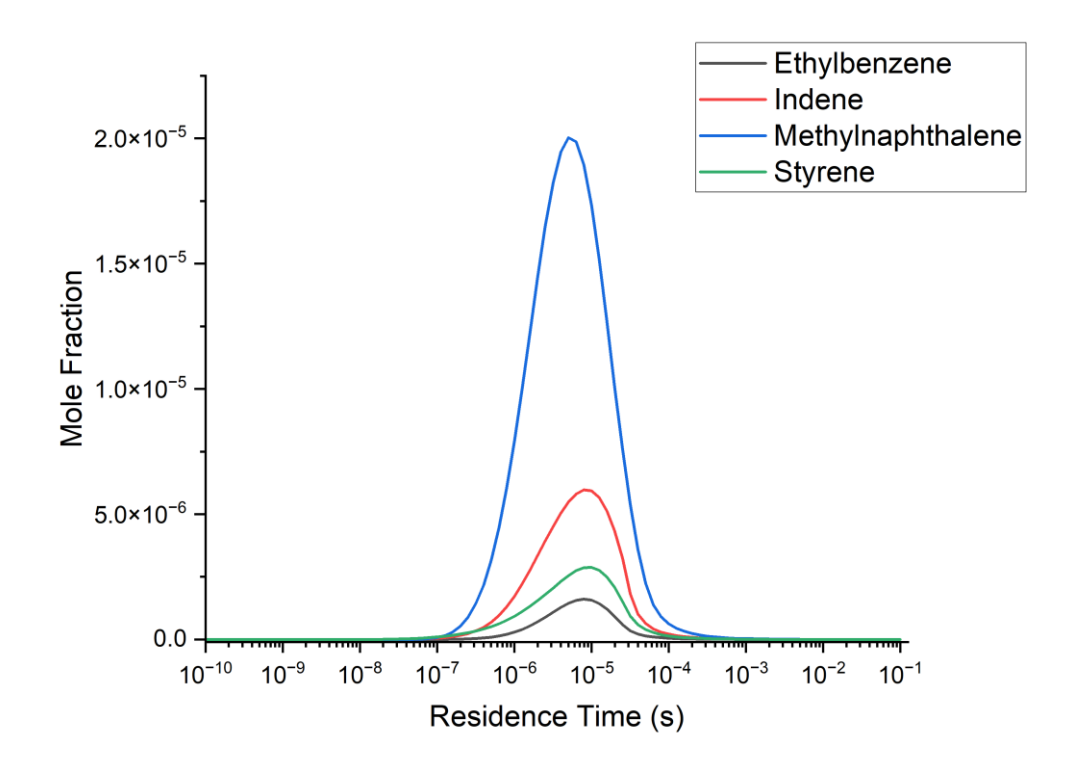


Figure 5. 7: Mole Fraction C<sub>14</sub>H<sub>10</sub> (phenanthrene + anthracene) at 1700 K as a function of residence time

The highest curve is methylnaphthalene, indene, styrene, and ethylbenzene. The sequence of fuel blends is the same compared with the 1500 K shown in Figure 5. 4, which indicates that C<sub>14</sub>H<sub>10</sub> can still predict soot at higher temperatures. However, some unique features appear in the 1700 K condition compared with Figure 5. 4. First, the peak value of all fuel blends has significantly increased. Second, the difference between each fuel blend in peak value is relatively smaller, especially for methylnaphthalene, whose peak value increased. Moreover, it also takes a shorter residence time for a fuel blend to reach the peak position of the mole fraction of C<sub>14</sub>H<sub>10</sub>. The peak position of methylnaphthalene is lower compared with 1500 K condition.

### 5.2.4.2 1300 K

Figure 5. 8 illustrates the mole fraction of  $C_{14}H_{10}$  of candidate fuel blends with a reaction temperature of 1300 K. Fuel blends show identical peak value rankings as at other temperatures.

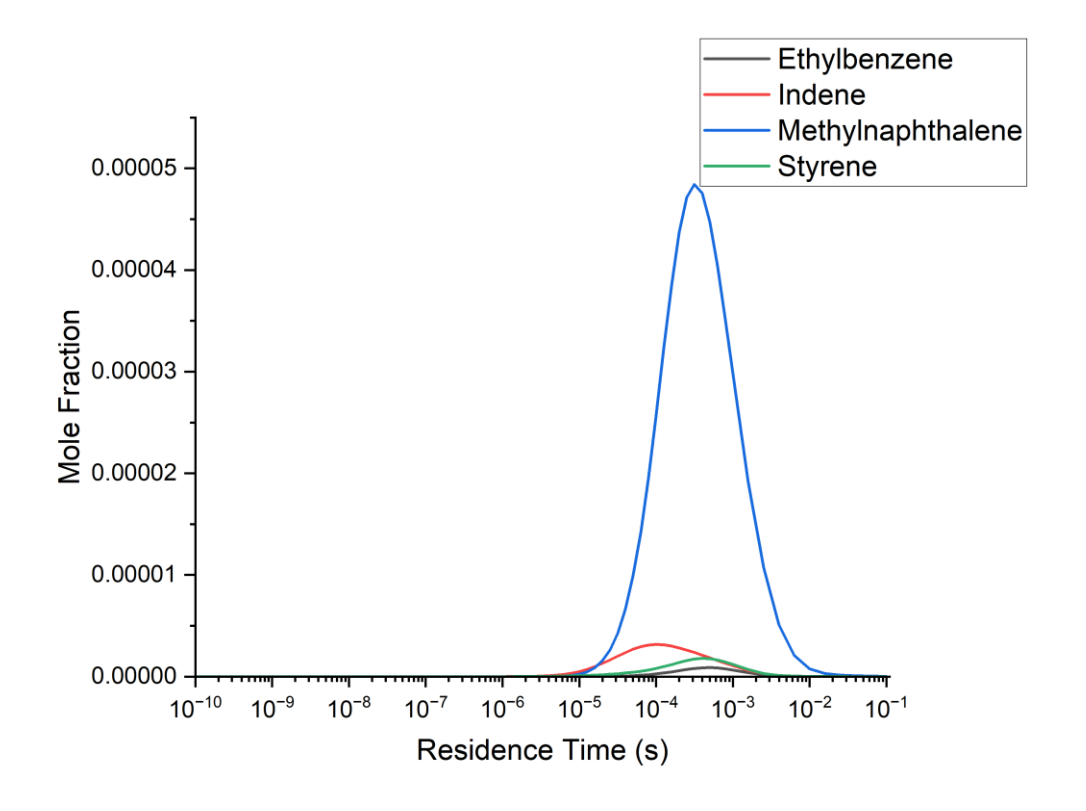


Figure 5. 8: Mole Fraction C14H10 (phenanthrene + anthracene) in 1300k

However, the peak value of indene shows a significant decrease. Moreover, the residence time required to reach the peak is noticeably increased. According to the simulation results, indene fuel blends exhibit inhibited formation of large soot particles in relatively low temperatures.

### 5.3 1-D model

Neither CRN Layout 2 nor Layout 3 provided valuable information in soot prediction using intermediate products under the same conditions as the experiment setup. In these two CRN layouts, no useful results were generated at the end of the primary zone. The major reason for this situation seems to be the selection of a recirculation model to represent the combustor's primary zone. This design for the primary zone significantly reduced the local residence time which is almost 10 times less than the model without recirculation. The is due the principle of recirculation, more flow will recirculate back to the first PSR, and residence time could be treated as the volume divided by flow rate for easy understanding. Therefore, a significant increase of flow into the reactor will dramatically reduce the residence time and preventing the reaction between reactants.

The experimental setup might not be suitable for simulation using these two layouts since the percentage of recirculation was directly obtain from the experiment findings, presented in Chapter 3. It might be possible to solve the problem by changing some operational variables such as the percentage of recirculation flow and reaction temperature. However, the principle of building the CRN model in the thesis aimed to represent an actual model Tay combustor, by alternating the combustion parameters, such as residence time, seems to reduce the value of the model. These two Layouts might still have value in the prediction of temperature and gaseous emissions with some modifications.

CRN Layout 1, which did not adapt by a recirculation model still could provide valuable information in terms of tracking the formation of soot by some pre-PAH content. Therefore, simulation results from CRN Layout 1 will be mainly presented and discussed in this section.

Among the results from all reactors, results in the first PFR, representing the intermediate zone in a combustor, will be presented and discussed in this section. The first two PSRs are essentially a 0-D model, and the 0-D model is already detailed and discussed previously in a wider range of AFRs, residence times and temperatures. Moreover, the last PFR is designed to represent the dilution process and the corresponding effect of the nozzle. The majority of reactants were fully consumed before entering the last PFR, which makes the results extremely difficult to investigate. Therefore, the results in the first PFR are the best choice for analysis, as they contain information from both the last PSR (primary zone) and the post-combustion process in the intermediate zone. Three positions in this reactor are of primary interest: the start position, middle position and end position.  $C_2H_2$ ,  $C_2H_3$  and  $C_6H_6$  are selected to investigate whether they are suitable for soot prediction purposes.

The mole fraction of  $C_2H_2$  of different fuel blends in the PFR is presented in Figure 5. 9. In general, the mole fraction of  $C_2H_2$  continues to decrease, and is completely consumed at the end of this reactor. The sudden decrease might primarily result from the increase in temperature and residence time, which enables the complete combustion of  $C_2H_2$  and other components. For more accurate simulations, investigating a more realistic temperature profile in post-flame region is required in the future work.

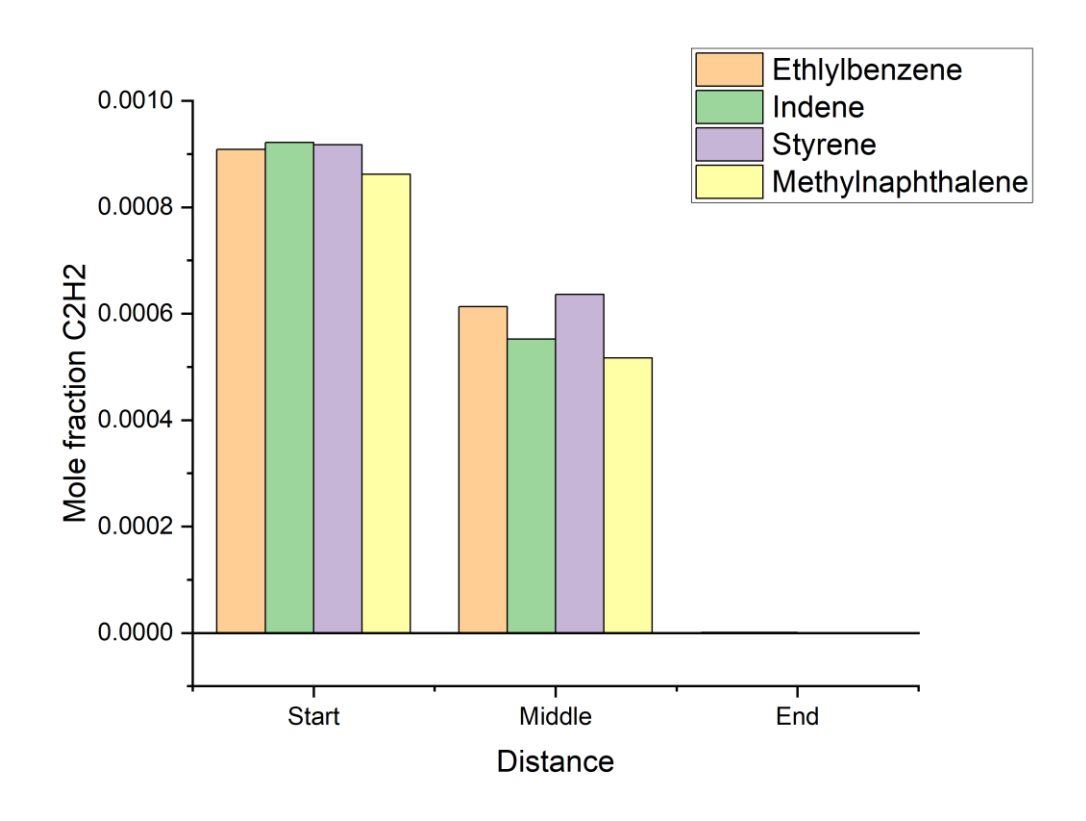


Figure 5. 9: Mole fraction of C2H2 of fuel blends in PFR

The mole fraction of  $C_2H_2$  is relatively high at the beginning of the PFR, which might indicate that the original fuel content was well-combusted in the primary zone. The difference in mole fraction between each fuel blend is also very small, and the order of mole fraction for different fuel blends is indene, styrene, ethylbenzene, and methylnaphthalene. Similar to the 0-D model, this order did not reflect the results found in the experiments. However, the order of the fuel blends changes in the middle of the reactor to styrene, ethylbenzene, indene, and methylnaphthalene. The differences between each fuel blend were also increased; the mole fraction of  $C_2H_2$  for ethylbenzene and styrene is noticeably higher than for indene and methylnaphthalene. In general,  $C_2H_2$  is not suitable to be selected as a soot tracer since it is unstable in a PFR and provides a different order of trend compared to experimental results. However, it might be able to distinguish the difference in soot production for larger aromatic groups such as diaromatics and monoaromatics.

The mole fraction of C<sub>2</sub>H<sub>3</sub> in three positions of the PFR is presented in Figure 5. 10.

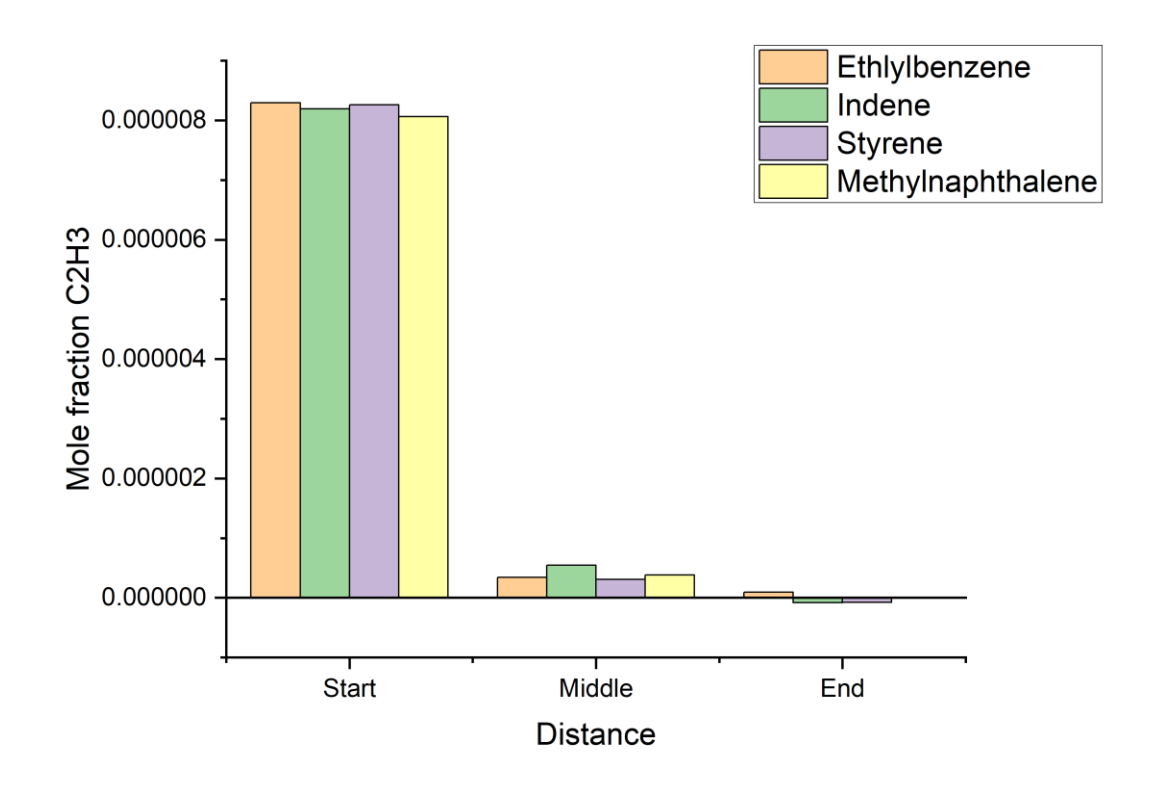


Figure 5. 10: Mole fraction of C2H3 of fuel blends in PFR

In the beginning of the PFR, the mole fraction of  $C_2H_3$  for four fuel blends are very similar. Only small differences are detected with the order: ethylbenzene, styrene, indene, methylnaphthalene. At the middle point of the PFR, the amount of  $C_2H_3$  was heavily consumed, and the trend of mole fraction changed to the order of indene, methylnaphthalene, ethylbenzene, styrene.

Findings from the results of C<sub>2</sub>H<sub>2</sub> and C<sub>2</sub>H<sub>3</sub> indicate that in a 1-D model, small molecules are not suitable for predicting soot formation since they are very easy to be consumed and regenerated simultaneously. Moreover, this also proves that the peak value method used in 0-D models may be insufficient for soot prediction, as it doesn't consider post-combustion behaviour affecting small molecule formation.

The more fraction of  $C_6H_6$  for four candidate fuel blends in the first PFR is shown in Figure 5. 11.

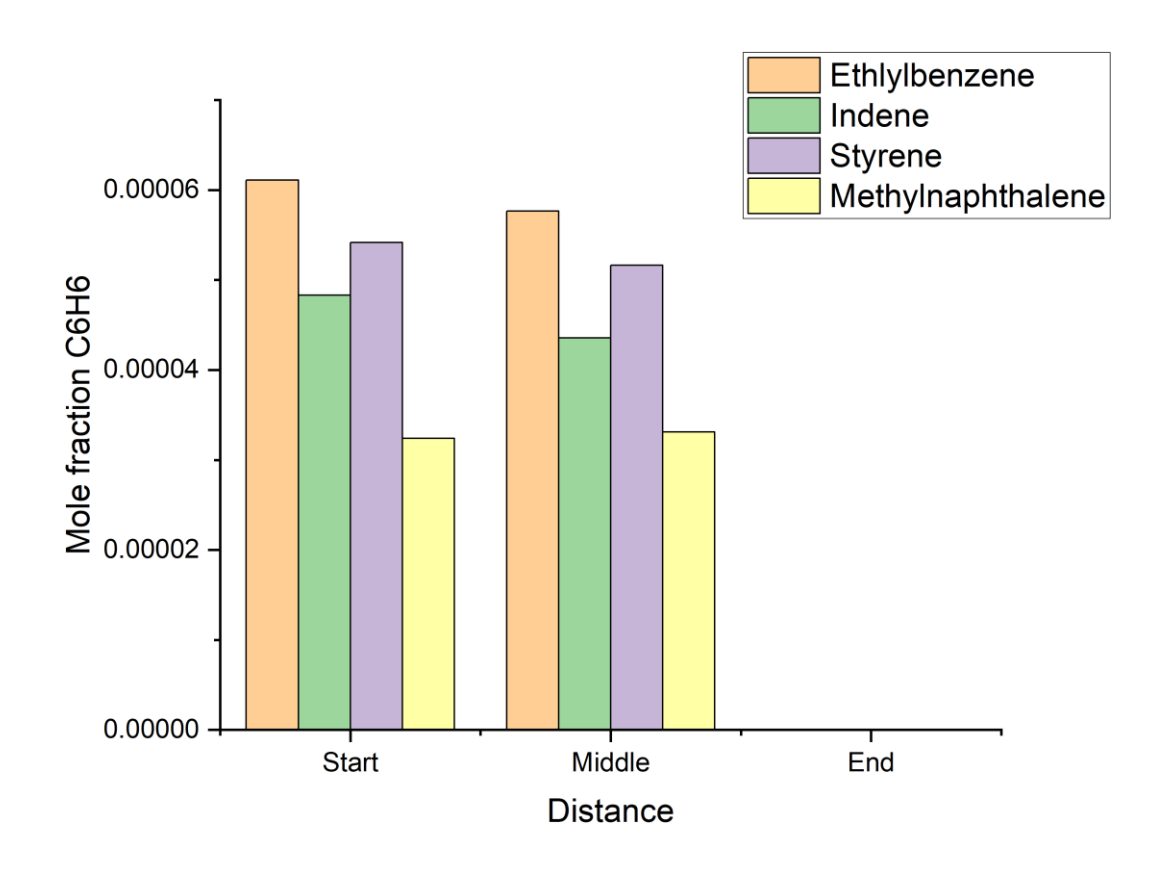


Figure 5. 11: Mole fraction (C6H6) in PFR

According to Figure 5. 11, the amount of  $C_6H_6$  was slightly consumed in the first half of the reactor. Moreover, the difference in mole fraction of  $C_6H_6$  between the four fuel blends is clear and similar in both the start and middle positions following the order: ethylbenzene, styrene, indene, and methylnaphthalene, which is much more stable compared to small molecules. It was also noticed that the amount of  $C_6H_6$  was quickly consumed in the remaining half of the PFR, possibly due to the increased reaction temperature along with the distance that triggered certain chemical mechanisms. However, the trend of  $C_6H_6$  for the four aromatic blends is found to be similar to the trend in the 0-D model, which has good agreement with experimental results. It also provides the possibility for soot prediction in the current setup of the 1-D model.

In general,  $C_6H_6$  is the preferred choice for soot prediction under the current 1-D model since other large molecules, such as  $C_{14}H_{10}$ , which is recommended in the 0-D model, were quickly consumed in the primary zone. This happened because  $C_6H_6$  is difficult to decompose compared to other smaller molecules since it is a ring-structured compound. It is also relatively easier to generate compared to large molecules meanwhile. It seems that larger molecules tend to convert to  $C_6H_6$  at high temperatures at first, but further decomposition does not happen, and PAH formation begins with  $C_6H_6$ .

Simulation results also show that a higher amount of soot is predicted for methylnaphthalene fuel blends. Only methylnaphthalene shows a strong ability to form BIN-group PAHs, which are small PAH groups such as C<sub>20</sub>H<sub>10</sub> and C<sub>20</sub>H<sub>16</sub>. The mole fraction of BIN-group PAHs in the first PFR for methylnaphthalene fuel blends is shown in Figure 5. 12.

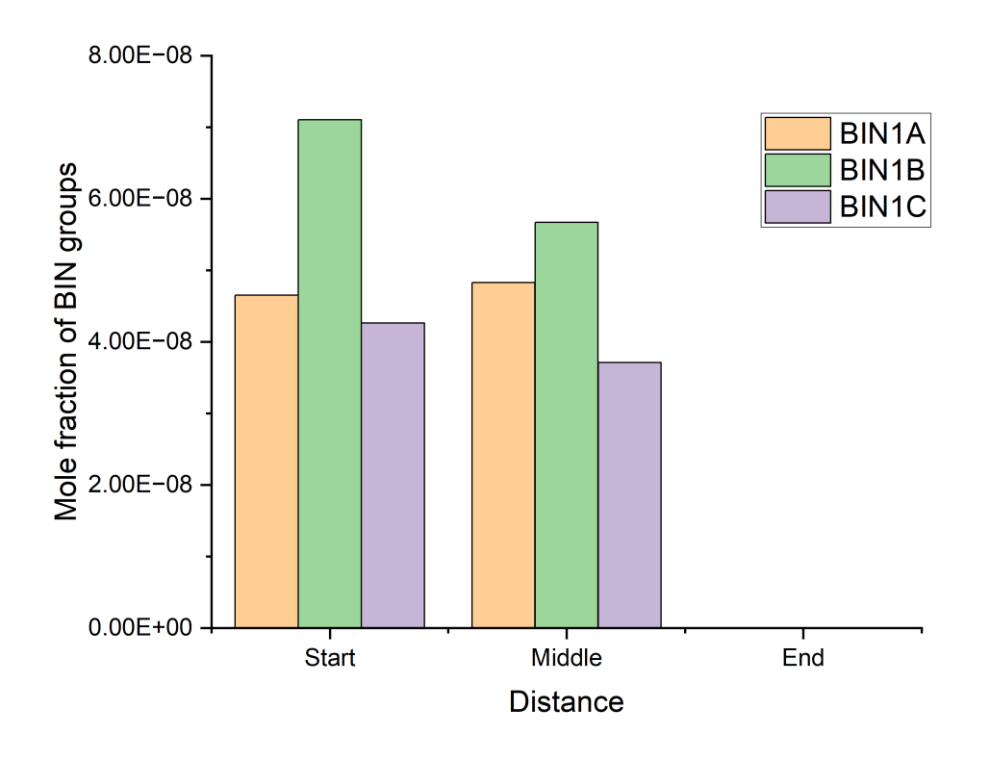
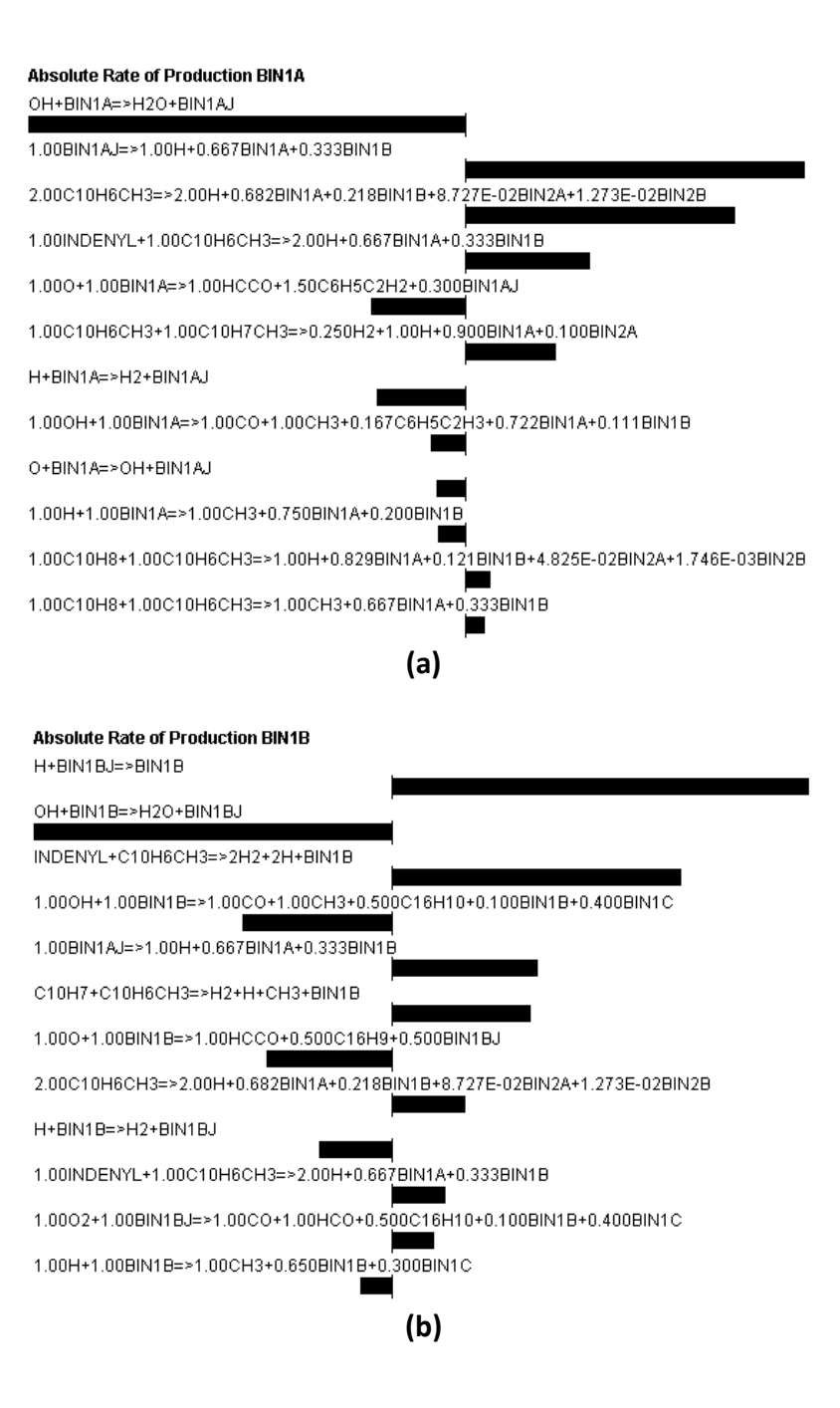


Figure 5. 12: Mole fraction of BIN groups for Methylnaphthalene fuel blends

The mole fraction of BIN groups has a very short, rapidly increasing period and then is fully consumed at the end of the reactor. It is also observed that BIN1A continues to increase until the middle point, which results in a delayed position of peak value. This behaviour is different from other BIN groups. The reason could be the internal transformation within BIN groups, and lower molecular weight species tend to aggregate into heavier species. The detailed reaction pathways to form BIN groups are shown in Figure 5. 13.



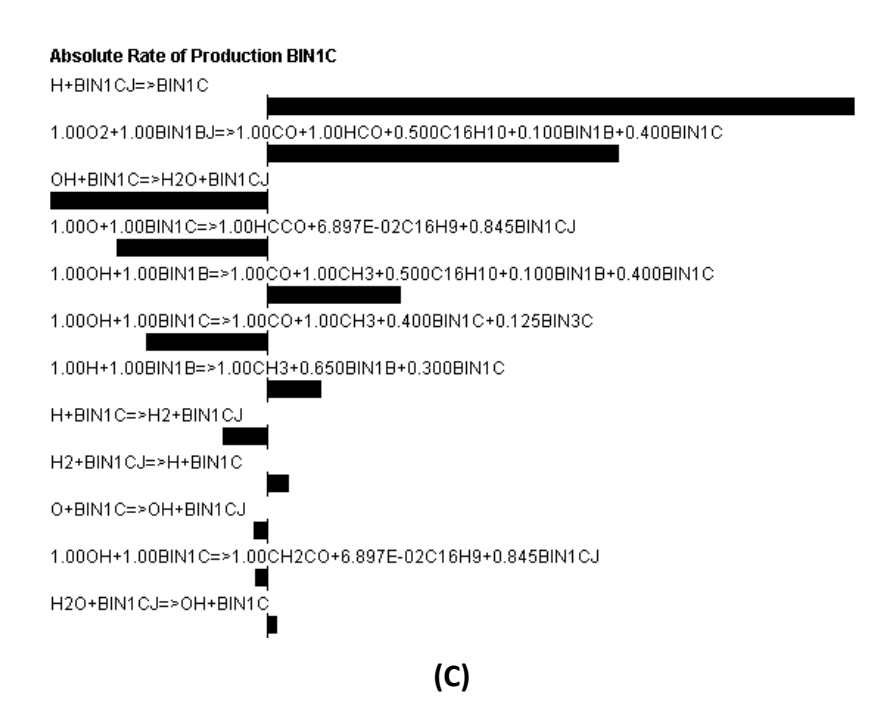


Figure 5. 13 (a)Production pathways to BIN1A, (b) Production pathways to BIN1B, (c)

Production pathways to BIN1C

Figure 5. 13 presents the strong transformation within BIN groups, it was also found that BIN groups could be generated from C10H6CH3 directly, which is also easily derived from methylnaphthalene as discussed previously through certain pathways. Typical formation routes are shown below:

$$OH + C10H7CH3 => H2O + C10H6CH3$$

$$INDENYL + C10H6CH3 => 2H2 + 2H + BIN1B$$

These explain the reason that using methylnaphthalene fuel blends in practical experiments will typically result in extremely high soot production. Moreover, indenyl could easily forms from indene, C6H6, and methylnaphthalene. The production pathways are complex, and possible reaction networks are presented in Figure 5. 14.

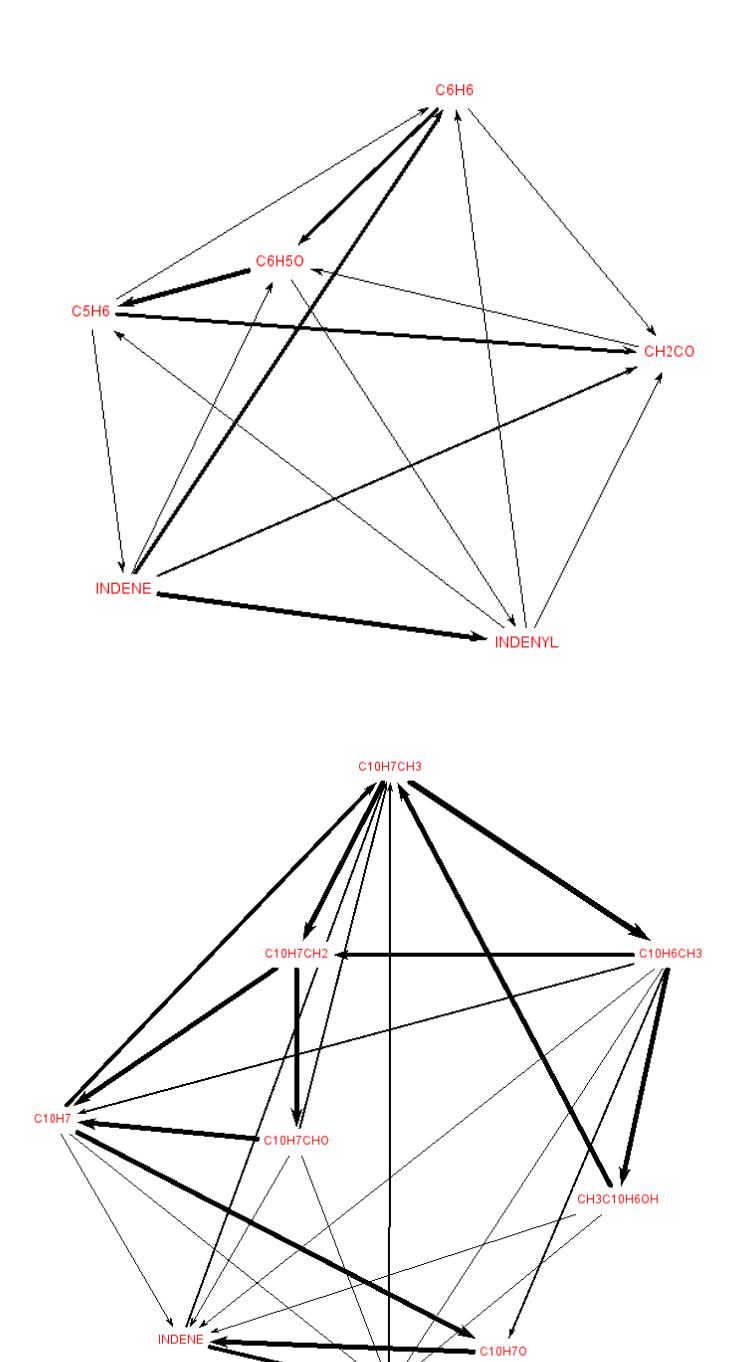


Figure 5. 14: Possible reaction net between methylnaphthalene, indenyl, and C6H6

# **5.4 Conclusion**

In conclusion, by using CHEMKIN-Pro, a simple, cost-efficient 0-D combustion model has been established and validated for investigating potential soot intermediates in this

model. A more complex 1-D model used to simulate more realistic combustion is also constructed based on a downscaled model Tay combustor.

For 0-D model, the results of four candidate intermediate tracers have been analysed, including  $C_2H_2$ ,  $C_2H_3$ ,  $C_6H_6$ , and  $C_{14}H_{10}$ . In conclusion, large molecules like  $C_6H_6$  and  $C_{14}H_{10}$  are more reliable for soot prediction than small intermediates such as acetylene. Moreover,  $C_{14}H_{10}$  performs better after crosschecking with the experimental results. One major drawback of  $C_6H_6$  is that it could not distinguish indene blends from other candidate fuel blends as accurately as  $C_{14}H_{10}$ .

The impact of different air-fuel ratios and reaction temperatures has also been investigated. Although these factors affect simulation results, such as peak value and position, all fuel blends' sequence remains identical. This finding supports the idea of using large PAH molecules as a soot tracer for most combustion conditions [130], in this case C<sub>14</sub>H<sub>10</sub>.

Possible theories regarding different behaviour among selected intermediate tracers have also been proposed. After the corroboration between the experimental and simulation results, a previously ignored factor (molecular structure) has been identified. Heavier, more structurally complex intermediates prove more accurate as soot predictors.

As a soot or PM predictor, a diaromatic is more accurate than a monoaromatic, and a monoaromatic is better than other smaller molecular species, such as acetylene. Intermediates containing a complete benzene ring in their structure are already suitable for PM prediction, but the accuracy differs depending on the species.

For example, other than C<sub>14</sub>H<sub>10</sub>, benzene is another intermediate that has the potential to predict soot production. Although less accurate than C<sub>14</sub>H<sub>10</sub>, benzene presents a

correct sequence of candidate fuel blends in inverse order of experimental results. This phenomenon may occur because benzene is the very beginning of PAH formation. The most challenging stage of PAH formation is establishing the first benzene ring. After the first benzene ring is generated, the stability of the molecular structure increases, inhibiting the molecule from being easily consumed. Based on this hypothesis, other intermediates with one complete benzene ring may show a similar predictive capability for soot, and the accuracy increases with the number of benzene rings.

For the 1-D model, using C<sub>6</sub>H<sub>6</sub> as a soot traces. Shows a good agreement between experimental and simulation results, which is also found in the 0-D model. Under the experimental setup, the 1-D model seems to have difficulty with soot prediction since the majority of fuel content is heavily consumed at the end of the primary zone. This likely results from the local AFR and residence time, which strongly promote chemical reactions. However, C<sub>6</sub>H<sub>6</sub> remains useful as a soot tracer in the current 1-D model. Methylnaphthalene is also predicted to have a strong ability for PM production through certain pathways, which agrees with the experimental results.

# 6. Impact of alternative fuels on seal compatibility

### 6.1 Introduction

The importance of using alternative jet fuel to reduce PM emissions has been discussed in the literature review. Since the promotion of drop-in alternative jet fuel blends, PM emissions are expected to decrease significantly in the foreseeable future. Meanwhile, with the increasing use of alternative jet fuels, the fuel leakage issue has drawn attention in the industry. One of the significant differences between alternative jet fuels and conventional jet fuel is that alternative jet fuels are synthetic materials, and conventional jet fuel comes from natural fossil fuel resources. Therefore, alternative jet fuels usually have a much simpler molecular composition than fossil fuels. Consequently, a reasonable hypothesis is that some missing chemical components in alternative jet fuels cause the leakage issue.

Some researchers have investigated how fuel composition affects seal compatibility [50], [90]. It is proven that the lack of aromatics in alternative jet fuels is the primary cause for the leakage problem since aromatics promote swelling of the O-ring, which enhances sealing ability. Although the study of alternative jet fuel leakage started in the past decade, the experimental platforms and methods need to be upgraded to investigate alternative jet fuel's impact on O-rings further. For example, although aromatics are the primary source for leakage issues with pure alternative jet fuels, different aromatic structures also impact the sealing performance differently. Since aromatics will become additives in the alternative jet fuel formulation, finding the precise

aromatic species that prevent leakage but do not significantly affect emissions simultaneously is essential.

In this test campaign, the experimental method was developed from previous research on stress relaxation tests [117] with many significant improvements. With the upgrade of test equipment and experimental configuration, the O-ring's response to high and low temperatures has been investigated. Moreover, new experimental configurations can provide more realistic test conditions. Results indicated that the new test configuration offers a more effective method to describe seal behaviour in different fuels.

In general, the primary objective of this investigation is to establish a new test configuration to examine seal compatibility in various O-ring materials, fuels and temperatures.

However, the experiment was cut short due to the flood in the autumn of 2019. All experimental equipment and samples were lost during the flood. Although the scheduled tests on candidate fuels and O-rings were not completed, the results still indicate the new test method is valid for examining seal compatibility in various fuels. Therefore, the primary goal was still accomplished.

This chapter will describe the development of an innovative method to assess seal compatibility in various jet fuels. The experimental setup and procedure design will be presented and explained in detail first. Experimental results will be divided and discussed in the order of changes in fuel blends. A discussion of temperature impact will also be presented. Finally, candidate O-rings used throughout all testing procedures will be presented, and the damage level caused by fuel changes and temperature variation will be analysed.

### 6.2 Result and Discussion

The entire experiment method was continuously improved during the test campaign. It took some test runs with the complete setup until all experimental apparatus, test procedures, and data collection methods were properly integrated and produced valid results. Data from these test attempts will not be discussed in this section, and all analyses and discussions are based on the data collected from the final two test sets before the flood mentioned previously.

In general, data from these two valid sets were obtained and processed using the counterforce method, which involves two types of forces, F(N) and F0 (N), shown in Equation 6. 1.

Counterforce method = 
$$\frac{F}{F0}$$

Equation 6. 1

F refers to the direct counterforce measured by a sensor over time. F0 represents the initial counterforce obtained after 30 minutes of finishing all compression procedures provided by the Elastocon rig. The reason for using the counterforce method instead of direct counterforce is due to the nature of the O-ring. A new O-ring is highly compressible since it does not lose elasticity. Thirty minutes is essential for stabilizing the O-ring samples and sensor for better measurement accuracy.

Results were plotted according to the counterforce method, which will be presented clearly in this section. Considering the complexity of the experiment, such as fuel change and time requirements, the results will be divided according to the type of fuels that O-rings were immersed in to facilitate presentation. The discussion section will compare different candidate O-rings based on their behaviour in the fuels. In addition,

the impact of fuel exchange on counterforce method accuracy will be discussed for possible future improvements.

Temperature effects are also one of the major investigation objectives. Therefore, the influence on sealing behaviour after the high-temperature ageing process will be presented and analysed. Stress relaxation behaviour under low temperatures will also be discussed at the end of this chapter.

It should be noted that some minor fluctuations were observed across all results, which are considered negligible noise. This noise for a given fuel type might be due to minor temperature variations and rig vibrations. For example, during the experiment, it was recorded that closing the lab door would cause the measurement curve to fluctuate slightly. However, the fluctuation intensity is too small, and all O-ring samples were affected uniformly. This noise will not affect the overall trend, and the scientific findings from this data will be valid.

In addition, due to the rig design, some noticeable fluctuations occur during fuel exchange. The entire stress relaxation unit must be removed from the Elastocon system, and the sensor records these vibrations. The same problem was observed after transferring jigs from the oven to the Elastocon system, and the influence is worse because the jigs need to be repositioned in the stress relaxation unit, which often causes vibration and distorts the results. These undesired fluctuations in data collection need to be carefully monitored since they cause an unpredicted rise or decrease in the stress relaxation curve. Many measures have been applied to try to eliminate these fluctuations.

The impact of these fluctuations might affect the appearance of the results, but these artifacts are readily identifiable during analysis. Moreover, the primary purpose was to

develop a new test method. In this regard, the objective is still considered accomplished overall.

### 6.2.1 Jet A-1

Jet A-1 was used to start the first stage of the experiment with all four types of O-rings. It also served as a reference result throughout the served. It is essential to use Jet A-1 as the first test fuel, and the reason is clear.

First, fossil fuel has been shown to cause the elastomer to swell heavily after contact, and Jet A-1 is the most representative fossil fuel. The rapid swell behaviour will be recorded and presented immediately in the stress relaxation curve using the counterforce method during testing. Identifying the initial swelling behaviour in Jet A-1 could help assess whether the system is functioning properly. Second, Jet A-1 is the primary jet fuel used in the aviation industry and the main component in alternative jet fuel blends. Therefore, investigating the O-ring behaviour in Jet A-1 under the new test configuration with high compression provides an essential reference for other fuel blends.

Samples were immersed in Jet A-1 for 94 hours before the fuel exchange. The first few hours after O-ring fuel contact are shown in Figure 6. 1, and the full 80-hour stress relaxation curve is presented in Figure 6. 2.

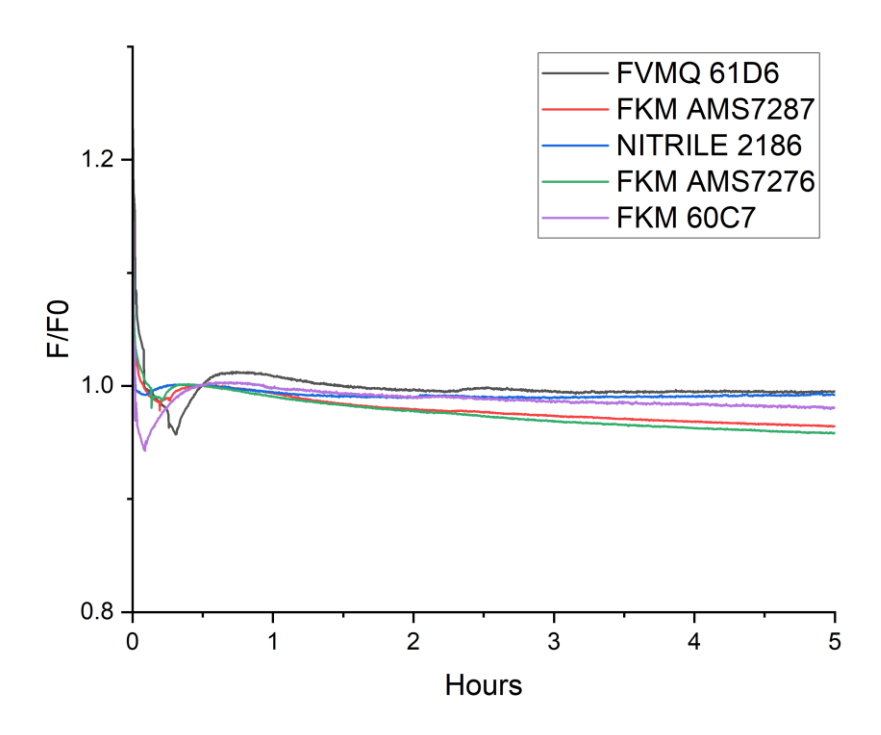


Figure 6. 1: Initial stress relaxation curve for 5 hours

Based on previous research [117], different types of O-rings exhibit their unique patterns in the initial stress relaxation curve. A typical nitrile O-ring undergoes three stages (quick reduction, swelling and further relaxation) in Jet A-1 during the first few hours. However, fluorosilicone (FS) O-rings show a continuous reduction trend regarding counterforce.

However, the conclusion from previous experiments was established under ideal conditions with full compression in the Elastocon system. Therefore, previous observations of distinct initial stress relaxation patterns may not be observed again in this test campaign, which is one of the key distinctions in this research.

Compared with previous O-ring behaviour patterns and according to Figure 6. 1, the new experiment reveals a different stress relaxation behaviour pattern. All O-ring samples decreased rapidly within the first 30 minutes due to the F/F0 calculation method, where F0 is the value of counterforce after 30 minutes. However, the rapid decrease indicates O-rings' high compressibility under such high compression.

Moreover, all O-ring samples exhibit swelling behaviour in the beginning. Additionally, expect for FKM type O-rings, FS (FVMQ 61D6) and nitrile (NITRILE 2186) show no further relaxation period, which will be more visible in Figure 6. 2.

In the 80-hour timeframe, the reaction force increases significantly for nitrile and FS, representing fuel penetration. Especially for nitrile, the trend becomes steeper after 10 hours, which shows the pronounced reactive behaviour of nitrile in Jet A-1 fuel.

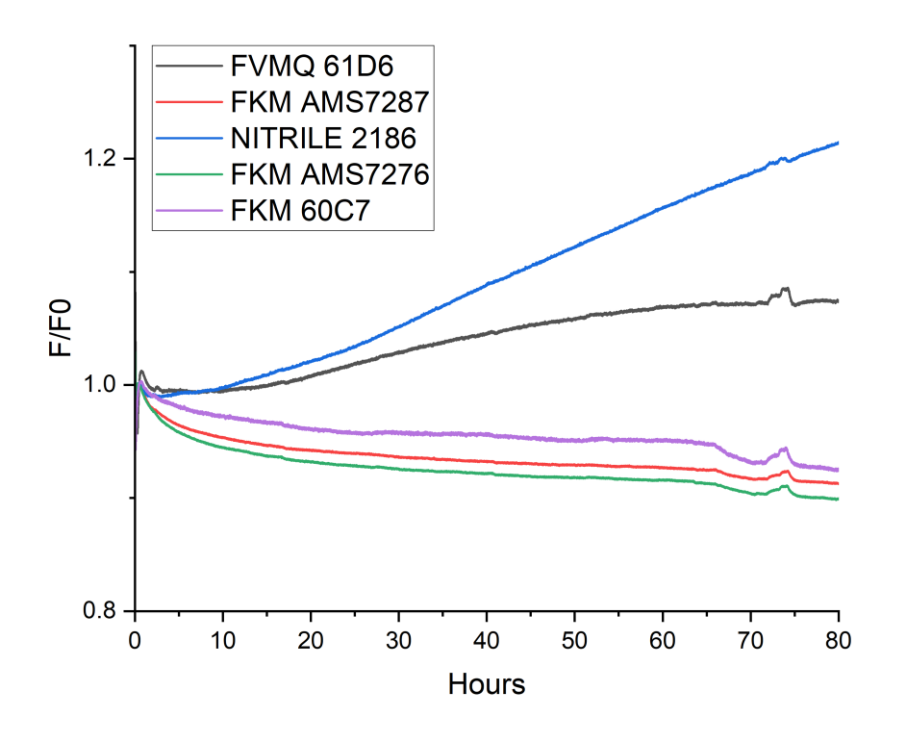


Figure 6. 2: The stress relaxation behaviour in Jet A-1 for 80 hours

In addition, all FKM type O-rings lost the ability to recover reaction force. The trend of F/F0 initially declined but stabilised at the end. The trend of the counterforce curve indicates that after a short period of influence caused by jet fuel contact, FKM quickly reaches equilibrium. The position of F/F0 is very close to the beginning position of FKM, which means that FKM maintained its sealing capability. This behaviour is due to the high fuel resistance properties of FKM, which prevent fuel molecules from penetrating the O-ring and causing seal swelling.

### 6.2.2 Jet A-1 to Alternative Jet Fuel (#13)

The fuel inside the Elastocon system was switched to Alternative Jet Fuel (#13) after testing with Jet A-1. The result of the corresponding O-ring behaviour is shown in Figure 6. 3. In theory, switching the fuel from Jet A-1 to any low aromatic alternative jet fuels should stop the aggressive O-ring swelling for some aromatic-sensitive materials such as nitrile. However, this effect has not been clearly demonstrated.

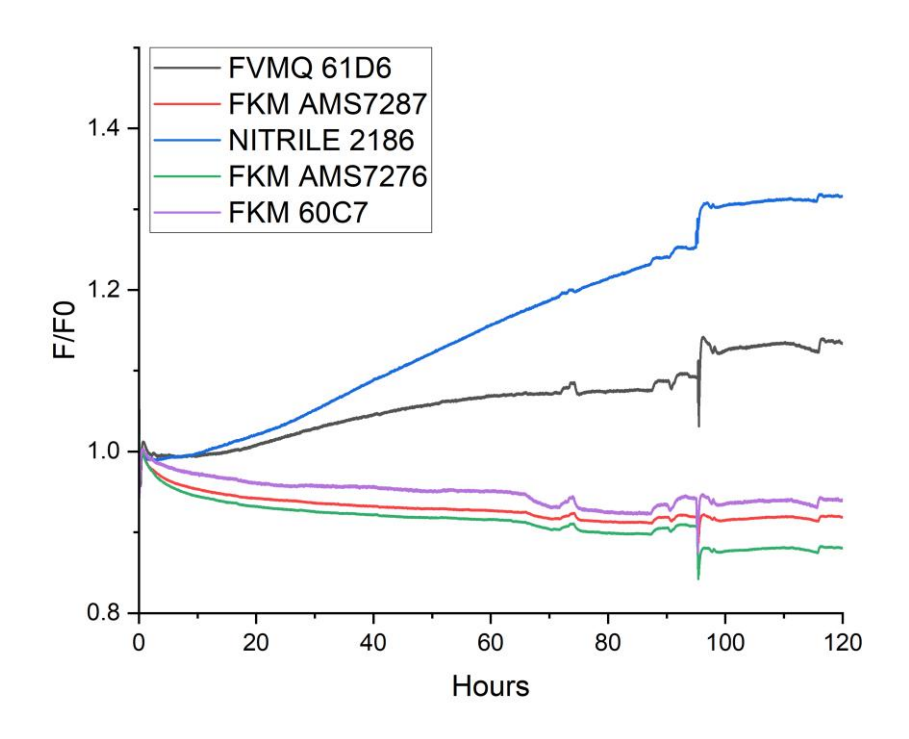


Figure 6. 3: The stress relaxation behaviour from Jet A-1 to Alternative Jet Fuel (#13)

Figure 6. 3 shows that all three FKM O-rings show no visible changes in counterforce. However, nitrile (NITRILE 2186) and FS (FVMQ 61D6) respond dramatically after contacting alternative jet fuels. The increasing trend on the stress relaxation curve (F/F0) stops immediately and remains flat throughout the alternative jet fuel exposure period. It is noticed that nitrile and FS showed the steepest increase before the alternative jet fuels treatment. This phenomenon indicates that low aromatic fuel restrains the swelling of the O-ring, reduces the sealing performance, and can lead to fuel leakage.

From a molecular perspective of nitrile, this behaviour suggests that fuel molecules cease penetrating the O-ring sample, which prevents the O-ring from swelling. In addition, the absorbed fuel component from Jet A-1 remain trapped inside the O-ring, which causes a flat trend in reaction force. This phenomenon also applies to the FS. However, for FKM, due to its high fuel resistance capacity, the fuel components cannot readily penetrate the O-ring, resulting in a flat trend of the F/F0 value shown in Figure 6. 3.

# 6.2.3 Alternative Jet Fuel (#13) to Alternative Jet Fuel (#4)

Fuel was switched from Alternative Jet Fuel #13 to Alternative Jet Fuel #4 in this experimental phase. The O-ring stress relaxation behaviour results are shown in Figure 6. 4. It is worth mentioning again that the only difference between #13 and #4 is the aromatic content, with approximately 10% greater concentration than Alternative Jet Fuel #4. All other fuel properties, including the specific aromatic species present are identical.

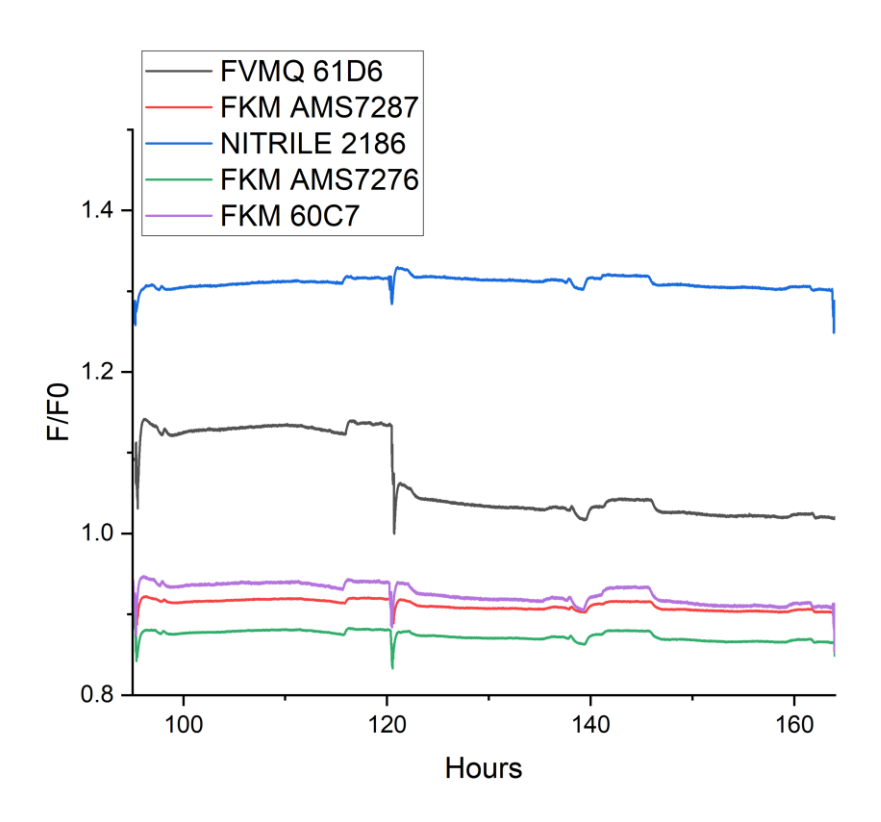


Figure 6. 4: The stress relaxation behaviour from Alternative Jet Fuel (#13) to Alternative Jet Fuel (#4)

According to Figure 6. 4, no significant change in the trend of the stress relaxation curve indicates that a slight shift in aromatic concentration will not affect swelling behaviour. It is an interesting finding since aromatic are known to significantly impact swelling behaviour. However, according to this figure, even aromatic-sensitive materials such as nitrile were unaffected by the reduced aromatic content. This phenomenon occurs because all O-rings samples have already reached molecular-level equilibrium conditions. Since the aromatic concentration Alternative Jet Fuel #4 is lower than in Alternative Jet Fuel #13, no additional molecules can penetrate the O-ring structure. However, when switched to a high aromatic concentration fuel, an increased trend in counterforce is predicted for aromatic-sensitive materials such as nitrile.

In addition, although the value of counterforce (F/F0) for nitrile and three FKM are similar before and after the fuel exchange, FS has a noticeable drop in counterforce. The reason behind this observation is complex.

This drop could be caused by undesirable vibrations during the fuel exchange. As mentioned previously, due to the instrument's design, fuel exchange requires removing the stress relaxation unit from the Elastocon, which could accidentally affect the sensor. However, the most crucial result requiring analysis is the trend of the counterforce curve, which remains unaffected by the initial drop in F/F0 after fuel exchange.

# 6.2.4 Alternative Jet Fuel (#4) to Jet A-1

Fresh Jet A-1 was used again to replace the alternative jet fuels in this experimental phase. This fuel change was designed to evaluate the recoverability of each O-ring material, especially aromatic-sensitive types such as nitrile and FS, which exhibited a dramatic increase in counterforce in the first 90 hours. In addition, the first thermal ageing process was performed after this fuel change, using Jet A-1 as the heating medium. This arrangement reflects the fact that Jet A-1 is the most widely used jet fuel in the aviation industry, making it ideal for establishing a reference line.

The stress relaxation curves for different O-ring materials are shown in Figure 6. 5. Although the exposure time to Jet A-1 in this phase was shorter than in other fuel-chang phases, the results shown in Figure 6. 5 provide sufficient data.

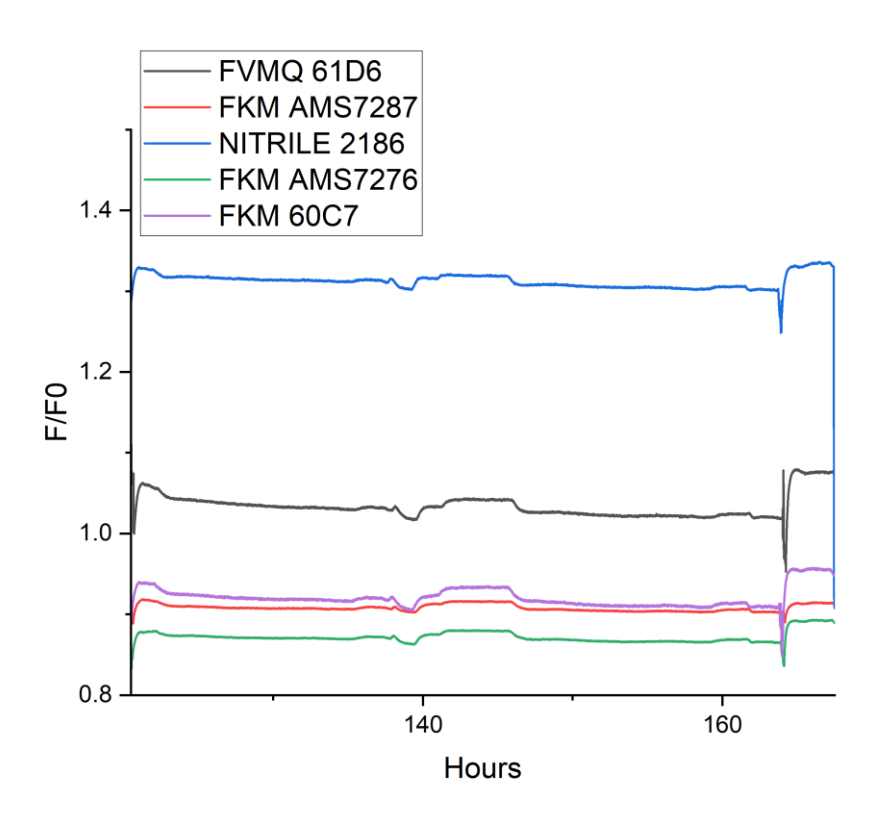


Figure 6. 5: The stress relaxation behaviour from Alternative Jet Fuel (#13) to Jet A-1

As presented in Figure 6. 5, most O-ring samples do not show any dramatic change in the trend of counterforce. This observation indicated that most O-ring samples lost the ability to absorb fuel molecules, and the exchange between elastomer and fuel molecules reached equilibrium. However, nitrile shows different behaviour. There has been a noticeable increase in counterforce. It indicated that nitrile is still sensitive to the increase in aromatic concentration, with continued fuel molecule absorption into the O-ring structure, more time is required to reach the equilibrium conditions. It could also be said that, at least at this point, nitrile could provide better sealing performance than other materials due to the swelling behaviour.

In addition, more time for the sample to immerse in Jet A-1 is preferred, which could potentially provide more precise exchange dynamics of fuel exchange, especially for nitrile. This improvement could be applied to future experiments. However, in general, the swelling behaviour of nitrile is successfully observed, so the scientific outcome is still valid.

### 6.2.5 High-temperature treatment

Heat treatment is mainly used to accelerate the ageing process in this investigation. Moreover, the temperature used in this experiment is relatively high compared with previous studies. A newly designed heating vessel and strategy were implemented as described in the previous section. Therefore, the performance and feasibility of adding a C11 jig and new heating method to the existing Elastocon stress relaxation system were evaluated. During the thermal ageing, vessels containing jigs are removed from the Elastocon system, meaning the temperature-dependent counterforce changes are not measurable. After high-temperature ageing, jigs containing O-ring samples will be reinstalled into the stress relaxation unit for Jet A-1 treatment for approximately 48 hours. Fresh Jet A-1 is used during this phase. The reason for using fresh Jet A-1 relates to oxidation during heating. Although this oxidation will not affect the O-ring samples, the fuel properties might change slightly. The results of the Jet A-1 treatment immediately after the first high-temperature treatment are shown in Figure 6. 6.

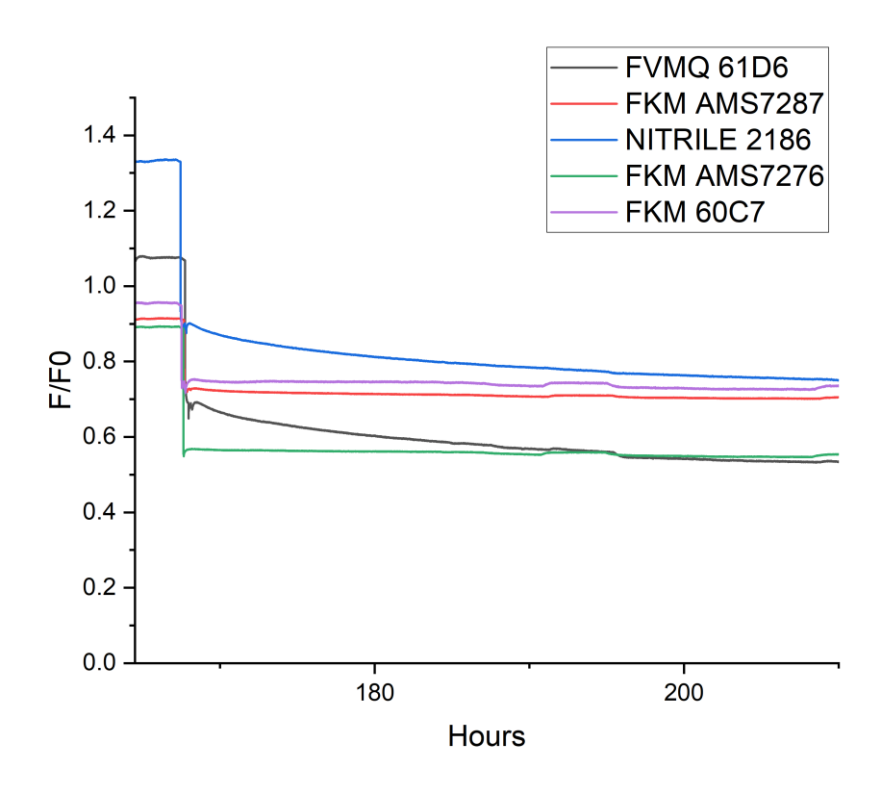


Figure 6. 6: Stress relaxation curve after the first heating process

Figure 6. 6 presents the reaction force curve immediately after heating jigs back into the Elastocon rig. As mentioned, the fuel used after the thermal ageing process is still Jet A-1.

After high-temperature treatment, all O-rings' reaction force values (F/F0) dropped dramatically. Moreover, the sequence of O-rings with different materials changed their pre-treatment sequence. FS showed a massive drop in counterforce, which is even lower than some FKM O-rings. Nitrile still has the highest counterforce among all samples, but the difference compared with FKM-type O-rings is decreased over time.

The reason for the immediate decrease in the value of counterforce might be the same as described in the previous fuel exchange section. The process of removing/reinstalling the stress relaxation unit could affect the readings. Moreover, jigs that contain O-rings were removed from the rig and placed in the heating vessel for the

heating process. Therefore, the major challenge is how to relocate jigs into stress relaxation rigs to their previous position after heating.

After the thermal ageing process and Jet A-1 treatment (shown in Figure 6. 6), fuel in the Elastocon rig were changed twice to fresh Alternative Jet Fuel #13 for 48 hours, then to Alternative Jet Fuel #4 for 67 hours. The respective stress relaxation curve is shown in Figure 6. 7.

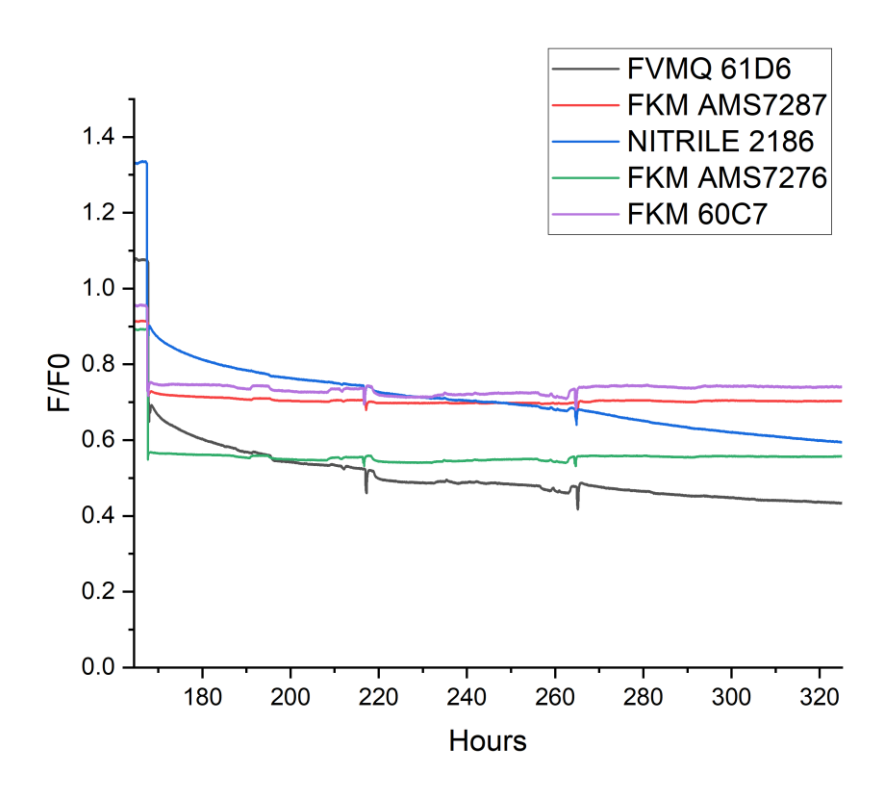


Figure 6. 7: Fuels impact on heat-treated sample after the first heating process

As Figure 6. 7 indicates, the trend of counterforce continues to decrease for nitrile and FS, the two types of material sensitive to aromatic content. For nitrile, although the value of counterforce is still higher than other FKM types in the first 48 hours of Jet A-1, after switching to Alternative Jet Fuel #13, the value is already lower than FKM AMS7287 and FKM 60C7. Moreover, the value of counterforce approaches FKM AMS7276 during the exposure of Alternative Jet Fuel #4. These phenomena indicate that the nitrile

completely loses its elasticity after high-temperature ageing, and the O-ring's internal components begin dissolving into the fuel. FS shows similar situation but severe degradation. The value of counterforce continues decreasing and becomes lower than all FKM O-rings by the final measurement.

Overall, FKM shows its ability to maintain the counterforce after the thermal ageing process, which indicates that for long service and multiple fuel exchange conditions, FKM is generally better than nitrile and FS in sealing ability. Moreover, it should be noted that the heating temperature is higher for FKM since FKM has a relatively high temperature resistance. Although the reason for using higher ageing temperature is to maximise the ageing effects, results show that the high-temperature resistance of FKM is still valid under high compression. Although FS and nitrile types lost their elasticity and sealing capability after the first ageing process, extra high-temperature heating is performed to assess the test configuration's reliability and investigate the limits of the other three FKM O-rings.

Figure 6. 8 presents the complete test sequence for Set 6. After 47 hours of treatment in Alternative Jet Fuel #4, the second thermal ageing process is performed. Fuel is then switched to Jet A-1 to determine whether swelling behaviour will occur in the test sample. According to the figure, the overall trend is similar to the trend discovered after the first ageing cycle, indicating that both FS and nitrile continue to decrease dramatically in counterforce. It suggests that FS and nitrile have lost their sealing capability.

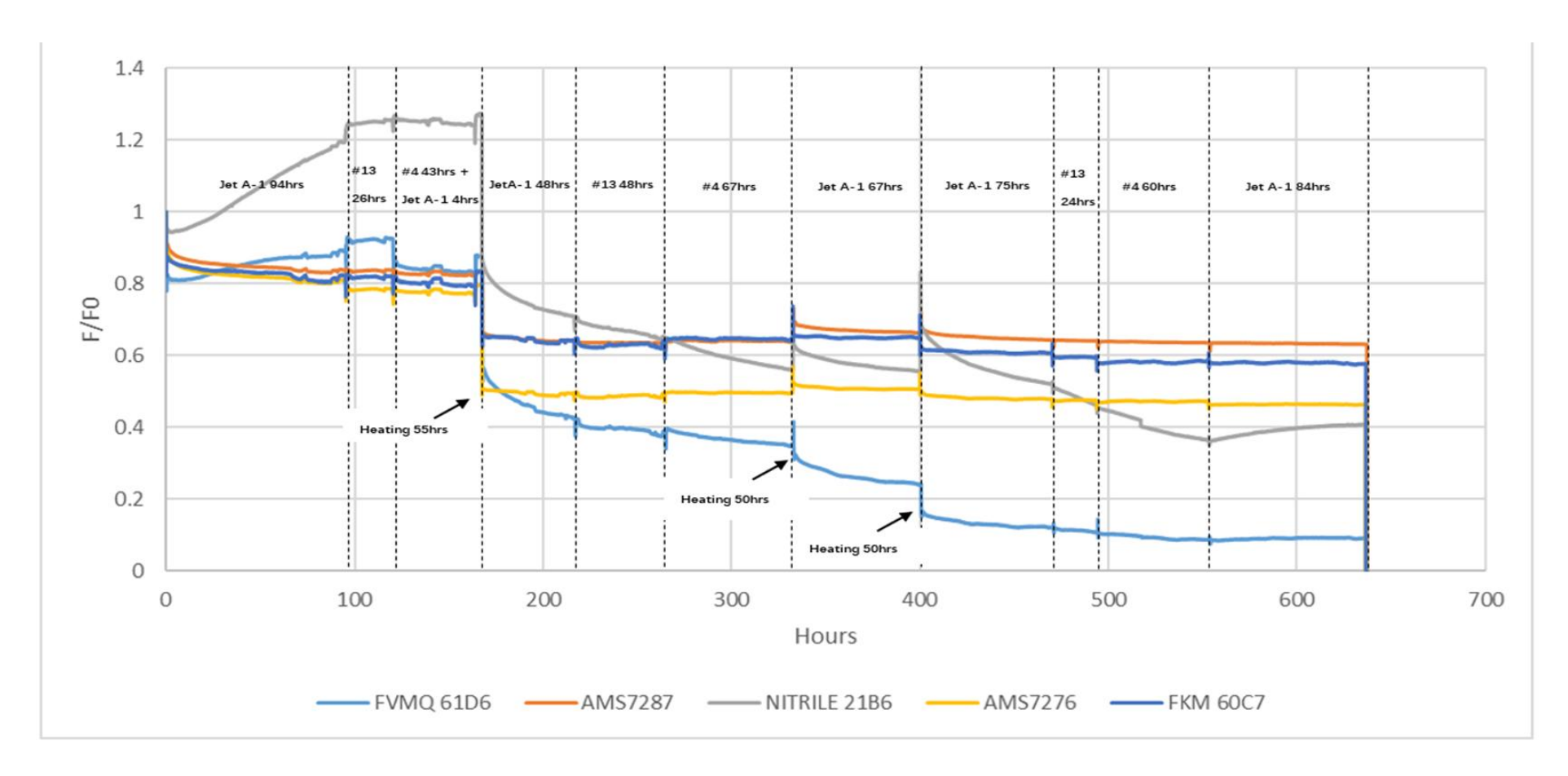


Figure 6. 8: All high-temperature ageing processes and fuel exchanges of Set 6

On the other hand, all three FKM O-rings still maintain the same level of counterforce, which indicates that this FKM has not yet lost selling ability completely. A final high-temperature ageing process is performed after 67 hours of Jet A-1 treatment. The behaviour of counterforce for this ageing process is unchanged from earlier tests.

In general, it could be concluded that FS and nitril quickly lose their sealing capability after the high-temperature ageing process. It suggests that, compared to FKM, these two materials do not have the advantage for long-term sealing applications.

### **6.2.6 Low-temperature impact**

Testing the sealing performance of an O-ring product in a realistic condition is one of the objectives for this investigation. As the experiment aims to provide the actual inservice condition, the lowest temperature selected in the test is -40 °C to simulate temperature while an aircraft is in the stratosphere. All test samples will ideally be placed in the rig for 24 hours per fuel at -40 °C. However, the actual experiment condition is more complex. As mentioned, only a few attempts have been successfully performed due to damage to the original chiller and the following flood.

The overall stress reaction curve is shown in Figure 6. 9 (a), and the corresponding fuel temperature is presented in Figure 6. 9 (b)

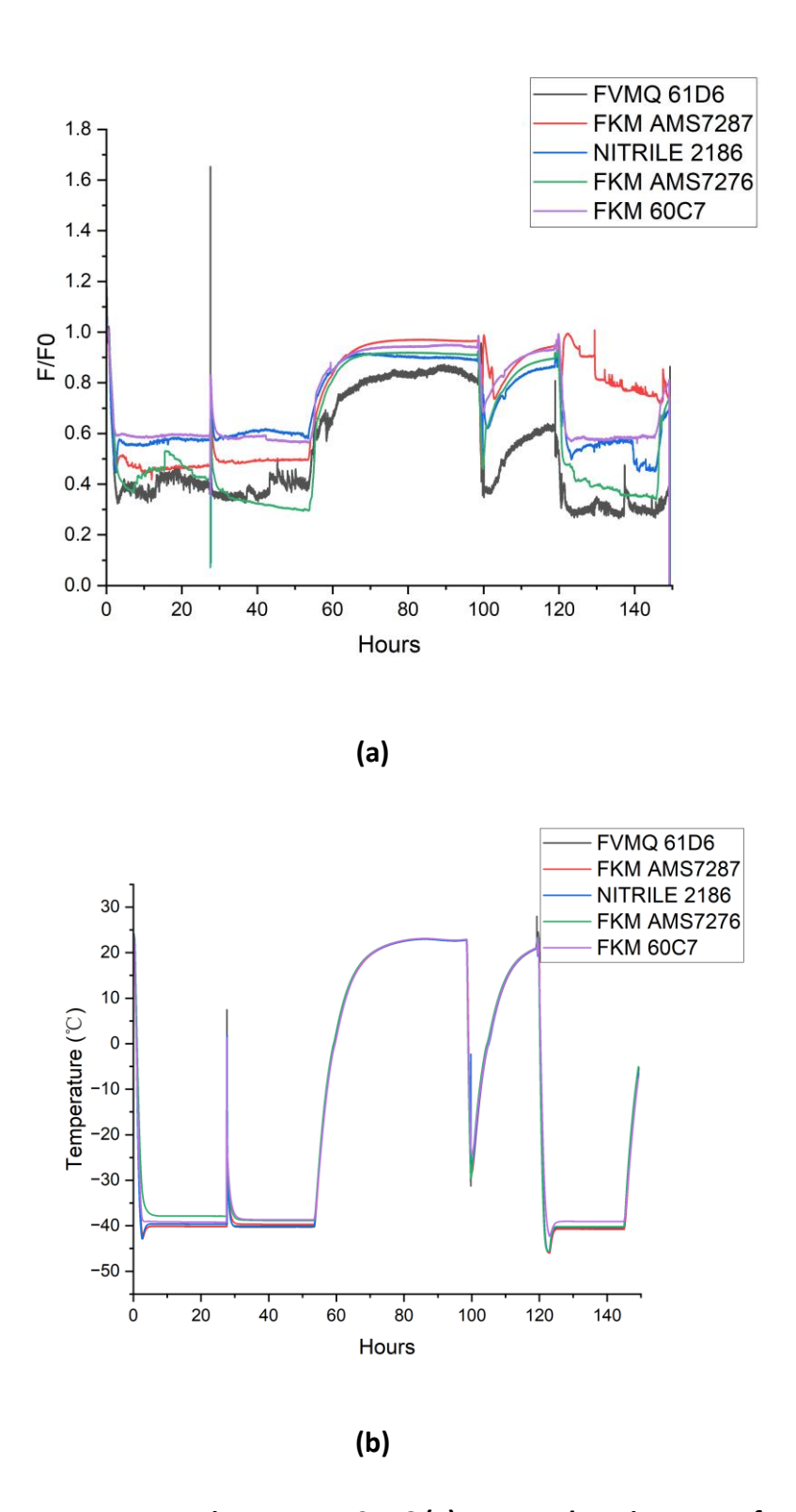


Figure 6. 9: Low-temperature impacts on Set 6 (a) stress relaxation curve for different materials (b) temperature curve.

O-ring samples in Jet A-1 are first reduced to -40  $^{\circ}$ C, and this temperature is maintained for 25 hours. It can be seen from Figure 6. 9 (a) that the counterforce decreases as

temperature drops. Although the temperature was maintained at -40°C for a long period, the reaction force was not stabilised for sample O-rings, especially for FS and FKM AMS 7276, which may indicate poor tolerance under low-temperature environments. It could also suggest that these two O-ring samples have already reached their physical limit, and low temperature amplified their counterforce/ sealing performance failure.

Fuel is then switched to Alternative Jet Fuel #13 for 25 hours, and the behaviour of test samples is similar to the Jet A-1 period. It indicates that for Set 6, the candidate O-ring is not sensitive to aromatic change under low temperatures. It is expected since all samples have lost their aromatic sensitivity after ageing.

Temperature is then increased to room temperature slowly. After samples reach the stable condition, another temperature-dropping process down to -40 °C is performed. The temperature of sample O-rings is then recovered to room temperature again, followed by a final temperature decrease treatment to -40 °C. This set of temperature circular processes is performed to assess the recovery ability of O-rings, and according to Figure 6. 9, the reaction force of all material increases with temperature rise, and it decreases rapidly with temperature reduction. Therefore, it could be concluded that sealing performance for all materials is highly sensitive to temperature changes.

# 6.2.7 Experiment replicability

Since the investigation uses a newly established testing rig and experiment methodology, the effectiveness of the results needs to be assessed. Therefore, another set of O-ring samples, Set 7, is established to check the replicability of these new test configurations. Set 7 runs in parallel with Set 6 as a control group and with careful time management. Both samples will not disturb each other even when using the same experiment equipment. There is no difference in the material for O-ring samples

between Set 6 and Set 7. However, due to the tolerance of O-rings and C11 jigs, the value of the precompression was still calculated based on the measurement of these new O-rings.

#### 6.2.7.1 Fuel impacts and heat ageing treatment

The overall results of Set 7 are presented in Figure 6. 10. Jet A-1 was used to establish a baseline in the first 67 hours. The behaviour of each type of O-rings is identical to that in Set 6, where FS and nitrile show an increased trend in counterforce.

The fuel exchange strategy of Set 7 is similar to that of Set 6, which followed the sequence of Jet A-1, Alternative Jet Fuel #13, and Alternative Jet Fuel #4. Each fuel period lasted 24 hours after the first heating ageing process. In total, two heat treatments of 50 and 67 hours respectively were performed to accelerate the ageing process.

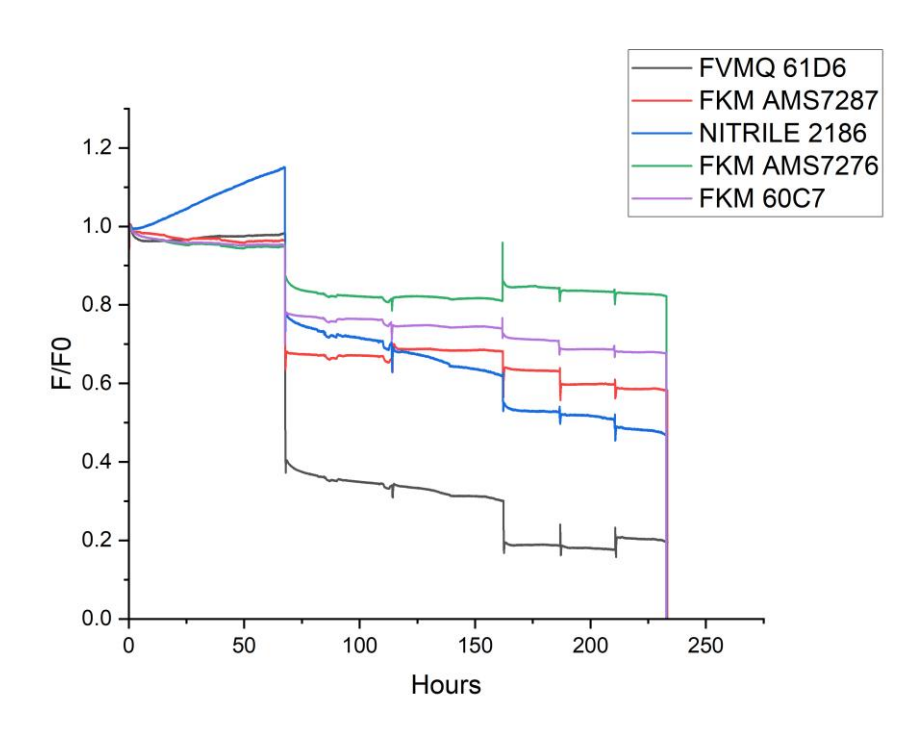


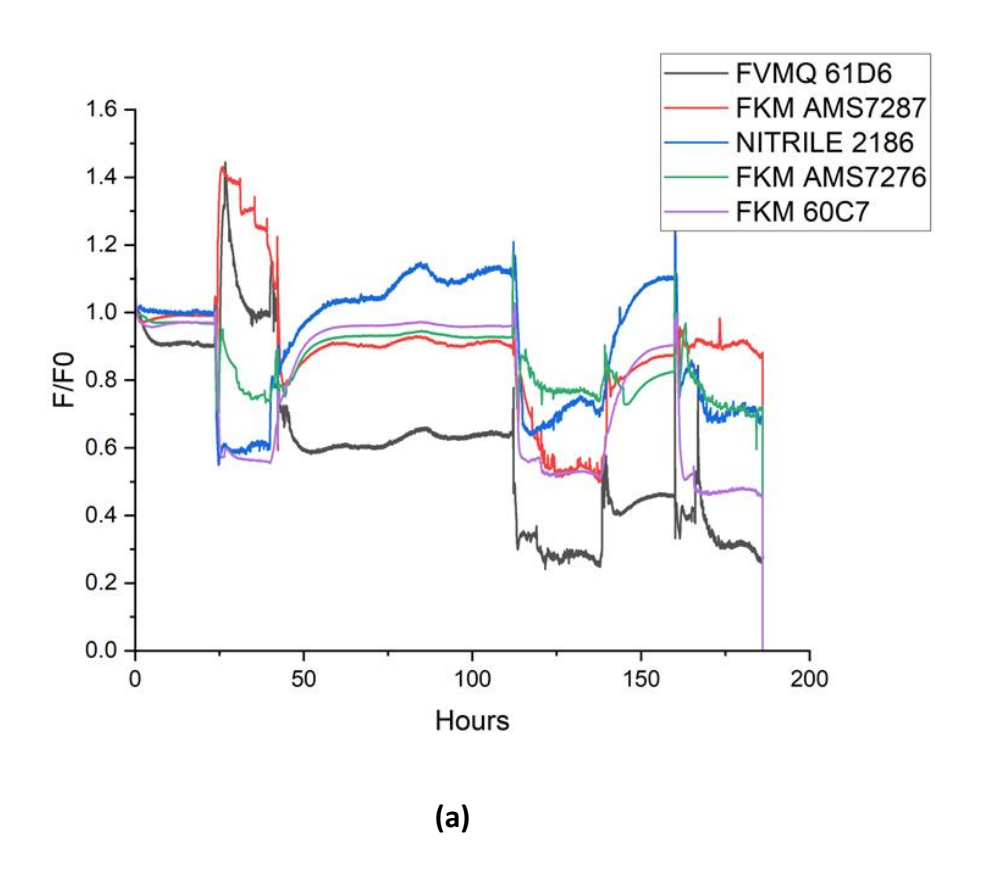
Figure 6. 10: Stress relaxation curve for Set 7

As presented in Figure 6. 10, nitrile dramatically increases counterforce while immersed in Jet A-1, and FS shows a slightly increasing trend of F/F0. Meanwhile, all FKM materials show a slight decline trend in terms of counterforce.

Generally, the behaviour of the test O-ring sample is the same between Set 6 and Set 7. The conclusion is that FS and nitrile have poor sealing ability during prolonged exposure to various fuel environments. It also confirms the reliability of the new test configuration.

#### 6.2.7.2 Low-temperature impact

The replicability of low-temperature impact on O-ring seal compatibility has also been examined. Figure 6. 11 presents the temperature cycling for Set 7 between room temperature and -40  $^{\circ}$ C.



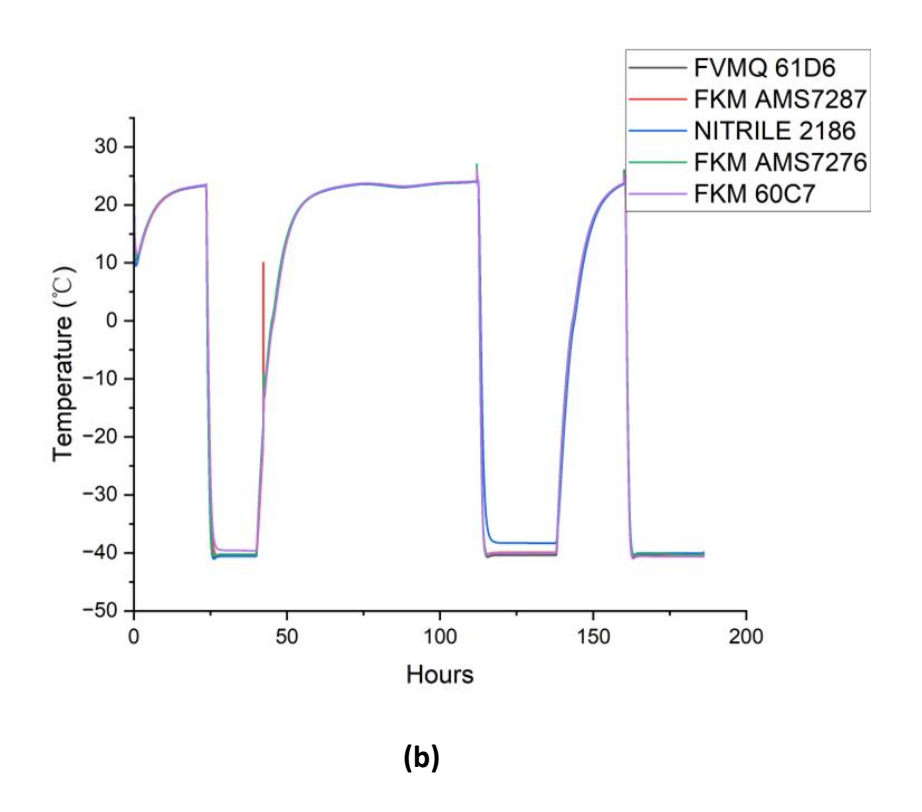


Figure 6. 11: Low-temperature impacts on Set 7 (a) stress relaxation curve for different materials (b) temperature curve.

According to Figure 6. 11, the stress relaxation curve indicated that the counterforce is sensitive to temperature changes, consistent with the results of Set 6, but the sequence of O-ring samples varied. It might be because all test samples had lost the sealing ability. Generally, the behaviour of counterforce during low-temperature treatment is similar between Set 6 and Set 7.

# 6.2.8 Physical appearance of O-rings after the experiment

Figure 6. 12 illustrates the O-ring condition for each set after completing the ageing process including complex fuel-changing process, high temperature ageing (180°C for FKM and FS, 110°C for nitrile) and low temperature ageing (-40°C), as detailed from Figure 6. 8 to Figure 6. 11. These damages were recorded through visual and tactile inspection. It would be ideal to send these samples for further analysis. However, the flood happened immediately after completing this experimental stage, and the photo is

the only evidence left. Nevertheless, the effect on different materials is significant enough to support the evaluation of each O-ring's performance. In general, all types of O-ring materials exhibit some physical deformation.



Figure 6. 12: O-ring physical appearance.

FS is the softest among all samples and is significantly softer than the original condition, which means it has lost its elasticity entirely and starts to dissolve into the fuel.

Nitrile samples are harder than in their initial condition. In addition, the surface of the nitrile O-ring is extremely flat, which could be evidence of extreme compression caused by aggressive swelling behaviour during the test. Too much swelling means a significant volume increase, and the volume dramatically decreases after the thermal ageing process. The massive change in volume is one of the primary reasons for fuel leaking problems.

All three FKM O-rings are harder than the original, indicating fuel absorption, which means an imbalance in molecular exchange between the fuel and O-ring material. However, only a few compression marks appear on the surface compared to nitrile, suggesting that FKM is more stable in various testing environments. Moreover, the same material has similar damage conditions in both sets of O-ring samples, demonstrating the experiment's replicability.

#### 6.3 Conclusion

Generally, one complete test run could be divided into four phases: precompression, fuel exchange, high-temperature ageing and low-temperature treatment. It should be mentioned that the experimental method was continually improved, which resulted in some flaws during the investigation. For example, ideally, the duration for each O-ring sample in a given fuel type should be the same, but this was not the case in the test due to the lab's opening schedule. However, it should be emphasised again this inconsistency does not affect the conclusion made from the experiment results since immersion time in one fuel across samples is still the same. The primary objective of this experiment is to establish a reliable experimental method to investigate the behaviour of O-ring in a wide range of materials, temperatures and fuels. Therefore, different times spent in one fuel will provide variability, making the experiment results closer to actual service conditions. The same principle applies to temperature treatment.

Three types of O-rings, FKM, FS and nitrile, have been tested under high compression (25% of original CSD). After analysing the experimental results, it could be concluded that FKM has the best sealing performance among these materials in different fuels and temperatures. Although nitrile shows strong swelling behaviour initially, it loses its elasticity after a long ageing process and will cause fuel leakage. Different manufacturing standards did not significantly impact the sealing performance for FKM.

Overall, the majority of the test rig and methodology were established successfully. The combination of the C11 jig and Elastocon provides a new approach to assess seal compatibility under high pressure, which offers a more realistic test environment than previous research.

Still, many questions remain unanswered, and significant improvements can be made. The test platform and methodology require further refinement, particularly regarding fuel exchange methods and strategies. The current fuel exchange procedure requires manual filling and pouring actions, which causes many problems during the test campaign. The compression applied to the O-ring is relatively high. Although most compression is fixed physically by C11 jigs, Elastocon is still extremely sensitive to any disturbance. Therefore, unwanted reaction force disturbances occur every time of fuel exchange. The same problem also affects the results of low-temperature treatment when using the manual fuel exchange method. The temperature of the fuel must return to room temperature to change the fuel. Otherwise, water in the air will freeze on the surface of the jigs, which will block the movement between jig plates and pollute the fuel. Time is also wasted waiting for the temperature to recover to room temperature.

Developing a suitable fuel exchange system will be the final component of this experiment methodology. For example, a simple micropump and tubing system could theoretically solve the problem.

# 7. Conclusions on alternative fuels on emissions and seal compatibility and future work

This section will discuss an overall conclusion combining all knowledge achieved from three result chapters. It will also provide potential improvements for future work that could enhance the current experimental methodology and extend the understanding of alternative jet fuels regarding both emission prediction and seal compatibility.

#### 7.1 Overall conclusions

A various of aromatics species were investigated for their effects on PM and gaseous emission using a combustor chamber from a Tay engine. Moreover, analytical models were establish based on a model Tay combustor to simulate the combustion process and investigate potential soot tracers. In addition, a more practical test platform for Oring sealing performance under various temperature and fuels were established.

The key findings of this thesis are summarised below:

Fuel blends with two different aromatic concentrations were tested for their soot
production in the Tay rig. The result indicates that the fuel blend with higher
aromatic content produces significantly more soot while using the Tay combustor.
This conclusion is consistent with the emissions tests on other gas turbine
combustors. The impact of various aromatic species on PM and gaseous emissions
was evaluated in the Tay combustor. Results indicated that different aromatics
affect emissions differently, especially for soot production.

- Aromatic structure seems to play an important role in soot production.
   Monoaromatics produce less soot compared to diaromatics under the same concentration level. This shows that aromatics with more complete benzene ring structures tend to produce more PM.
- Within monoaromatic species, different species exhibit varying soot production. It was found that the presence of alicyclic compounds in the molecular structure significantly promotes soot production. This may occur because ring structures are difficult to decompose during the combustion process. This finding is also valuable for selecting soot tracers in the simulation model. Molecules with complete ring structure, such as benzene, were considered, different from other studies using very small molecules as soot racers
- Density also presents relatively high correlations with PM production. This is because fuel blends with higher density usually contain more fuel components which requires a longer residence time to complete combust in the same volume. However, it should be pointed out that fuel blends used in this thesis are relatively simple compared to actual commercial fuels, as the main objective of this thesis is to investigate the differences between aromatic species. Therefore, for real inservice jet fuels, density cannot be used as the only indicator of soot production. Multiple fuel properties are necessary to be considered for accurate prediction.
- A 0-D simulation model has been established using Ansys Chemkin-Pro analysing various residence times, AFR and reaction temperature. Potential tracers were evaluated as well. In general, large molecules like C<sub>6</sub>H<sub>6</sub> and C<sub>14</sub>H<sub>10</sub> provide more reliable soot prediction than small intermediates such as acetylene in the 0-D model.

- CRN models were also developed to represent the combustion process inside a model Tay combustor. A detailed methodology on how to build a CRN model was presented. The CRN results indicate that C<sub>6</sub>H<sub>6</sub> might be a suitable candidate for soot prediction, since it is difficult to consume and can form larger PAHs through certain pathways. Methylnaphthalene was also found to have the ability to produce more soot intermediates than other aromatics. These results agree with the experimental results presented in Chapter 4.
- A new experimental method for evaluating the reliability of seal compatibility under various temperatures and fuel types has been established. High pressure and extreme temperature testing become an option to test elastomer samples in fuel systems. In general, this test configuration works as desired, and it shows high experimental replicability.
- Three types of O-rings, FKM, FS, and nitrile, were tested using a complex fuel-switching process and temperature treatment. In general, nitrile showed strong sealing ability initially with conventional aromatic-rich jet fuel, due to its ability to absorb fuel components into its molecular structure. However, after switching to alternative jet fuels with lower aromatic concentrations, the advantage of nitrile disappeared rapidly. This explains the fuel leakage problems in gas turbine engines are usually found after switching from conventional to alternative jet fuels when using nitrile in the fuel system.
- FKM (Viton) shows relatively stable sealing performance in alternative jet fuels
  compare to other test materials which agree with the findings in previous research.
  Unlike previous studies, this study applied more realistic multiple fuel-switching
  procedures and temperature treatment under high compression, which did not

significantly compromise its sealing performance compare with others. This makes it a viable option to use in the future fuel systems using alternative jet fuels.

FS shows strong sensitivity to high temperatures and fuel switching under new test
configurations. Since the high-temperature treatment in this thesis was used to
accelerate the ageing effect on O-rings, this rapid decrease in seal performance
might indicate a shorter lifespan compared to other O-ring materials.

# 7.2 Suggestions on future work

According to the knowledge achieved during the research, some possible future work is recommended here which might be worth for further study.

The most important improvement that could be considered in the future would be the perfection of the test methodology for the seal compatibility experiment. Although the new test method works fine in general, some improvements still need to be implemented. For example, the fuel-changing process could be improved during the experiment. Cells containing fuel and samples need to be pulled out for fuel exchange. The jigs and samples are under high compression, so the process of fuel change would affect test results noticeably. Moreover, in low-temperature experiments, a new fuel exchange system is essential. Fuel cannot be changed under extremely low temperatures to prevent the generation of ice from air on test samples. Some fuel exchange units are commercially available and could be introduced into the current experiment setup. In addition, the impact of aromatic species on the sealing ability of various elastomer materials is also worth investigating.

More work could be done regarding the soot simulation model. Further investigation
or modification of the 1-D model proposed in this thesis could be done for more
accurate simulation of a gas turbine combustor. A physical model to simulate the
fuel mixture in the primary zone is recommended.

# **Bibliography**

- (EIA). [Online]. Available: https://www.eia.gov/energyexplained/oil-and-petroleum-products/
- [2] B. R. Swopes, "1 January 1914," This day in aviation. Accessed: Apr. 10, 2023. [Online].

  Available: https://www.thisdayinaviation.com/1-january-1914/
- [3] International Civil Aviation Organization (ICAO), "Effects of Novel Coronavirus (COVID-19) on Civil Aviation: Economic Impact Analysis," International Civil Aviation Organization (ICAO). Accessed: Jun. 25, 2023. [Online]. Available: https://www.icao.int/sustainability/Documents/COVID-19/ICAO\_Coronavirus\_Econ\_Impact.pdf
- [4] Ihssane Mounir, "Commercial Market Outlook 2022-2041." Accessed: Jun. 01, 2023.

  [Online]. Available: https://www.boeing.com/resources/boeingdotcom/market/assets/downloads/CM

  O\_2022\_Report\_FINAL\_v02.pdf
- [5] S. Shparberg and B. Lange, "Global Market Forecast 2022." Accessed: Jun. 01, 2023.

  [Online]. Available: https://www.airbus.com/sites/g/files/jlcbta136/files/2022-07/GMF-Presentation-2022-2041.pdf
- [6] National Air and Space Museum, "Jumo 004B Engine." Accessed: Jul. 01, 2022. [Online]. Available: https://airandspace.si.edu/collection-objects/junkers-jumo-004-b-turbojet-engine/nasm\_A19670124000

- [7] Royal Air Force Museum, "Comet The First Jet Airliner." Accessed: Jul. 03, 2022.

  [Online]. Available: https://www.rafmuseum.org.uk/research/archive-exhibitions/comet-the-worlds-first-jet-airliner/
- [8] H. Saravanamuttoo, C. Rogers, H. Cohen, and P. Straznicky, *Gas Turbine Theory*, Sixth. Harlow: Pearson Education Limited, 2009.
- [9] A. j. Colozza, "Hydrogen Storage for Aircraft Applications Overview," Ohio, 2002.
- [10] G. D. Brewer, *Hydrogen aircraft technology*. London: CRC Press, 1991.
- [11] M. Masiol and R. M. Harrison, "Aircraft engine exhaust emissions and other airport-related contributions to ambient air pollution: A review," *Atmos Environ*, vol. 95, pp. 409–455, 2014, doi: 10.1016/j.atmosenv.2014.05.070.
- [12] U. S. Senate, "Health impacts of PM-2.5 associated with power plant emissions: hearing before the Committee on Environment and Public Works," Washington, D.C, 2002.
- [13] H. Bockhorn, *Soot formation in combustion: mechanisms and models.* Berlin: London: Springer, 1994.
- [14] E. E. M. and V. G. M. E.D. Banús, M.A. Ulla, "Structured Catalysts for Soot Combustion for Diesel Engines," in *Diesel Engine Combustion, Emissions and Condition Monitoring*, London: InTech, 2013, ch. 5, p. 118. doi: 10.5772/54516.
- [15] M. Thomson and T. Mitra, "A radical approach to soot formation," *Science (1979)*, vol. 361, no. 6406, pp. 978–979, 2018, doi: 10.1126/science.aau5941.
- [16] A. H. Lefebvre and D. R. Ballal, *Gas turbine combustion alternative fuels and emissions*, 3rd ed. London: CRC Press, 2010.

- [17] G. A. Kelesidis, A. Nagarkar, U. Trivanovic, and S. E. Pratsinis, "Toward Elimination of Soot Emissions from Jet Fuel Combustion," *Environ Sci Technol*, vol. 57, no. 28, pp. 10276–10283, Jul. 2023, doi: 10.1021/acs.est.3c01048.
- [18] R. L. Schalla and G. E. McDonald, "Variation in Smoking Tendency," *Ind Eng Chem*, vol. 53, no. 7, pp. 1497–1500, 1953.
- [19] R. A. Hunt, "Relation of Smoke Point to Molecular Structure," *Ind Eng Chem*, vol. 45, no. 3, pp. 602–606, 1953, doi: 10.1021/ie50519a039.
- [20] X. Xue, X. Hui, P. Singh, and C. J. Sung, "Soot formation in non-premixed counterflow flames of conventional and alternative jet fuels," *Fuel*, vol. 210, no. May, pp. 343–351, 2017, doi: 10.1016/j.fuel.2017.08.079.
- [21] A. Macintosh and L. Wallace, "International aviation emissions to 2025: Can emissions be stabilised without restricting demand?," *Energy Policy*, vol. 37, no. 1, pp. 264–273, 2009, doi: 10.1016/j.enpol.2008.08.029.
- [22] S. M. Palash, M. A. Kalam, H. H. Masjuki, B. M. Masum, I. M. Rizwanul Fattah, and M. Mofijur, "Impacts of biodiesel combustion on NOx emissions and their reduction approaches," *Renewable and Sustainable Energy Reviews*, vol. 23, no. x, pp. 473–490, 2013, doi: 10.1016/j.rser.2013.03.003.
- [23] I. Jhun, B. A. Coull, A. Zanobetti, and P. Koutrakis, "The impact of nitrogen oxides concentration decreases on ozone trends in the USA," *Air Qual Atmos Health*, vol. 8, no. 3, pp. 283–292, 2015, doi: 10.1007/s11869-014-0279-2.
- [24] K. M. Latha and K. V. S. Badarinath, "Correlation between black carbon aerosols, carbon monoxide and tropospheric ozone over a tropical urban site," *Atmos Res*,

- vol. 71, no. 4, pp. 265–274, 2004, doi: 10.1016/j.atmosres.2004.06.004.
- [25] IPCC, "Aviation and the Global Atmosphere." Accessed: Mar. 04, 2019. [Online]. Available: https://archive.ipcc.ch/ipccreports/sres/aviation/110.htm
- [26] Aviation Fuels Technical Review. 2007.
- [27] C. Saggese *et al.*, "A physics-based approach to modeling real-fuel combustion chemistry V. NOx formation from a typical Jet A," *Combust Flame*, vol. 212, no. x, pp. 270–278, 2020, doi: 10.1016/j.combustflame.2019.10.038.
- [28] N. Asgari and B. Padak, "Effect of fuel composition on NOx formation in high-pressure syngas/air combustion," *AIChE Journal*, vol. 64, no. 8, pp. 3134–3140, 2018, doi: 10.1002/aic.16170.
- [29] G. S. Samuelsen, J. Brouwer, M. A. Vardakas, and J. D. Holdeman, "Experimental and modeling investigation of the effect of air preheat on the formation of NOx in an RQL combustor," *Heat and Mass Transfer/Waerme- und Stoffuebertragung*, vol. 49, no. 2, pp. 219–231, 2013, doi: 10.1007/s00231-012-1080-0.
- [30] J. Harper, E. Durand, P. Bowen, D. Pugh, M. Johnson, and A. Crayford, "Influence of alternative fuel properties and combustor operating conditions on the nvPM and gaseous emissions produced by a small-scale RQL combustor," *Fuel*, vol. 315, no. October 2021, p. 123045, 2022, doi: 10.1016/j.fuel.2021.123045.
- [31] "What is the greenhouse effect?," NASA. Accessed: Jul. 28, 2022. [Online]. Available: https://climate.nasa.gov/faq/19/what-is-the-greenhouse-effect/
- [32] W. A. Majewski and M. K. Khair, *Diesel Emissions and Their Control*. SAE International, 2006.

- [33] ATAG, "Aviation: Benefits Beyond Borders," 2020.
- [34] R. Mawhood, E. Gazis, S. de Jong, R. Hoefnagels, and R. Slade, "Production pathways for renewable jet fuel: a review of commercialization status and future prospects," *Biofuels, Bioproducts and Biorefining*, vol. 10, no. 4, pp. 462–484, 2016, doi: 10.1002/bbb.1644.
- [35] P. D. S. Lee, L. L. Lim, and B. Owen, "Bridging the aviation CO2 emissions gap: why emissions trading is needed," 2013.
- [36] C. Zhang, X. Hui, Y. Lin, and C. J. Sung, "Recent development in studies of alternative jet fuel combustion: Progress, challenges, and opportunities," *Renewable and Sustainable Energy Reviews*, vol. 54, pp. 120–138, 2016, doi: 10.1016/j.rser.2015.09.056.
- [37] J. Curtis, E. Metheny, and S. R. Sergent, "Hydrocarbon Toxicity," National library of Medicine. [Online]. Available: https://www.ncbi.nlm.nih.gov/books/NBK499883/
- [38] "Use of oil," U.S. Energy Information Administration (EIA). [Online]. Available: https://www.eia.gov/energyexplained/oil-and-petroleum-products/use-of-oil.php
- [39] H. W. Pohl and V. V. Malychev, "Hydrogen in future civil aviation," *Int J Hydrogen Energy*, vol. 22, no. 10–11, pp. 1061–1069, 1997, doi: 10.1016/s0360-3199(95)00140-9.
- [40] Congress of the United States, "Aircraft nuclear propulsion program. Hearing before the subcommittee on Research and Development of the Joint Committee on Atomic Energy," Washington, D.C, 1969.
- [41] L. Zheng et al., "Effects of Alternative Fuel Properties on Particulate Matter Produced

- in a Gas Turbine Combustor," *Energy and Fuels*, vol. 32, no. 9, pp. 9883–9897, 2018, doi: 10.1021/acs.energyfuels.8b01442.
- [42] S. Geleynse, K. Brandt, M. Garcia-Perez, M. Wolcott, and X. Zhang, "The Alcohol-to-Jet Conversion Pathway for Drop-In Biofuels: Techno-Economic Evaluation," *ChemSusChem*, vol. 11, no. 21, pp. 3728–3741, 2018, doi: 10.1002/cssc.201801690.
- [43] U. Trivanovic and S. E. Pratsinis, "Opinion: Eliminating aircraft soot emissions," Oct. 27, 2023. doi: 10.5194/ar-2023-15.
- [44] B. T. Brem *et al.*, "Effects of Fuel Aromatic Content on Nonvolatile Particulate Emissions of an In-Production Aircraft Gas Turbine," *Environ Sci Technol*, vol. 49, no. 22, pp. 13149–13157, 2015, doi: 10.1021/acs.est.5b04167.
- [45] G. Karavalakis *et al.*, "Evaluating the effects of aromatics content in gasoline on gaseous and particulate matter emissions from SI-PFI and SIDI vehicles," *Environ Sci Technol*, vol. 49, no. 11, pp. 7021–7031, 2015, doi: 10.1021/es5061726.
- [46] M. L. Botero, S. Mosbach, J. Akroyd, and M. Kraft, "Sooting tendency of surrogates for the aromatic fractions of diesel and gasoline in a wick-fed diffusion flame," *Fuel*, vol. 153, pp. 31–39, 2015, doi: 10.1016/j.fuel.2015.02.108.
- [47] Y. Qian, Y. Qiu, Y. Zhang, and X. Lu, "Effects of different aromatics blended with diesel on combustion and emission characteristics with a common rail diesel engine," *Appl Therm Eng*, vol. 125, pp. 1530–1538, 2017, doi: 10.1016/j.applthermaleng.2017.07.145.
- [48] W. E. Betts *et al.*, "Diesel Fuel Aromatic Content and Its Relationship With Emissions From Diesel Engines," *Concave*, no. 92, 1992.

- [49] C. S. Casal, G. Arbilla, and S. M. Corrêa, "Alkyl polycyclic aromatic hydrocarbons emissions in diesel/biodiesel exhaust," *Atmos Environ*, vol. 96, pp. 107–116, 2014, doi: 10.1016/j.atmosenv.2014.07.028.
- [50] K. Chen, H. Liu, and Z. xia, "The Impacts of Aromatic Contents in Aviation Jet Fuel on the Volume Swell of the Aircraft Fuel Tank Sealants," *SAE International Journal of Aerospace*, vol. 6, no. 1, pp. 2013-01–9001, 2013, doi: 10.4271/2013-01-9001.
- [51] Y. Liu, X. Sun, V. Sethi, D. Nalianda, Y. Li, and L. Wang, "Review of modern low emissions combustion technologies for aero gas turbine engines," *Progress in Aerospace Sciences*, vol. 94, no. November 2016, pp. 12–45, Oct. 2017, doi: 10.1016/j.paerosci.2017.08.001.
- [52] I. El Helou, A. W. Skiba, and E. Mastorakos, "Experimental Investigation of Soot Production and Oxidation in a Lab-Scale Rich-Quench-Lean (RQL) Burner," *Flow Turbul Combust*, vol. 106, no. 4, pp. 1019–1041, 2021, doi: 10.1007/s10494-020-00113-5.
- [53] I. El Helou, J. M. Foale, R. S. Pathania, R. Ciardiello, A. W. Skiba, and E. Mastorakos, "A comparison between fossil and synthetic kerosene flames from the perspective of soot emissions in a swirl spray RQL burner," *Fuel*, vol. 331, no. P1, p. 125608, 2023, doi: 10.1016/j.fuel.2022.125608.
- [54] G. Jeong and K. Ahn, "One-dimensional analysis of double annular combustor for reducing harmful emissions," *Energies (Basel)*, vol. 14, no. 13, 2021, doi: 10.3390/en14133930.
- [55] A. M. Boies et al., "Particle emission characteristics of a gas turbine with a double

- annular combustor," *Aerosol Science and Technology*, vol. 49, no. 9, pp. 842–855, 2015, doi: 10.1080/02786826.2015.1078452.
- [56] D. F. Schultz, *Exhaust emissions of a double annular combustor: parametric study.*Washington, D.C: National Aeronautics and Space Administration, 1975.
- [57] M. Chmielewski and M. Gieras, "Impact of variable geometry combustor on performance and emissions from miniature gas turbine engine," *Journal of the Energy Institute*, vol. 90, no. 2, pp. 257–264, 2017, doi: 10.1016/j.joei.2016.01.004.
- [58] Y. G. Li and R. L. Hales, "Steady and dynamic performance and emissions of a variable geometry combustor in a gas turbine engine," *J Eng Gas Turbine Power*, vol. 125, no. 4, pp. 961–971, 2003, doi: 10.1115/1.1615253.
- [59] J. A. Saintsbury and P. Sampath, "Atmospheric Tests of a Variable Combustor Geometry for Reducing Gas Turbine Emissions," *J Fluids Eng*, pp. 327–333, 1975, doi: 10.1115/1.3447311.
- [60] S. A. Mosier and R. M. Pierce, "Advanced Combustor Systems for Stationary Gas Turbine Engines Contract," Mar. 1980.
- [61] Y. Liu, X. Sun, V. Sethi, D. Nalianda, Y. Li, and L. Wang, "Review of modern low emissions combustion technologies for aero gas turbine engines," *Progress in Aerospace Sciences*, vol. 94, no. November 2016, pp. 12–45, Oct. 2017, doi: 10.1016/j.paerosci.2017.08.001.
- [62] A. S. Feitelberg and M. A. Lacey, "The GE Rich-Quench-Lean Gas Turbine Combustor," 1998. [Online]. Available: http://asmedigitalcollection.asme.org/gasturbinespower/article-

- pdf/120/3/502/5889487/502\_1.pdf
- [63] M. Makida, H. Yamada, Y. Kurosawa, T. Yamamoto, K. Matsuura, and S. Hayashi, "PRELIMINARY EXPERIMENTAL RESEARCH TO DEVELOP A COMBUSTOR FOR SMALL CLASS AIRCRAFT ENGINE UTILIZING PRIMARY RICH COMBUSTION APPROACH," Power for Land, 2006. [Online]. Available: http://www.asme.org/about-asme/terms-of-use
- [64] J. Harper, "An Experimental Study of the nvPM Emissions Produced by Alternative Aviation Fuels in a Newly-Developed RQL Research Combustor," 2022.
- [65] C. Ling, J. Hamilton, and B. Khandelwal, "Chapter 1 Feedstock and pathways for alternative aviation fuels," in *Aviation Fuels*, B. Khandelwal, Ed., Elsevier Science Publishing Co Inc, 2021, ch. 1, pp. 1–22.
- [66] S. Blakey, L. Rye, and C. W. Wilson, "Aviation gas turbine alternative fuels: A review," *Proceedings of the Combustion Institute*, vol. 33, no. 2, pp. 2863–2885, 2011, doi: 10.1016/j.proci.2010.09.011.
- [67] R. Przysowa, B. Gawron, T. Białecki, A. Łęgowik, J. Merkisz, and R. Jasiński, "Performance and emissions of a microturbine and turbofan powered by alternative fuels," *Aerospace*, vol. 8, no. 2, pp. 1–20, 2021, doi: 10.3390/aerospace8020025.
- [68] E. Corporan *et al.*, "Emissions characteristics of a turbine engine and research combustor burning a Fischer-Tropsch jet fuel," *Energy and Fuels*, vol. 21, no. 5, pp. 2615–2626, 2007, doi: 10.1021/ef070015j.
- [69] M. Cheng, "A Comprehensive Program for Measurement of Military Aircraft Emissions," 2009. doi: 10.1590/S0066-782X2010000400019.

- [70] C. C. Wey, B. E. Anderson, and C. Hampton, "Aircraft Particle Emissions experiment (APEX)," 2006.
- [71] M. L. Botero, S. Mosbach, and M. Kraft, "Sooting tendency of paraffin components of diesel and gasoline in diffusion flames," *Fuel*, vol. 126, pp. 8–15, 2014, doi: 10.1016/j.fuel.2014.02.005.
- [72] R. Howard and N. Carolina, "Alternative Aviation Fuel Experiment ( AAFEX )," 2011.
- [73] R. Del Rosario, J. Koudelka, R. Wahls, N. Madavan, and D. Bulzan, "Alternative Aviation Fuel Experiment II (AAFEX II) Overview," NASA. Accessed: Mar. 04, 2018.

  [Online]. Available: https://ntrs.nasa.gov/citations/20150010381
- [74] M. T. Timko *et al.*, "Particulate emissions of gas turbine engine combustion of a fischer-tropsch synthetic fuel," *Energy and Fuels*, vol. 24, no. 11, pp. 5883–5896, 2010, doi: 10.1021/ef100727t.
- [75] B. A. Almohammadi, P. Singh, S. Sharma, S. Kumar, and B. Khandelwal, "Impact of alkylbenzenes in formulated surrogate fuel on characteristics of compression ignition engine," *Fuel*, vol. 266, no. December 2019, p. 116981, 2020, doi: 10.1016/j.fuel.2019.116981.
- [76] J. P. Longwell, E. E. Frost, and M. A. Weiss, "Flame Stability in Bluff Body Recirculation Zones," *Ind Eng Chem*, vol. 45, no. 8, pp. 1629–1633, 1953, [Online]. Available: https://pubs.acs.org/sharingguidelines
- [77] S. R. Turns, *An introduction to combustion*, Second. McGraw-Hill, 1996.
- [78] H. C. Hottel, G. C. Wii, and A. H. Bonnell, "Application of Well-stirred Reactor Theory to the Prediction of Combustor Performance," 1958.

- [79] A. M. Mellor and D. C. Hammond, "A Preliminary Investigation of Gas Turbine Combustor Modelling," *Combustion Science and Technology*, vol. 2, no. 2–3, pp. 67–80, Nov. 1970, doi: 10.1080/00102207008952236.
- [80] D. Mavris, "Enhanced Emission Prediction Modeling and Analysis for Conceptual Design," 2007. [Online]. Available: www.asdl.gatech.edu
- [81] D. L. Allaire, "A Physics-Based Emissions Model for Aircraft Gas Turbine Combustors," 2006.
- [82] I. T. OSGERBY, "Literature Review of Turbine Combustor Modeling and Emissions," *AIAA Journal*, vol. 12, no. 6, pp. 743–754, Jun. 1974, doi: 10.2514/3.49345.
- [83] F. Di Mare, W. P. Jones, and K. R. Menzies, "Large eddy simulation of a model gas turbine combustor," *Combust Flame*, vol. 137, no. 3, pp. 278–294, May 2004, doi: 10.1016/j.combustflame.2004.01.008.
- [84] K. Zhang, "Turbulent Combustion Simulation in Realistic Gas-Turbine Combustors,"2017.
- [85] M. J. Dewitt, E. Corporan, J. Graham, and D. Minus, "Effects of aromatic type and concentration in Fischer— Tropsch fuel on emissions production and material compatibility," *Energy & Fuels*, no. 9, pp. 2411–2418, 2008.
- [86] N. Jeyashekar, E. Frame, G. Wilson, S. Hutzler, and S. O. Brien, "Elastomer Fuel Compatibility Studies With Alternative Jet Fuels," in *ASME Turbo Expo 2013: Turbine Technical Conference and Exposition*, Texas, 2013, pp. 1–8.
- [87] E. Corporan *et al.*, "Chemical, thermal stability, seal swell, and emissions studies of alternative jet fuels," *Energy and Fuels*, vol. 25, no. 3, pp. 955–966, 2011, doi:

- 10.1021/ef101520v.
- [88] N. Chopde, G. H. Borse, O. Kuchanwar, and A. T. Ghodke, "Compatibility Assessment of Fuel System Elastomers with Bio-oil and Diesel Fuel," *Energy Fuels*, vol. 30, p. 6486–6494, 2016, doi: 10.1021/acs.energyfuels.6b01138.
- [89] L. I. Farfán-Cabrera, J. Pérez-González, and E. A. Gallardo-Hernández, "Deterioration of seals of automotive fuel systems upon exposure to straight Jatropha oil and diesel," *Renew Energy*, vol. 127, pp. 125–133, 2018, doi: 10.1016/j.renene.2018.04.048.
- [90] J. L. Graham, "Impact of Alternative Jet Fuel and Fuel Blends on Non- Metallic Materials Used in Commercial Aircraft Fuel Systems," 2014.
- [91] Y. Liu, "Investigation on Elastomer Compatibility with Alternative Aviation Fuels.," 2013.
- [92] A. F. Bicen, D. G. N. Tse, and J. H. Whitelaw, "Combustion Characteristics of a Model Can-Type Combustor," 1990.
- [93] L. Zheng, J. Cronly, E. Ubogu, I. Ahmed, Y. Zhang, and B. Khandelwal, "Experimental investigation on alternative fuel combustion performance using a gas turbine combustor," *Appl Energy*, vol. 238, no. October 2018, pp. 1530–1542, 2019, doi: 10.1016/j.apenergy.2019.01.175.
- [94] N. J. Wilson, "Developing the Rolls-Royce Tay," *THE AMERICAN SOCIETY OF MECHANICAL ENGINEERS*, 1988, [Online]. Available: http://asmedigitalcollection.asme.org/GT/proceedings-pdf/GT1988/79191/V002T02A017/2397656/v002t02a017-88-gt-302.pdf

- [95] L. Zheng, J. Cronly, E. Ubogu, I. Ahmed, Y. Zhang, and B. Khandelwal, "Experimental investigation on alternative fuel combustion performance using a gas turbine combustor," *Appl Energy*, vol. 238, no. October 2018, pp. 1530–1542, 2019, doi: 10.1016/j.apenergy.2019.01.175.
- [96] P. J. Ashmole, "INTRODUCING THE ROLLS-ROYCE TAY," *AIAA Paper*, 1983, doi: 10.2514/6.1983-1377.
- [97] "Laser Induced Incandescence Theory of Operation," Artium. [Online]. Available: https://www.artium.com/lii-theory-of-operation
- [98] L. Zheng, "Sheffield Gaseous Emission Profile of Alternative Fuel in a Gas Turbine Combustor [Unpublished manuscript]]."
- [99] B. A. A. Almohammadi, "Investigating the Effects of Alternative Fuels with Different Aromatic Species on Compression Ignition Engine Emissions and Performance," The University of Sheffield, 2020.
- [100] S. K. Chaulya and G. M. Prasad, "Gas Sensors for Underground Mines and Hazardous Areas," in *Sensing and Monitoring Technologies for Mines and Hazardous Areas*, S.
  K. Chaulya and G. M. Prasad, Eds., Elsevier, 2016, ch. Chapter 3, pp. 161–212. doi: 10.1016/b978-0-12-803194-0.00003-9.
- [101] "Infrared Non Dispersive CO2 Analyzer Working Principle," Inst Tools. Accessed: Aug. 03, 2022. [Online]. Available: https://instrumentationtools.com/infrared-non-dispersive-co2-analyzer-working-principle/
- [102] N. E. Sánchez, A. Callejas, A. Millera, R. Bilbao, and M. U. Alzueta, "Formation of PAH and soot during acetylene pyrolysis at different gas residence times and reaction

- temperatures," *Energy*, vol. 43, no. 1, pp. 30–36, 2012, doi: 10.1016/j.energy.2011.12.009.
- [103] N. Chindaprasert, E. Hassel, J. Nocke, C. Janssen, M. Schultalbers, and O. Magnor, "Prediction of CO Emissions from a Gasoline Direct Injection Engine Using CHEMKIN®," in *SAE technical paper series*, Oct. 2006. doi: 10.4271/2006-01-3240.
- [104] "The CRECK Modeling Group." Accessed: May 20, 2020. [Online]. Available: http://creckmodeling.chem.polimi.it/menu-kinetics/menu-kinetics-detailed-mechanisms
- [105] W. Pejpichestakul *et al.*, "Examination of a soot model in premixed laminar flames at fuel-rich conditions," *Proceedings of the Combustion Institute*, vol. 37, no. 1, pp. 1013–1021, 2019, doi: 10.1016/j.proci.2018.06.104.
- [106] E. Ranzi, A. Frassoldati, A. Stagni, M. Pelucchi, A. Cuoci, and T. Faravelli, *Reduced kinetic schemes of complex reaction systems: Fossil and biomass-derived transportation fuels*, vol. 46, no. 9. 2014. doi: 10.1002/kin.20867.
- [107] E. Ranzi, C. Cavallotti, A. Cuoci, A. Frassoldati, M. Pelucchi, and T. Faravelli, "New reaction classes in the kinetic modeling of low temperature oxidation of n-alkanes," *Combust Flame*, vol. 162, no. 5, pp. 1679–1691, 2015, doi: 10.1016/j.combustflame.2014.11.030.
- [108] M. P. Boyce, "Gas Turbine Performance Test," in *Gas Turbine Engineering Handbook*, 4th ed., M. P. Boyce, Ed., Elsevier, 2012, ch. 20, pp. 769–802. doi: 10.1016/B978-0-12-383842-1.00020-2.
- [109] K. Gleason and A. Gomez, "Detailed Study of the Formation of Soot Precursors and

- Soot in Highly Controlled Ethylene(/Toluene) Counterflow Diffusion Flames," *J Phys Chem A*, vol. 127, no. 1, pp. 276–285, Jan. 2023, doi: 10.1021/acs.jpca.2c06538.
- [110] D. Golea, Y. Rezgui, M. Guemini, and S. Hamdane, "Reduction of PAH and Soot Precursors in Benzene Flames by Addition of Ethanol," *J Phys Chem A*, vol. 116, no. 14, pp. 3625–3642, Apr. 2012, doi: 10.1021/jp211350f.
- [111] K. Zhang, A. Ghobadian, and J. M. Nouri, "Scale-resolving simulation of a propane-fuelled industrial gas turbine combustor using finite-rate tabulated chemistry," *Fluids*, vol. 5, no. 3, Sep. 2020, doi: 10.3390/fluids5030126.
- [112] M. C. Paul and W. P. Jones, "Radiative heat transfer in a model gas turbine combustor," in *WIT Transactions on Engineering Sciences*, 2006, pp. 413–421. doi: 10.2495/HT060401.
- [113] A. F. Bicen and J. M. L. M. Palma, "Report Number FS/86/36," 1986.
- [114] J. SWITHENBANK and N. A. CHIGIER, "VORTEX MIXING FOR SUPERSONIC COMBUSTION".
- [115] J. Swithenbank, I. Poll, M. W. Vincent, and D. D. Wright, "COMBUSTION DESIGN FUNDAMENTALS."
- [116] J. Rosenthal, "ARL/ME Note 235," 1959.
- [117] Y. Liu, "Investigation on Elastomer Compatibility with Alternative Aviation Fuels.," 2013.
- [118] R. Hornig, "Comparison of various CSR methods regarding the static long-term sealing behaviour of AEM, ACM and HNBR compounds," *International Polymer Science and Technology*, vol. 37, no. 11, pp. 1–15, 2010.

- [119] S. Blakey and C. Ling, "Compatibility of Elastomeric Materials -Stress Relaxation Testing [Unpublished manuscript]," Sheffield, 2019.
- [120] Y. Liu, C. W. Wilson, S. Blakey, and T. Dolmansley, "Elastomer compatibility test of alternative fuels using stress-relaxation test and FTIR spectroscopy," *Proceedings of the ASME Turbo Expo*, vol. 1, pp. 637–647, 2011, doi: 10.1115/GT2011-46100.
- [121] K. G. Kyprianidis, D. Nalianda, and E. Dahlquist, "A NOx Emissions Correlation for Modern RQL Combustors," *Energy Procedia*, vol. 75, no. x, pp. 2323–2330, 2015, doi: 10.1016/j.egypro.2015.07.433.
- [122] P. Lobo, D. E. Hagen, and P. D. Whitefield, "Comparison of PM emissions from a commercial jet engine burning conventional, biomass, and fischer-tropsch fuels," *Environ Sci Technol*, vol. 45, no. 24, pp. 10744–10749, 2011, doi: 10.1021/es201902e.
- [123] Y. Qian, Y. Qiu, Y. Zhang, and X. Lu, "Effects of different aromatics blended with diesel on combustion and emission characteristics with a common rail diesel engine," *Appl Therm Eng*, vol. 125, pp. 1530–1538, 2017, doi: 10.1016/j.applthermaleng.2017.07.145.
- [124] C. S. Casal, G. Arbilla, and S. M. Corrêa, "Alkyl polycyclic aromatic hydrocarbons emissions in diesel/biodiesel exhaust," *Atmos Environ*, vol. 96, pp. 107–116, 2014, doi: 10.1016/j.atmosenv.2014.07.028.
- [125] W. E. Betts *et al.*, "Diesel Fuel Aromatic Content and Its Relationship With Emissions From Diesel Engines," *Concave*, no. 92, 1992.
- [126] G. Karavalakis *et al.*, "Evaluating the effects of aromatics content in gasoline on gaseous and particulate matter emissions from SI-PFI and SIDI vehicles," *Environ Sci*

- Technol, vol. 49, no. 11, pp. 7021-7031, 2015, doi: 10.1021/es5061726.
- [127] J. E. *et al.*, "Soot formation mechanism of modern automobile engines and methods of reducing soot emissions: A review," *Fuel Processing Technology*, vol. 235, no. February, p. 107373, 2022, doi: 10.1016/j.fuproc.2022.107373.
- [128] B. Owen *et al.*, "Review: Particulate Matter Emissions from Aircraft," *Atmosphere* (*Basel*), vol. 13, no. 8, pp. 1–19, 2022, doi: 10.3390/atmos13081230.
- [129] L. Miniero, K. Pandey, G. De Falco, A. D'Anna, and N. Noiray, "Soot-free and low-NO combustion of Jet A-1 in a lean azimuthal flame (LEAF) combustor with hydrogen injection," *Proceedings of the Combustion Institute*, vol. 39, no. 4, pp. 4309–4318, 2023, doi: 10.1016/j.proci.2022.08.006.
- [130] S. H. Park, "Simulation of the Formation and Growth of Soot Aerosol Particles in a Premixed Combustion Process Using a Soot Aerosol Dynamics Model," *Atmosphere* (*Basel*), vol. 13, no. 5, p. 847, May 2022, doi: 10.3390/atmos13050847.
- [131] J. I. Hileman and R. W. Stratton, "Alternative jet fuel feasibility," *Transp Policy (Oxf)*, vol. 34, pp. 52–62, 2014, doi: 10.1016/j.tranpol.2014.02.018.
- [132] M. Patel and A. Kumar, "Production of renewable diesel through the hydroprocessing of lignocellulosic biomass-derived bio-oil: A review," *Renewable and Sustainable Energy Reviews*, vol. 58, pp. 1293–1307, 2016, doi: 10.1016/j.rser.2015.12.146.
- [133] "Summit Next Gen to use Honeywell Ethanol to Jet fuel technology for production of sustainable aviation fuel," *Focus on catalysts*, p. 23, 2023, doi: 10.1016/j.focat.2023.06.020.

- [134] "Crop information: Maize," Food and Agriculture Organization of the United Nation.

  Accessed: Jul. 20, 2022. [Online]. Available: https://www.fao.org/land-water/databases-and-software/crop-information/maize/en/
- [135] U. Lee, H. Kwon, M. Wu, and M. Wang, "Retrospective analysis of the U.S. corn ethanol industry for 2005–2019: implications for greenhouse gas emission reductions," *Biofuels, Bioproducts and Biorefining*, vol. 15, no. 5, pp. 1318–1331, 2021, doi: 10.1002/bbb.2225.
- [136] K. E. Thome and C. Y. C. Lin Lawell, "Corn ethanol in the Midwestern USA: Local competition, entry and agglomeration," *J Econ Geogr*, vol. 22, no. 6, pp. 1247–1273, 2022, doi: 10.1093/jeg/lbab038.
- [137] G. Hochman and D. Zilberman, "Corn Ethanol and U.S. Biofuel Policy 10 Years Later:

  A Quantitative Assessment," *Am J Agric Econ*, vol. 100, no. 2, pp. 570–584, 2018, doi: 10.1093/ajae/aax105.
- [138] M. A. F. D. de Moraes, M. R. P. Bacchi, and C. E. Caldarelli, "Accelerated growth of the sugarcane, sugar, and ethanol sectors in Brazil (2000-2008): Effects on municipal gross domestic product per capita in the south-central region," *Biomass Bioenergy*, vol. 91, pp. 116–125, 2016, doi: 10.1016/j.biombioe.2016.05.004.
- [139] A. P. D. Turetta, T. Kuyper, T. F. Malheiros, and H. L. da C. Coutinho, "Corrigendum to 'A framework proposal for sustainability assessment of sugarcane in Brazil' [Land Use Policy 68 (2017) 597–603]," *Land use policy*, vol. 72, no. December 2017, pp. 578–585, 2018, doi: 10.1016/j.landusepol.2017.11.044.
- [140] M. S. Buckeridge, A. P. de Souza, R. A. Arundale, K. J. Anderson-Teixeira, and E.

- Delucia, "Ethanol from sugarcane in Brazil: A 'midway' strategy for increasing ethanol production while maximizing environmental benefits," *GCB Bioenergy*, vol. 4, no. 2, pp. 119–126, 2012, doi: 10.1111/j.1757-1707.2011.01122.x.
- [141] Y. D. Tan and J. S. Lim, "Feasibility of palm oil mill effluent elimination towards sustainable Malaysian palm oil industry," *Renewable and Sustainable Energy Reviews*, vol. 111, no. January, pp. 507–522, 2019, doi: 10.1016/j.rser.2019.05.043.
- [142] D. Darshini, P. Dwivedi, and K. Glenk, "Capturing stakeholdersĎ views on oil palmbased biofuel and biomass utilisation in Malaysia," *Energy Policy*, vol. 62, pp. 1128–1137, 2013, doi: 10.1016/j.enpol.2013.07.017.
- [143] T. Burimsitthigul, B. Yoosuk, C. Ngamcharussrivichai, and P. Prasassarakich, "Hydrocarbon biofuel from hydrotreating of palm oil over unsupported Ni–Mo sulfide catalysts," *Renew Energy*, vol. 163, pp. 1648–1659, 2021, doi: 10.1016/j.renene.2020.10.044.
- [144] M. H. Mat Yasin, R. Mamat, G. Najafi, O. M. Ali, A. F. Yusop, and M. H. Ali, "Potentials of palm oil as new feedstock oil for a global alternative fuel: A review," *Renewable and Sustainable Energy Reviews*, vol. 79, no. April 2016, pp. 1034–1049, 2017, doi: 10.1016/j.rser.2017.05.186.
- [145] A. Papini and M. C. Simeone, "Forest resources for second generation biofuel production," *Scand J For Res*, vol. 25, no. SUPPL. 8, pp. 126–133, 2010, doi: 10.1080/02827581.2010.485827.
- [146] J. D. Murphy and N. M. Power, "An argument for using biomethane generated from grass as a biofuel in Ireland," *Biomass Bioenergy*, vol. 33, no. 3, pp. 504–512, 2009,

- doi: 10.1016/j.biombioe.2008.08.018.
- [147] K. Mihajlovski, A. Buntić, M. Milić, M. Rajilić-Stojanović, and S. Dimitrijević-Branković, "From Agricultural Waste to Biofuel: Enzymatic Potential of a Bacterial Isolate Streptomyces fulvissimus CKS7 for Bioethanol Production," *Waste Biomass Valorization*, vol. 12, no. 1, pp. 165–174, 2021, doi: 10.1007/s12649-020-00960-3.
- [148] J. D. McMillan, "Biochemical refining of lignocellulose to biofuels: status and prospects," 2010.
- [149] M. Sainger, A. Jaiwal, P. A. Sainger, D. Chaudhary, R. Jaiwal, and P. K. Jaiwal, "Advances in genetic improvement of Camelina sativa for biofuel and industrial bioproducts," *Renewable and Sustainable Energy Reviews*, vol. 68, no. October 2016, pp. 623–637, 2017, doi: 10.1016/j.rser.2016.10.023.
- [150] Y. Herreras, V. Stern, and A. Capuano, "Sustainable Biofuel Raw Material Production for the Aviation Industry," 2010.
- [151] H. D. Belayneh, R. L. Wehling, Y. Zhang, and O. N. Ciftci, "Development of omega-3-rich Camelina sativa seed oil emulsions," *Food Sci Nutr*, vol. 6, no. 2, pp. 440–449, 2018. doi: 10.1002/fsn3.572.
- [152] H. A. Romijn and M. C. J. Caniëls, "The Jatropha biofuels sector in Tanzania 2005-2009: Evolution towards sustainability?," *Res Policy*, vol. 40, no. 4, pp. 618–636, 2011, doi: 10.1016/j.respol.2011.01.005.
- [153] J. Li, B. Bluemling, A. P. J. Mol, and T. Herzfeld, "Stagnating jatropha biofuel development in southwest China: An institutional approach," *Sustainability* (Switzerland), vol. 6, no. 6, pp. 3192–3212, 2014, doi: 10.3390/su6063192.

- [154] K. Kashe, D. L. Kgathi, M. Murray-Hudson, and K. B. Mfundisi, "Assessment of benefits and risks of growing Jatropha (Jatropha curcas) as a biofuel crop in sub-Saharan Africa: a contribution to agronomic and socio-economic policies," *J For Res* (*Harbin*), vol. 29, no. 1, pp. 1–12, 2018, doi: 10.1007/s11676-017-0460-1.
- [155] J. Wang *et al.*, "Creating values from wastes: Producing biofuels from waste cooking oil via a tandem vapor-phase hydrotreating process," *Appl Energy*, vol. 323, no. July, p. 119629, 2022, doi: 10.1016/j.apenergy.2022.119629.
- [156] V. R. Wiggers, A. Wisniewski, L. A. S. Madureira, A. A. C. Barros, and H. F. Meier, "Biofuels from waste fish oil pyrolysis: Continuous production in a pilot plant," *Fuel*, vol. 88, no. 11, pp. 2135–2141, 2009, doi: 10.1016/j.fuel.2009.02.006.
- [157] Y. Wang, Y. Cao, and J. Li, "Preparation of biofuels with waste cooking oil by fluid catalytic cracking: The effect of catalyst performance on the products," *Renew Energy*, vol. 124, pp. 34–39, 2018, doi: 10.1016/j.renene.2017.08.084.
- [158] W. Zhang *et al.*, "Green preparation of branched biolubricant by chemically modifying waste cooking oil with lipase and ionic liquid," *J Clean Prod*, vol. 274, p. 122918, 2020, doi: 10.1016/j.jclepro.2020.122918.
- [159] V. Makareviciene, V. Skorupskaite, and V. Andruleviciute, "Biodiesel fuel from microalgae-promising alternative fuel for the future: A review," *Rev Environ Sci Biotechnol*, vol. 12, no. 2, pp. 119–130, 2013, doi: 10.1007/s11157-013-9312-4.
- [160] S. Y. A. Siddiki *et al.*, "Microalgae biomass as a sustainable source for biofuel, biochemical and biobased value-added products: An integrated biorefinery concept," *Fuel*, vol. 307, no. September 2021, p. 121782, 2022, doi:

- 10.1016/j.fuel.2021.121782.
- [161] S. Nair and H. Paulose, "Emergence of green business models: The case of algae biofuel for aviation," *Energy Policy*, vol. 65, pp. 175–184, 2014, doi: 10.1016/j.enpol.2013.10.034.
- [162] J. Cowen and A. F. Hepp, "Synthesis and characterization of cobalt-containing nanoparticles on alumina: a potential catalyst for gas-to-liquid fuels production," 2016.
- [163] Q. Fei, M. T. Guarnieri, L. Tao, L. M. L. Laurens, N. Dowe, and P. T. Pienkos, "Bioconversion of natural gas to liquid fuel: Opportunities and challenges," *Biotechnol Adv*, vol. 32, no. 3, pp. 596–614, 2014, doi: 10.1016/j.biotechadv.2014.03.011.
- [164] J. A. Elia, J. Li, and C. A. Floudas, "Strategic planning optimization for natural gas to liquid transportation fuel (GTL) systems," *Comput Chem Eng*, vol. 72, pp. 109–125, 2015, doi: 10.1016/j.compchemeng.2014.04.010.
- [165] J. E. A. Graciano, B. Chachuat, and R. M. B. Alves, "Conversion of CO2-Rich Natural Gas to Liquid Transportation Fuels via Trireforming and Fischer-Tropsch Synthesis: Model-Based Assessment," *Ind Eng Chem Res*, vol. 57, no. 30, pp. 9964–9976, 2018, doi: 10.1021/acs.iecr.8b00135.
- [166] U.S. Energy Information Administration, "Global gas-to-liquids growth is dominated by two projects in South Africa and Uzbekistan." Accessed: Jun. 23, 2022. [Online].

  Available: https://www.eia.gov/todayinenergy/detail.php?id=33192
- [167] T. Qi, L. Zhou, X. Zhang, and X. Ren, "Regional economic output and employment

- impact of coal-to-liquids (CTL) industry in China: An input-output analysis," *Energy*, vol. 46, no. 1, pp. 259–263, 2012, doi: 10.1016/j.energy.2012.08.024.
- [168] M. Höök and K. Aleklett, "A review on coal-to-liquid fuels and its coal consumption," *Int J Energy Res*, vol. 34, no. 10, pp. 848–864, Aug. 2010, doi: 10.1002/er.1596.
- [169] Z. Liu, S. Shi, and Y. Li, "Coal liquefaction technologies-Development in China and challenges in chemical reaction engineering," *Chem Eng Sci*, vol. 65, no. 1, pp. 12–17, 2010, doi: 10.1016/j.ces.2009.05.014.
- [170] L. Zhou, M. Duan, and Y. Yu, "Exergy and economic analyses of indirect coal-to-liquid technology coupling carbon capture and storage," *J Clean Prod*, vol. 174, pp. 87–95, 2018, doi: 10.1016/j.jclepro.2017.10.229.
- [171] H. C. Mantripragada and E. S. Rubin, "Techno-economic evaluation of coal-to-liquids (CTL) plants with carbon capture and sequestration," *Energy Policy*, vol. 39, no. 5, pp. 2808–2816, 2011, doi: 10.1016/j.enpol.2011.02.053.
- [172] A. P. Steynberg, M. E. Dry, B. H. Davis, and B. B. Breman, "Fischer-Tropsch Reactors," in *Studies in Surface Science and Catalysis*, A. Steynberg and M. Dry, Eds., Elsevier, 2004, ch. Chapter 2, pp. 64–195. doi: 10.1016/S0167-2991(04)80459-2.
- [173] A. de Klerk *et al.*, "Sustainable aviation fuel: Pathways to fully formulated synthetic jet fuel via Fischer–Tropsch synthesis," *Energy Sci Eng*, no. November 2022, 2022, doi: 10.1002/ese3.1379.
- [174] M. Ojeda and S. Rojas, *Biofuels from Fischer-Tropsch synthesis*. NOVA, 2010.
- [175] Y. Jiang and D. Bhattacharyya, "Plant-wide modeling of an indirect coal-biomass to liquids (CBTL) plant with CO2 capture and storage (CCS)," *International Journal of*

- Greenhouse Gas Control, vol. 31, pp. 1–15, 2014, doi: 10.1016/j.ijggc.2014.09.022.
- [176] L. Tao, A. Milbrandt, Y. Zhang, and W. C. Wang, "Techno-economic and resource analysis of hydroprocessed renewable jet fuel," *Biotechnol Biofuels*, vol. 10, no. 1, pp. 1–16, 2017, doi: 10.1186/s13068-017-0945-3.
- [177] A. G. Romero-Izquierdo, F. I. Gómez-Castro, C. Gutiérrez-Antonio, S. Hernández, and M. Errico, "Intensification of the alcohol-to-jet process to produce renewable aviation fuel," *Chemical Engineering and Processing Process Intensification*, vol. 160, no. December 2020, pp. 1–11, 2021, doi: 10.1016/j.cep.2020.108270.
- [178] W. C. Wang and L. Tao, "Bio-jet fuel conversion technologies," *Renewable and Sustainable Energy Reviews*, vol. 53, pp. 801–822, 2016, doi: 10.1016/j.rser.2015.09.016.
- [179] J. Han, L. Tao, and M. Wang, "Well-to-wake analysis of ethanol-to-jet and sugar-to-jet pathways," *Biotechnol Biofuels*, vol. 10, no. 1, pp. 1–15, 2017, doi: 10.1186/s13068-017-0698-z.
- [180] M. Moreira, A. C. Gurgel, and J. E. A. Seabra, "Life cycle greenhouse gas emissions of sugar cane renewable jet fuel," *Environ Sci Technol*, vol. 48, no. 24, pp. 14756–14763, 2014, doi: 10.1021/es503217g.
- [181] C. T. Chong and J.-H. Ng, "Biojet fuel production pathways," in *Biojet Fuel in Aviation Applications*, C. T. Chong and J.-H. Ng, Eds., Elsevier, 2021, ch. Chapter 2, pp. 81–141. doi: 10.1016/B978-0-12-822854-8.00003-2.
- [182] S. Eswaran, S. Subramaniam, S. Geleynse, K. Brandt, M. Wolcott, and X. Zhang, "Techno-economic analysis of catalytic hydrothermolysis pathway for jet fuel

- production," *Renewable and Sustainable Energy Reviews*, vol. 151, no. July, p. 111516, 2021, doi: 10.1016/j.rser.2021.111516.
- [183] R. W. Stratton, H. Min Wong, and J. I. Hileman, "Life Cycle Greenhouse Gas Emissions from Alternative Jet Fuels," 2010. doi: PARTNER-COE-2010-001.

# **APPENDIX A - Feedstock of alternative jet fuels**

# A.1 Feedstock of alternative jet fuels

The classification of alternative jet fuels is complex due to various feedstocks and production pathways. A general alternative jet fuels feedstock and production pathway are present in Figure A. 1.

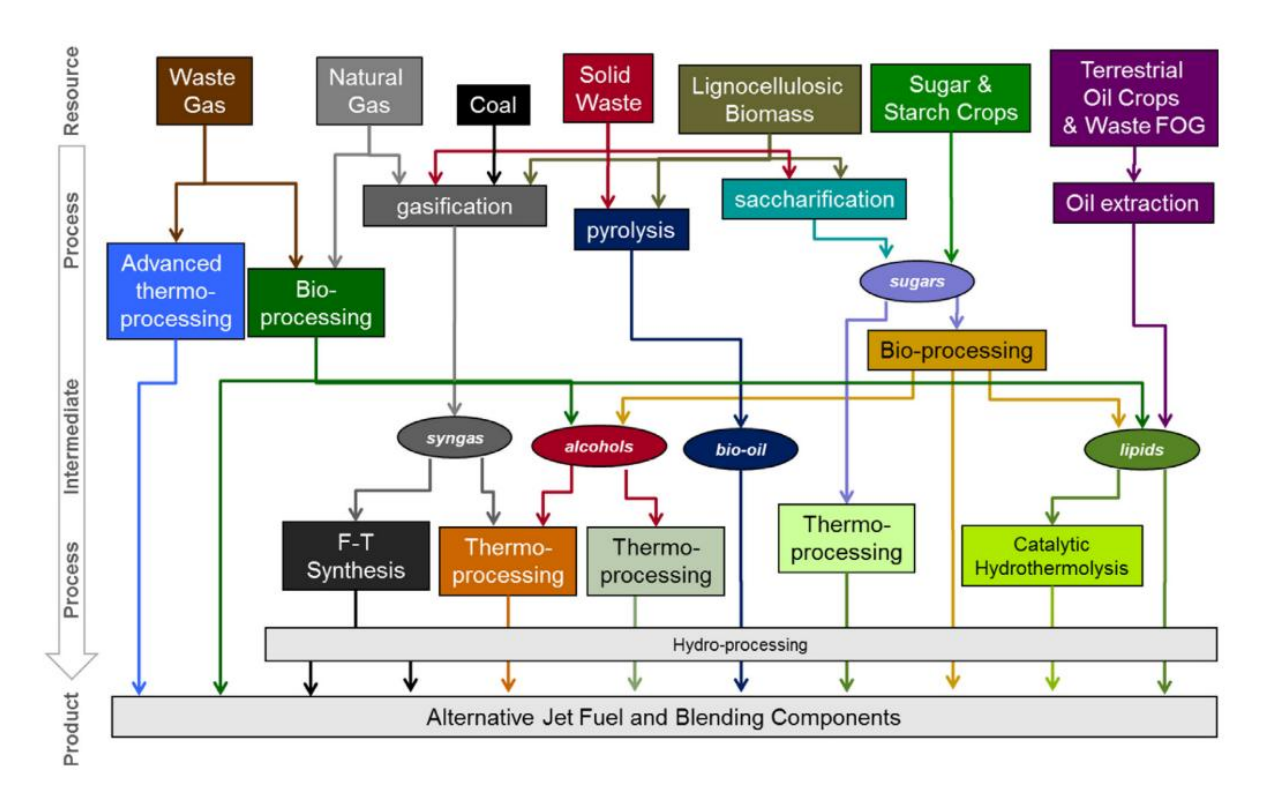


Figure A. 1: alternative jet fuels feedstocks and pathway. Reproduced from [131]

According to Figure A. 1, alternative jet fuels could generally be divided into two categories according to the feedstock: fossil-based and bio-based. Fossil-based synthetic fuels such as coal to liquids (CTL) and gas to liquids (GTL) are produced from fossil feedstocks using the Fischer-Tropsch (FT) process. Bio-based jet fuel uses biomass or crop oil, which usually requires additional bio-processing or hydrotreatment to achieve jet fuel requirements.

#### A.2 Bio-based feedstock

Biofuel is considered renewable since it is reproducible. A general classification of biobased feedstock is present in Figure A. 2.

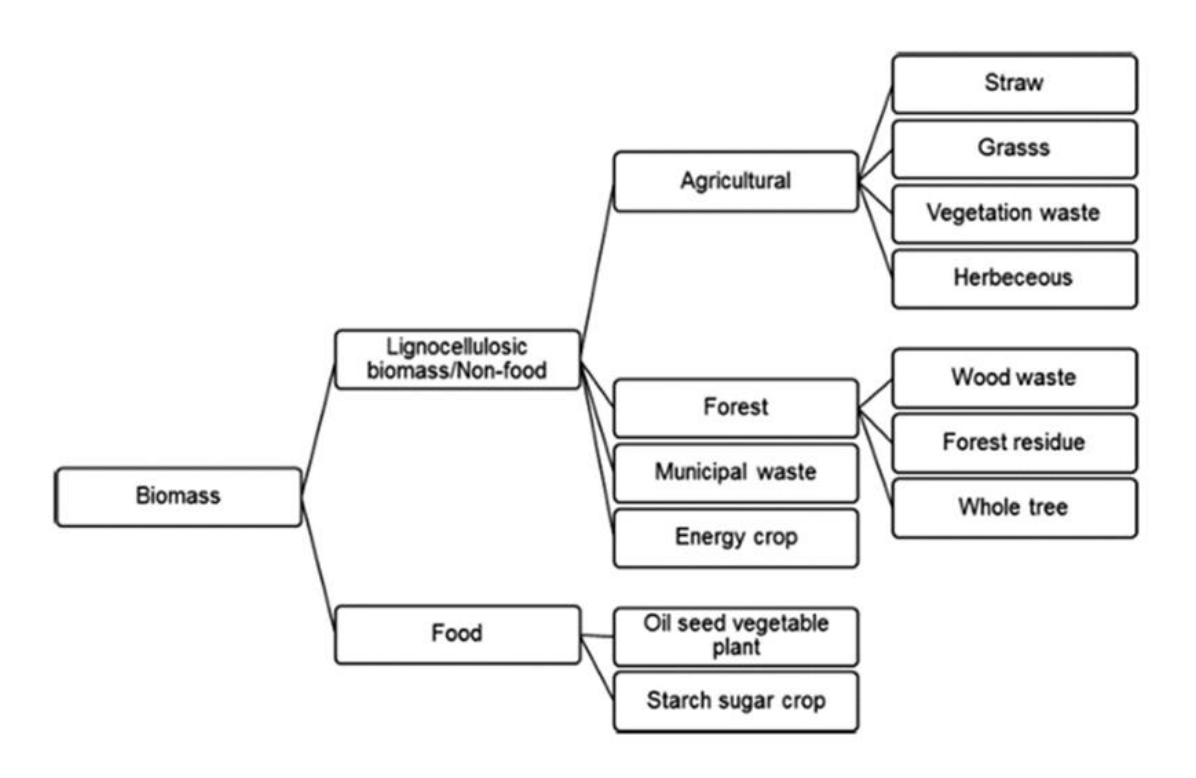


Figure A. 2: Classification of biomass. Reproduced from [132]

According to Figure A. 2, biofuel feedstocks could be divided into an edible group and an inedible group. Edible types are food-related sources such as oil seed, corn, and sugarcane. This group of feedstocks is also referred to as first-generation feedstock. The majority of biofuel is made from edible. Inedible feedstock mainly includes lignocellulosic biomass and energy crops. This type of feedstock also refers to second-generation feedstock. The third-generation feedstock is microalga, which has been developed recently. The main requirement of biofuel feedstock is the low price and the high production rate. The majority of the total cost of producing biofuel is its feedstock, and therefore, finding a cheap type of feedstock is essential. In addition, biomass

production is sensitive to species properties, place of origin and climate. Thus, a species that could provide colossal output and have high energy security is precious.

Compared with traditional fossil-based feedstock, biomass has a significant advantage in terms of solving energy security issues, which provides an alternative resource to produce jet fuel. Moreover, since bio-jet fuel is alternative jet fuels, which is less aromatic, it also reduces PM emissions compared with conventional jet fuels. Other than PM emissions, the carbon emission of biofuel is considered low as the carbon released during the combustion will be consumed during the growth of the plants. However, a detailed investigation is required for a specific bio-based feedstock since the total carbon life cycle should be involved in the calculation. For example, if land is needed for cultivation, carbon stored inside the soil will be released into the atmosphere during the cultivation. A more detailed discussion of the carbon life cycle will be presented in this chapter later.

#### A.2.1 Starch and sugar

Starch and sugar could be produced from first-generation feedstock. As mentioned, the food-related source is considered a first-generation feedstock of biofuels. In general, corn and sugarcane are all of the primary sources of this category of feedstock. More procedure is usually required to produce biofuel by using these feedstocks since both starch and sugar are also primary resources of ethanol production. A further process is essential to transfer ethanol into biobased alternative jet fuels [133].

As one of the most important crops, corn, known as maize, is widely cultivated on every continent. According to the statistics from the Food and Agriculture Organization of the United Nations (FAO), world production was about 594 million tons in 2020 [134], and the United States contributed the largest percentage of the total. Corn is one of the

primary ethanol feedstocks in the United States [135], [136], [137], and large corn harvests have contributed to increased ethanol production in recent years. Increased corn production and relatively stable corn prices have helped make increased ethanol production more profitable and less susceptible to corn price shocks.

Besides corn, sugar extract from sugarcane can be converted directly into ethanol through fermentation. Originating in Asia, sugarcane is one of the most significant feedstocks of ethanol production. Developing country like Brazil uses sugarcane as the ethanol feedstock, which is one of the leading countries of sugarcane cultivation in the global market [138], [139], [140].

#### A.2.2 Palm oil

Oil extracted from the palm is also considered a potential renewable jet fuel feedstock [141], [142], [143]. As one of the most extensively cultivated plants in the world, the palm family has a position in human history. It is difficult to identify whether palm oil is the first or second generation of feedstock. Plam is considered an energy plant, but many places also use palm oil as cooking oil, which makes it edible.

Most of the content in palm oil is saturated fat, which will become semisolid at room temperature. One of the advantages of using the palm as fuel feedstock is that the waste material during the oil extraction process, such as shells and fruit bunches, could also be treated as biomass for energy production [144]. Indonesia, Malaysia and Nigeria have a long history of producing palm since the desired cultivation environment for palm is tropical and subtropical climates.

#### A.2.3 Lignocellulose resources

Lignocellulose resources are referred to as second-generation feedstock of biofuels. Some typical feedstocks of lignocellulose resources include forest resources, grass and agricultural waste [145], [146], [147]. An overall production pathway of biofuel using lignocellulose resources as feedstock is present in Figure A. 3.

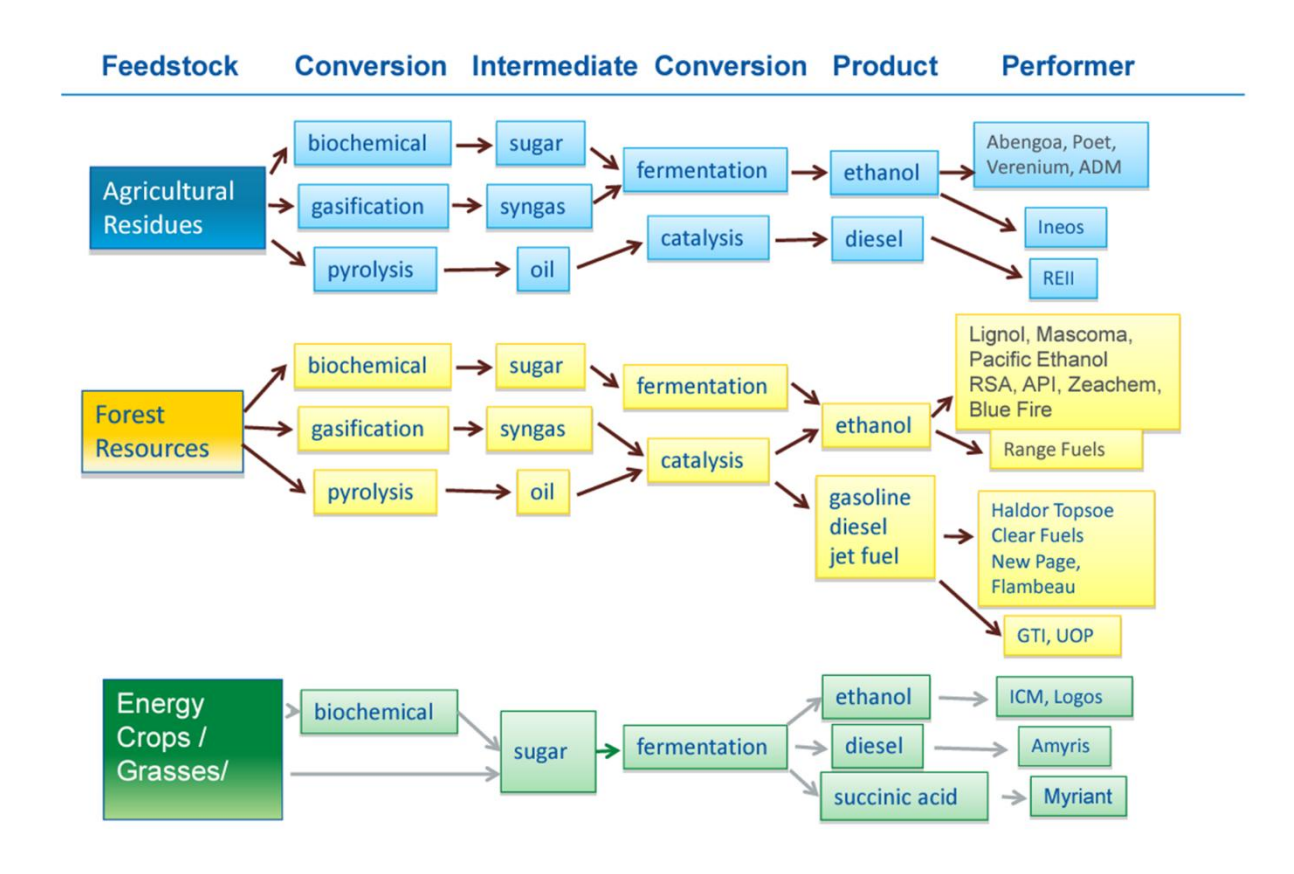


Figure A. 3: Production pathway of biofuel for lignocellulose resources [148]

Compared with traditional food-related crops, lignocellulose feedstock has a huge advantage. Since the majority of lignocellulose resources are wasted from other fields, such as agricultural activity, no additional water and fertilizer are required during the production. Moreover, using lignocellulose will not cause problems in food security, and the feedstock price is acceptable as well.

#### A.2.4 Energy crops

Oil from edible oil crops such as sunflower, palm and soybean are the major sources of biodiesel. However, the increased demand for biofuel also worsens the competition for food supply. Therefore, oil from nonedible oil plants is introduced as an alternative feedstock of biofuel belonging to second-generation feedstock. These non-edible crops, also called energy crops, include various species such as camelina sativa and jatropha.

Camelina sativa is a species belonging to the family of Brassicaceae, which is an annual flowering plant. Various oil-producing plant is also included in this family, such as rapeseed, canola and mustard. Using camelina sativa as biofuel feedstock has been widely investigated [149]. The main advantage of camelina is its high oil content, almost 38%-40% [150]. In addition, compared with conventional oil crops, camelina shows a high tolerance to dry environments during its lifetime. It is a massive advantage as a large scale of land unsuitable for biofuel plants can grow camelina. Furthermore, low input, such as fertilization and water, is required for camelina. However, some research [151] indicates that cameline is full of omega-3 fatty acids, which could potentially be used as a high-quality food oil. Since it is not included in the primary food market, using camelina as a biofuel feedstock will not compete with the food supply.

Jatropha is another non-edible energy plant widely grown in Africa, Asia, and America [152], [153], [154]. Traditionally, the jatropha family provide oil feedstock for the medicinal soap industry. Seedcakes of jatropha could also be used for fertilization and animal food. The oil derived from jatropha has been selected as a biofuel feedstock in the last decade and labelled as a miracle crop since it provides high-quality biofuel with low input. Compared with conventional food crops, jatropha can survive in unproductive land and is insensitive to extreme weather. Moreover, the water necessary for the growth of jatropha is extremely low. These properties of jatropha result in a high

potential for biofuel production, which does not need to compete with food crops. However, jatropha has recently lost its position, as the total yield is far lower than predicted. The main drawback of jatropha is that it has not yet been domesticated completely, which means it will struggle in massive cultivation due to increasing biofuel demand.

#### A.2.5 Waste oil

Waste oil is considered the second-generation biofuel feedstock which has the potential to procure commercialised biofuel [155], [156], [157]. Every year around 16.54 million tons of waste cooking oils is produced world with approximately 5 million tons in China [158]. The advantage of waste oil is the price, as this feedstock is usually abandoned waste. Moreover, using waste oil is believed to be environmentally friendly. However, the major problem with waste oil is that the production is unstable, and the collection point is dispersion. Therefore, it does not have enough ability as a long-term feedstock supplement for the large demand of the market. Moreover, waste oil and animal fat usually contain saturated fatty acids, increasing production prices.

#### A.2.6 Algae

Algae, one of the oldest life forms on earth, has already evolved into thousands of species worldwide. As the fundamental species inside the food chain, algae perform the energy donor through photosynthesis. Algae is recently considered the third generation of biofuel feedstock due to its high oil content, high growth rate and easiness of cultivation [159], [160], [161]. Like oil plants, Algae grow by consuming water, carbon dioxide and sunlight, but far more efficiently than conventional plants. Cultivation of microalgae is much easier and faster than oil plants, which is almost 30 times higher yields per acre. In the wild, algae species can be found in every habitat in earth,

including extreme salt water or even glaciers. In the case of the amount of carbon dioxide absorption during their lifetime, microalgae show a stronger advantage than conventional biomass producers. Moreover, considering its extremely high growth rate, microalgae seem to be the only feedstock with the potential to satisfy the world's liquid fuel demand. The relative technology relative to Algae could be predicted to develop rapidly soon.

#### A.3 Fossil feedstock

Instead of renewable bio-based feedstock, fossil feedstock beside crude oil could also produce alternative jet fuel. For example, coal and natural gas can all be converted into jet fuel though FT process. Fossil feedstock has a longer production history and more mature converting technology than bio-based feedstock [162]. The largest portion of alternative jet fuel is produced by coal and natural gas through the Fischer-Tropsch process. The advantage of fossil feedstock is the fully developed production pathway and the less input in term of feedstock. No additional process is required as all fossil feedstock is generated from geologically sequestered carbon sources.

However, one of most significant drawbacks of using fossil feedstock is that the carbon dioxide generated through the combustion process will interrupt the carbon balance in the atmosphere. Moreover, as large-scale production is involved, there is a potential energy competition between jet fuel feedstock and daily energy usage such as electricity and heating.

#### A.3.1 Natural gas

Natural gas is a fossil-based resources which could be used as feedstock of alternative jet fuels [162]. In general, it is a gas mixture which majority contain low molecular weight hydrocarbon [163]. The impurity of natural gas is various base on the place of

production, but usually include other types of alkanes and CO<sub>2</sub>. The process that converts natural gas to liquified fuel is called Gas to Liquids (GTL) [164]. Synthesis gas, which contains carbon monoxide and hydrogen, is produced first from natural gas. The FT process is then applied to convert synthesis gas into liquid hydrocarbons [165]. The U.S. Energy Information Administration estimated that by 2017, the average production of GTL will be 230,000 barrels per day, 0.2 per cent of global liquids production [166]. Figure A. 4 indicates the global production of liquid hydrocarbons through the GTL process.

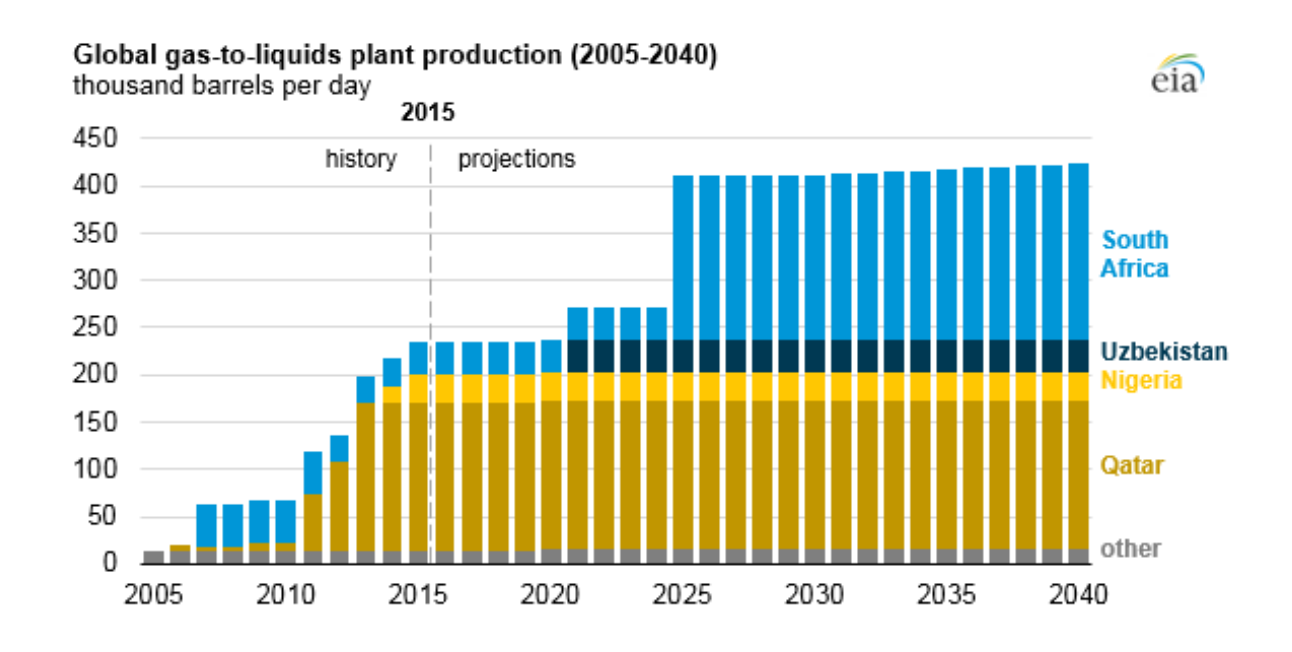


Figure A. 4: Global GTL plant production [166]

It is clear that fuel production has dramatically increased in the last decade, and it could be predicted that a huge increase in GTL fuels demand and production in the future.

#### A.3.2 Coal

Similar to natural gas, coal could convert to liquid jet fuel as well. The usage of coal as fuel feedstock has been well investigated for decades [167], [168], [169]. Coal-rich

country such as China has broad types of coal that could be used as feedstock for CTL processing, as shown in Table A. 1.

**Table A. 1: Composition difference of coal in China** [170]

|                          | Mass frac | tion (%) |      |      | Mass fraction (%) |       |       |              |           |       |
|--------------------------|-----------|----------|------|------|-------------------|-------|-------|--------------|-----------|-------|
|                          | Ash       | С        | Н    | N    | S                 | 0     | Water | Fixed carbon | Volatiles | Ash   |
| Anthracite coal (760524) | 5.20      | 90.93    | 1.13 | 0.30 | 0.25              | 1.27  | 3.21  | 88.27        | 3.32      | 5.2   |
| Meager coal (760527)     | 9.81      | 85.13    | 3.74 | 1.23 | 1.34              | 2.49  | 1.57  | 78.5         | 10.12     | 9.81  |
| Lean coal (73-1)         | 15.63     | 84.16    | 4.30 | 1.46 | 0.43              | 3.60  | 1.47  | 69.27        | 13.63     | 15.63 |
| Coking coal (73-6)       | 20.57     | 80.65    | 4.66 | 1.23 | 0.17              | 2.82  | 0.93  | 60.79        | 17.71     | 20.57 |
| Gas coal (73-7)          | 9.45      | 76.40    | 5.27 | 0.99 | 0.27              | 11.10 | 4.12  | 51.62        | 34.81     | 9.45  |

In addition, the performance as well as the fuel production of a CTL plant is different for each type of coal. Table A. 2 indicates the amount of fuel production by different types of coal in China.

Table A. 2: FT oil production and composition [170].

|                          | Tops<br>(kg/s) | Gasoil<br>(kg/s) | Keo<br>(kg/s) | FT oil<br>(kg/s) |
|--------------------------|----------------|------------------|---------------|------------------|
| Anthracite coal (760524) | 0.044          | 0.215            | 0.102         | 0.361            |
| Meager coal (760527)     | 0.045          | 0.219            | 0.105         | 0.369            |
| Lean coal (73-1)         | 0.042          | 0.0204           | 0.097         | 0.344            |
| Coking coal (73-6)       | 0.041          | 0.0199           | 0.095         | 0.334            |
| Gas coal (73-7)          | 0.044          | 0.0211           | 0.101         | 0.356            |

Same as other alternative jet fuels due to the lack of aromatic content in CTL jet fuels, the PM production is much lower compare with conventional jet fuel. In addition, due to the unique production pathway, less amount of sulphur contains in CTL jet fuels, making it more environmentally friendly. Although the emission from CTL is lower than conventional fuel during the combustion, the total carbon emission could be twice as high if the carbon lifecycle analysis is included in the consideration. Therefore, carbon capture and sequestration (CCS) must be applied to reduce the total carbon emission [171]. However, the result of combining CCS with CTL is the high capital-intensive which also potentially prevent its promotion.

# APPENDIX B - Production pathways of alternative jet fuels

Beside feedstock, alternative jet fuels could also be classified based on the production pathway. The most mature alternative fuel production pathway is Fischer-Tropsch (FT) process. As mentioned, some synthetic alternative jet fuels produced from fossil feedstocks such as natural gas and coal using the FT process. Recently, synthetic alternative jet fuels using the FT process have also targeted bio-based feedstock, which has enormous potential in term of feedstock availability and cost efficiency.

Other pathways have also dramatically developed recently due to the feedstock crisis of conventional jet fuel. For example, Hydrotreatment Easter and Fatty Acid technology provided an alternative method to produce aviation jet fuel by bio-oil type feedstocks. Figure B. 1 gives a general summary of the alternative jet fuels pathway and suitable feedstock which will be discussed in this chapter.

Table B. 1: A summary of the alternative jet fuels pathway and corresponding feedstock

| Pathway                                      | Feedstock   |  |  |  |  |  |
|--|---|--|--|--|--|--|
| Fischer-Tropsch (FT)                         | Natural gas, Coal, Biomass  |  |  |  |  |  |
| Hydrotreatment Esters and Fatty Acids        | Crops Oil (Camelina, Jatropha, etc.),<br>Tallow, Waste Oil, Algae |  |  |  |  |  |
| Alcohol to Jet                               | Corn, Sugarcane, Lignocellulose                                   |  |  |  |  |  |
| Direct Sugars to hydrocarbons                | Sugarcane   |  |  |  |  |  |
| Co-processing and catalytic hydrothermolysis | vegetable oil   |  |  |  |  |  |
| Gas fermentation                             | Industrial waste gas  |  |  |  |  |  |

# **B.1 Fischer-Tropsch (FT)**

Fischer-Tropsch (FT) as mentioned has been developed well in the past decades. Feedstock of FT pathways dominated by coal, natural gas and biomass. The final jet fuel product uses the FT process also called synthetic paraffinic kerosene (SPK). A general concept of Fischer-Tropsch reactor used in FT present in Figure B. 1.

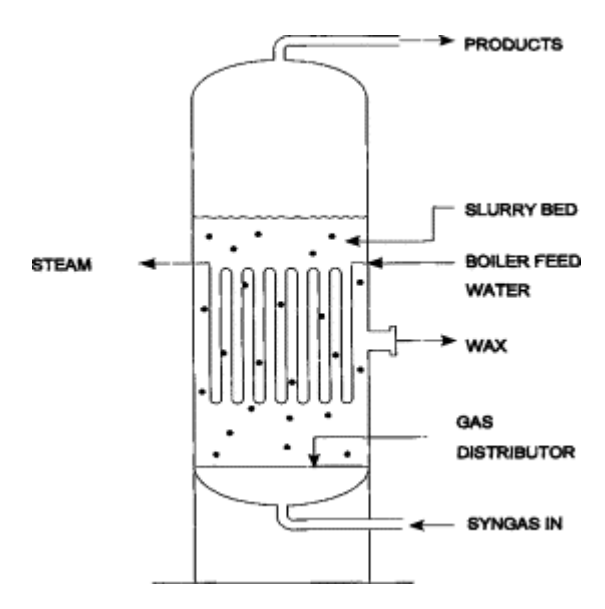


Figure B. 1: Fischer-Tropsch reactor. Reproduced from [172]

The advantage of using SPK as jet fuel is huge. First, FT fuels can be used directly in the jet engine, with no significant negative impact on engine preference reported in the past few years. Second, like other types of alternative jet fuels, FT fuels have a cleaner fuel formula and fewer aromatic compounds than conventional jet fuel, giving its massive advantage in PM reduction.

Depending on the producer, the basic feedstock, final fuel formula for the FT process varies (coal for Sasol, natural gas for Sell). However, all processes are required to produce synthesis gas first must first go through gasification [173]. FT jet fuel produced by Sasol is the first approved AJF to blend conventional jet fuel. In addition, The FT fuel

produced by Shell is a narrow-cut kerosene compared with JP8 and has been used commercially as a blending feedstock with conventional jet fuel since 2012.

Compared with fossil-based feedstock, biomass as FT feedstock has shorter history [174]. Agriculture waste and straw mattresses could all be converted into jet fuel through gasification and FT process. The cheap raw material price is the most significant advantage of using biomass as feedstock. Moreover, biomass is also considered environmentally friendly as it absorbs carbon during the recovery phase. It could predict that biomass's portion of FT fuels will increase soon.

In addition, some recent research indicates the possibility of using coal and biomass as feedstock, sometimes referred to as coal—biomass to liquids (CBTL) [175]. Liquid Fuel is generated through the new, more efficient signal-step hydrolysis process. The bypass product is high-purity carbon dioxide, which could be reused. The detailed information on this novel pathway is limited as it still needs further development. The potential economic and lifecycle is not analysed in any research.

# **B.2 Hydrotreatment Esters and fatty acids (HEFA)**

HEFA technology generally transfers raw feedstock to paraffinic through hydrotreatment and isomerization. For biobased alternative jet fuels, HEFA is the one of the most developed methods. The most advantage of using HEFA in alternative jet fuels production is the wide range of feedstock selection. Feedstocks of HEFA is mainly edible vegetable oil, but some inedible feedstocks such animal fat, waste oil, camelina and jatropha are also widely used. In addition, oil derived from algae has also rapidly developed, which has the possibility to start a revolutionary change in biofuel market. An overlook of oil yield from various crops and corresponding price is provided in Figure B. 2.

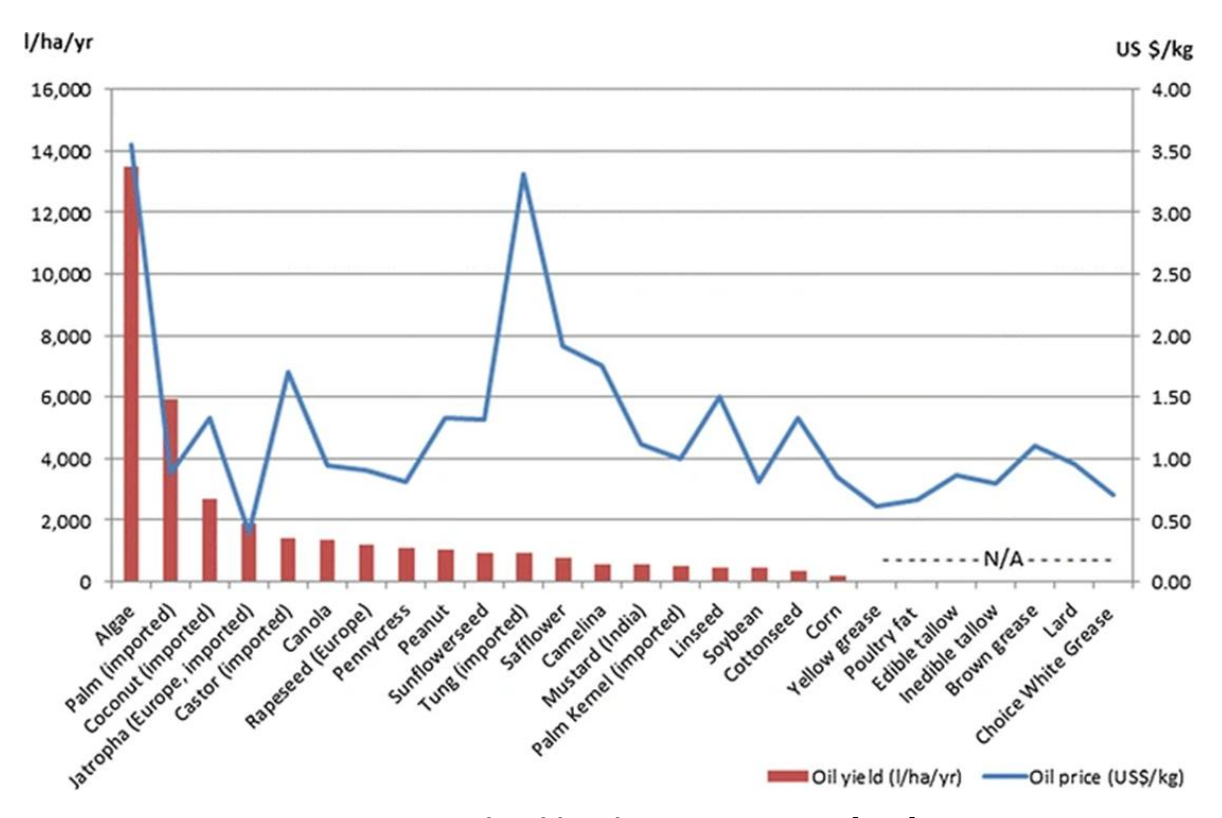


Figure B. 2: Oil yield and price in US 2014 [176]

Overall, the world vegetable oil supply was 178 million tonnes in 2015, and due to the development jet fuel demand, the aviation industry has recently increased the amount of oil feedstock to convert into AJF. However, not all crops are suitable to be the feedstock of alternative jet fuels using HEFA. Both price and yield need to be considered. Figure B. 2 indicates that oil price does not follow the oil yield for all crops. According to the tung has the highest oil price but a relatively low oil yield. Moreover, algae have a massive advantage in oil yield due to their high growth in cultivation, but the price is highest as well [159]. Palm and coconut also show their ability to provide a sustainable oil supply. Moreover, some oil crop is also used as cooking oil which rise the concern of food security.

One of the significant drawbacks of using edible feedstock is that when the demand and production increase dramatically, it may affect food security. In addition, the price of vegetable oil has increased more than ten times during the last ten years. Therefore, development nonedible is reasonable. Compared with edible plants, nonedible plants

cannot compete with the demand of food supply, and most of these plants can survive on land unsuitable for growing edible oil plants. Therefore, the price is significantly lower than edible plants.

Due to the concern of competition with food supply and environmental impact, wasted oils are also investigated as alternative HEFA feedstock as well. Used cooking oil (UCO) is the most widely obtainable resources, but the production is way smaller than the traditional vegetable oil. It has been estimated that 54200 tons per year of UCO could be collected in the USA.

Both Honeywell and Neste use HEFA technologies to produce alternative fuels. However, the final output is various due to the different production techniques. Honeywell uses hydrotreatment followed by selective cracking with the combination of isomerization, and the quantity of jet fuel in the output is maximised. Neste's HEFA process targets diesel production, and it is still possible to produce alternative jet fuels, but further adjustment is required.

# **B.3 Alcohol-to-Jet (ATJ)**

Alcohol, include ethanol and butanol are produced usually from biomass such as corn and sugarcane. As mentioned, the world's leading alcohol producers are the United States and Brazil. In the US, corn is the major feedstock of ethanol because of its rich cultivation and reserve quantity. Moreover, other feedstock could also use for Alcohol-to-Jet process such as lignocellulose resources.

The method transfers alcohol intermediates to jet fuel are called Alcohol-to-jet, and the core steps of Alcohol-to-Jet is shown in Figure B. 3.



Figure B. 3: The core catalytic steps in the Alcohol-to-Jet process [42].

In general, two steps are required to convert bio-feedstock into jet fuel. First, alcohol should be derived from sugar or starch through a process such as fermentation. This pathway for converting biomass feedstock to alcohol intermediates is a fully mature technology, especially in America and Brazil, providing strong technology for this type of alternative jet fuel. Second, convert alcohol into jet fuel through catalytic process include dehydration, oligomerization and hydrogeneration [177], [178]. Jet fuel produced though Alcohol-to-Jet is approved to blend with conventional jet fuel up to 50%.

### **B.4 Direct sugars to hydrocarbons (DSHC)**

The feedstock of the DSHC process is similar to Alcohol-to-Jet process. The difference is that this method converts sugar directly to alkane-type fuels through anaerobic fermentation. The detail production pathway of DSHC is presented in Figure B. 4.

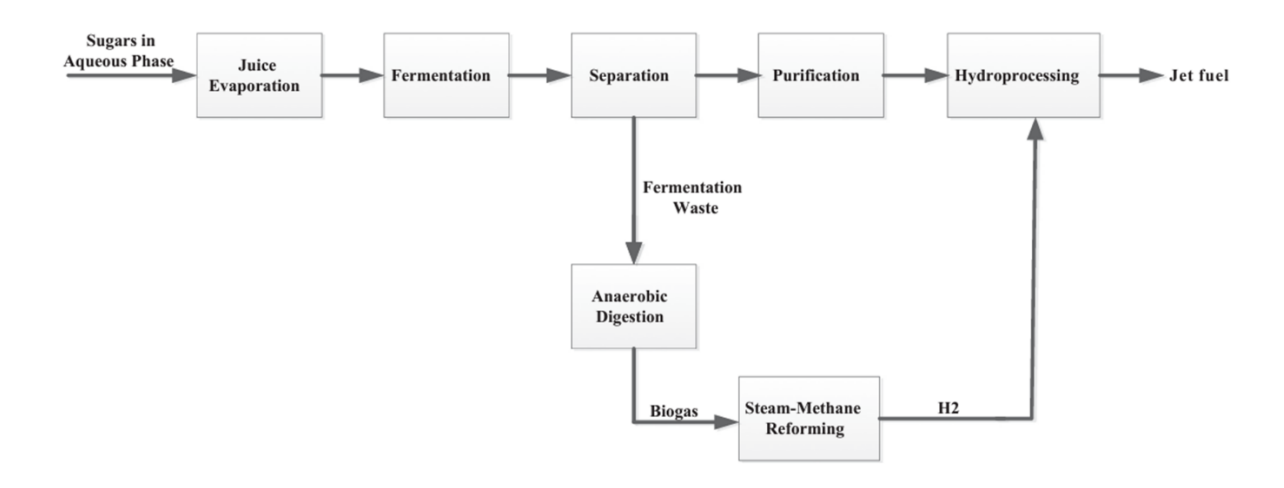


Figure B. 4: Direct sugar-to-jet fuel [178].

Compare with Alcohol-to-Jet process, DSHC do not need to produce alcohol as an intermediate to convert into jet fuel [179]. Moreover, considering the complexity of fermentation, simple hexose sugars generated from sugarcane can be used as the primary feedstock [180]. In addition, this technology can transfer more complex sugar structures, such as the sugar extract, from lignocellulosic biomass feedstock.

# **B.5 Catalytic hydrothermolysis (CH)**

This pathway transfers vegetable oil to jet fuel with the middle distillation in the refineries. A general production pathway is shown in Figure B. 5. The investment cost is low because the existing hydrotreated technology references this pathway. Catalytic hydrothermolysis uses water to produce aromatic and paraffinic, with less hydrogen consumption [181]. The result fuel achieved the requirement to be used as a 100% drop-in fuel.

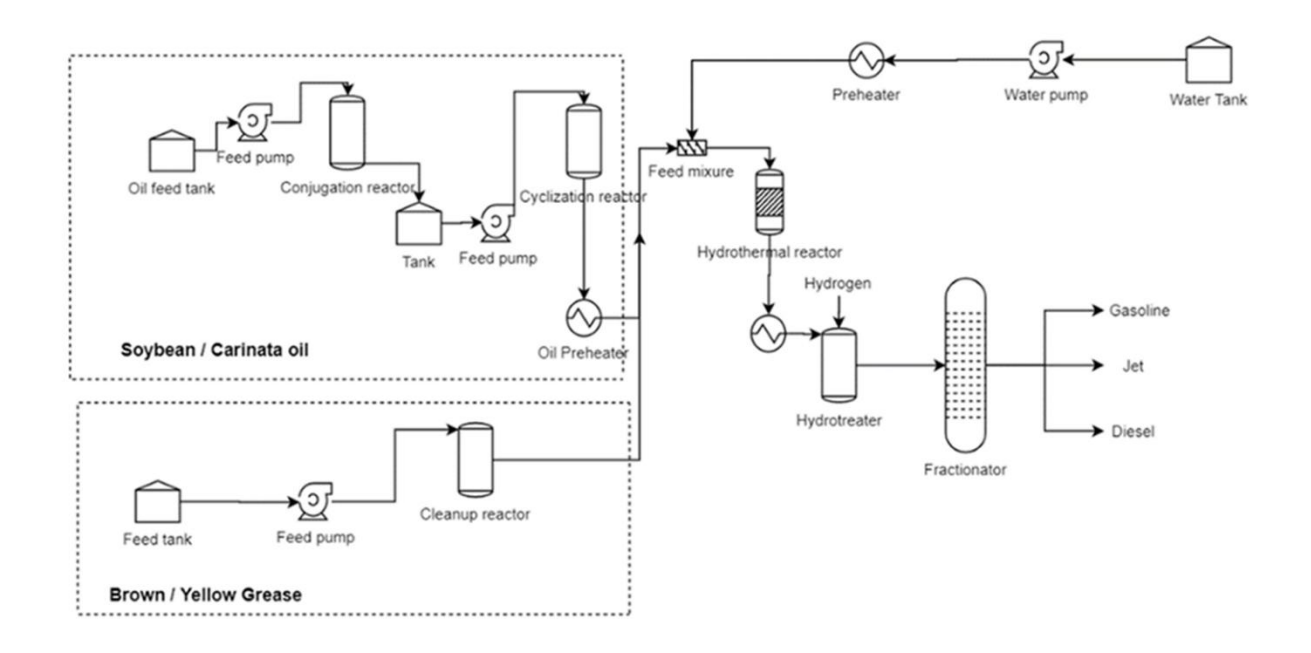


Figure B. 5: Catalytic Hydrothermolysis process [182].

#### **B.6 Life cycle analysis**

A lot of research focussing on developing new feedstock for jet fuel production due to the energy security and emission reduction purposes. It has been approved that alternative jet fuels have significantly reduce emissions compare with conventional jet fuel. However, In the past, research only focused on emission at the combustion stage which is not in the case of alternative fuel. A huge amount of alternative jet fuels feedstocks are crops, which require water, fertilizer and land during cultivation. Moreover, feedstocks of alternative jet fuels usually require complex process into order to achieve desire jet fuel which able to use in the gas turbine engines. Therefore, an overall carbon emission calculation should be processed as the production pathway usually generates much higher carbon than the combustion phase.

A detailed life cycle GHG calculation of fossil-based alternative jet fuel is present in Figure B. 6.

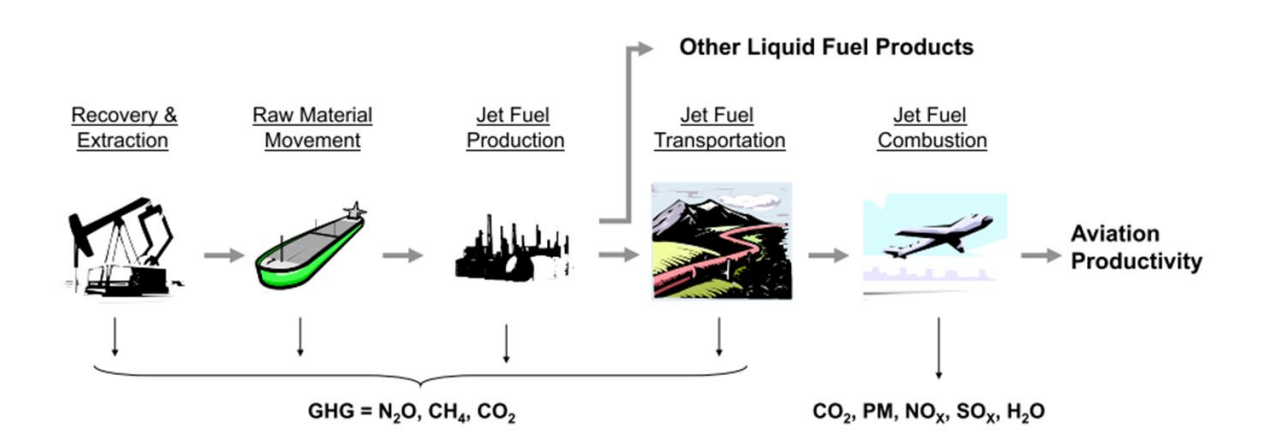


Figure B. 6: Septs need to consider for the life cycle GHG calculation of fossil-based jet fuel [183].

One typical example of fossil based alternative jet fuels is the jet fuel produced through CTL process. The Carbon emissions of CTL fuel will be lower than conventional jet fuel if the stage of combustion in a gas turbine engine is consider only. However, additional

carbon will be produced during the production of CTL, and the total carbon emission (production stage + combustion stage) will be twice as high as conventional fuel. Moreover, since coal is a fossil-based resources. Using fossil-based feedstock will release the amount of carbon that is originally fixed under the ground thought the crustal movements. A detailed life cycle GHG calculation of fossil-base jet fuel is present in Figure B. 7.

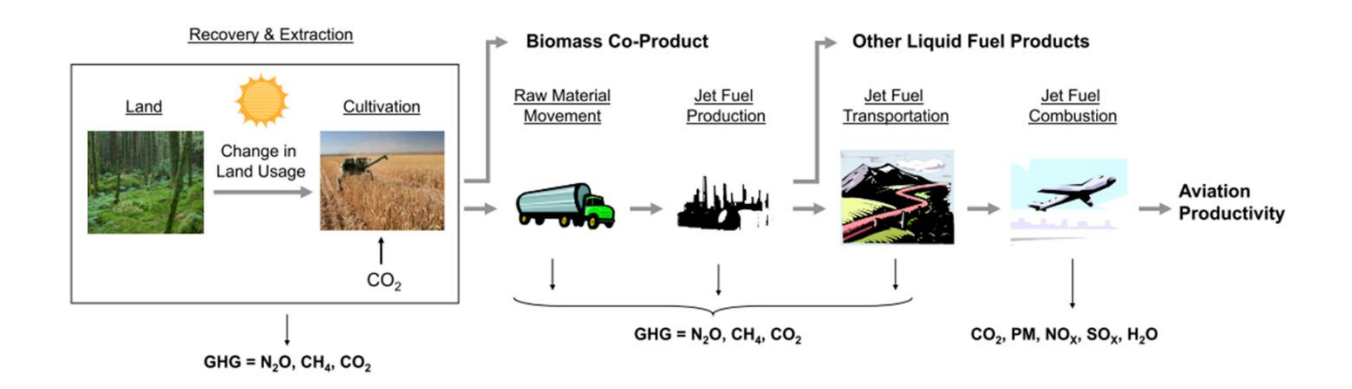


Figure B. 7: Septs need to consider for the life cycle GHG calculation of bio-based jet fuel [183].

Another example is the jet fuel produced by biomass. For a long time, biomass has been considered the raw material for jet fuel with zero carbon emission. This theory is based on the carbon balance between the growth phase of the bio plant (absorbing carbon from the atmosphere) and the combustion phase (releasing carbon to the atmosphere). In this hypothesis, the amount of absorbed and released carbon could be cancelled, which did not introduce extra carbon to the environment. However, recent research indicated the opposite results. Carbon, such as fertilisation during growth phase which will cause addition carbon released into the atmosphere. In addition, in the case of large-scale cultivation, deforestation, land exploitation, and reclamation will release the carbon which is fixed inside the soil and plants previously.

Therefore, to have a complete understanding of emissions cause by using alternative jet fuels both production stage and combustion stage should put into the consideration.

For example, for an energy plant, carbon emissions from cultivation, land use, feedstock transportation, production process and combustion are all essential to put in the calculation of total carbon emissions.

A complex life cycle calculation for selected feedstock based on the data from PARTNER-Partnership for Air Transportation Noise and Emission Reduction is shown in Figure B. 8.

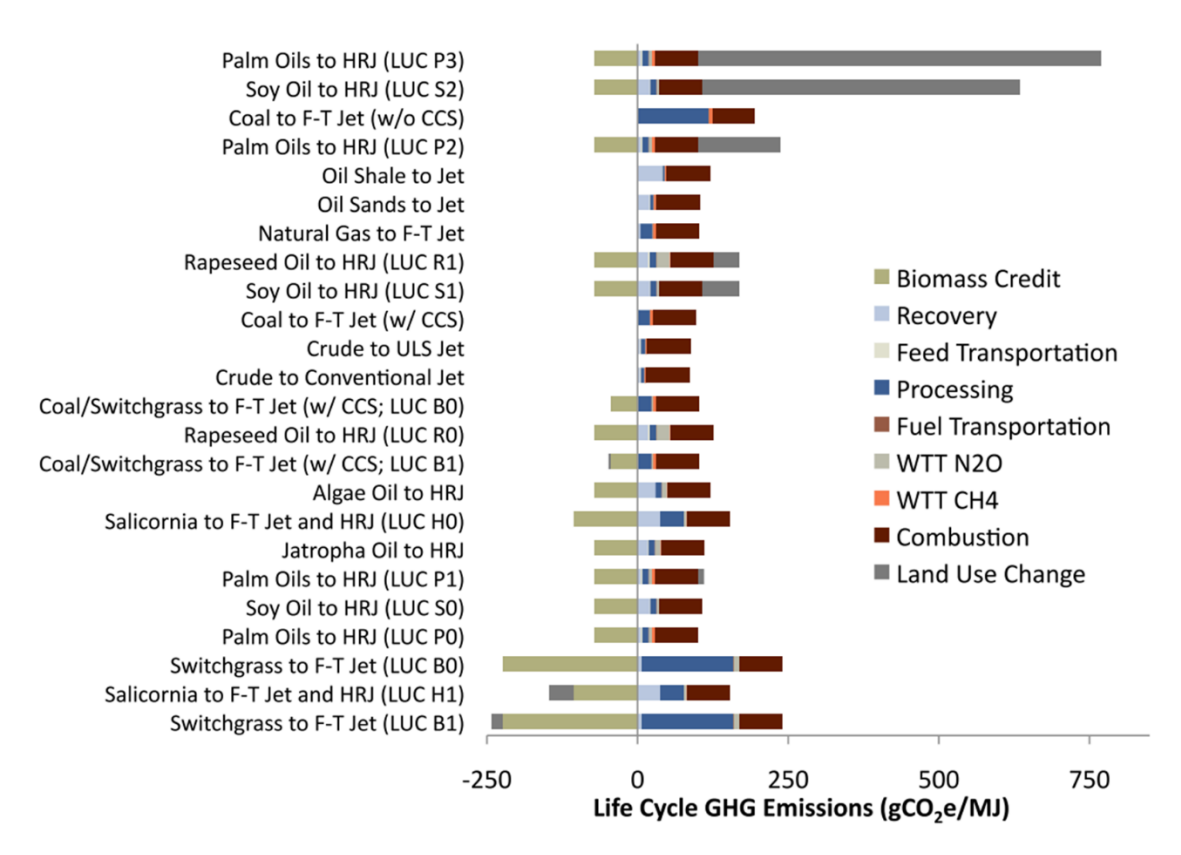


Figure B. 8: Life cycle GHG emissions for selected feedstock and pathway [183]

According to Figure B. 8, the highest whole carbon emission is hydro-processed renewable fuel produced by palm oil and soy oil, and Land Use Change produces a large portion of the emission. It is reasonable as cultivation of these energy plants will involve deforestation and reclamation. In the case of Palm, rainforest, tropical rainforest

and peat land, the rainforest will be converted into palm plantation fields. Plant oil production generally produces massive carbon emissions during the Land Use Phase.

Compared with bio feedstock, fossil feedstock such as coal and natural gas has the emission advantage in the recovery stage. Still, the major carbon emission is due to the processing phase, which is more than 50% of total carbon emission. However, with Carbon Capture and Sequestration (CCS) technology, the amount of carbon emission during the converting process has been dramatically reduced. Bio-based feedstock has a considerable advantage over fossil feedstock due to reduced total carbon emissions through the growth phase. However, further investigation should still be conducted as large-scale demand is required. The balance of food and fuel feedstock and potential output reduction due to the environment is still challenging.